

ABSTRACT

Title of Dissertation: DEVELOPMENT OF A COMPONENT BASED
SIMULATION TOOL FOR THE STEADY
STATE AND TRANSIENT ANALYSIS OF
VAPOR COMPRESSION SYSTEMS

Jonathan M. Winkler
Doctor of Philosophy, 2009

Dissertation Directed By: Reinhard Radermacher, Professor
Department of Mechanical Engineering

Computer simulations have become a commonly used tool to aid engineers design and optimize vapor compression systems. Generally, the simulation of vapor compression heat pump systems falls into one of two categories; steady state and transient. Steady state simulations are typically very accurate and highly detailed, and used for design and optimization of vapor compression systems and components. Transient simulations generally utilize more assumptions to reduce complexity and computational time, and are used to design and evaluate control strategies. However, utilizing two separate simulation tools to perform steady state and transient simulations presents the challenge and burden

of increased software development and maintenance effort and inconsistency in the predicted results.

This thesis presents a simulation tool that simultaneously serves the industry needs of an integrated steady state and transient vapor compression simulation tool. The tool is developed using a component-based architecture allowing for the users to incorporate in-house component models into the simulation and the component-based framework is discussed in detail. Particular emphasis is placed on transient heat exchanger simulation; resulting in an algorithm that reduces complex and detailed heat exchanger models into simplified, faster versions that still have sufficient accuracy so that transient and steady state results converge to the same performance under steady state conditions. Thus, consistency in the results between the steady state and transient simulations is preserved.

Nearly all pre-existing vapor compression system simulation tools are limited to the standard four component cycle. However, for enhanced efficiency and thermal comfort, multi-component systems are gaining in popularity. The component-based framework implemented by the simulation tool allows for the simulation of cycles with additional components.

During the development of the simulation tool, the need of a faster, more robust solution algorithm to solve a steady state vapor compression system became evident. Thus, a new solution algorithm was developed, thoroughly tested, and compared with existing solution techniques in the literature. An improvement of 50% was achieved in the solution algorithm's robustness. A more advanced method to determining initial guess values for steady simulations was developed and reduced the number of component evaluations by approximately 40%.

DEVELOPMENT OF A COMPONENT BASED SIMULATION TOOL FOR THE
STEADY STATE AND TRANSIENT ANALYSIS OF VAPOR COMPRESSION
SYSTEMS

By

Jonathan M. Winkler

Dissertation submitted to the Faculty of the Graduate School of the
University of Maryland, College Park, in partial fulfillment
of the requirements for the degree of
Doctor of Philosophy
2009

Advisory Committee:
Professor Reinhard Radermacher, Chair
Professor Jung-ho Kim
Associate Professor Tien-Mo Shih
Assistant Professor Bao Yang
Associate Dean Gary Pertmer

© Copyright by
Jonathan M. Winkler
2009

Acknowledgements

I am forever grateful for my advisor, Dr. Reinhard Radermacher; for his patience, guidance, and encouragement. I have had the unique pleasure of working with Dr. Radermacher on a variety of projects and have greatly benefitted, in many ways, from this opportunity. I would like to express gratitude to my advisory committee, Dr. Jungho Kim, Dr. Tien-Mo Shih, Dr. Bao Yang, and Dr. Gary Pertmer, for their service and contribution to making this thesis as strong as possible.

I would like to offer a special thanks to Vikrant Aute, who is most responsible for teaching me the day-to-day lessons on how to perform high level research. He has shown infinite patience in always taking the time to answer my questions and has been very successful at helping me learn software development skills. I am thankful for my colleagues, Omar AbdElAziz and Varun Singh, who have always lent open ears when I needed advice. I wish them both the best of luck in the completion of their Ph.D.'s and continued success in all future endeavors. I am very appreciative of Xudong Wang for providing experimental data allowing me to complete my thesis.

I would like to thank all ISOC students, past and present, for influencing my graduate student career and contributing to my success. I would specifically like to thank David Richardson, for taking the time to introduce me to VapCyc and component-based programming, and Andy Schwentker, for helping me figure out graduate school.

Most importantly, I would like to thank my wife, Larissa, and my family for their love and support. Without the continuous love and sacrifice by my wife, this achievement would not have been possible.

Table of Contents

Acknowledgements.....	ii
Table of Contents.....	iii
List of Tables	vii
List of Figures.....	viii
Nomenclature.....	x
1 Introduction.....	1
1.1 Vapor Compression Systems.....	1
1.2 Introduction to Steady State and Transient Simulation of Vapor Compression Systems.....	3
1.2.1 Steady State Simulation.....	3
1.2.2 Transient Simulation.....	5
1.2.2.1 Heat Exchanger Modeling Overview.....	7
1.2.2.2 Compressor Modeling Overview.....	9
1.2.3 Quasi Steady State Simulation.....	11
1.3 Literature Review	11
1.3.1 Steady State Vapor Compression System Solution Techniques.....	11
1.3.2 Transient Vapor Compression System Simulations	15
1.3.3 Transient Compressor Simulations.....	20
1.3.4 Existing Vapor Compression System Simulation Packages.....	22
1.3.4.1 Steady State Simulation Software Packages.....	22
1.3.4.2 Transient Simulation Software Packages.....	24
1.3.5 Summary of Background	27
1.4 Research Objectives.....	28
1.5 Completed Tasks / Thesis Organization	29
2 Component-Based Simulation Framework.....	31
2.1 Motivation.....	31
2.2 Definitions	32
2.2.1 Components	32
2.2.2 Ports	33
2.2.3 Component Boundary Condition Types	33
2.2.4 Junctions	34
2.3 Background Information.....	36
2.4 Standardized Framework	37
2.4.1 Port States	38
2.4.2 Parameters.....	38
2.4.3 Vapor Compression Component Standard.....	40
2.4.4 Load Component Standard	43
2.4.5 Fan Component Standard.....	45

2.4.6 Control Block Standard.....	47
2.5 Sample Equation Set for the Steady State Solution of a Vapor Compression System	47
2.5.1 System Definition	47
2.5.2 Component Model Equation Set.....	48
2.5.2.1 Compressor Model.....	49
2.5.2.2 Condenser Model.....	50
2.5.2.3 Expansion Device Model.....	52
2.5.2.4 Evaporator Model	53
2.5.3 System-Level Solution Variables.....	54
2.5.4 Application of Component-Based Simulation	57
3 Steady State Component Simulation	58
3.1 Air-to-Refrigerant Heat Exchanger Simulation.....	58
3.1.1 Generic Heat Exchanger Model.....	58
3.1.2 CoilDesigner Heat Exchanger Model	59
3.2 Compressor Simulation.....	60
3.2.1 Isentropic Compressor Model.....	60
3.2.2 ARI-540 Coefficient Compressor Model.....	61
3.2.3 Two-Stage Isentropic Compressor Model	62
3.3 Expansion Device Simulation.....	64
3.3.1 Fixed Orifice Model.....	64
3.3.2 Short Tube Orifice Model.....	65
3.3.3 Adiabatic Capillary Tube Model	65
3.3.4 Linear TXV Model	66
4 Investigation into Steady State Solver Performance and Its Improvement	68
4.1 Motivation.....	68
4.1.1 Relevance to Transient Simulation	70
4.2 System Solver Evaluation Procedure.....	70
4.2.1 Vapor Compression Cycle Configurations	71
4.2.2 Nonlinear Equation Solver Selection.....	72
4.2.3 Vapor Compression System Input Specification	72
4.2.4 System Operating Conditions Test Matrix	73
4.2.5 Guess Value Calculations	75
4.2.5.1 Design Point Guess Values.....	75
4.2.5.2 Adjusted Guess Values	75
4.2.6 Numerical Experiments	76
4.3 System Solver Performance Metrics.....	77
4.3.1 Solver Robustness.....	77
4.3.2 Computational Efficiency	78
4.4 Algorithms for Solving a Component-Based Vapor Compression System	
Simulation.....	78
4.4.1 Junction Solver.....	79
4.4.1.1 Junction Solver Advantages.....	80
4.4.1.2 Junction Solver Disadvantages	81

4.4.2 Enthalpy Marching Solver	81
4.4.2.1 Enthalpy Marching Solver Advantages	85
4.4.2.2 Enthalpy Marching Solver Disadvantages	85
4.4.3 Decoupled Energy and Hydraulic Solver	85
4.4.3.1 Decoupled Energy and Hydraulic Solver Advantages	87
4.4.3.2 Decoupled Energy and Hydraulic Solver Disadvantages	88
4.5 Results and Discussion	88
4.5.1 Junction Solver Results	91
4.5.2 Enthalpy Marching Solver Results	93
4.5.3 Decoupled Energy and Hydraulic Solver Results	95
4.5.4 System Input Specification Type Comparison	97
4.5.5 Numerical Equation Solver Convergence Comparison	98
5 Steady State Simulation of Additional Cycle Types	100
5.1 Two Stage Flash Tank Cycle	100
5.1.1 Two Stage Flash Tank Cycle Solution Procedure	101
5.1.2 Two Stage Flash Tank Cycle Validation	103
5.2 Cascade Vapor Compression System with Multiple Components	108
5.2.1 Cascade System Solution Procedure	111
5.2.2 Cascade System Validation	115
5.2.2.1 Experimental System	115
5.2.2.2 Modeling Procedure and Assumptions	116
5.2.2.3 Validation Results	117
6 Transient Component Simulation	121
6.1 Tank and Tube Heat Exchanger Simulation	121
6.1.1 Heat Transfer Elements (Tanks)	122
6.1.1.1 Heat Exchanger Dehumidification	126
6.1.2 Pressure Drop Elements (Friction Tubes)	129
6.1.2.1 Inlet and Outlet Friction Tubes	129
6.1.2.2 Internal Friction Tubes	132
6.1.3 Heat Exchanger Modeling Procedure	133
6.1.3.1 Modeling of Multiple Row Heat Exchangers	134
6.1.4 Heat Exchanger Model Dependence on Number of Tanks	136
6.1.5 Numerical Issues	142
6.1.6 CoilDesigner Input File Translator	143
6.1.7 Steady State Heat Exchanger Validation	144
6.1.7.1 Single Row Heat Exchanger	145
6.1.7.2 Multiple Row Heat Exchanger	149
6.2 Compressor Simulation	153
6.2.1 Compressor Modeling Approach	154
6.2.1.1 Boundary Conditions	156
6.2.1.2 Compressor Model Formulation and General Equation Set	156
6.2.1.3 Reciprocating Compressor Heat Transfer Calculations	159
6.2.1.4 Scroll Compressor Heat Transfer Calculations	162
6.2.2 Summary of Required Input Parameters	163

6.2.3 Compressor Model Validation	164
6.2.3.1 Steady State Validation	166
6.2.3.2 Transient Validation	172
6.3 Expansion Device Simulation	180
7 Transient System Simulation	182
7.1 System Simulation Procedure	182
7.1.1 System Level Solution Variables and Conservation Equations	182
7.1.2 Solution Procedure	185
7.2 Time Stepping Procedure	186
7.2.1 Variable Time Step Procedure	187
7.3 Transient and Steady State Comparison - Example Simulation	187
7.3.1 System Description	188
7.3.2 Simulation Results	190
7.3.3 Results Comparison	195
7.4 Transient Validation Study	197
7.4.1 System Description and Procedure	197
7.4.2 Validation Results	198
7.4.3 Validation Discussion	203
8 Summary and Conclusions	205
8.1 Component-Based Simulation	205
8.2 Steady State Component Simulation	206
8.3 Investigation into Steady State Solver Performance and Its Improvement	206
8.4 Transient Component Simulation	208
8.5 Transient System Simulation	209
9 List of Major Contributions and Future Work	210
9.1 Major Contributions	210
9.2 Future Work	212
References	213

List of Tables

Table 1.1 Summary of transient compressor models found in the literature	21
Table 2.1 List of Vapor Compression Component Standard methods	41
Table 2.2 List of Vapor Compression Component Standard properties	42
Table 2.3 List Fan Provider methods	46
Table 4.1 ASHRAE Rating Conditions (Reproduced from ASHRAE Std. 116, 1995) ...	74
Table 4.2 System solver test matrix values	75
Table 4.3 Average number of function evaluations required to simulate the basic cycle	90
Table 5.1 ASHRAE test conditions and extended condition	104
Table 5.2 Desired R404A saturation temperatures and R404A condenser configuration	116
Table 5.3 Cascade system compressor configuration	116
Table 6.1 Test heat exchanger input parameters	137
Table 6.2 Outdoor heat exchanger input parameters	145
Table 6.3 Heat transfer correlations and corresponding correction factors	146
Table 6.4 Pressure drop correlations and corresponding correction factors	146
Table 6.5 Cooling mode air-side and refrigerant-side inlet conditions	147
Table 6.6 Heating mode air-side and refrigerant-side inlet conditions	147
Table 6.7 Indoor heat exchanger input parameters	150
Table 6.8 Heat transfer correlations and corresponding correction factors	150
Table 6.9 Pressure drop correlations and corresponding correction factors	151
Table 6.10 Air-side and refrigerant-side inlet conditions	151
Table 6.11 Parameters required to simulate reciprocating and scroll compressors	163
Table 6.12 Input parameters used during compressor model validation	165
Table 6.13 Steady state compressor operating conditions	166
Table 6.14 Steady state and transient performance comparison	179
Table 7.1 Example simulation heat exchanger input parameters	188
Table 7.2 Example simulation reciprocating compressor input parameters	189
Table 7.3 Comparison of steady state and transient results for the example system	196

List of Figures

Figure 1.1 Standard vapor compression system	2
Figure 1.2 (a) Pressure-enthalpy diagram and (b) temperature-entropy diagrams for a typical vapor compression system	2
Figure 1.3 Finite volume discretized heat exchanger tube	8
Figure 1.4 Moving boundary heat exchanger tube	8
Figure 1.5 Multiple evaporator vapor compression cycle	18
Figure 2.1 An example component.....	33
Figure 2.2 A simple junction	35
Figure 2.3 System, vapor compression component, and load component interaction.....	45
Figure 2.4 Flow chart shown fan component initialization	46
Figure 2.5 Control block and component interaction	47
Figure 2.6 Diagram of a conventional vapor compression system.....	48
Figure 2.7 Diagram showing component model interaction.....	55
Figure 3.1 Two-stage compressor options	63
Figure 3.2 Two-stage compressor options with an intermediate suction port	64
Figure 3.3 TXV mass flow rate at a fixed pressure drop vs. superheat	66
Figure 4.1 Two cycle configurations used in evaluating solver performance	71
Figure 4.2 Flow chart describing the Junction Solver solution procedure	80
Figure 4.3 Flow chart describing the Enthalpy Marching Solver solution procedure	84
Figure 4.4 Flow chart describing the Decoupled Energy and Hydraulic Solver solution procedure.....	86
Figure 4.5 Fractional step convergence for the Decoupled Energy Hydraulic Solver	88
Figure 4.6 Standard cycle test matrix results	89
Figure 4.7 Advanced cycle test matrix results	90
Figure 4.8 Enthalpy Marching Solver results based on simulation specification type	97
Figure 4.9 Solver convergence for the Enthalpy Marching Solver	99
Figure 5.1 Diagram of a two-stage flash tank cycle	101
Figure 5.2 Diagram of two-stage flash tank cycle as modeled.....	102
Figure 5.3 Baseline cycle validation results for system capacity	105
Figure 5.4 Baseline cycle validation results for compressor power consumption.....	106
Figure 5.5 Baseline cycle validation results for system mass flow rate	106
Figure 5.6 Flash tank cycle validation results for system capacity.....	107
Figure 5.7 Flash tank cycle validation results for compressor power consumption.....	107
Figure 5.8 Flash tank cycle validation results for system mass flow rate.....	108
Figure 5.9 Diagram of a cascade vapor compression system	109
Figure 5.10 Temperature entropy diagram of a theoretical cascade system.....	110
Figure 5.11 Pressure enthalpy diagram of a theoretical cascade system	111
Figure 5.12 Diagram of a multi-component vapor compression system	112
Figure 5.13 Flow chart describing the cascade simulation solution approach	112
Figure 5.14 Diagram of a cascade vapor compression system junction numbers	114
Figure 5.15 Diagram of experimental cascade system	115
Figure 5.16 Cascade system validation results for system capacity	119
Figure 5.17 Cascade system validation results for compressor power consumption	119
Figure 5.18 Cascade system validation results for system mass flow rate	120

Figure 5.19 Cascade system validation results for saturation temperatures	120
Figure 6.1 Conceptual diagram showing the tank model	123
Figure 6.2 Discretized tank model	124
Figure 6.3 Inlet and outlet friction tubes.....	130
Figure 6.4 Internal friction tube connected to two tanks	132
Figure 6.5 Tank tube heat exchanger	134
Figure 6.6 An example of a multiple row heat exchanger.....	134
Figure 6.7 Using three tank to model a multiple row heat exchanger	136
Figure 6.8 Refrigerant enthalpy profile along the heat exchanger length for heat exchanger models constructed from various number of tank models.....	138
Figure 6.9 Percent difference in heat load compared to CoilDesigner	139
Figure 6.10 Refrigerant pressure profile along the heat exchanger length for heat exchanger models constructed from various number of tank models.....	140
Figure 6.11 Percent difference in pressure compared to CoilDesigner	141
Figure 6.12 Heat transfer coefficient correlation trends	143
Figure 6.13 Heat load validation results for the outdoor heat exchanger	148
Figure 6.14 Refrigerant pressure drop validation results for the outdoor heat exchanger	149
Figure 6.15 Heat load validation results for the indoor heat exchanger	152
Figure 6.16 Pressure drop validation results for the indoor heat exchanger.....	153
Figure 6.17 Reciprocating compressor model schematic	154
Figure 6.18 Scroll compressor model schematic	155
Figure 6.19 Compressor power consumption validation results (steady state operation)	170
Figure 6.20 Compressor mass flow rate validation results (steady state operation).....	171
Figure 6.21 Discharge temperature validation results (steady state operation)	171
Figure 6.22 Compressor shell temperature validation results (steady state operation) ..	172
Figure 6.23 Experimental suction and discharge pressures during startup test	173
Figure 6.24 Compressor mass flow rate validation results (transient operation)	174
Figure 6.25 Compressor outlet temperature validation results (transient operation).....	175
Figure 6.26 Compressor power consumption validation results (transient operation) ..	176
Figure 6.27 Compressor shell temperature validation results (transient operation)	177
Figure 7.1 Basic four component system and unknown variables.....	182
Figure 7.2 Flow chart describing the transient simulation solution procedure.....	185
Figure 7.3 Example simulation results - system pressures	191
Figure 7.4 Example simulation results – heat loads	192
Figure 7.5 Example simulation results – mass flow rate	193
Figure 7.6 Example simulation results – compressor power consumption	194
Figure 7.7 Example simulation results – system charge distribution	195
Figure 7.8 Transient validation results – system pressures.....	198
Figure 7.9 Transient validation results – refrigerant mass flow rates.....	199
Figure 7.10 Transient validation results – air-side capacity	200
Figure 7.11 Photograph of evaporator (courtesy of Wang (2008a)).....	201
Figure 7.12 Transient validation results – refrigerant-side capacity.....	202
Figure 7.13 Transient validation results – compressor power consumption	203

Nomenclature

A	Heat transfer area (m ²)
c	Constant
C	Heat capacity (J/kg·K)
C_v	Valve flow coefficient
C_p	Specific heat at constant pressure (J/kg·K)
D	Tube diameter (m)
DP	Pressure drop (Pa)
D_v	Compressor displacement volume (m ³)
f	Friction factor
\vec{f}	Vector of residual functions
g_{ca}	Dimensional gravitational constant
h	Specific enthalpy (J/kg)
h_d	Mass transfer coefficient (m/s)
h_{fg}	Latent heat of vaporization (J/kg)
\dot{H}	Energy flow, J/s
HX	Heat exchanger
K	Valve constant
L	Length (m)
Le	Lewis number
\dot{m}	Mass flow rate (kg/s)
M	Refrigerant charge, mass (kg)
N_{cells}	Number of cells
N_J	Number of junctions
P	Pressure (Pa)
\dot{P}	Power consumption (W)
\dot{Q}	Heat transfer rate (W)
r	Mass flow rate ratio
$r_{\dot{m}}$	Mass flow rate residual value
$r_{\dot{H}}$	Energy flow residual value
r_P	Pressure residual value
r_M	System charge residual value
r_{SC}	Subcooling residual value

\vec{r}	Vector of residual values
Re	Reynolds number
<i>RPM</i>	Compressor speed in revolutions per minute
<i>s</i>	Entropy (J/K)
<i>t</i>	Time (s)
<i>T</i>	Temperature (K)
<i>U</i>	Internal energy (J)
<i>U</i>	Overall heat transfer coefficient (W/m ² ·K)
<i>v</i>	Velocity (m/s)
<i>V</i>	Internal volume (m ³)
<i>x</i>	Length (m)
\vec{x}	Vector of unknown values
<i>X</i>	ARI compressor model output parameter

Greek Symbols

α	Heat transfer coefficient (W/m ² ·K)
ε_f	Equation solver tolerance in the <i>f</i> -domain
ε_x	Equation solver tolerance in the <i>x</i> -domain
η	Efficiency
μ	Dynamic viscosity (Pa·s)
ρ	Density (kg/m ³)
ω	Humidity ratio of moist air

Subscripts

<i>2ph</i>	Two-phase/two-phase region
<i>air</i>	Air-side
<i>c</i>	Cell
<i>comp</i>	Compressor
<i>cond</i>	Condenser
<i>evap</i>	Evaporator
<i>exp</i>	Expansion device
<i>f</i>	Saturated liquid state
<i>high</i>	High-side/high-temperature
<i>i</i>	Index parameter, iteration

<i>in</i>	Flow into a junction or component
<i>isen</i>	Isentropic
<i>J</i>	Junction
<i>liq</i>	Liquid/liquid region
<i>low</i>	Low-side/low-temperature
<i>mech</i>	Mechanical
<i>mix</i>	Mixing value of multiple streams
<i>out</i>	Flow outlet of component or junction
<i>ref</i>	Refrigerant-side
<i>sat</i>	Saturation
<i>sc</i>	Subcooling
<i>sh</i>	Superheat
<i>shell</i>	Compressor shell
<i>vap</i>	Vapor/vapor region
<i>vol</i>	Volumetric

1 Introduction

1.1 Vapor Compression Systems

Vapor compression systems are the most widely used method for cooling with applications ranging from the refrigerated food chain to air-conditioning of residences and commercial buildings. In temperate climate regions, vapor compression systems are commonly used to provide space heating as well. According to the Energy Information Administration, approximately 31% of the electricity consumed by U.S. households in 2001 was for the purpose of heating, ventilation, and air-conditioning (HVAC) and nearly half of the HVAC total was dedicated only to central air-conditioning (Energy Information Administration, 2005). Along similar lines, kitchen and laundry appliances accounted for nearly one-third of U.S. household electricity consumption and nearly 64% of this total went towards powering refrigerators and freezers.

The standard vapor compression system, shown in Figure 1.1, consists of four key components; the compressor, condenser, expansion valve, and evaporator. The typical process is plotted in Figure 1.2 on a pressure-enthalpy diagram and a temperature-entropy diagram. Starting at state point 1, the work input to the compressor compresses the low pressure refrigerant vapor to a high pressure, high temperature superheated vapor. The refrigerant then flows through the condenser where the vapor refrigerant condenses to a subcooled state as heat is rejected to the ambient. The liquid refrigerant is throttled in the expansion device resulting in a low temperature, two-phase mixture at the evaporator inlet. As the refrigerant flows through the evaporator, heat is absorbed from the conditioned space evaporating the refrigerant.

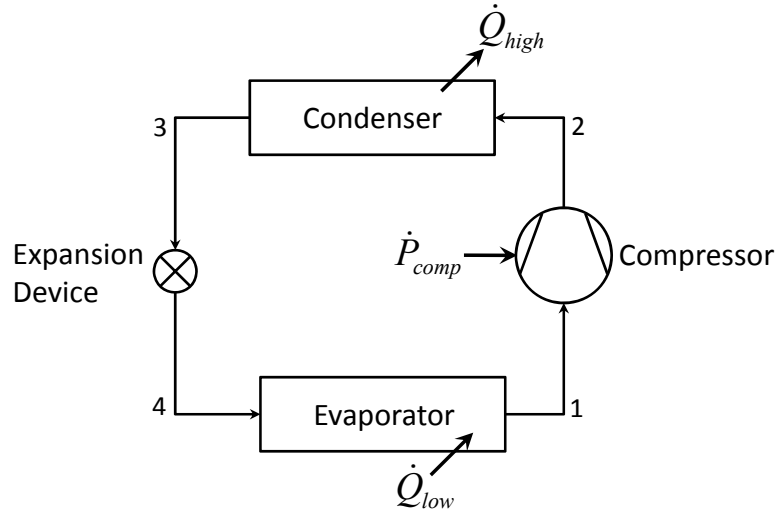


Figure 1.1 Standard vapor compression system

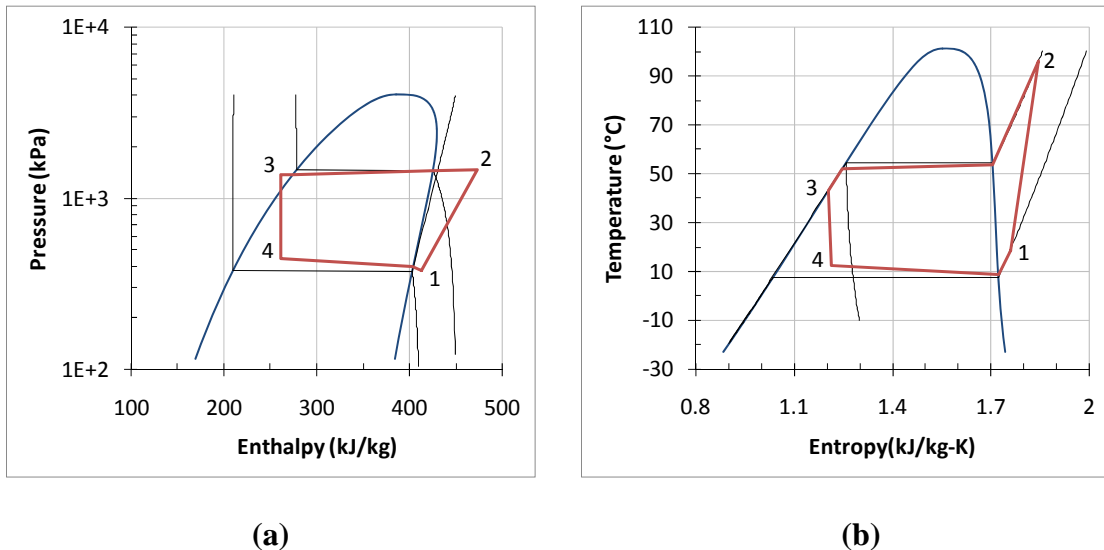


Figure 1.2 (a) Pressure-enthalpy diagram and (b) temperature-entropy diagrams for a typical vapor compression system

With increasing emphasis being placed on energy efficiency, the enhancement of vapor compression system performance is receiving much attention due to their high level of energy intensity. A promising option is to move away from the standard four component vapor compression system and include additional components to offer better control over the spaces that require air-conditioning. Variable refrigerant flow (VRF) air-conditioning systems are gaining in popularity to condition residential and commercial

buildings (Masuda *et al.*, 1991; Aynur *et al.*, 2006). VRF systems utilize an inverter driven compressor to control the refrigerant flow rate and multiple evaporator coils each with their own expansion valve to control the temperature of a specific zone. Thus, the evaporator of a properly conditioned space can essentially be turned off as the VRF system conditions the zones that require additional cooling. As vapor compression system configurations grow in complexity, the functionality of the simulation tools used to model such systems must also grow to allow for the continued enhancement of vapor compression system performance.

1.2 Introduction to Steady State and Transient Simulation of Vapor Compression Systems

Computer simulation has become a required tool in the design phase of vapor compression systems; however with relatively few exceptions most simulations focus on the basic four component system. With an increasing focus being placed on energy efficiency, the simulation of multi-component vapor compression systems (having multiple evaporators, condenser or compressors) will become essential to assist in the design of these more complicated systems. The implementation of a component-based framework will facilitate the simulation of multi-component systems.

Vapor compression system simulation can take place in one of two major time domains; namely steady state or transient. Both types of simulation offer distinct advantages and disadvantages to the design engineer.

1.2.1 Steady State Simulation

A steady state simulation provides details regarding the system performance at a set of specific design points and describes how the system will perform at off-design conditions. The computational time for a steady state simulation is generally much less

than for a transient simulation, thus steady state simulation tools have been most commonly used in designing vapor compression systems. Vapor compression systems are rated and designed using steady state performance (ASHRAE 1995; ARI 1999) and thus system optimization and performance studies have been most commonly completed using steady state simulations.

It is important for the simulation tool be numerically efficient, robust, and highly accurate when conducting system optimization and performance studies. It is not feasible for a design engineer to conduct an optimization study requiring an execution time on the order of weeks or months, and thus the simulation must be capable of running multiple times over the course of a few days. When incorporating gradient-based optimization routines, the simulation tool must be robust at solving a wide range of possible systems. If the simulation fails to solve for an intermediate set of input variables during a gradient-based optimization, the optimization must terminate without determining an optimum solution. Generally, numerical optimization of a vapor compression system or one of the components will yield a performance improvement of approximately 10-20% (Aute *et al.*, 2004; Winkler *et al.*, 2006). The uncertainty of the improvement predicted by any optimization routine will be high if the simulation does not accurately calculate the performance of the baseline system.

In order for steady state simulation to be useful to the design engineer, the simulation tool must display high levels of (i) accuracy, (ii) robustness, and (iii) computational efficiency (Ding, 2007). The accuracy of a system simulation tool is dictated by the accuracy of the component models used to construct the system. The simulation tool's robustness is important when attempting to simulate a system at off-

design conditions. The simulation of more complicated cycle configurations to enhance energy efficiency also places greater emphasis on the simulation tool's robustness. The computational efficiency of the simulation tool is important because the main advantage of steady state simulation over transient simulation is the computational effort. There has been much research in the area of steady state vapor compression system simulation; however few researchers have developed simulation tools capable of simulating cycle configurations beyond the basic four component system. Often a simulation procedure is presented without describing the robustness of the approach in handling off-design conditions.

1.2.2 Transient Simulation

A transient simulation can provide detailed information regarding the system performance during start-up, cycling operations, and other capacity control measures at a cost of an increase in computational time. Vapor compression systems tend not to operate in steady state for significant periods of time; thus a transient simulation can more accurately capture the overall system performance. The steady state performance of the system can be obtained by running the transient simulation until steady state is reached; however, this is a rather expensive approach to attain such information and is rarely utilized by vapor compression system design engineers.

Transient simulation of vapor compression systems have been most commonly used in the area of control algorithm development. Since vapor compression systems tend not to operate in steady state for significant periods of time and controls are inherently time dependent, transient simulation and/or experiments are required to design optimized control strategies. Vapor compression system manufacturers typically have separate design teams responsible for designing the components of the vapor compression system

and the control strategies; both of which use simulation packages designed to meet the respective needs. Design engineers assigned to design the components of the vapor compression system typically utilize steady state simulations to aid in the design process, whereas the controls design team will typically utilize transient simulation in the design process. The transient performance of a vapor compression system is inherently coupled to many aspects of the components that make up that system, such as the heat exchanger thermal mass, refrigerant charge, compressor characteristics, etc. Therefore, it is imperative for the two design groups to communicate when designing the system and it would be ideal if they could utilize a single simulation tool that would meet the unique needs of both teams.

Transient simulation will start playing a larger role in the design of vapor compression systems as cycle configurations and their controls increase in complexity. As multi-evaporator systems gain in popularity due to enhanced efficiency and thermal comfort, the development of controls for such systems will be an important step in attaining maximum efficiency. A transient simulation tool capable of handling cycle configurations beyond that of the basic four component system can vastly aid the engineer in developing control algorithms for such systems. Multi-component systems undergo a greater amount of transient phenomena than basic systems and it is important to catch such phenomena during the design process. Steady state simulation can be useful in sizing components of large systems to operate at a specific design point and thus can be an important tool when designing large systems. Despite the large amount of research in the area of transient simulation of vapor compression systems, there has not yet been

the development of an integrated vapor compression simulation tool capable of performing transient and steady state simulations.

1.2.2.1 Heat Exchanger Modeling Overview

Transient heat exchanger models generally fall into one of two categories; namely phase-independent finite difference models and phase-dependent moving boundary models (Bendapudi and Braun, 2002). In finite difference models, the heat exchanger is subdivided into a fixed number of constant volume regions and the manner in which the heat exchanger is subdivided is independent of the refrigerant phase. Each control volume represents a single refrigerant state point throughout the length of the heat exchanger. The transient mass, energy, and sometimes momentum conservation equations are then discretized over these control volumes using a finite difference scheme to develop a set of coupled first-order differential equations. The set of differential equations are then solved to update the heat exchanger state variables as the simulation progresses in time. Figure 1.3 depicts a heat exchanger tube discretized using a finite volume approach. There are three zones in the heat exchanger; namely, a superheat vapor zone, two phase zone, and subcooled liquid zone. The heat exchanger tube is subdivided into N_{cells} fixed volume cells each with length L_c , however these cells are created independently of the three zones in the heat exchanger.

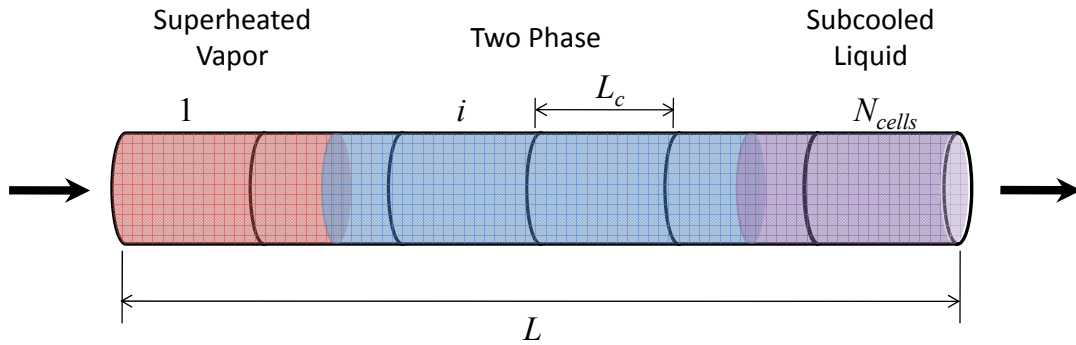


Figure 1.3 Finite volume discretized heat exchanger tube

In moving boundary models, the heat exchanger is subdivided based on the location of the phase transition points. The volume of each region changes as the phase transition points move throughout the heat exchanger. The refrigerant properties, and thus heat transfer coefficients, are typically assumed to be constant in each zone of the heat exchanger. The moving boundary heat exchanger concept is shown in Figure 1.4, which consists of three different zones and thus two transition points. The length of each zone changes in time as the transition points move throughout the heat exchanger.

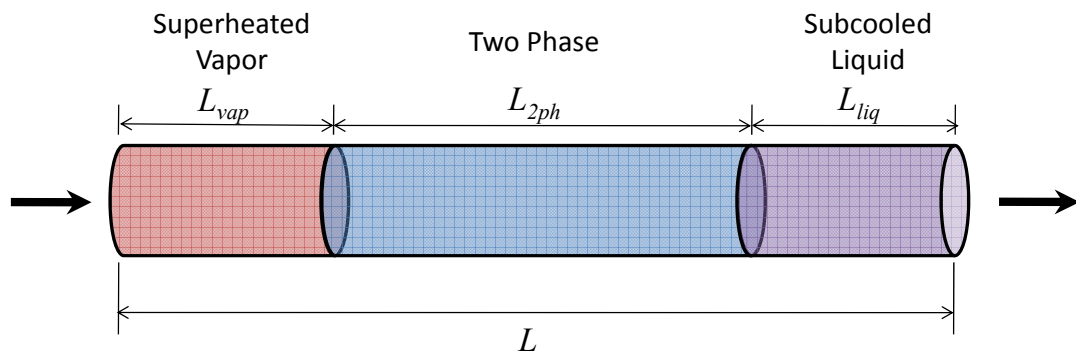


Figure 1.4 Moving boundary heat exchanger tube

It is possible for phase transition points to enter and leave the heat exchanger under transient operation and special consideration needs to be included in the moving boundary heat exchanger modeling approach to handle such cases.

The two modeling approaches each have advantages and disadvantages associated with them. The finite volume approach provides information concerning the spatial variation of the refrigerant properties throughout the entire length of the heat exchanger. Since the heat exchanger tube is discretized into a fixed number of control volumes each with a fixed length, it is possible for the model to take into account air-side maldistribution along the tube length. The downside of the finite volume approach is the added computational cost compared to the moving boundary formulation. In addition, numerical instabilities are more likely in the finite volume approach due to the large set of differential equations that must be solved for each time step.

1.2.2.2 Compressor Modeling Overview

The compressor is essentially the heart of the vapor compression system and generally, along with the expansion valve capacity, dictates the refrigerant mass flow rate through the system. In a vapor compression system model, typically the compressor model calculates the refrigerant mass flow through the system. Compressor models usually use the suction (inlet) pressure and temperature (or enthalpy) along with the discharge (outlet) pressure as input. These parameters are then used to calculate the compressor mass flow rate, compressor power consumption, and discharge refrigerant temperature.

In the transient simulation of a vapor compression system, the compressor is often treated as a quasi steady state component; meaning the calculated mass flow rate and discharge temperature instantaneously update based on the current suction conditions and discharge pressure. This is a valid assumption since the timescales associated with the variation of the compressor mass flow rate are very small compared to timescales associated with heat exchanger performance and charge distribution. Dynamic

compressor models that capture valve dynamics and mass flow rate variation for each cycle of the compressor motor are too computationally expensive and require too small of time steps to be included in a system level simulation (Ding, 2007). Compressor models utilized in a system simulation generally fall into one of two categories: map-based models and efficiency-based models.

Map-based models are based on manufacturer data and therefore the performance will most likely match the experimental results. However, the published data provided by compressor manufacturers is valid only over a specific range, which is likely to be violated during a transient simulation. Most manufacturer data has been taken under steady state operation, and thus all the transient phenomena likely to effect the compressor performance during transient time periods will not be taken into account.

Efficiency-based models can capture the trends and can match experimental results after the model has been tuned accordingly. However, this approach requires more effort than using a map-based model. Efficiency-based models can make use of either the compressor isentropic efficiency or the refrigerant polytropic coefficient. The refrigerant polytropic coefficient is typically not constant under varying conditions and attaining a value for the polytropic coefficient for a variety of refrigerants is often difficult.

After a vapor compression system has been turned on, the compressor shell temperature increases, and thus rejects heat to the environment. The change in shell temperature affects the performance of the compressor. In order to model the shell temperature the heat loss from the compressor shell must be modeled. During steady state calculation, the heat loss from the compressor shell can be calculated using the mechanical efficiency of the compressor, and thus the shell temperature does not need to

be calculated. In order to model the heat loss from the compressor shell during a transient simulation, heat transfer coefficients and heat transfer areas must be provided as input. These types of parameters are often difficult to describe since refrigerant-side heat transfer coefficient correlations for the inside of a compressor shell are difficult to find and heat transfer areas are unknown to the design engineer.

1.2.3 Quasi Steady State Simulation

In actuality, there exists a third time regime in which vapor compression systems can be simulated; namely quasi steady state simulation. In a quasi steady state simulation, the time dependent variables are assumed to come to equilibrium at a much faster rate than the transients of the inputs. This assumption is valid when the system responds at a much faster rate than the rate at which the boundary conditions are changing. Browne and Bansal (2002) incorporated a quasi steady state assumption when modeling the refrigerant mass flow rate through a vapor compression liquid chiller. The mass flow rate throughout the entire vapor compression system was assumed to be equal to the mass flow rate predicted by the compressor for the current operating conditions. This assumption does not allow for the refrigerant distribution to be captured by the model during transient operation.

1.3 Literature Review

1.3.1 Steady State Vapor Compression System Solution Techniques

Many steady state vapor compression simulations exist in the literature and all solve for a set of unknown variables that can be used to determine the system performance. Generally, there are two approaches in which these variables are solved: (i) using a non-simultaneous, successive approach where a variable is solved to convergence

prior to moving on the next unknown variable (Davis and Scott, 1976; Hiller and Glicksman, 1976; Ellison and Creswick, 1978; Tassou *et al.*, 1982; Domanski and Didion, 1983; Fischer and Rice, 1983; Domanski and McLinden, 1992; Robinson and Groll, 2000; Koury *et al.*, 2001; Joudi and Namik, 2003; Sarkar *et al.*, 2006) and (ii) using a multi-variable nonlinear equation solver to resolve the unknown variables simultaneously (Parise, 1986; Almedia *et al.*, 1990; Jolly *et al.*, 1990; Herbas *et al.*, 1993; Bourdouxhe *et al.*, 1994; Rossi, 1995; Browne and Bansal, 1998; Hwang and Radermacher, 1998; Corberan *et al.*, 2000; Corberan *et al.*, 2002; Richardson *et al.*, 2002; Richardson *et al.*, 2004; Sanaye and Malekmohammadi, 2004; Agrawal *et al.*, 2007).

The non-simultaneous, successive approach to simulating the vapor compression system generally results in the implementation of a global solution scheme. In a global solution scheme the mathematical equations describing each component model are generally hard-coded within the system solver. When a global solution scheme has been implemented the vapor compression system configuration is generally fixed and therefore additional components cannot be inserted with any ease into the original configuration. A global solution scheme can offer advantages in the area of robustness since the system solver is directly evaluating all mathematical equations; however the flexibility of the simulation is limited. The underlying reason behind the inflexibility of such simulations is that the set of solution variables cannot be dynamically formulated based on an arbitrary system configuration.

In a component-based solution scheme the component models can more readily be located outside the system solver since the component models are being treated as “black-box” objects. Thus, this approach can be extended to handle arbitrary system

configurations since the solver requires only knowledge of how the component models have been connected. This increase in flexibility can lead to decreased robustness since the system solver cannot assume a functional form of the mathematical equations being solved by the component models. The development of a component-based solution scheme to handle a large variety of complicated cycle configurations was originally presented in the area of absorption system simulation (Grossman and Michelson, 1985). The authors describe the requirement of a component-based simulation tool for the purposes of modeling absorption systems with complicated configurations and elaborate on the simultaneous algorithm used to solve the simulation. The solution algorithm was later enhanced to model more complicated cycle configurations (Grossman and Gommed, 1987; Grossman and Zaltash, 2001).

Stoecker (1971, 1989) provides a good definition of component-based simulation and discusses the advantages/disadvantages of solving a system successively or simultaneously. Stoecker presented concepts dealing with a general simulation tool capable of simulating any thermal system. In this approach, the user would incorporate previously developed subroutines representing the component models and the simulation tool would solve the component models to satisfy system-level conservation of mass and energy equations.

Parise (1986) describes an algorithm to simulate a vapor compression system that successively steps around the system, starting at the compressor suction, and propagates the refrigerant enthalpies around the cycle. Simple component models are used and consequentially the system solver solved for only two unknown values. This model was enhanced to incorporate more detailed component models and re-presented by Herbas *et*

al. (1993), in which the authors mention the unknown variables are solved for simultaneously using the Newton-Raphson method. Though the authors solve for the equations simultaneously, the author's implement a global solution strategy to facilitate in the reduction of unknown variables.

Rossi (1995) describes a modular vapor compression system simulation that solves a fixed system configuration simultaneously by marching around the cycle starting at the compressor. The simulation tool was primarily developed to analyze and evaluate fault detection and diagnostics for vapor compression systems.

Corberan *et al.* (2000) introduced a simulation tool for the modeling of water-to-air heat pumps. The simulation employed a modular solution strategy to solve the state equations of a fixed system configuration consisting of the basic components and accessories; therefore, sub-models were used to model the individual components within the cycle. The authors mention the program uses the Hybrid method to solve for the unknown variables simultaneously. Corberan *et al.* (2002) enhanced the model to include air-to-air heat pumps and introduced the program as being commercially available software for the design of vapor compression systems.

Richardson *et al.* (2002) introduced the modular/component-based simulation tool called VapCyc. The solution methodology was briefly discussed for a fixed four component system. Richardson *et al.* (2004) expanded on the original version of the VapCyc solver and formulated the solution algorithm in a more general manner allowing for the simulation of a vapor compression cycle with additional components. The Junction Solver was introduced as being the modular/component-based solver behind

VapCyc (Richardson, 2006). The Junction Solver was designed to provide complete flexibility in designing vapor compression system configurations.

1.3.2 Transient Vapor Compression System Simulations

Dating back nearly 30 years, there have been numerous publications on the transient simulation of vapor compression systems. Dhar (1978) was among the first to present the transient simulation of an entire vapor compression system. The simulation was constructed in a modular format by using subroutines for each of the component models in the system. A room model was constructed to fully capture the transients on the air-side and refrigerant-side of the system. Dhar implemented a moving boundary heat exchanger model that assumed each control volume acted as a “stirred tank” and thus, the refrigerant condition flowing out of each control volume was equal to the bulk conditions in the control volume. Dhar was very successful at capturing all the major transients in the system.

Chi and Didion (1982) were the first to incorporate the transient one-dimensional momentum equation into the simulation. The heat exchangers were modeled using a moving boundary formulation and the simulation incorporated the dynamic effects associated with the refrigerant, the air flowing across the heat exchanger, the fans, the heat exchanger walls, the motor shaft, the compression, the expansion valve, and the accumulator. The transient system was reduced to a set of 32 ordinary differential equations solved using the explicit Euler method with fixed time steps of 0.005 seconds. Though the equations were solved globally, the model was developed in a modular format allowing for alternative systems to be simulated.

MacArthur (1984) was the first to incorporate a finite volume discretization approach to simulating the heat exchangers. MacArthur was also among the first

researchers to develop individual component models and use these component models to construct the vapor compression system. The author mentioned the functionality of being able to switch between two flow-control devices; namely a fixed orifice and a thermostatic expansion valve. The heat exchanger models used an overly simplistic assumption that the pressure response of the heat exchanger was independent of the thermal response and thus a uniform velocity through the heat exchanger was assumed. Later work by MacArthur and Grald (MacArthur and Grald, 1987) overcame this assumption by coupling the mass balance and energy balance in the heat exchanger model. The authors developed a modified energy equation that included the conservation of energy and momentum equations to reduce the computational intensity of the simulation (MacArthur and Grald, 1987). The same authors presented a moving boundary formulation to model the heat exchangers in an independent piece of work (Grald and MacArthur, 1992).

Murphy and Goldschmidt (1985, 1986) constructed a simplified model of a vapor compression system to analyze the start-up and shutdown characteristics of a residential air-conditioning system. In the start-up analysis, the authors modeled the compressor, condenser, liquid line, and capillary tube to determine the start-up losses of the system. In the shutdown analysis, the flow between the condenser and evaporator is analyzed as the system pressures come to equilibrium.

Sami *et al.* (1987) represented the vapor compression system by using discrete control volumes. The model was unique in that various component models were included. The simulation included the following models: shell-tube condenser, air-cooled

condenser, direct expansion evaporator, shell-tube evaporator, coil evaporator, capillary tube, thermostatic expansion valve, and reciprocating compressor.

Vargas and Parise (1995) developed a simplified dynamic model of a heat pump for the purpose of developing control strategies aimed at reducing energy consumption. The heat exchanger models were simple compared to previous references; however, the authors included a model of the DC servomotor to control the compressor speed. The DC servomotor modeled the change in current and angular frequency over time and was coupled to the compressor model via the angular frequency term.

He *et al.* (1998) developed a multi-input multi-output (MIMO) control strategy through the use of simple dynamic vapor compression system model. A low order, lumped-parameter developed to model the dominating dynamic variables of the vapor compression system. This paper serves as a good example of a simple dynamic vapor compression system model developed for the sole use of control algorithm development.

Rossi and Braun (1999) developed a real-time fully distributed model of a roof-top air conditioning unit. The heat exchangers neglected the pressure drop and used the inlet and outlet mass flow rates along with the inlet enthalpy as the boundary condition. The conservation of mass and energy equations were manipulated to form a set of algebraic ordinary differential equations used to calculate the pressure and enthalpy time derivatives for each heat exchanger. The compressor was modeled using polynomial curve fits taken from manufacturer data.

Gordon *et al.* (1999) presented the dynamic modeling of a multiple-zone vapor compression system consisting of four parallel evaporators with each evaporator having an upstream expansion device, similar to the system shown in Figure 1.5. A moving

boundary approach was used to model the conservation of mass and energy equations for each heat exchanger in the system. The authors used a steady state momentum equation to handle the system level mass balance at the evaporator outlets which ultimately determines the mass flow distribution exiting the parallel evaporators. The pressure drop through each evaporator was calculated from the center of the two phase region to the evaporator outlet using the outlet refrigerant mass flow rate. The reasoning behind selecting this length to calculate the pressure drop was not presented and this assumption might lead to an inaccurate calculation of the outlet refrigerant mass flow rate.

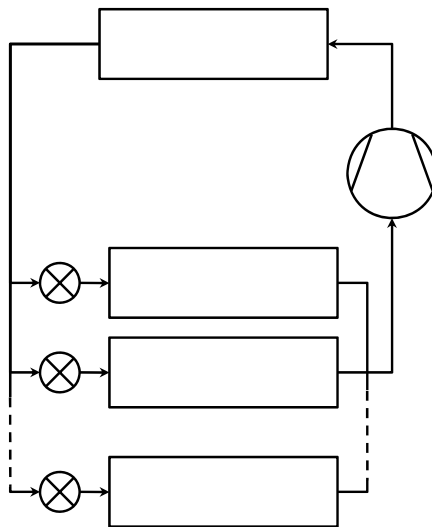


Figure 1.5 Multiple evaporator vapor compression cycle

Browne and Bansal (2002) looked at the transient simulation of large scale liquid chillers. The authors pointed out that a majority of the dynamic simulation to date had been in the area of small scale, residential units. Though the authors modeled a large scale system, a majority of the system transients were neglected. The simulation was designed to capture the dynamic behavior of the vapor compression system with changing water set points, and thus the heat exchangers were modeled using quasi-steady state assumptions.

Bendapudi *et al.* (2002) expanded the model by Rossi and Braun (1999) to a liquid chiller (Bendapudi *et al.*, 2002). A detailed summary of this work was presented in Bendapudi *et al.* (2005) along with a numerical study presenting the results of a mesh independence study for the Rossi and Braun (1999) model. Bendapudi *et al.* (2004) analyzed the differences between a moving boundary approach and a finite volume approach for simulating heat exchangers in a transient simulation. The finite volume approach was taken from Rossi and Braun (1999) while the moving boundary approach was similar to the approach used by Grald and MacArthur (1992). Bendapudi *et al.* (2004) concluded that the models had comparable results; however the moving boundary model was approximately twice as fast.

Shah *et al.* (2004) simulated and validated a similar system as shown in Figure 1.5 with having two parallel evaporators. The authors mentioned the approach could be extended to any number of evaporators. The authors assumed a steady flow through a suction pipe connecting each evaporator to the compression suction port. The pressure drop through each suction line was used to determine the outlet mass flow rate from each evaporator. This approach fails to take into account the change in refrigerant mass in each suction line by assuming steady state flow through each pipe section.

Rasmussen and Alleyne (2004) developed a low order dynamic model of a transcritical air-conditioning system, with the focus being placed on the multivariable controller design. The compressor is treated as a static component and the heat exchanger models neglect the refrigerant pressure drop. Though the simulation handles transcritical cycle, the modeling approach of the gas cooler assumes only single phase refrigerant is

present in the heat exchanger. Thus, the simulation can not capture subcritical operation during start up conditions.

Ding et al. (2004) developed a dynamic model of a bypass two-circuit cycle refrigerator freezer. The authors implement a moving boundary approach to simulate the heat exchangers and make the common assumptions of homogenous two-phase flow and neglecting refrigerant pressure drop. The authors make the additional assumption that a portion of the heat exchanger wall temperature can be approximated as equal to the refrigerant temperature since the convective heat transfer on the refrigerant-side is much greater than that on the air-side. The method implemented by the authors is called the effective metal method.

Hermes and Melo (2008) developed a transient model to simulate the startup and cycling characteristics of household refrigerators. The authors implement a fixed volume approach to simulate the heat exchangers and adopt the approach presented by Rossi and Brown (1999). The authors neglected the refrigerant-side pressure drop and applied the trapezoidal rule to average the heat transfer coefficient for each control volume.

1.3.3 Transient Compressor Simulations

Table 1.1 summarizes the variety of transient compressor models found in the literature.

A majority of the compressor models found in the literature use the compressor efficiency as input; however a number of these use a set of coefficients based on manufacturer data to determine the efficiency. With the exception of the Chi and Didion (1982) model, all the efficiency-based models that don't rely on a set of coefficients use a constant efficiency independent of operating conditions to determine the compressor performance.

Half of the compressor models listed in Table 1.1 includes the heat loss from the compressor shell, Q_{shell} . All of these compressor models also predict the compressor shell temperature, with the exception of the model presented by Bendapudi *et al.* (2005). In the Bendapudi *et al.* (2005) compressor model the shell heat loss is modeled assuming the heat generated by the motor is instantly rejected by the compressor shell. This assumption results in the compressor model not requiring heat transfer coefficients and heat transfer areas. All the other compressor models that take into account the heat loss from the compressor shell require heat transfer coefficient values and heat transfer areas.

The compressor models implemented by MacArthur (1984) and Chi and Didion (1982) are the most detailed compressor models listed in Table 1.1. The MacArthur model includes five modes of heat transfer within the compressor and thus requires five overall heat transfer coefficient values. The Chi and Didion model includes pressure losses due the valve dynamics and thus properties of the compressor cylinder valves must be input to the compressor model.

Table 1.1 Summary of transient compressor models found in the literature

Author(s)	Map- /Eff.- Based	Const. Eff.?	Isentropic/ Polytropic	Includes Q_{shell}?	Includes T_{shell}?	No. of UA Values
MacArthur (1984)	Eff.	Yes	Isentropic	Yes	Yes	5
Chi and Didion (1982)	Eff. w/ Coeff.	No	Polytropic	Yes	Yes	2
He <i>et al.</i> (1998)	Eff.	Yes	Isentropic	No	No	-
Rossi & Braun (1999)	Map	No	-	Yes	Yes	2
Anand (1999)	Eff.	Yes	Both	Yes	Yes	1
Cullimore (2000)	Eff. w/ Coeff.	No	Isentropic	No	No	-
Browne & Bansal (2002)	Eff.	Yes	Isentropic	No	No	-
Tummescheit <i>et al.</i> (2005)	Eff. & Map	No	Isentropic	No	No	-

Rasmussen and Alleyne (2004)	Eff.	Yes	Isentropic	No	No	-
Shah <i>et al.</i> (2004)	Eff.	Yes	Isentropic	No	No	-
Ding <i>et al.</i> (2004)	Eff.	Yes	Polytropic	Yes	Yes	1
Bendapudi <i>et al.</i> (2005)	Eff. w/ Coeff.	No	Polytropic	Yes	No	0

1.3.4 Existing Vapor Compression System Simulation Packages

A majority of the vapor compression system simulations discussed in Sections 1.3.1 and 1.3.2 were developed for academic purposes and their use was limited to the principal investigators. In several instances, these simulations progressed to a commercially available software package.

1.3.4.1 Steady State Simulation Software Packages

The Oak Ridge National Laboratory (ORNL) Heat Pump Design Model (Fischer and Rice, 1983) was the first vapor compression system simulation tool developed to aid engineers in the design of vapor compression systems. The simulation tool was created by merging two vapor compression system simulations from ORNL (Ellison and Creswick, 1978) and the Massachusetts Institute of Technology (MIT) (Hiller and Glicksman, 1976). The tool remains in use today by design engineers and has undergone a number of enhancements over the years. The design engineer is limited to steady state air-to-air heat pump simulations for the fixed four component vapor compression system.

The National Institute of Standards and Technology (NIST) offers CYCLE_D for the theoretical analysis of a vapor compression system (Domanski *et al.*, 2003) CYCLE_D is intended to provide engineers with information regarding the performance of pure and mixed refrigerants and is not intended to be a detailed vapor compression

simulation tool. The program has seen a few revisions over the years and originated from CYCLE-11, which was an upgrade from CYCLE-7 (Domanski and McLinden, 1992).

Herrick Laboratories at Purdue University offer ACMODEL, a detailed steady-state simulation model, originally developed by Rossi (1995). All input parameters required to run ACMODEL are provided using batch files, and thus the program lacks a user-friendly interface. Though the simulation tool is constructed in a modular, object-oriented format, the component library is limited to a single finite difference based heat exchanger model and a single ARI map-based compressor model. (Shen *et al.*, 2004)

FKW – Research Center for Refrigeration Technology and Heat Pumps offers Cycle Calculation Program KMKreis, a simple but widely used thermodynamic model that calculates system state points for nine different cycle configurations. The program requires a large set of system-level input variables, such as condensing temperature, evaporating temperature, system subcooling, and system superheat, and does not allow for a detailed specification of the vapor compression system components. The program does include a list of 57 available refrigerants. The program is along the same lines as CYCLE_D, offered by NIST, and is not intended to be very detailed simulation tool for vapor compression system design.

Thermal Systems Research and Modeling (IMST) of the Universidad Politécnica de Valencia developed and released Advanced Refrigeration Technologies (ART) in 2002 (Corberan *et al.*, 2002). The simulation tool limits the user to the basic four component system; however various accessories can be added to the simulation such as piping, liquid-suction line heat exchanger, and a four-way valve. The simulation tool allows the user to select between different types of heat exchanger, compressor, and

expansion device models all of which vary in level of detail. The model is modular, thus allowing for different component models to be run by the program; however the program is not component-based, meaning the user cannot develop components for use in the program. ART is strictly a steady state simulation tool.

NIST introduced a beta version of ACSIM in 2004 (Domanski, 2004). ACSIM simulates the standard four component configuration; however, the program is unique in that it allows the user to design evaporator and condenser circuitries. The program requires the user input an ARI compressor map and a constant system superheat. Therefore, the simulation tool can not simulate various throttling devices.

Emerson Climate Technologies offers System Design Simulation for purchase by customers interested in Emerson products. The program allows the user to directly include Emerson products into the simulation; which include Copeland compressors, Copeland air-cooled condensing units, Emerson accumulators, and Emerson thermostatic expansion valves. The program is based on the ORNL Heat Pump Model.

Richardson (2006) presented VapCyc, a steady-state component-based simulation tool allowing for the simulation of cycles with additional components. VapCyc is continually being developed according to the interests of industrial partners belonging to the Center for Environmental Energy Engineering (CEEE) Integrated Systems and Optimization Consortium (ISOC).

1.3.4.2 Transient Simulation Software Packages

C&R Technologies offers SINDA/FLUINT, a general-purpose simulation environment for the arbitrary modeling of thermal-fluid systems (Cullimore *et al.*, 2004). The programming environment is most commonly used to model the transient response of thermal systems; however steady state simulations can be carried out through a

relaxation of the time dependent variables. FLUINT, which is the calculation engine behind the fluid flow analysis portion of the program, uses two types of submodels, namely lumps and paths, to perform the system analysis. C&R Technologies offer Sinaps Plus as a pre- and post- processor for SINDA/FLUID which allows user to design and connect various submodels. SINDA/FLUINT then creates a FORTRAN executable every time the program is run using the system layout and corresponding submodel code and solves for the transient variables simultaneously.

SINDA/FLUINT has been used to model the transient performance of a vapor compression system and a pre-built vapor compression cycle model can be purchased (Ploug-Sorensen *et al.*, 1997; Cullimore, 2000). The simulation tool has been extensively used within the aerospace industry for heat transfer and fluid flow analysis, but has not been well accepted by the vapor compression industry. Constructing a system in SINDA/FLUINT is considered rather time consuming and the flexibility of the tool increases the lead time to conducting meaningful simulations.

TRNSYS (Solar Energy Laboratory, University of Wisconsin-Madison, 2007) is a simulation environment for the transient simulation of systems. The simulation tool implements a component-based framework allowing the user to develop component models and load them into the TRNSYS environment. Initially developed for the transient analysis of solar thermal systems, the program has been extended to include a large variety of systems. TRNSYS has been used to simulate a supermarket refrigeration system (Ge and Tassou, 2000). Generally, the TRNSYS environment is more suitable to simulate systems with large time steps (Bradley, 2007) and thus component models designed to simulate a vapor compression system tend to be overly simplistic compared

to models described in Section 1.3.2. The model constructed by Ge and Tassou (2000) was designed to predict and control the energy consumption of the refrigeration system, and thus details such as heat exchanger pressure drop, refrigerant charge migration, and cabinet pull-down times were not included in the simulation.

Tummescheit *et al.* (2005) presented an air conditioning component library using Modelica (Modelica Association, 2007), an open object-oriented modeling language, for use in Dymola. Dymola is a component-based, dynamic simulation environment allowing users to integrate their own component models into the simulation through use of the Modelica modeling language (Dynasim AB, 2007). The Air Conditioning library is suited for steady state and transient simulation (Tummescheit *et al.*, 2005); however the mathematics describing how this is accomplished is not presented. According to Gauthier (2007), when running a steady state simulation the model does not quite start out in steady state and the simulation must run for approximately 20 seconds to reach a steady state value. Initial values close to the steady state solution must be entered into the simulation. Though steady state simulation has been selected a transient simulation is run to achieve the steady state performance. This approach fails to take advantage of the strengths of steady state simulation.

TransRef, a transient vapor compression simulation package developed by Anand (1999) at CEEE, was designed to simulate transient performance of a household refrigerator. The simulation tool was later enhanced to include the transient simulation of an automotive air-conditioning system (Gado, 2006). ElAziz (2006) modified the simulation tool to implement a component-based framework allowing for the development of additional component models (ElAziz *et al.*, 2006). The current

limitation of the program is with the available cycle configurations. The program allows for the simulation of four cycle configurations commonly used in household refrigerators. Each of the four cycle configuration implements a unique solver only to be used for that particular configuration. The simulation procedure does not allow for heat exchanger pressure drop to be taken into account.

1.3.5 Summary of Background

The area of vapor compression simulation, both steady state and transient, though a relatively mature research field requires significant improvements in order to further advance the current state of technology: increasing speed, accuracy, capabilities, and robustness. Furthermore, based on the literature review, there exists a clear need to develop an integrated transient and steady state simulation tool that is internally consistent, but also takes advantage of the inherent strengths of the steady state and transient simulation approaches.

Many techniques to simulate a vapor compression system operating in steady state have been presented in the literature; however, the numerical advantages and disadvantages of the various approaches have not been discussed. There is still a need for a robust, efficient, accurate, and flexible steady state vapor compression system solver, and hence the development of a new steady state solution algorithm. These aspects of a numerical routine tend to be conflicting in nature, and thus progress in these areas is required to continue the enhancement of vapor compression system simulation. The robustness and efficiency of a solution algorithm is dependent on the closeness between the initial guess values and the actual solution. Few authors describe a generic procedure used to determine guess values and thus a new approach has been developed and tested in the investigation.

The advantage of steady state simulation is the relatively high execution speed for a very detailed simulation. The advantage of the transient simulation is that the transient performance can be captured; however simpler models are required in order to achieve reasonable execution speed. Though relatively simple when compared to steady state models, transient models must maintain a high level of dependability. Regardless of whether a transient or steady state simulation was performed, the steady state performance should be consistently predicted with both types of simulation. Current modeling approaches are not capable of doing so while simultaneously taking advantage of the respective strengths of current techniques. This thesis addresses the underlying challenges.

1.4 Research Objectives

The proposed work focuses on steady state and transient vapor compression system simulation. There are two key areas that the thesis addresses, both of which include additional areas of development:

- Integration of steady state and transient simulation in a single component-based simulation environment
 - Vapor compression simulation component standard development allowing for system-to-component communication supporting steady state and transient simulation
 - Approximation of steady state component models for use in a transient simulation such that transient and steady state calculations converge to the same steady state result while taking advantage of the respective strengths of each type of simulation

- Steady state system solver performance analysis and improvement
 - Steady state solution procedure development enhancing calculation speed and robustness
 - Enhanced guess value calculation procedure development

1.5 Completed Tasks / Thesis Organization

A series of tasks had to be completed in order to develop an integrated steady state and transient component-based simulation package and fulfill the objectives of this thesis.

A vapor compression component standard was developed to provide a mechanism for all system-to-component and component-to-component communication supporting steady state and transient simulation. Both the steady state and transient simulation engines rely on a component standard dictating the component-based framework. Chapter 2 of this thesis describes the concept of component-based simulation and contains a detailed description of the implemented component-based framework. A sample equation set is provided for a simple vapor compression system simulation to serve as an example of component-based simulation of a vapor compression system.

In a component-based simulation environment, the component models contain the appropriate engineering equations. Suitable steady-state component models have been developed and incorporated into the simulation tool. Chapter 3 describes the steady state component library currently available in the simulation tool.

The simulation tool can perform steady state and transient calculations. However in order to take full advantage of both simulation approaches, two separate simulation engines were developed to handle the corresponding calculation procedure. The requirements of a steady state simulation algorithm have been mentioned in Section 1.2.1

and Section 1.3.5 mentions there is still a need for a robust, efficient, accurate, and flexible steady state vapor compression system solver. Chapter 4 describes an investigation into the performance of three steady state solution algorithms. The solution algorithm deemed the highest performing was selected as the steady state solution scheme implemented by the simulation tool.

Numerical validation of the steady state component models and vapor compression system have been presented in earlier works (Jiang, 2003; Aute *et al.*, 2004; Richardson, 2006; Winkler *et al.*, 2006) and thus are not included in this thesis.

The component-based approach used in developing the solver allows the solver to be easily extended to model different types of vapor compression systems. Chapter 5 describes solution procedures for simulating two-stage vapor injection cycles and cascade vapor compression systems. Validation results for both types of systems are presented.

Suitable transient component models were not available for use in the simulation tool, and thus new transient component models were developed and are described in Chapter 6.

As previously mentioned, in order to take full advantage of both simulation approaches, two separate simulation engines were developed to handle the corresponding calculation procedure. Chapter 7 describes the transient simulation scheme implemented by the system solver. A system-level validation of a 9.5kW R410A residential air conditioner is presented using the component models described in Chapter 6.

2 Component-Based Simulation Framework

A component-based simulation environment consists of two main modules; namely the component models and the system solver. Component models contain all the necessary engineering equations to simulate a specific thermodynamic process. The system solver is responsible for determining the system state points at each component inlet and outlet such that all system-level conservation laws are obeyed. The system solver accomplishes this task by executing the component models and evaluating system level conservation equations based on the configuration in which the components have been connected.

2.1 Motivation

The underlying rationale of conducting a simulation in a component-based format is the system solver does not require any prior knowledge of or relation to the component models that make up the system. This feature enhances the flexibility of the simulation tool while increasing the overall usefulness.

The flexibility of component-based software allows the users of the software to interchange component models without any modification to the procedure in which the system solver interacts with the component models. Since the component models are loaded into the program from external libraries at run-time, the users of the simulation tool have the option of developing their own component models for use within the program without requiring access to the source code of the simulation tool.

The flexibility of component-based software increases the usefulness of the software to a larger audience. The interchanging of component models is a mechanism of controlling the level of detail carried out by the simulation. For example, when

investigating the effect of system performance with respect to a particular variable, it might not be necessary to use a very detailed heat exchanger model when a simple model capable of representing the performance trends is available.

The component-based nature of a simulation tool also allows component selection optimization studies to be carried out. Since the component models can be loaded into the solver at any point prior to executing the solver, the general engine that selects component models and places them into the system could be any optimization routine capable of handling discrete variables. This type of optimization would be useful when designing a system using “off the shelf” components since there is a discrete set of available components that can be used to construct the system.

2.2 Definitions

2.2.1 Components

Components represent the vapor compression system components such as the evaporator, compressor, expansion device, etc. Thus, component models find solutions to the appropriate engineering equations describing that particular type of component. For example, a heat exchanger model representing a condenser will contain the necessary equations to satisfy the conservation laws of mass, energy, and momentum. Component models are responsible for satisfying the necessary conservation equations corresponding to the thermodynamic process occurring within the component.

In a component-based solution scheme, the system solver lacks information concerning the equations each component is solving. For example, the system solver can decipher between a compressor model and a condenser model, but the system solver will lack information concerning the type of condenser being modeled, i.e. a tube-fin heat

exchanger, a micro-channel heat exchanger, or a refrigerant to water tube-in-shell heat exchanger. Therefore, the component models are treated as “black box” objects and communication between the system and the component must occur via a structured framework (Winkler et al., 2006). The system solver communicates with a component model by assigning refrigerant states (e.g. pressure and specific enthalpy) at the components’ inlet and outlet ports, as shown in Figure 2.1. For the purposes of this thesis, it will be assumed that all system-to-component working fluid communication is carried out via the component inlet and outlet pressures, enthalpies, and mass flow rates.

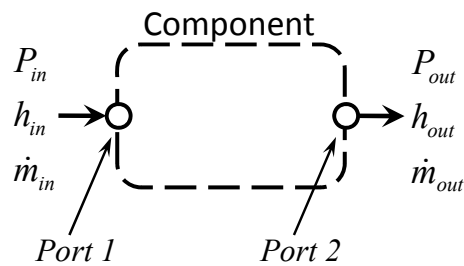


Figure 2.1 An example component

2.2.2 Ports

Ports are the mechanism through which the system solver communicates with the component models, and represent the refrigerant inlets and outlets of the component model. Through use of the components’ ports the system can:

- i. provide the component model with the appropriate inlet parameters
- ii. acquire the appropriate outlet parameters upon a successful execution of the component model

2.2.3 Component Boundary Condition Types

The solution procedure implemented by a component model is designed to use a specific type of boundary condition. The type of boundary condition a component model

implements ultimately determines the manner in which the system-to-component communication must take place. This thesis will focus on system solvers that utilize the following two types of boundary conditions.

Boundary pressure based component models require the inlet pressure, inlet enthalpy, and outlet pressure to execute. These parameters are provided by the system solver and would be passed to the component prior to the execution. Upon successful execution, the system solver would query the component model for the mass flow rate at each inlet and outlet port and the enthalpy at each outlet port. The most common component models to implement this boundary condition type are the compressor and expansion device. Heat exchangers can also implement this type of boundary condition; however execution speed is often slow due the computational requirement associated with solving the required equations.

Mass flow rate based components require the inlet pressure, inlet enthalpy, and inlet mass flow rate to execute and return the pressure and enthalpy for each outlet. Heat exchanger models typically implement this type of boundary condition.

2.2.4 Junctions

A junction represents an infinitesimal point within the cycle that allows for system-to-component interaction and provides the mechanism in which component ports are connected. A junction can be thought of as a system “state point”, whereas a single pressure and enthalpy value characterize the state of a junction. Even though junctions do not directly apply to component-based simulation, their description is provided here since junctions are used in system-to-component communication.

A simple junction is shown in Figure 2.2. In this diagram the junction represents the connection point between three ports; two of these being component outlets and one

being a component inlet. In theory, a junction can represent the connection point between any number of components, however in a conventional vapor compression system the number of components connected to a junction is two. Since a junction has a single pressure value, P , it is quite obvious that all component ports connected to this junction must have an equivalent pressure. Since junctions do not contain any process for separating the fluid into different states, it is concluded that all streams flowing from a junction must have an equal specific enthalpy, h_{mix} . The mixture specific enthalpy, h_{mix} , is used as the enthalpy value to describe the state of a junction and is calculated according to Equation 2.1.

$$h_{mix} = \frac{\sum_{i=1}^{NPorts,In} \dot{m}_i h_i}{\sum_{i=1}^{NPorts,Out} \dot{m}_i} \quad (2.1)$$

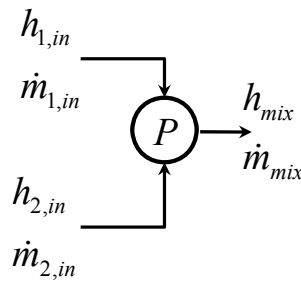


Figure 2.2 A simple junction

It is important to state that junctions do not represent pipes used to connect components, and thus represent “ideal connections” in between two component models. If the pressure drop or heat transferred to the refrigerant between two components is expected to be significant, a pipe model can be inserted in between the two component models. In this case, an additional junction would be added to the system.

2.3 Background Information

The fundamental requirement of a component-based simulation is the development of a standardized framework implementing the required system-to-component and component-to-component communication. The standardized framework developed for the simulation is presented in the following section.

Modelica is an object-oriented computer programming language designed for modeling engineering systems. The nature of the programming language is component-based, however one could argue that the components are not treated using a “black-box” approach since symbolic transformation algorithms must be applied to Modelica codes to solve the component modeling equations (Otter and Elmqvist, 2000). The two most common Modelica simulation environments are Dymola from Dynasim and MathModelica from MathCore. A variety of component model libraries exist on the open market; however the more detailed component libraries, such as the air-conditioning component library, are sold by third party vendors. Since component models programmed using the Modelica language require the purchase of a secondary simulation environment, the Modelica environment could not be used for this work.

The CAPE-OPEN Laboratories Network (CO-LaN) offers and supports the CAPE-OPEN (CO) standard. The CO standard defines a set of rules that allow CO component models to interact with CO-based applications. The standard is very comprehensive and essentially contains a subset of standards for a variety of process engineering applications. Even though the standard includes a thermodynamic and physical properties interface specification, the standard’s intention to be completely general has increased the complexity to a point where implementing the standard is quite burdensome. Vapor

compression system design engineers with a limited programming background would not have adequate knowledge to develop component models using the CO standard, and thus a component standard specifically targeted to vapor compression systems would better serve the community.

Richardson (2006) presented a component-based framework for the steady-state simulation of a vapor compression system and its components. Much of the vapor compression component standard presented in Section 2.4.3 is adopted from this work; however necessary additions were required to support transient component models. Richardson's vapor compression component standard also included additional fields that were determined to be unnecessary. It is important to limit the number of required fields in the component standard in order to simplify the development of new component models as much as possible.

2.4 Standardized Framework

The standardized framework includes a mechanism for the system solver to provide the component model with the required boundary conditions to run the model and for the output from the model to be passed back to the system solver after the component has been successfully executed. It is important that all component models within the system follow the same framework and that all communication between the system and the component models be conducted through the use of the methods provided by the framework. The manner in which this framework is implemented is quite flexible, however once the framework is in place it must be obeyed by all component models used by the program. The standardized framework developed consists of a set of structures and class interfaces that are described in the following sections.

2.4.1 Port States

Port States are used to represent the working fluid state point at each component port. Even though it is assumed for this thesis that working fluid states will be specified through the use of pressures and enthalpies, it is possible for additional information to be required when specifying the boundary conditions. Enthalpy values, by definition, are meaningful quantities only when being compared to a common reference point. Thus, using enthalpy to specify the refrigerant condition is only feasible when all component models in the system are using an identical reference point which cannot be guaranteed when component models are developed externally from the simulation environment. For this reason, temperature and refrigerant mass quality are included in the Port State. Port States included each of the following parameters, which are passed to the component model ports prior to the model being executed:

- Mass Flow Rate
- Pressure
- Enthalpy
- Temperature
- Quality
- Mass Fraction

2.4.2 Parameters

Parameters are structures used as a means to provide user interaction with a component model. A collection of parameters serve to specify component independent properties, dependent properties, transient properties, control sensors, and control actuators.

Independent properties are generally physical inputs that the user must provide prior to running the simulation that describe the component being modeled. Possible independent properties include heat exchanger tube length, compressor displacement, etc.

Dependent properties are values calculated by the component model during execution which are to be displayed to the user upon the successful completion of the system solver. Dependent properties are generally properties that are calculated by the component model that would go unknown to user unless they were contained in the dependent property list. Example dependent properties include heat exchanger air-side pressure drop and compressor shell cooling, but values such as heat exchanger outlet pressure or outlet temperature are generally not dependent properties since these are calculated as the system solver resolves the system.

Transient properties are reserved for transient simulations and are properties that are updated by the component model as the simulation marches in time. Transient properties must be provided with an initial value by the user prior to the start of the simulation. Examples of transient parameters include compressor shell temperature and cabinet wall temperature.

Control sensors and actuators serve only purpose in transient simulations and are used to provide component-to-component communication through the use of a control algorithm and controller. Control sensors are parameters that are output by each component model during each time step that are used to actuate a response by other component models. Example control sensors include the air temperature in a freezer compartment, compressor shell temperature, etc. Control actuators are parameters that are used by component models to generate a specific response based on the values

determined by a control algorithm. For example, a thermostat controls the compressor status (i.e. whether the compressor is running or shut off). Example control actuators include the compressor status (dictating where the refrigeration system is running) and refrigerator damper setting (dictating the portion of conditioned air flowing to the freezer and food compartments).

2.4.3 Vapor Compression Component Standard

In component-based simulation all vapor compression system component models must follow a standardized framework and the Component Standard primarily dictates the structure of this framework. At the center of the Component Standard is a class interface that ultimately determines the set of properties and methods that each component model must implement. The simulation tool will not load a component model unless the component model implements the required class interface. The Component Standard was developed with the intent of keeping the number of required methods to a minimum, in order to promote ease of use amongst component model developers, while attempting to maximize the overall flexibility. The component standard has been developed to support multiple types of boundary conditions and both steady state and transient simulation.

The Vapor Compression Component Standard contains the methods (Table 2.1) and properties (Table 2.2) that each vapor compression component model must implement.

Table 2.1 List of Vapor Compression Component Standard methods

Method	Description
InitializeComponent	Initializes the component model and returns true if the component has been successfully initialized.
GetRefrigerantList	Returns an array of integers indicating the predefined integers corresponding to refrigerants supported by the component model.
CanHandleProperties	Returns true if the component model will handle user interaction for changing independent properties.
EditProperties	Displays a modal dialog where the user can change the independent properties of the component.
SetPropertyRoutineData	Sets the necessary information to initialize the property routine library required for component model execution.
HasBoundaryCondition	Tests if the boundary condition (pressure, mass flow rate, etc.) passed in to this method is supported by the component model.
HasOperatingMode	Tests if the operating model (steady state or transient) passed in to this method is supported by the component model.
PreProcess	Allows the component model to conduct any pre-processing immediately prior the component model being executed.
Run	Executes the component model and returns 0 if the model was successfully run, a negative integer if an error occurred, or a positive integer if a warning was generated.
PostProcess	Runs any post-processing on the component model and is called immediately after the component model has been successfully executed.
UpdateTimeStep	Updates the component time step for transient operation.
GetStockProperty	Given a type of stock property (cost, weight, volume, etc.) returns the corresponding values. Certain stock property indices are pre-defined in the standard as enumerations.
SaveState	Saves all the component models properties to an XML node.
LoadState	Loads all the component model properties given an XML node.
Terminate	Used to terminate the component model and is called prior to the component model being unloaded from the system to release any resources.

Table 2.2 List of Vapor Compression Component Standard properties

Property	Description
PortCount	Returns the number of ports the component has.
BoundaryCondition	Sets the boundary condition types implemented by the system solver (if the boundary condition type is supported by the component model).
OperatingMode	Sets the operating mode (steady state or transient) implemented by the system solver (if the operating mode is supported by the component model).
OperatingContext	Sets the operating context (AC, heat pump, low temperature refrigeration, etc.) to the component model.
IndependentProperties	Returns a list of all the independent properties available to the user.
Refrigerant	Sets the working fluid to the component model.
SolverParameters	Sets any required tolerances to the component model that may be required during execution.
PortStates	Returns a given port state for the component model.
ControlActuators	Returns a list of control actuators the component requires in order to execute.
ControlSensors	Returns a list of control sensors the component will output after each execution.
ExternalSensorsRequired	Returns a list of sensors that must be set in order for the component model to run. An example includes a thermostatic expansion valve which requires the suction superheat in order to be executed.
TransientProperties	Returns a list of transient properties for the component model.
DependentProperties	Returns a list of all the dependent properties output from the component model.
HeatOut	Returns the heat load calculated by the component model. Heat out is taken as positive.
WorkOut	Returns the work calculated by the component model. Work out is taken as positive.
PowerConsumption	Returns the power consumption calculated by the component model.
Charge	Returns the working fluid charge calculated by the component model.
SystemUnits	Sets the unit system selected by the user to be used for display purposes only.
TraceSwitch	Sets the trace switch used for debugging a component model.
WorkingFolder	Sets the current working folder path for the component model.
Message	Returns any error messages or warnings that might have been generated during execution.

2.4.4 Load Component Standard

The purpose of a vapor compression system is to condition a space, which can be a refrigerator cabinet, automotive passenger cabin, room in a building, etc. When operating in steady state the heat load of the space must equal the capacity of the vapor compression system and thus simulating the load is generally not required. However in transient simulation, simulating the load becomes important in order to capture the rate of temperature change occurring within the space. Load components, such as a refrigerator cabinet, an automotive passenger cabin, and a room in a building, must be treated differently than vapor compression components since they directly interact with a vapor compression component.

The methods and properties implemented by load components are quite similar to the methods and properties listed in Table 2.1 and Table 2.2. The purpose of developing a separate class definition for load components is due to the way load components are handled and to distinguish load component models from other types of component models. Load component models are directly handled by the vapor compression components they are coupled to. For example, in a household refrigerator the air in the cabinet is cooled by the evaporator. The fan pulls air from the cabinet, directs it over the evaporator coil, and returns the conditioned air back to the cabinet. The simulation procedure of this process is quite similar to the actual process. Prior to executing the evaporator model, the inlet air condition to the evaporator is retrieved from the load model. The evaporator model is then executed and the outlet air condition from the evaporator model is passed to the load model as input. The system solver does not

execute the load model; instead the vapor compression component coupled to the load model executes the load model as required.

The Load Component Standard consists of two parts. The first being for load component models, which was described in the previous paragraph. The second part the Load Component Standard dictates which vapor compression component models can be coupled with a load model. Vapor compression component models that have been designed to execute a load model also must implement a Load Provider class interface. This class interface contains only one method allowing the load component model be passed into the vapor compression component model. Once the load component model has been passed into the vapor compression component model, the vapor compression component can execute the load component model as required.

Figure 2.3 depicts the communication flow between the system solver, vapor compression component models, and load component models. The system sets the Port States to the vapor compression component prior to execution. Once the system executes the vapor compression component model, the component model retrieves the inlet air condition from Port₂, executes the heat exchanger model, and passes the outlet air condition to Port₁ of the load model.

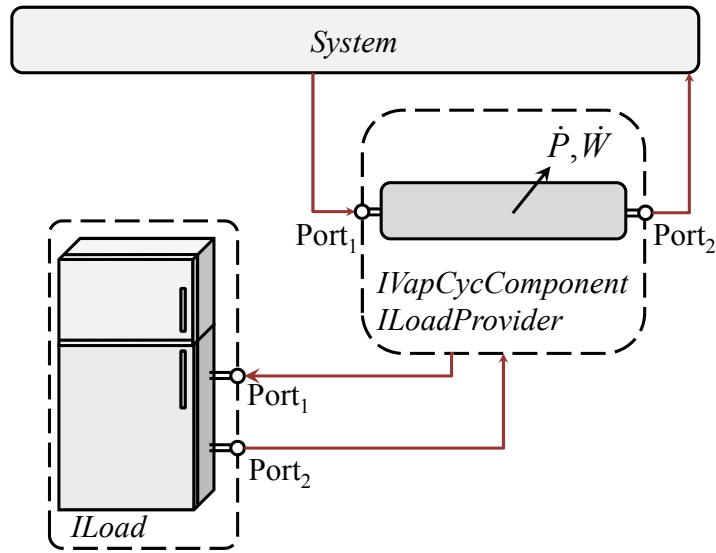


Figure 2.3 System, vapor compression component, and load component interaction

2.4.5 Fan Component Standard

Heat exchanger models used in the simulation of air-to-air heat pumps generally require the air-side flow rate to be specified prior to being executed. In some scenarios the air-side flow rate can be directly specified by the user; however in certain circumstances it can be useful to simulate the fan responsible for forcing air across the heat exchanger. Similar to the load component, a fan component standard has been developed in order to distinguish fan component models. The fan component standard also consists of two entities; namely the Fan Component Standard and the Fan Provider. These entities are similar in nature to the Load Component Standard.

A fan component model must be coupled to a heat exchanger component model and the two models must internally iterate to determine the air-side flow rate. The air-side flow rate is generally iterated over until the air-side pressure drop calculated by the heat exchanger matches the pressure head calculated by the fan.

As previously mentioned, not all heat exchanger models require a fan model to determine the air-side flow rate and in some cases use of a fan model is optional. Thus,

the Fan Provider class interface determines if a heat exchanger model supports the use of the fan. The Fan Provider class interface contains a small set of method as listed in Table 2.3.

Table 2.3 List Fan Provider methods

Method	Description
GetFanCount	Returns the number of fans a heat exchanger model is using.
IsFanRequired	Returns true if the heat exchanger model must be couple with a fan model and returns false if otherwise.
SetFan	Sets the fan component model to the heat exchanger. This method can be called multiple times if a set of fans are being used for a single heat exchanger.

The following flow chart shows the initialization procedure for a vapor compression component model and the steps to specify the fan component model to the vapor compression component model.

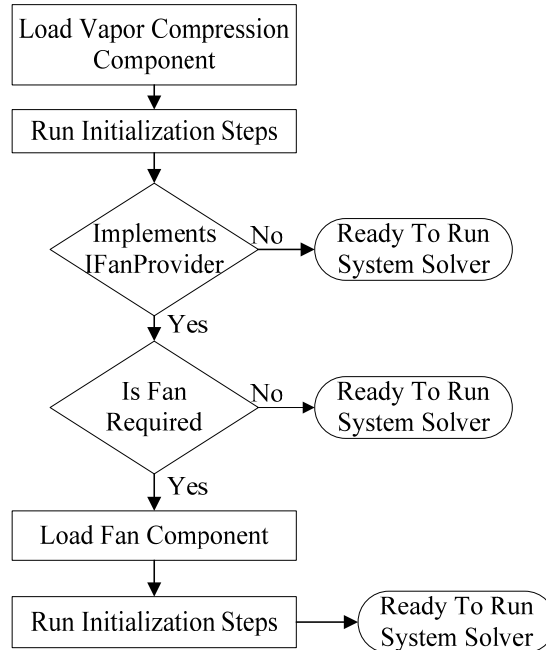


Figure 2.4 Flow chart shown fan component initialization

2.4.6 Control Block Standard

Transient simulation is commonly used to develop control algorithms. Control sensors and actuators are built into the vapor compression component standard; however an additional class interface is required for the control algorithms. The Control Block Standard dictates the implementation of control algorithms in the overall framework. Control blocks use the sensor values output by a set of a component models and determine what signals to send to the corresponding actuators. A thermostat serves as an example in Figure 2.5. The air temperature in the freezer compartment of the cabinet model, $T_{air, freezer}$, is used by the thermostat model to determine the on/off status of the compressor.

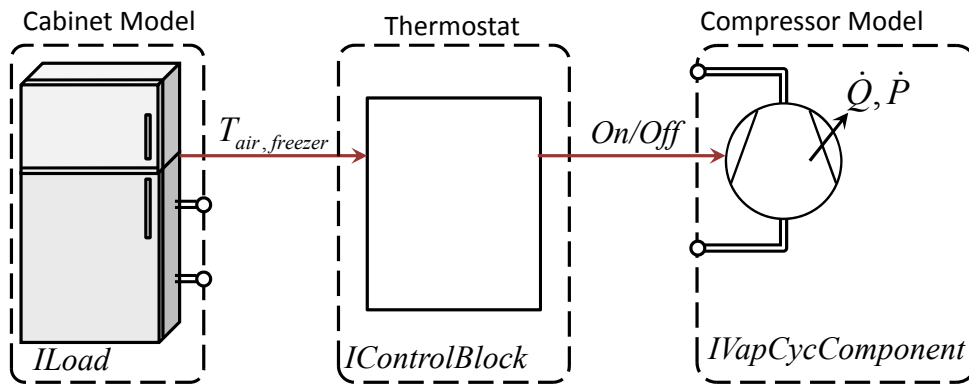


Figure 2.5 Control block and component interaction

2.5 Sample Equation Set for the Steady State Solution of a Vapor Compression System

2.5.1 System Definition

In general, to simulate a vapor compression system the solution algorithm must ascertain the refrigerant condition at each state point within the cycle along with the mass flow rate through each component. Particular state points and mass flow rates can be calculated using various component models. For example, a compressor model typically

calculates a mass flow rate given an inlet pressure and enthalpy along with the outlet pressure. The mass flow rate calculated by the compressor in Figure 2.6 can be used to execute the condenser model. Similar to the compressor, an expansion valve model typically calculates a mass flow rate which can be used to execute the evaporator model connected downstream of the valve. The solution algorithm designed to simulate the vapor compression system ultimately determines which state points and mass flow rates can be explicitly calculated by various component models and which state points must be solved for through iteration.

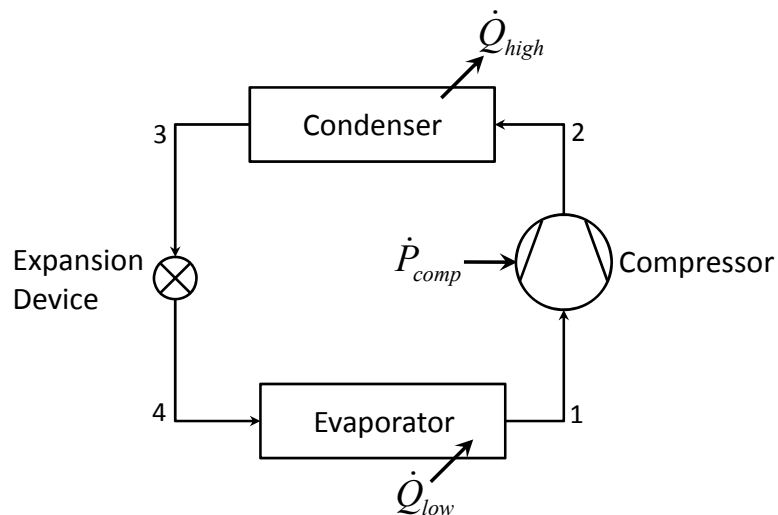


Figure 2.6 Diagram of a conventional vapor compression system

2.5.2 Component Model Equation Set

In order to provide a complete description of component-based simulation for a vapor compression system, this section provides a sample equation set for each component model. The system shown in Figure 2.6 is a conventional vapor compression system consisting of four components connected via four junctions. This system will serve as the example system for this section of the thesis. Since the system is being simulated under steady state assumptions, a load model will not be included in the

simulation. Simple component models will be used to serve as this example, thus a fan component model will not be coupled with either heat exchanger model. All component models have access to a refrigerant property routine library that allows for the calculation of thermophysical properties corresponding to a specific refrigerant condition.

The following four component models are assumed to operate using the inlet pressure and enthalpy. The compressor model and expansion device models also require the refrigerant outlet pressure to calculate the refrigerant mass flow rate. The evaporator model and condenser models require the refrigerant mass flow rate as input and calculate the outlet pressure.

2.5.2.1 Compressor Model

As previously mentioned, the compressor model uses the inlet pressure, inlet enthalpy, and outlet pressure as input to calculate the mass flow rate and outlet enthalpy.

The model requires the following input variables:

- Refrigerant conditions: h_{in}, P_{in}, P_{out}
- Physical parameters: $D_v, RPM, \eta_{isen}, \eta_{vol}$

The model uses these input parameters to calculate the following output:

- Refrigerant outlet condition: h_{out}, \dot{m}_{comp}
- System level output: \dot{P}_{comp}

The compressor model uses the following assumptions:

- Constant volumetric efficiency
- Constant isentropic efficiency
- Constant mechanical efficiency
- Heat loss from the compressor shell is neglected

- Refrigerant charge is neglected

Using the inlet refrigerant condition, the compressor model uses the refrigerant property library to calculate the inlet density and entropy.

$$(\rho_{in}, s_{in}) = fn(P_{in}, h_{in}) \quad (2.2)$$

The refrigerant mass flow rate is then calculated using the required physical parameters and inlet density.

$$\dot{m}_{comp} = \rho_{in} D_v \eta_{vol} \frac{RPM}{60} \quad (2.3)$$

The isentropic outlet enthalpy is calculated by the refrigerant property library using the outlet pressure and inlet entropy.

$$h_{out,isen} = fn(P_{out}, s_{in}) \quad (2.4)$$

The outlet enthalpy and the compressor power consumption can then be calculated to fulfill the required output from the compressor model.

$$h_{out} = h_{in} + \frac{h_{out,isen} - h_{in}}{\eta_{isen}} \quad (2.5)$$

$$\dot{P}_{comp} = \frac{\dot{m}_{comp} (h_{out} - h_{in})}{\eta_{mech}} \quad (2.6)$$

2.5.2.2 Condenser Model

The accuracy of the heat exchanger models, namely the condenser model and evaporator model, typically has a more significant impact than the compressor model and expansion valve model on the ability of the system simulation to reproduce experimental results. For that reason, the heat exchanger models typically involve a more detailed calculation procedure. However for the example, the heat exchanger model will be made very simple. The condenser model for this example will use the following input variables:

- Refrigerant conditions: $h_{in}, P_{in}, \dot{m}_{ref}$
- Physical parameters: $L, D, UA)_{cond}, f, \dot{m}_{air}, T_{air,in}, C_{p,air}$

The condenser model will use the above input parameters to calculate the following set of outputs:

- Refrigerant outlet condition: $h_{out}, P_{out}, M_{cond}$
- System level output: $\dot{Q}_{cond}, DP_{ref}, T_{air,out}$

The condenser model uses the following assumptions:

- Constant heat transfer coefficients
- Constant friction factor
- Air-side pressure drop is neglected
- Refrigerant pressure drop is calculated based on the inlet condition

The refrigerant pressure drop is calculated using the friction factor and inlet density.

$$DP_{ref} = f \frac{2L}{\pi \rho_{in} D} \dot{m}_{ref}^2 \quad (2.7)$$

The outlet refrigerant pressure is then easily calculated.

$$P_{out} = P_{in} - DP_{ref} \quad (2.8)$$

A condenser typically has three distinct zones; namely the de-superheating zone, the two-phase zone, and the subcooled liquid zone. Generally, the two-phase zone is the largest of the three zones, and thus the heat transfer will be modeled using the two-phase temperature,

$$T_{sat} = f_n \left(\frac{P_{in} + P_{out}}{2} \right) \quad (2.9)$$

Using the two-phase temperature, inlet air temperature, and overall heat transfer coefficient of the heat exchanger, the heat load, outlet refrigerant enthalpy, and outlet air temperature can be calculated.

$$\dot{Q}_{cond} = UA)_{cond} (T_{sat} - T_{air,in}) \quad (2.10)$$

$$h_{out} = h_{in} - \frac{\dot{Q}_{cond}}{\dot{m}_{ref}} \quad (2.11)$$

$$T_{air,out} = T_{air,in} + \frac{\dot{Q}_{cond}}{\dot{m}_{air} C_{p,air}} \quad (2.12)$$

2.5.2.3 Expansion Device Model

The expansion device can be modeled as a fixed orifice, capillary tube, short tube orifice, thermostatic expansion valve, etc. The sample component model will simulate a fixed orifice. The model requires the following input variables:

- Refrigerant conditions: h_{in}, P_{in}, P_{out}
- Physical parameters: C_f, D

The fixed orifice model uses these input parameters to calculate the following output:

- Refrigerant outlet condition: h_{out}, \dot{m}_{exp}

The model uses the following assumptions:

- Constant flow coefficient
- Isenthalpic expansion
- Refrigerant charge is neglected

Using the inlet refrigerant condition, the expansion device model uses the refrigerant property library to calculate the inlet density.

$$\rho_{in} = fn(P_{in}, h_{in}) \quad (2.13)$$

The refrigerant mass flow rate is then calculated using the flow coefficient, inlet density, and pressure drop across the valve.

$$\dot{m}_{exp} = C_f D^2 \sqrt{\rho_{in} (P_{in} - P_{out})} \quad (2.14)$$

Since the model assumes isenthalpic expansion, the outlet enthalpy is equal the inlet enthalpy.

$$h_{out} = h_{in} \quad (2.15)$$

2.5.2.4 Evaporator Model

The evaporator model for this example will use the following input variables:

- Refrigerant conditions: $h_{in}, P_{in}, \dot{m}_{ref}$
- Physical parameters: $L, D, UA)_{evap}, f, \dot{m}_{air}, T_{air,in}, C_{p,air}$

The evaporator model will calculate the following set of outputs:

- Refrigerant outlet condition: $h_{out}, P_{out}, M_{evap}$
- System level output: $\dot{Q}_{evap}, DP_{ref}, T_{air,out}$

The evaporator model uses the following assumptions:

- Constant heat transfer coefficients
- Constant friction factor
- Air-side pressure drop is neglected
- Refrigerant pressure drop is calculated based on the inlet condition

The refrigerant pressure drop is calculated using the friction factor and inlet density.

$$DP_{ref} = f \frac{2L}{\pi \rho_{in} D} \dot{m}_{ref}^2 \quad (2.16)$$

The outlet refrigerant pressure is then easily calculated.

$$P_{out} = P_{in} - DP_{ref} \quad (2.17)$$

An evaporator typically has two distinct zones; namely the two-phase zone and the superheated vapor zone. Generally, the two-phase zone is the larger of the two zones, and thus the heat transfer will be modeled using the two-phase temperature,

$$T_{sat} = fn\left(\frac{P_{in} + P_{out}}{2}\right) \quad (2.18)$$

Using the two-phase temperature, inlet air temperature, and overall heat transfer coefficient of the heat exchanger, the heat load, outlet refrigerant enthalpy, and outlet air temperature can be calculated.

$$\dot{Q}_{evap} = UA)_{evap} (T_{sat} - T_{air,in}) \quad (2.19)$$

$$h_{out} = h_{in} - \frac{\dot{Q}_{evap}}{\dot{m}_{ref}} \quad (2.20)$$

$$T_{air,out} = T_{air,in} + \frac{\dot{Q}_{evap}}{\dot{m}_{air} C_{p,air}} \quad (2.21)$$

It should be noted that the evaporator model and condenser model implement similar calculation procedures, which is typical in heat exchanger simulation.

2.5.3 System-Level Solution Variables

The purpose of the system solver is to resolve the thermodynamic state of all the junctions within the cycle. For the simple component models implemented in this example, all the output values can be explicitly calculated from the physical parameters and refrigerant boundary conditions, but this does not guarantee that mass, momentum, and energy will be conserved throughout the system. The thermodynamic states at each junction must be determined such that the system balances.

The vapor compression system consisting of the sample component models is shown in Figure 2.7. As previously described, the required variables to determine the thermodynamic state of a junction include the pressure and the specific enthalpy. Since the output for each component model can be explicitly calculated using the input parameters, the number of unknown variables can be reduced to the set of pressures and enthalpies for each junction. The set of unknown variables can be placed in a vector, x .

$$\bar{x} = [P_1 \quad P_2 \quad P_3 \quad P_4 \quad h_1 \quad h_2 \quad h_3 \quad h_4]^T \quad (2.22)$$

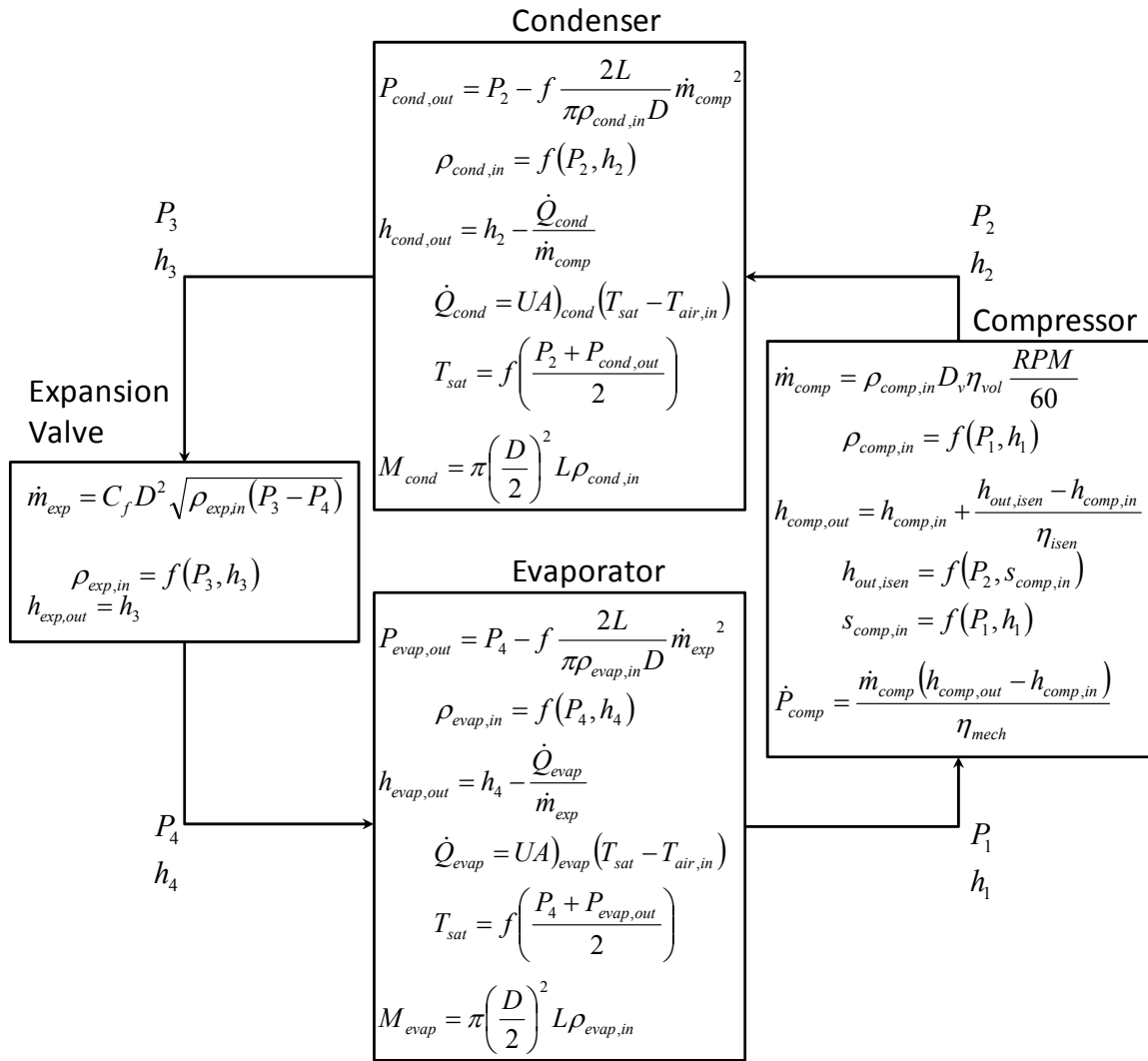


Figure 2.7 Diagram showing component model interaction

Based on the algorithm implemented by the system solver, it is possible for certain variables in \bar{x} to be eliminated. The component modeling equations are used to formulate a set of equations corresponding to the set of unknown variables shown in Equation 2.22. An example of such an equation set is shown below. In this example, it is assumed that the system charge, $M_{sys,user}$, has been specified as input to the simulation and represents the total mass of refrigerant in the system.

$$\bar{r} = \begin{bmatrix} \dot{m}_{comp} - m_{exp} \\ h_{comp,out} - h_2 \\ P_{cond,out} - P_3 \\ h_{cond,out} - h_3 \\ h_{exp,out} - h_4 \\ P_{evap,out} - P_1 \\ h_{evap,out} - h_1 \\ (M_{evap} + M_{cond}) - M_{sys,user} \end{bmatrix} = \bar{0} \quad (2.23)$$

The system solver algorithm must formulate a set of equations equal to the number of unknown variables remaining after the simplifications have been made. Chapter 4 will discuss three possible algorithms for solving a vapor compression system simulation. In all approaches, the system solver utilizes a nonlinear equation solver to solve for the unknown variables using the formulated set of equations. The formulated equation set can always be written in the following form.

$$\bar{f}(\bar{x}) = \bar{0} \quad (2.24)$$

All nonlinear solvers require an initial point in which to start searching for a solution, thus in each approach an initial or guessed value for each unknown variable must be determined. All systems of nonlinear equations are solved using an iterative procedure, and therefore the set of equations described in Equation 2.24 cannot be

satisfied exactly. Alternatively, the set of equations are used to formulate a residual value and a tolerance is set to determine when the equation solver should terminate. Typically, the Euclidean norm of the residual vector is used.

$$\|\vec{f}(\vec{x})\|_2 \leq \varepsilon_f \quad (2.25)$$

2.5.4 Application of Component-Based Simulation

Despite the fact that component models described in this example might be suitable at estimating performance trends associated with an actual vapor compression system, the component models are generally too simplistic to accurately capture the behavior of a vapor compression system. Component-based simulation essentially allows the equations in Figure 2.7 to be replaced with any set of equations suitable at modeling that particular component without having to change the approach to simulate the entire system. The condenser model can range from a simple UA-based heat exchanger model, as described here, to a complex discretized model requiring internal iteration to determine the outlet conditions. Component-based simulation allows all the component model equations to remain in their corresponding “black-box”.

3 Steady State Component Simulation

The steady state component library is fairly extensive and though a majority of the component models have been created by outside sources, this chapter is included for completeness. Even though most of the component models have been developed by external sources, all the component models were adopted to fit in the framework presented in Chapter 2.

3.1 Air-to-Refrigerant Heat Exchanger Simulation

The focus of the heat exchanger component library will be placed on air-to-refrigerant heat exchangers, however the very nature of component-based simulation allows for the flexibility to be extended to water-to-refrigerant heat exchangers as well. However, the initial development of the simulation tool has been geared towards air-to-refrigerant vapor compression systems, and hence the focus of this section.

3.1.1 Generic Heat Exchanger Model

Richardson (2006) introduced the Generic Heat Exchanger Model, a lumped 3 zone, UA-based heat exchanger model. The model treats the heat exchanger as a single tube, and thus the effects of changing air temperature are neglected. The model assumes constant heat transfer coefficients for the air-side and refrigerant-side vapor, two-phase, and liquid regions, which must be entered by the user. The model also assumes a friction factor and only uses the refrigerant inlet conditions to evaluate the pressure drop. The original model was developed to calculate a mass flow rate given boundary pressures; however the model has been extended to handle both types of boundary conditions mentioned in Section 2.2.3. Though the assumptions included in this model are overly simplistic and don't allow for accurate prediction of experimental performance, the

model does provide accurate trends at an inexpensive cost making the model suitable for capturing vapor compression system performance trends and conducting preliminary investigational studies.

3.1.2 CoilDesigner Heat Exchanger Model

Jiang (2003) and Jiang *et al.* (2006) introduced CoilDesigner, a general purpose simulation tool for the steady state analysis air-to-refrigerant heat exchangers. CoilDesigner is a segment-based model that divides each heat exchanger tube in a number of segments and evaluates refrigerant-side correlations for each segment as the thermophysical properties of the refrigerant change along the heat exchanger tube. The model is highly detailed and allows for the simulation of arbitrary heat exchanger circuitries. The model includes calculations for not only tube-fin heat exchangers, but microchannel heat exchangers as well.

CoilDesigner includes a rich user-interface allowing users to save and load CoilDesigner files. The component model developed using the CoilDesigner solver routines uses a CoilDesigner file as input to provide all the heat exchanger information, such as tube and fin geometries, heat exchanger circuitry, heat transfer and pressure correlation settings, etc. The vapor compression system simulation tool then sets the refrigerant-side inputs as the system solver attempts to balance the entire vapor compression system (the procedure for which is described in the following chapter).

Though the increase in accuracy comes with a higher computational cost, the CoilDesigner Heat Exchanger Model component will be the most utilized steady state heat exchanger model by those who use the steady state portion of the simulation tool. The increase in computational cost places a higher demand on the overall computational

efficiency of the vapor compression system solver, and hence the importance of computational efficiency described in Chapter 4.

3.2 Compressor Simulation

Section 1.3.3 mentions that there are generally two main types of transient compressor models: efficiency-based models and map-based models. Since in transient simulations, the compressor model is modeled using quasi-steady assumptions, it is not surprising that compressor models found in steady-state simulations tend to be one of the same two types. Compressor models generally operate using the suction pressure, suction enthalpy (or temperature), and discharge pressure as inputs and calculate the mass flow rate, power consumption, and discharge enthalpy (or temperature).

3.2.1 Isentropic Compressor Model

Though relatively simple, the standard isentropic compressor model is utilized by many authors (see Table 1.1). The isentropic compressor model presented here is suitable in both steady state and transient system-level simulations under the quasi-steady state assumptions. The model assumes constant isentropic and volumetric efficiency and neglects shell cooling effects. The compressor mass flow rate is calculated using the following equation.

$$\dot{m} = \eta_{vol} \rho_{suction} D_v \frac{RPM}{60} \quad (3.1)$$

The compressor discharge enthalpy is calculated assuming a constant isentropic efficiency, shown in Equation 3.2, where $h_{isen,out}$ is determined from the suction entropy and discharge pressure.

$$h_{out} = h_{in} + \frac{h_{isen,out} - h_{in}}{\eta_{isen}} \quad (3.2)$$

The compressor power consumption is calculated using the compressor inlet and outlet enthalpy and a constant motor efficiency.

$$\dot{P} = \frac{\dot{m}(h_{out} - h_{in})}{\eta_{motor}} \quad (3.3)$$

Though the model does not explicitly calculate the compressor shell cooling effects, the shell cooling is implied by the compressor motor efficiency. Since the model is operating under steady state, the energy imbalance between the compressor motor power and change in the refrigerant enthalpy is taken into account through heat being rejected through the compressor shell.

$$\dot{Q}_{shell} = \dot{P} - \dot{m}(h_{out} - h_{in}) = \dot{P}(1 - \eta_{motor}) \quad (3.4)$$

3.2.2 ARI-540 Coefficient Compressor Model

The Air-Conditioning, Heating, and Refrigeration Institute (AHRI), formerly known as the Air-Conditioning and Refrigeration Institute (ARI), provides performance rating standard for positive displacement compressors (ARI, 1999). The compressor performance, X , is modeled using a standardized 10 coefficient polynomial format, as shown in Equation 3.5.

$$X = c_0 + c_1 T_e + c_2 T_c + c_3 T_e^2 + c_4 T_e T_c + c_5 T_c^2 + c_6 T_e^3 + c_7 T_c T_e^2 + c_8 T_e T_c^2 + c_9 T_c^3 \quad (3.5)$$

In Equation 3.5, T_e represents the suction dew point temperature calculated from the suction pressure and T_c represents the discharge dew point temperature calculated from the discharge pressure. The coefficients, c_i , are provided by compressor manufacturers and are determined from conducting a series of steady state tests at a set of operating conditions also mentioned in the standard. The output of the model, X , is the compressor

mass flow rate, power consumption, rated system capacity, and current draw. A different set of coefficients must be used for each output parameter.

3.2.3 Two-Stage Isentropic Compressor Model

Two stage cycles are gaining in popularity due to the continued effort towards more energy efficient vapor compression systems and the favorability of environmentally benign refrigerants. The simulation of two-stage cycles requires a two-stage compressor model. Huff *et al.* (2002) numerically investigated three distinct two-stage transcritical CO₂ cycle configurations, which also discussed the benefits of using an intercooler to reject heat at an intermediate pressure in between the two compression stages.

The two-stage compressor configurations shown in Figure 3.1 and Figure 3.2 are treated as “black-box” compressor models, meaning the low stage compressor, high stage compressor, and possibly the intercooler are all contained within a single component model. The low and high stage compressors are modeled using the isentropic compressor model described in Section 3.2.1.

The two compressor configurations shown in Figure 3.1 must iteratively solve for the intermediate pressure at the low stage compressor discharge such that mass flow rate balances through both compressors. The mass flow rate through the low stage and high stage must be equivalent since the model is operating under steady state. The model must internally iterate for the intermediate pressure since the high stage compressor mass flow rate calculate is dependent on the intermediate suction density, as shown in Equation 3.1.

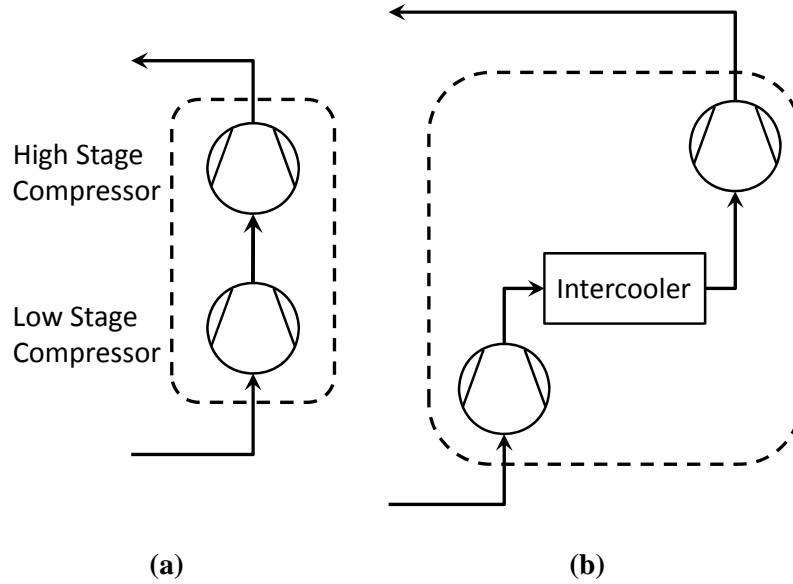


Figure 3.1 Two-stage compressor options

The two compressor configurations shown in Figure 3.2 are slightly different in that they have an intermediate suction port. The compressor model shown in Figure 3.2a was utilized by Winkler *et al.* (2008a) to simulate a residential R410A two-stage flash tank cycle. Since these two compressor configurations use an intermediate suction port, the intermediate suction pressure and enthalpy must be passed into the component prior to execution. The two-stage compressor model then calculates the suction, intermediate, and discharge mass flow rates, and the discharge enthalpy.

The compressor shown in Figure 3.2a requires an iteration to determine the mixing enthalpy at the high stage suction port, $h_{suction,high}$, to ensure energy balance within the compressor. The suction enthalpy at the high stage compressor inlet is the unknown variable iterated over until the following energy balance is satisfied.

$$\dot{m}_{dis} h_{suction,high} = \dot{m}_{suction} h_{suction} + \dot{m}_{int} h_{int} \quad (3.6)$$

The compressor configuration shown in Figure 3.2b must iterate on the low stage compressor discharge pressure, $P_{discharge,low}$, to ensure the outlet pressure of the intercooler

is equal to the intermediate suction pressure, P_{int} . The model must also iterate over the mixing enthalpy at the high stage suction port, $h_{suction,high}$, to ensure energy balance within the compressor, as explained above.

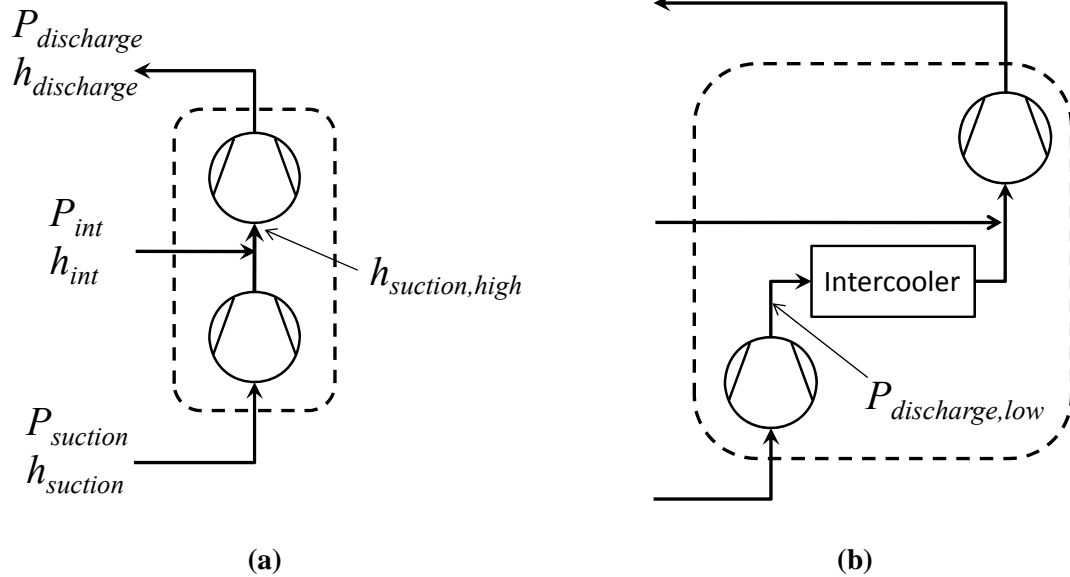


Figure 3.2 Two-stage compressor options with an intermediate suction port

3.3 Expansion Device Simulation

The expansion device component model tends to be the simplest component model when simulating the entire vapor compression system, mostly due to the reason that such models tend to be correlation based. Expansion device models tend to calculate a refrigerant mass flow rate given the refrigerant inlet condition and outlet pressure. The models presented here are suitable for use in transient simulation of vapor compression systems for the reasons mentioned in Section 6.3.

3.3.1 Fixed Orifice Model

Stoecker (1983) provides a simple equation to calculate the mass flow rate through a fixed orifice using the inlet and outlet pressure, inlet density, and certain valve characteristics such the diameter, D , and valve constant, K . (Stoecker, 1983)

$$\dot{m} = KD^2 \sqrt{\rho_{in} (P_{in} - P_{out})} \quad (3.7)$$

3.3.2 Short Tube Orifice Model

Kim et al. (1994) and Kim and O'Neal (1994) developed correlations to model two-phase refrigerant flow through short tube orifices specifically for R134a, R22, and R12. Both works use the same basic form of equation to calculate the refrigerant mass flow rate through the orifice. (Kim and O'Neal, 1994; Kim *et al.*, 1994)

$$\dot{m} = C_c A_c \sqrt{2g_{ca} \rho_{in} (P_{in} - P_f)} \quad (3.8)$$

In the above equation, A_c represents the short tube cross sectional area, g_{ca} is the dimensional gravity constant, and C_c and P_f are determined by correlations developed specifically for each refrigerant.

3.3.3 Adiabatic Capillary Tube Model

Two adiabatic capillary tube models are included in the component library. The models presented by Choi *et al.* (2003) and by ASHRAE (2002) are both formulated using Pi-groups based correlation. Both correlations operate using the functional form presented below. (ASHRAE, 2002; Choi *et al.*, 2003)

$$\pi_8 = K \cdot \pi_1^a \cdot \pi_2^b \cdot \pi_3^c \cdot \pi_4^d \cdot \pi_5^e \cdot \pi_6^f \cdot \pi_7^g \quad (3.9)$$

where,

$$\pi_8 = \frac{\dot{m}}{D\mu_f} \quad (3.10)$$

The π terms in each model are not the same dimensionless parameter, but each π term represents a physical parameter. The constants, a through g , in the above equation are determined empirically.

3.3.4 Linear TXV Model

Li *et al.* (2004) presented a globally linear thermostatic expansion valve (TXV) model. TXV's automatically adjust the valve opening based on the refrigerant superheat at the evaporator outlet or compressor inlet. The model is considered linear because the valve mass flow rate varies linearly as a function of superheat, as shown in Figure 3.3. (Li *et al.*, 2004) In the figure below, the distance from point O to point A is the static superheat, $T_{sh,static}$, and represents the superheat at which the valve starts to open. The distance from point O to point A represents the maximum opening superheat, at which point the valve cannot provide any additional capacity.

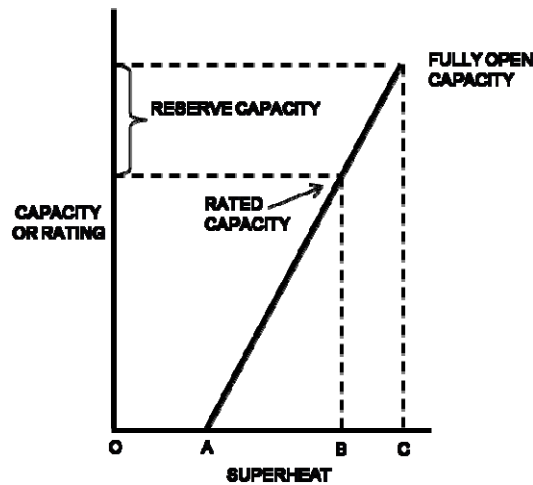


Figure 3.3 TXV mass flow rate at a fixed pressure drop vs. superheat

The general form of the model is shown below

$$\dot{m} = C(T_{sh,operating} - T_{sh,static})\sqrt{\rho_{in}(P_{in} - P_{down})} \quad (3.11)$$

where, C represents the valve flow coefficient. The static superheat setting and the valve flow coefficient must be provided by the valve manufacturer. The current system superheat, $T_{sh,operating}$, must be passed into the TXV component model prior to execution.

As pointed out in Table 2.2, this is conducted using the `ExternalSensorsRequired` property of the component standard.

4 Investigation into Steady State Solver Performance and Its Improvement

The work completed in this chapter has been published by Winkler *et al.*, 2008b.

4.1 Motivation

Chapter 2 concludes that in component-based simulation the system solution algorithm is as important as the approach used to model the individual components. The reason being that in a component-based solver the component models can be easily interchanged and created by outside developers, thus placing the stricter requirement on being able to simulate the entire system, i.e. a set of component models connected together to form a vapor compression system.

Many techniques to simulate a vapor compression system operating in steady state have been presented in the literature; however, the numerical advantages and disadvantages of the various approaches have not been discussed. The key performance metric to determine the value of a solution algorithm should be the algorithm's robustness and efficiency at simulating a system at off-design conditions. In order to simulate a vapor compression system consisting of multiple components, the algorithm's ability to be extended beyond the basic four component vapor compression system should be examined. The solver with the best performance was selected as the primary solver in the integrated steady state and transient simulation tool.

There is still a need for a robust, efficient, accurate, and flexible steady state vapor compression system solver, and hence the development of a new steady state solution algorithm. These aspects of a numerical routine tend to be conflicting in nature, and thus progress in these areas is required to continue the enhancement of vapor compression

system simulation. The robustness and efficiency of a solution algorithm is dependent on the closeness between the initial guess values and the actual solution. Few authors describe a generic procedure used to determine guess values and thus a new approach has been developed and tested in the investigation.

A numerical study investigating the performance of steady state vapor compression system simulation techniques has been conducted to determine a set of best practices when simulating a vapor compression system. The investigation included two algorithms from the literature along with a new solution technique developed for the simulation of complex vapor compression system configurations. Each algorithm's robustness at handling a large variety of operating conditions for a set of different cycle configurations has been quantified. All three solution algorithms were implemented using a component-based approach capable of simulating vapor compression systems consisting of multiple components. The solution algorithms to be analyzed include the following:

- Junction Solver (Richardson, 2006)
- Decoupled Energy and Hydraulic Solver (Jiang, 2003; Richardson, 2006)
- Enthalpy Marching Solver

The Enthalpy Marching Solver is a new component-based solution technique allowing for the simulation of generic system configurations. The algorithm was developed to have increased robustness and efficiency over the first two solvers in the above list. The details of the Enthalpy Marching Solver solution technique have been presented in Winkler *et al.* (2008b).

4.1.1 Relevance to Transient Simulation

The investigation into steady solver performance will provide insight for conducting transient simulations as well. Features from the best performing steady state solver can be used in constructing a transient system solution scheme since a solution algorithm must be implemented to solve each time step of the transient simulation. The details concerning the transient system solution procedure are described in Chapter 7.

4.2 System Solver Evaluation Procedure

A series of numerical experiments were conducted to characterize the performance of the previously listed system solver algorithms. These numerical experiments were designed to determine the robustness and computational effort required for each solution algorithm. In order to determine the robustness of each algorithm a test matrix was designed to test the solver's ability to simulate a cycle operating under off-design conditions. The effect of different approaches used to close the system of equations and chosen guess values were also studied. In summary, the following aspects were analyzed when evaluating each vapor compression system solver:

- Cycle configuration (the basic vapor compression system and a system consisting of additional components)
- Nonlinear equation solver algorithm
- Vapor compression system input specification option (system refrigerant mass and system subcooling)
- Operating conditions (ambient and space temperatures)
- Guess value dependence

4.2.1 Vapor Compression Cycle Configurations

Two cycle configurations were analyzed to test each solution algorithm. The basic four component vapor compression system cycle, shown in Figure 4.1a, is the simplest cycle configuration for any solution algorithm to solve. This cycle configuration was chosen since it is the simplest form of a vapor compression cycle and will therefore help to determine the upper bound of the performance of each solution scheme. For this purposes of this investigation, piping and additional accessories were not be accounted for since these types of components don't contribute to the overall complexity of the cycle.

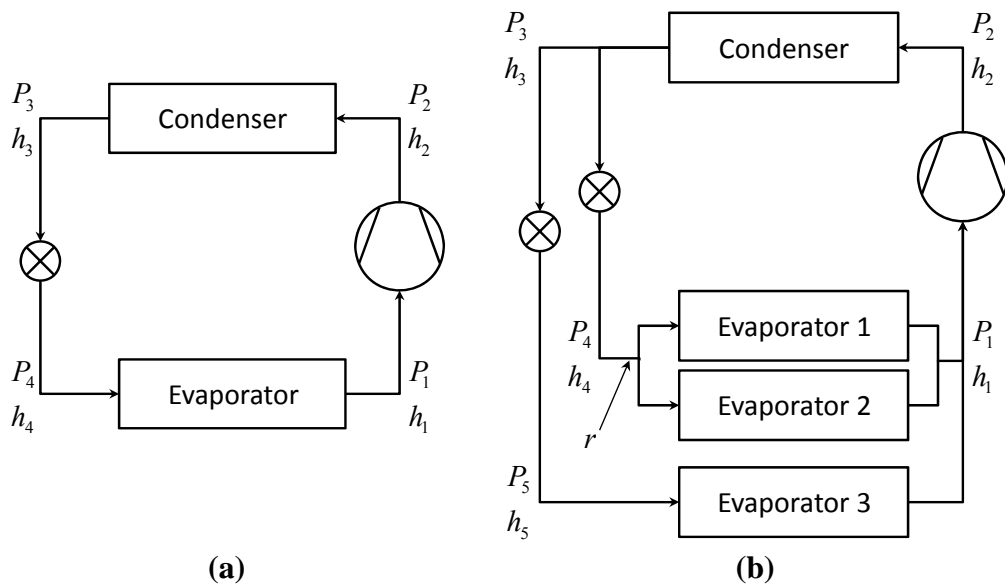


Figure 4.1 Two cycle configurations used in evaluating solver performance

A more complicated cycle configuration is shown in Figure 4.1b. Theoretically there is no limit on the number of components in a vapor compression system and thus the most difficult cycle configuration for a solution scheme to simulate cannot be determined. However, there are certain features of this cycle configuration that enhance the system's complexity:

- Additional unknown values (i.e. additional state points within the cycle)

- Merging of three components at the compressor suction port
- Splitting of refrigerant flow at the inlet to Evaporator 1 and Evaporator 2

4.2.2 Nonlinear Equation Solver Selection

All three algorithms utilize a nonlinear equation solver to solve the resulting mass and energy balance equations. Three nonlinear equation solvers were tested with each algorithm in a further attempt to develop a robust vapor compression system solver. The three nonlinear equation solvers tested include:

- Newton-Raphson method (Press *et al.*, 1992)
- Broyden's method (Press *et al.*, 1992)
- The Hybrid method (More *et al.*, 1980)

The purpose of testing three nonlinear equations solvers was to eliminate the dependence of the nonlinear equation solver on the performance of the three vapor compression system simulation algorithms.

4.2.3 Vapor Compression System Input Specification

For sub-critical vapor compression cycles, there exist two common options to close the system of equations and therefore all three solution schemes were tested using the following specification types:

- System refrigerant mass specification (i.e. system charge)
- System subcooling specification

When choosing to specify the system refrigerant charge, the simulation must satisfy a mass balance between the mass input by the user and the total mass calculated by the component models. In order to conduct the mass balance, the system charge (M_{system}) must be specified to the solution algorithm and the component models must implement

algorithms to calculate the charge internal to the component, $M_{Component,i}$. Equation 4.1 provides the corresponding equation to calculate the system level mass balance residual.

$$r_M = M_{System} - \sum_{i=1}^{NComponents} M_{Component,i} \quad (4.1)$$

The refrigerant subcooling at the condenser outlet can be specified to the solution algorithm in order to close the set of equations. Vapor compression systems are typically designed for a standardized amount of refrigerant subcooling. When specifying the refrigerant subcooling it is important for the corresponding residual equation to be in terms of enthalpy to ensure numerical stability in the event two-phase flow is exiting the condenser. The equation to calculate the subcooling residual is shown in Equation 4.2.

$$r_{SC} = h_{SC} - h_{Cond,out} \quad (4.2)$$

In Equation 4.2 , h_{SC} is calculated as follows.

$$h_{SC} = f(P = P_{Exp,in}, T = T_{sat@P} - T_{SC}) \quad (4.3)$$

The above two equations assume the liquid line connecting the condenser and expansion device has been neglected.

4.2.4 System Operating Conditions Test Matrix

Conventional vapor compression systems interact with the environment through the evaporator(s) and condenser(s) and a secondary fluid. For the purposes of this study the secondary fluid for all heat exchangers was assumed to be air. Vapor compression systems are designed using a specified operating point. The systems shown in Figure 4.1a and Figure 4.1b were initially designed using a specified design point from which the nominal system charge for each system was determined. The design point was taken from ASHRAE Standard 116 and ARI Standard 540. The operating conditions from these

standards are listed in Table 4.1. The chosen refrigerant for both systems was R134a and details concerning the component models have been described by Richardson (2002).

Table 4.1 ASHRAE Rating Conditions (Reproduced from ASHRAE Std. 116, 1995)

	Parameter	Temperature [°F / °C]
Refrigeration System Parameters	Suction Dew Point Temperature	45 / 7.2
	Discharge Dew Point Temperature	130 / 54.4
	Suction Superheat	20 / 11.1
	Liquid Subcooling	15 / 8.3
Air-side Parameters	Indoor Air Inlet Temperature	80 / 26.67
	Outdoor Air Inlet Temperature	95 / 35

The system solver test matrix is presented in Table 4.2. The indoor heat exchanger air inlet temperature was chosen to range from 15°C below the design point to 5°C above the design point in increments of 1°C. The outdoor heat exchanger air inlet temperature was chosen to range from 8°C below the design point to 12°C above the design point also in increments of 1°C. As previously stated, the system solvers were designed to operate using a specified input value for either the system charge or the system subcooling. The nominal system charge was calculated by simulating each system using the subcooling specified by the design point. The specified system charge was varied by $\pm 30\%$ of the nominal system charge using a set of five different charge values. Similarly, the system subcooling was varied between 2°C and 10°C by increments of 1°C. The total number of operating points in the test matrix was $21 \cdot 21 \cdot 5 + 21 \cdot 21 \cdot 9 = 6174$. The test matrix for each cycle was run using the following three non-linear equation solvers: Newton's method, Broyden's method, and the Hybrid method. The purpose of choosing these nonlinear equation solvers was to study the performance of the classical Newton-Raphson method as compared to several quasi-Newton methods.

Table 4.2 System solver test matrix values

Parameter	Minimum [°F / °C]	Maximum [°F / °C]	Step [°F / °C]	No. of Points
Indoor Air Inlet Temperature	53.6 / 11.67	89.6 / 33.67	9/5 / 1.0	21
Outdoor Air Inlet Temperature	80.6 / 27.0	116.6 / 47.0	9/5 / 1.0	21
System Charge (M_{sys})	-30 %	+30 %	---	5
System Subcooling	3.6 / 2.0	18.0 / 10.0	9/5 / 1.0	9

4.2.5 Guess Value Calculations

For each unknown value an initial or guessed value must be determined and passed to the numerical equation solver. In solving any set of equations the likelihood of finding a solution is highly dependent on the accuracy of the guess values. Therefore, the effect of guess value accuracy has been studied by using two different approaches to determine guess values.

4.2.5.1 Design Point Guess Values

The first approach was to use the design point conditions in Table 4.1 to determine the required guess values. By using the values in Table 4.1 along with an assumed discharge superheat, evaporator superheat, and heat exchanger pressure drop, a guess value for each junction within the cycle can be easily calculated. This procedure is independent of the current operating condition and only utilizes the design point in determining the guess values.

4.2.5.2 Adjusted Guess Values

A set of more accurate guess values can be calculated by first running the components prior to attempting to solve the simulation. Running the components can provide information describing how the system is reacting to the current operating point. Since the high side pressure dictates both the amount of subcooling and calculated system

charge, the high side pressure can be iteratively adjusted to achieve a better initial point. This procedure requires that the components be run several times prior to running the system solver; however the better guess value can compensate for the computational time required to calculate more accurate guess values. The additional time spent running the components to determine accurate guess values must be considered when evaluating the system solver's performance utilizing the procedure.

4.2.6 Numerical Experiments

Each system solution procedure was tested with the previously described operating point test matrix using each of the previously listed numerical equation solvers with both the design point guess values and adjusted guess values. Thus, for each solution algorithm the operating test point matrix was run a total of eight times for each cycle configuration.

The implementation of Newton's method used in this study is based on the classical derivation using the Taylor series expansion of a vector valued function. The Newton step, which determines a new set of x variables closer to the solution, is evaluated through the calculation of the finite difference Jacobian. The Jacobian calculation requires n function evaluations, where n is the number of unknown variables, making it a costly operation. However, the full Newton step guarantees quadratic convergence once the solver is close to the solution. Broyden's method is a quasi-Newton, often called a secant method, which approximates the Jacobian using residual values from the previous iteration. The method converges super linearly as the solution is reached but is often done with far fewer function evaluations. Newton's method and Broyden's method are based on line searches. The Hybrid method is a quasi-Newton method based on the model trust region approach, which has been proven to be quite robust.

4.3 System Solver Performance Metrics

The results from the numerical experiments have been used to measure the robustness and efficiency of each solver.

4.3.1 Solver Robustness

The robustness for each solver has been quantified by determining the percentage of operating conditions in which the simulation did not solve. For a given operating condition the system solver might be unable to find the solution for the following three reasons:

- i. Current junction pressure and enthalpy values were out of the available range provided by the refrigerant property library
- ii. Allowed maximum number of iterations was reached
- iii. Equation solver stalled in the \bar{x} domain

It is possible for the equation solver to reach invalid values when attempting to find the solution since the equation solver lacks knowledge concerning the thermodynamic system being simulated. The junction pressure and enthalpies are provided by the equation solver, and thus it is possible for the equation solver to reach pressure and enthalpy values incompatible with the refrigerant property library. In this situation the system solver can no longer continue and must terminate prior to finding the solution.

A maximum number of iterations must be specified to the equation solver. If the equation solver should reach this limit the solution procedure must be terminated prior to reaching the solution.

In addition to the tolerance specified to the equation solver mentioned in Equation 2.25, an additional tolerance must be specified. Equation 4.4 calculates the change in x variables from iteration $i-1$ to iteration i . In this equation, ε_x is the specified tolerance in

the \bar{x} domain. An equation solver can converge based on the criteria of Equation 4.4 without satisfying the criteria mentioned in Equation 2.25, and thus the equation solver can terminate prior to reaching the actual solution. This situation can be monitored by analyzing the system energy balance and the calculated convergence criteria value upon solver termination and therefore can be taken into account when determining system solver robustness.

$$\|\bar{x}_i - \bar{x}_{i-1}\| \leq \epsilon_x \quad (4.4)$$

4.3.2 Computational Efficiency

The computational cost per iteration associated with each of the equation solvers varies depending on the method and therefore the number of iterations required to simulate a cycle cannot be used to characterize a solver's efficiency. The number of function evaluations required to reach the specified tolerance is a better metric of computational efficiency. With regard to the system solvers presented in this thesis, a function evaluation can be thought of as the number of times all the component models are executed. As previously stated, the number of times a component model is run must be taken into account when using the adjusted guess values. The number of times a component need to be run to attain a better guess depends on the current operating point. The average number of function evaluations required to attain a better set of guess values for the basic cycle was five.

4.4 Algorithms for Solving a Component-Based Vapor Compression System Simulation

This section describes the algorithms of each of three vapor compression system solvers evaluated in this investigation.

4.4.1 Junction Solver

In the Junction Solver algorithm the thermodynamic state at each junction is solved for simultaneously through the use of boundary pressure based components and junction level conservation equations (Richardson et al., 2004). Since all component models calculate the inlet and outlet mass flow rates using the inlet conditions and outlet pressure, the mass flow rates can be removed from the set of unknown variables in Equation 2.22. Thus, the set of unknown variables will contain an unknown pressure and an unknown enthalpy for each junction. For any system configuration with N_J junctions, the set of unknowns can be simplified as follows.

$$\bar{x} = [P_1 \quad \cdots \quad P_{N_J} \quad h_1 \quad \cdots \quad h_{N_J}]^T \quad (4.5)$$

The Junction Solver applies junction level conservation equations of mass and energy to satisfy the required number of residual equations. For a closed system, there are $N_J - 1$ unique junction mass balance equations and N_J unique junction energy balance equations, where N_J is the number of junctions in a given cycle. Equation 4.6 describes the junction mass flow balance residual equation.

$$r_{\dot{m}} = \sum_{i=1}^{N_{Ports,In}} \dot{m}_i - \sum_{i=1}^{N_{Ports,Out}} \dot{m}_i \quad (4.6)$$

Similarly, Equation 4.7 describes the junction energy balance residual equation, where h_J represents the current enthalpy value assigned to junction J .

$$r_{\dot{H}} = \sum_{i=1}^{N_{Ports,In}} \dot{m}_i h_i - \sum_{i=1}^{N_{Ports,Out}} \dot{m}_i h_J \quad (4.7)$$

These two sets of equations only provide $2N_J - 1$ equations when $2N_J$ equations are required to close the system of unknown variables. The additional closure equation required to simulate the system results from system specification type described in

Section 4.2.3. The flow chart in Figure 4.2 describes the Junction Solver solution procedure.

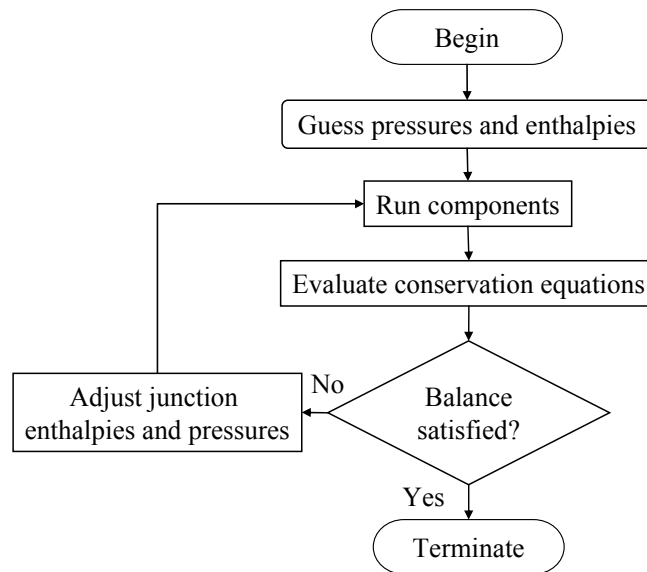


Figure 4.2 Flow chart describing the Junction Solver solution procedure

4.4.1.1 Junction Solver Advantages

The most obvious advantage of the Junction Solver, as shown in Equations 4.5 through 4.7, is the ease in which the algorithm can be extended to handle more advanced cycle configurations. The set of unknown variables and corresponding conservation equations can be easily constructed in a generic fashion to handle any system configuration. The order in which component models are executed is unimportant since component models are being executed simultaneously. Therefore, the Junction Solver can easily handle cycles with internal heat transfer such as cycles with a suction line heat exchanger. Refrigerant mass flow distribution due to splits and merges within the system are easily handled.

A less obvious advantage of this approach is the independence of component type. All components in the cycle are boundary pressure based components, and thus

distinction between different component types is not required. This advantage is most noticeable when the component models are being run, since the component models are not required to be run in a particular order. Consequently, the component models can be executed in parallel taking advantage of multiprocessor computers.

4.4.1.2 Junction Solver Disadvantages

The most noticeable disadvantage of this approach is the requirement that heat exchanger models implement the inlet/outlet pressure boundary condition. Boundary pressure based heat exchanger models require an additional iterative procedure to determine the refrigerant mass flow rate thus increasing the computational effort required to evaluate the model while decreasing the model's robustness.

This solution scheme fails to take advantage of the fact that enthalpies within the cycle are not completely independent. For example, if the suction enthalpy increases, the condenser inlet enthalpy also will increase. Additional iterations might be required to resolve the cycle since all junction enthalpies are treated as being independent of one another.

4.4.2 Enthalpy Marching Solver

In the Enthalpy Marching Solver, the thermodynamic state at each junction is determined by marching or propagating enthalpy around the cycle beginning at the junction connected to the compressor suction. In order to march the enthalpy around the cycle, the components must be executed in the order of refrigerant flow.

Unlike the Junction Solver, the Enthalpy Marching Solver utilizes both boundary pressure based and mass flow rate based component models. The Enthalpy Marching Solver requires that all flow control devices (e.g. compressors and expansion devices) operate using boundary pressures and all friction dictated components (e.g. heat

exchangers and pipes) operate using the mass flow rate based boundary condition. Thus, the compressor and expansion device models calculate the refrigerant mass flow rates and the heat exchanger models calculate the refrigerant pressure drop using the calculated refrigerant mass flow rates. Since enthalpy values are being marched around the cycle there is only one unknown enthalpy value, and thus all remaining unknown enthalpy values in Equation 2.22 can be removed and replaced by a single enthalpy value, h_1 . For the basic cycle shown in Figure 4.1a the set of unknown variables can be simplified to the following.

$$\bar{x} = [P_1 \quad P_2 \quad P_3 \quad P_4 \quad h_1]^T \quad (4.8)$$

Due to the marching nature of the solver and the fact that mixed boundary condition types are implemented, the junction level conservation equations cannot be directly applied to all junctions. An alternative set of equations must be formulated. In the Enthalpy Marching Solver, the conservation equations described in Equations 4.6 and 4.7 are applied only to junction 1. Since a pressure value is assigned to each junction, residual equations can be formulated using the pressure drop calculations performed by the heat exchanger models. In the following residual equation, $P_{HX,i}$ is the calculated outlet pressure for heat exchanger i and P_J is the pressure assigned to the downstream junction J .

$$r_P = P_{HX,i} - P_J \quad (4.9)$$

Equation 4.9 states that the calculated outlet pressure for a given heat exchanger must equal the pressure assigned to the corresponding downstream junction. For the basic cycle, Equations 4.6, 4.7, and 4.9 provide a total of four equations. The additional closure

equation required to simulate the system results from system specification type described in Section 4.2.3.

When simplifying Equation 2.22 to arrive at Equation 4.8, it is important to retain unknown pressure values for the inlet and outlet of each boundary pressure based component even though it is possible to eliminate certain pressure values when using mass flow rate based heat exchanger models. Taking the basic cycle as an example, it is possible to eliminate P_3 from Equation 4.8. The condenser takes the compressor mass flow rate, discharge pressure (P_2), and discharge enthalpy as input and calculates the outlet pressure and enthalpy. Therefore, it is possible to eliminate P_3 from Equation 4.8 and simply passing the outlet pressure from the condenser directly to the expansion device. This is not a feasible approach for two reasons. First, the two mass flow rate values being used to conduct the mass balance at junction 1 would no longer be independent of one another. Second, if there happen to be two condensers in parallel to one another, during iteration the outlet pressures of each heat exchanger might not be equal. The difficulty arises when determining how to propagate a pressure to the expansion device in this case.

The Enthalpy Marching Solver cannot directly handle parallel components without including additional variables to the set of unknowns described in Equation 4.8. Taking the advanced cycle in Figure 4.2b as an example, in order to provide each evaporator downstream of junction 4 with a unique mass flow rate a mass flow rate ratio must be added to list of unknown variables. For the advanced cycle, the vector of unknown variables is described in Equation 4.10.

$$\bar{x} = [P_1 \quad P_2 \quad P_3 \quad P_4 \quad P_5 \quad h_1 \quad r]^T \quad (4.10)$$

A comprehensive list of the residual equations for this cycle is included in Equation 4.11.

$$\vec{r} = \begin{bmatrix} \sum_{i=1}^3 \dot{m}_{Evap,i} - \dot{m}_{Comp} \\ \sum_{i=1}^3 \dot{m}_{Evap,i} h_{Evap,i,out} - \dot{m}_{Comp} h_1 \\ P_{Evap,1,out} - P_1 \\ P_{Evap,2,out} - P_1 \\ P_{Evap,3,out} - P_1 \\ P_{Cond,out} - P_3 \\ \text{Closure Equation} \end{bmatrix} \quad (4.11)$$

The flow chart in Figure 4.3 describes the solution procedure utilized by the Enthalpy Marching Solver.

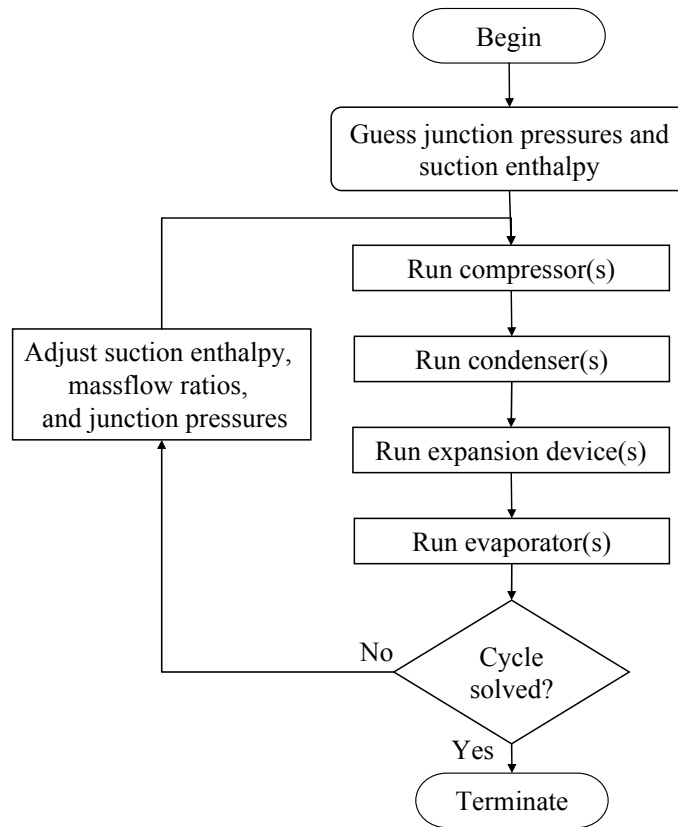


Figure 4.3 Flow chart describing the Enthalpy Marching Solver solution procedure

4.4.2.1 Enthalpy Marching Solver Advantages

The most noticeable advantage of the Enthalpy Marching Solver over the Junction Solver can be seen by comparing Equations 4.8 and 4.5. For simple cycles the Enthalpy Marching Solver needs to solve for fewer unknown variables. Since numerical equation solvers require the computation of the Jacobian, fewer variables will result in fewer component model executions per equation solver iteration. The Enthalpy Marching Solver also utilizes mass flow rate based heat exchanger models which are faster to execute as compared with pressure boundary condition models. This will have a large impact on computational time.

4.4.2.2 Enthalpy Marching Solver Disadvantages

The most noticeable disadvantage of the Enthalpy Marching Solver is the manner in which parallel components must be handled. For each additional parallel heat exchanger i , there will exist an additional unknown mass flow rate ratio, r_i . It is possible for the set of unknown variables for the Enthalpy Marching Solver to become larger than the corresponding set for the Junction Solver when the cycles become increasingly complicated. Since the components are being executed in a set order and enthalpy is being propagated around the cycle, cycles with internal heat exchange must be distinctly handled.

4.4.3 Decoupled Energy and Hydraulic Solver

The Decoupled Energy and Hydraulic Solver is quite similar to the Junction Solver, however the junction level mass and energy balances are solved separately. The solution procedure attempts to take advantage of the fact that the heat exchanger mass flow rates are primarily dictated by the junction pressures and the conservation of energy equations

are primarily dictated by the junction enthalpy values. This procedure is shown in Figure 4.4.

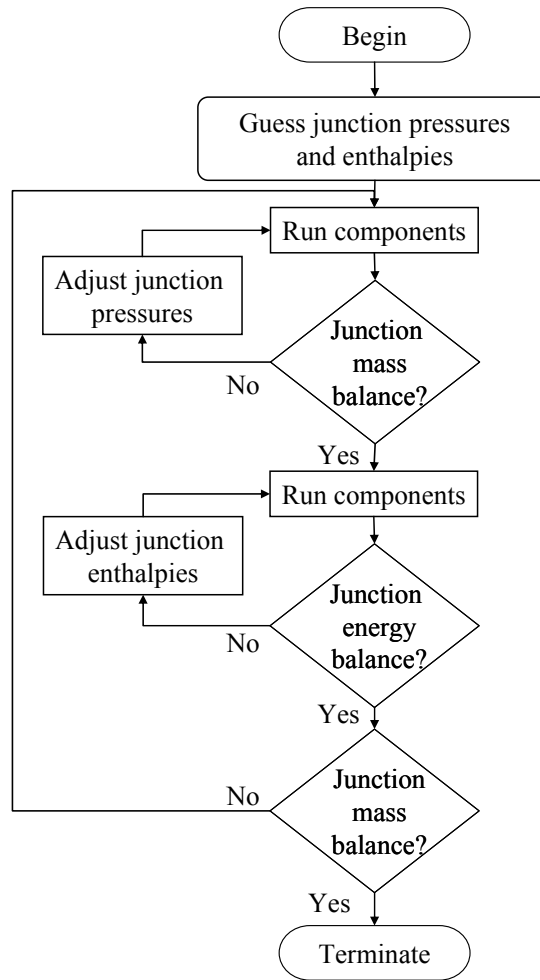


Figure 4.4 Flow chart describing the Decoupled Energy and Hydraulic Solver solution procedure

Since the algorithm attempts to simulate a cycle in two parts, there are two sets of unknown variables and residual equations used by the algorithm both of which are subsets of the variables and equations used by the Junction Solver. Equations 4.12 and 4.13 list the unknown variables in a decoupled format.

$$\bar{x}_{Hydraulic} = [P_1 \quad \cdots \quad P_{N_J}]^T \quad (4.12)$$

$$\bar{x}_{Energy} = [h_1 \quad \cdots \quad h_{N_J}]^T \quad (4.13)$$

The set of equations used to solve for the unknown pressures listed in Equation 4.12 are the junction level mass balances described in Equation 4.6 and the closure equation described in Section 4.2.3. Similarly, the set of equations used to solve for the unknown enthalpies in Equation 4.13 are the junction level conservation of energy equations described in Equation 4.7. Since there are N_J unique junction level conservation of energy equations an additional closure equation is not required to solve for the set of unknown enthalpies.

The junction enthalpies are held constant while the solver calculates the junction pressures and similarly, the component mass flow rates are held constant while the solver calculates the junction enthalpies. However, the compressor and expansion device mass flow rate tend to be quite dependent on the inlet enthalpy and therefore adjustment of the junction enthalpies might alter the junction mass balances. Thus, upon solving for the junction enthalpies the algorithm re-runs all the components using the updated pressures and enthalpies to determine if the mass flow balances are still satisfied. The procedure is repeated until the mass and energy balances are simultaneously satisfied.

4.4.3.1 Decoupled Energy and Hydraulic Solver Advantages

Since this algorithm is quite similar to the Junction Solver, the advantages listed for the Junction Solver apply to this algorithm as well. The general principle of this algorithm was adapted from an algorithm presented by Jiang (2003) for the steady state solution of a heat exchanger simulation using inlet/outlet pressures as the boundary condition. In the simulation of heat exchanger this algorithm has proven to be quite robust, and thus, it has been extended to simulate the entire vapor compression system.

4.4.3.2 Decoupled Energy and Hydraulic Solver Disadvantages

The disadvantages associated with the Junction Solver can be applied to this algorithm as well.

The outermost iteration of the solver is a fractional step method since the iterative procedure repeats the same calculations until convergence is met. A disadvantage of fractional step methods is the slow rate of convergence. Fractional step methods at best exhibit linear convergence. Figure 4.5 shows the residual value after each outer-most iteration of the Decoupled Energy and Hydraulic Solver. The plot shows that solver converges linearly at best since only one decimal place (at most) in accuracy is gained per iteration.

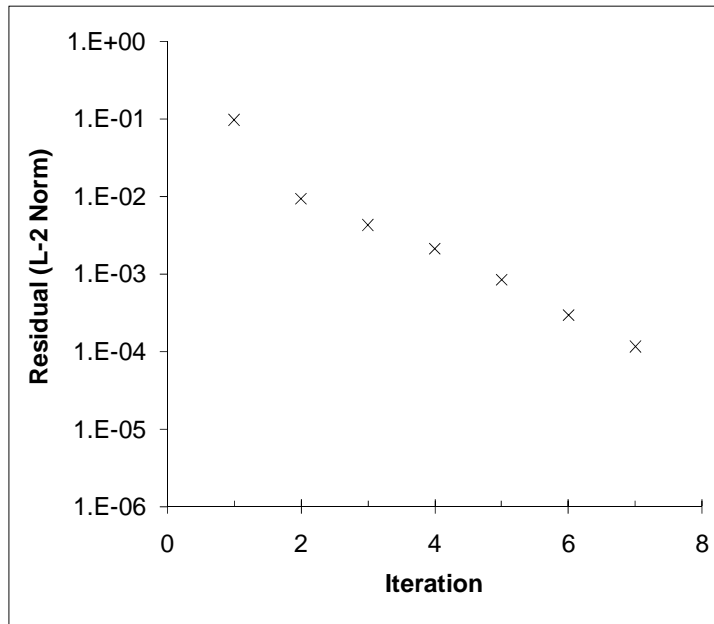


Figure 4.5 Fractional step convergence for the Decoupled Energy Hydraulic Solver

4.5 Results and Discussion

The test matrix results for the three solution algorithms simulating the standard vapor compression cycle displayed in Figure 4.1a are plotted in Figure 4.6 and the results for the three solvers are discussed in the following three sections. The results for the

vapor compression system with additional components shown in Figure 4.1b are plotted in Figure 4.7. The more complicated cycle configuration was not tested with the Decoupled Energy and Hydraulic Solver since the algorithm performed so poorly for the standard cycle configuration.

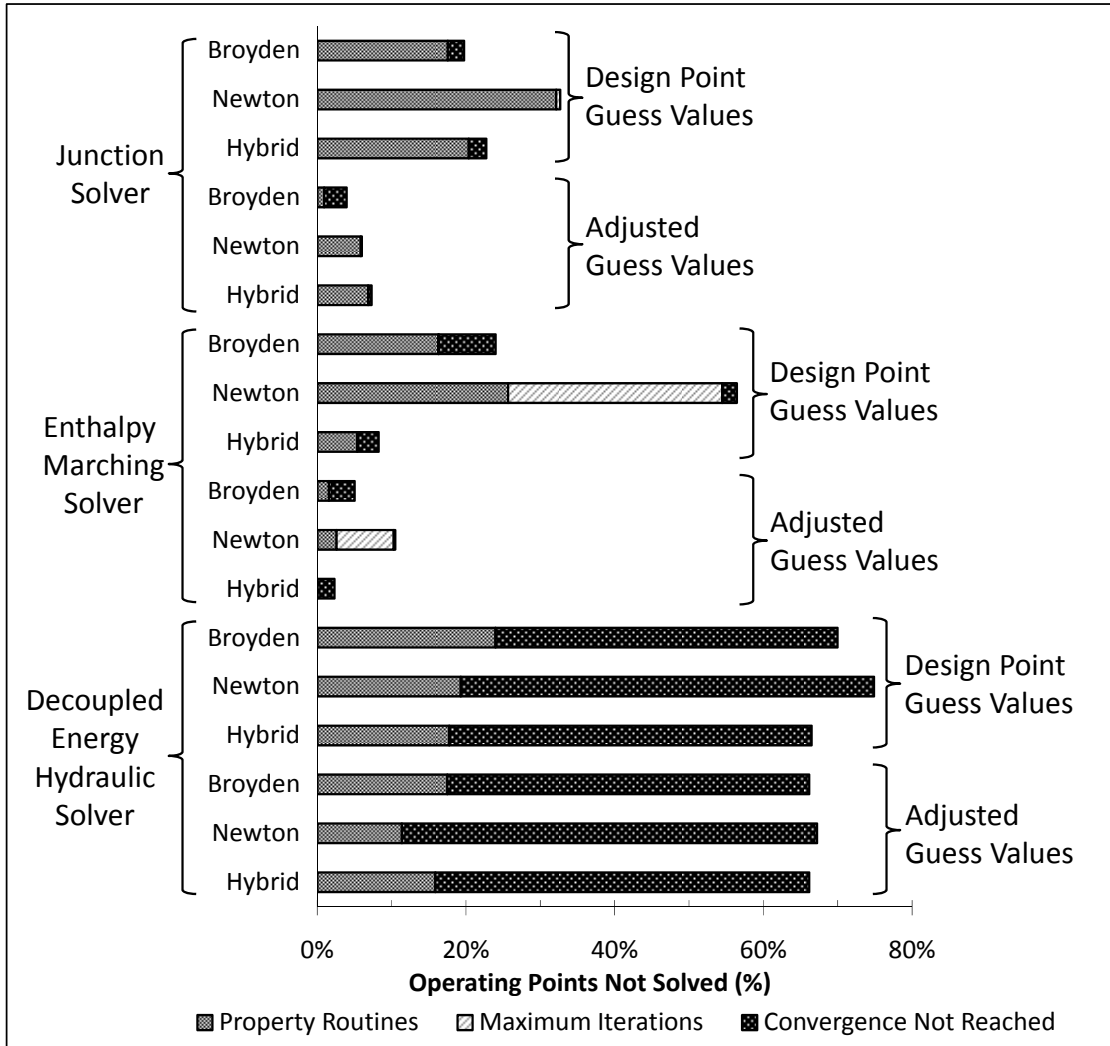


Figure 4.6 Standard cycle test matrix results

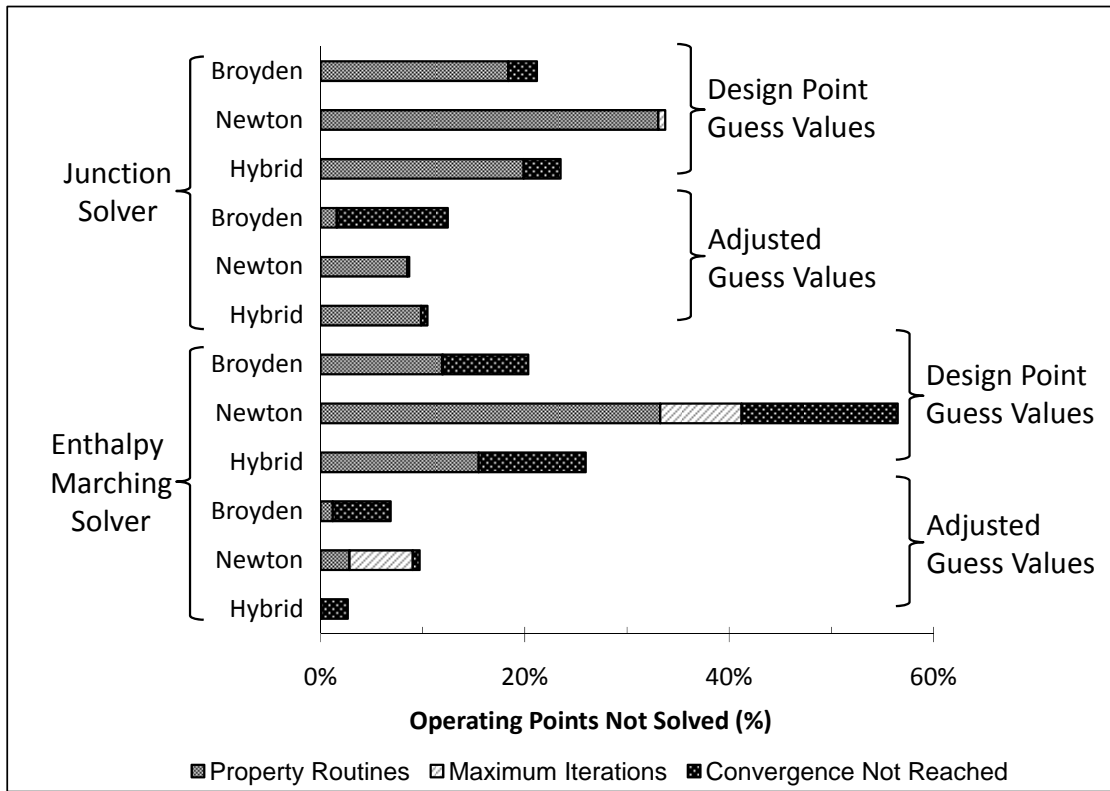


Figure 4.7 Advanced cycle test matrix results

The average number of function evaluations required to simulate the basic cycle for the various solvers are listed in Table 4.3.

Table 4.3 Average number of function evaluations required to simulate the basic cycle

System Solver Type	System Spec. Type	Design Point Guess Values			Adjusted Guess Values		
		Broy.	Newt.	Hybrid	Broy.	Newt.	Hybrid
Junction Solver	Charge	31.1	46.2	39.0	22.6	41.7	21.5
	Subcooling	21.3	43.7	18.0	17.7	40.8	16.2
	Overall	24.0	44.1	23.2	19.3	41.1	18.1
Enthalpy Marching Solver	Charge	26.3	33.4	26.9	19.6	29.9	17.1
	Subcooling	22.9	35.9	20.2	14.7	26.0	11.4
	Overall	23.8	35.2	22.2	16.4	27.4	13.4
Decoupled Energy & Hydraulic Solver	Charge	839.3	1067.4	4507.3	193.1	254.9	1138.4
	Subcooling	733.5	990.8	672.7	153.6	216.1	141.5
	Overall	771.9	1005.5	1980.5	166.8	228.7	472.7

4.5.1 Junction Solver Results

Broyden's method resulted in the highest percentage of successful runs for both types of guess value formulations when simulating the basic four component cycle. When using Broyden's method the Junction Solver was able to successfully simulate approximately 80% of the operating points when using the design point guess values and approximately 96% of the operating points when using the adjusted guess values. The results when using the Hybrid method were within 2% of the results when using Broyden's method.

The results were quite similar for the advanced cycle when using the design point guess values. However, not as many operating points were successfully simulated when using the adjusted guess values as for the basic cycle. Approximately 79% of the operating points were successfully simulated when using Broyden's method with the design point guess values. The results for all three solvers were within 2% of one another ranging from 88% for Broyden's method and 91% for Newton's method when using the adjusted guess values.

The results show that when using Broyden's method the Junction Solver successfully simulates approximately 8% more operating points for the basic cycle than it does for the advanced cycle. Even though the advanced cycle contains only two more unknown variables than the basic configuration, the number of components connected to the junctions has increased the number of terms in each junction level mass and energy balance equation. More specifically, the mass and energy balances at junctions 1, 3, and 4 are dependent on the behavior of more than one component model. This additional

complexity is compounded when parallel components are of different sizes resulting in a refrigerant mass flow distribution through the components.

As can be seen from Figure 4.6 and Figure 4.7 property routine errors are the most common reason for an operating point not being successfully simulated. This is in part due to the Junction Solver's solution algorithm. The Junction Solver uses junction pressure and enthalpy values passed from the equation solver to run the component models and calculate the residuals. Therefore, in this case the thermodynamic state at all junctions is determined by the values provided by the equation solver. Each component model uses the thermodynamic state of the upstream junction and a property routine library to calculate the corresponding thermophysical properties of the refrigerant. The equation solver is likely to take large steps for operating points when the initial residuals are large resulting in values incompatible with the property routine library.

Newton's method, which performed the worst in terms of robustness, also performed the worst in terms of speed. This behavior can be partially attributed to the fact that Newton's method evaluates the actual Jacobian on every iteration while the other two methods use an approximation to the Jacobian after the first iteration. On average, the Hybrid method was one function evaluation faster than Broyden's method. Using the adjusted guess values with either Broyden's method or the Hybrid method resulted in approximately five fewer required function evaluations. Therefore, there was little or no additional computational cost associated with determining a better set of guess values since approximately five additional function evaluations were used in determining the better guess values.

4.5.2 Enthalpy Marching Solver Results

The Hybrid method had the highest rate of success when simulating the basic cycle when using either the design point guess values or the adjusted guess values. The Enthalpy Marching Solver using the Hybrid method successfully simulated approximately 92% of the test matrix when using the design point guess values, which corresponds to approximately 12% more operating points than the Junction Solver using Broyden's method. The percentage of successfully simulated test points increased to approximately 98% when using the adjusted guess values. The Hybrid method did significantly better with the Enthalpy Marching solver than either Newton's or Broyden's method.

The Hybrid method was not as successful when simulating the advanced cycle when using the design point guess values; however the results for Broyden's method and Newton's method were quite similar to the results for the basic cycle. The Hybrid method only simulated 0.3% less operating points than basic cycle when using the adjusted guess values. The results for Broyden's method and Newton's method when used to simulate the advanced cycle were also quite similar to the results for the basic cycle when using the adjusted guess values. A contributing factor to the dependence on the type of guess value calculation for the advanced cycle is the guess value used for the mass flow rate ratio, r . It is not possible to attain a reasonable guess for the mass flow rate ratio without running the parallel evaporators at least once. Therefore, when using the design point guess values the only reasonable guess value for the mass flow rate ratio is 0.5. However, the component models are run at least a single time when using the adjusted guess values and a significantly more accurate mass flow rate ratio can easily be estimated.

Unlike the Junction Solver, the robustness of the Enthalpy Marching solver does not change much between the basic and advanced cycles. Similar to the Junction Solver two additional unknown variables must be solved for, namely P_5 and r ; however the total number of unknown variables is still less for the Enthalpy Marching Solver. When looking at the residual equation formulation for this cycle, only two of the seven residual equations have increased in complexity.

As shown in Figure 4.6 and Figure 4.7, the solver terminating prior to reaching convergence is the primary reason for an operating point not being simulated when using the adjusted guess values. The single energy balance residual equation is most often the equation that fails to converge. The equation solver must vary the suction enthalpy in an attempt to satisfy the energy balance described in Equation 4.11. The enthalpy value provided by the equation solver is marched around the cycle by running the various component models and is ultimately used to determine the evaporator outlet enthalpy. The equation solvers on occasion have difficulty determining the suction enthalpy required to satisfy the junction 1 energy balance.

Property routine errors are not a significant cause of unsuccessful simulations when using adjusted guess values with either Broyden's method or the Hybrid method. The Enthalpy Marching Solver contains only a single enthalpy value in the set of unknowns regardless of the cycle configuration, whereas the set of unknowns for the Junction Solver contain an enthalpy value for each junction in the cycle. Therefore, provided that the suction enthalpy supplied by the equation solver is valid, the calculated enthalpy at all remaining junctions will also be valid.

The component boundary condition type implemented by the Enthalpy Marching Solver also plays a role in the solver's robustness. In the Junction Solver the component mass flow rates are calculated using the corresponding junction pressures, and therefore the junction pressures must be adjusted to achieve the junction mass and energy balances. In the Enthalpy Marching Solver the heat exchangers operate taking the mass flow rate as input which reduces the dependence on the junction pressures supplied by the equation solver. Therefore, the equation solver is less likely to provide pressure values outside the applicable range of the property routine library.

As seen in Table 4.3, the Enthalpy Marching Solver was computationally more efficient than the Junction Solver. The Enthalpy Marching Solver required approximately 4.5 fewer function evaluations than the Junction Solver when using the adjusted guess values. The Enthalpy Marching Solver performance saw much benefit from using adjusted guess values. Approximately nine fewer function evaluations were required when using the adjusted guess values; resulting in a net decrease in approximately four function evaluations.

4.5.3 Decoupled Energy and Hydraulic Solver Results

The choice of equation solver did not have a significant impact on the results. The solver failed to find a solution for nearly 70% of the operating points and the use of adjusted guess values did not have a noticeable impact on the performance of the solver. Convergence was not reached for approximately 50% of the operating points and the remaining points that did not solve failed due to property routine errors.

As previously mentioned, this algorithm was originally implemented by Jiang (2003) for the steady state simulation of a heat exchanger model using inlet/outlet pressures as the type of boundary condition. Jiang essentially treats each heat exchanger

tube as a component and solves for the pressure distribution throughout the heat exchanger on a per tube basis. The Decoupled Energy and Hydraulic algorithm was adapted to simulate a system since it was proven to be quite robust when simulating a heat exchanger. However, as the results have shown the algorithm performs quite poorly when simulating an entire vapor compression system. This can be explained by analyzing some of the differences between the simulation of a heat exchanger and the simulation of the entire vapor compression system.

In both cases the pressures at each junction are being solved for by conducting junction level mass balances. However, a heat exchanger is an open system and thus there are N_J independent junction mass balances. The vapor compression system is a closed system and thus there are only N_J-1 independent junction level mass balance equations. In both cases there are N_J unknown pressures and therefore the closure equation is required when simulating the closed system. The closure equations previously described are strongly dependent on the junction enthalpy values which creates an inherent coupling between the hydraulic and energy solver. This coupling cannot be avoided due to the nature of the unknown variables and the equations being formulated to solve for these variables. The open system simulation is at an advantage in this case.

The use of specified inlet and outlet pressure when simulating a heat exchanger provides a known range of the junction pressures since all junction pressures must lie between the inlet and outlet pressures. However, the range of junction pressures is unknown when simulating a system.

The mass flow rate calculations performed by a heat exchanger are relatively independent of the enthalpy calculations. However, the expansion device component in

the vapor compression is very sensitive to changes in the inlet enthalpy. This is because the inlet density of the expansion device is very dependent on the inlet enthalpy and thus small changes in the inlet enthalpy can greatly affect the mass flow rate calculation. Therefore, the mass flow calculation can be dramatically altered after the solver exits the energy loop. In the case of the heat exchanger, the mass flow rate calculations won't require much adjustment after running the energy portion of the solver.

The advanced cycle was not tested with the Decoupled Energy and Hydraulic Solver since the algorithm performed so poorly for the basic cycle.

4.5.4 System Input Specification Type Comparison

The results shown in Figure 4.8 show the effect of the type of system input specification used in the simulation. The results plotted in Figure 4.8 are for the Enthalpy Marching Solver using adjusted guess values; however the trends in this figure are consistent for the other solvers as well.

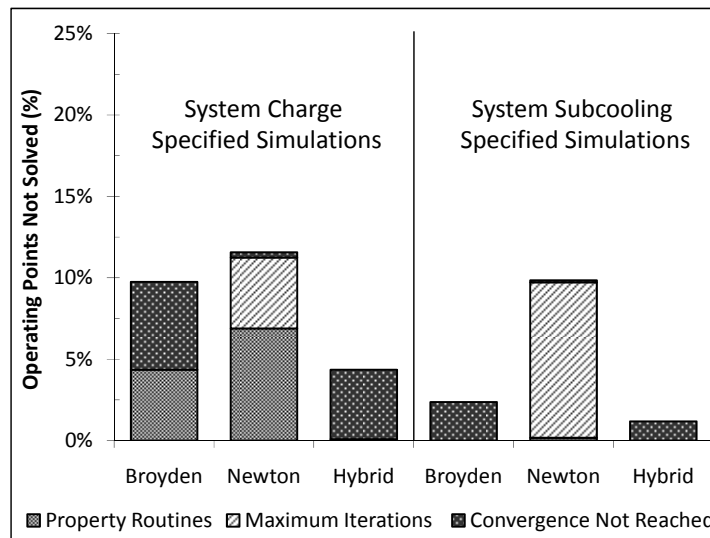


Figure 4.8 Enthalpy Marching Solver results based on simulation specification type

The three solution schemes are more robust when solving a system when the subcooling has been specified. The type of errors between the two specification types

also differs. As previously stated, the only difference between the two types of system specification is the closure equation used in the set of residual equations. The contributing factor to this difference in robustness is the sensitivity of the heat exchanger void fraction correlation to changes in the junction pressures. The calculated system charge can have sudden changes based on the refrigerant phase at the condenser outlet since one or two degrees of subcooling can change the calculated charge by approximately 20%. This problem does not exist for subcooling specified cycles since the residual is formulated using the enthalpy at the condenser outlet. It is this difference that results in property routine errors for the charge specified cycles and not the subcooling specified cycles. The equation solvers tend to use infeasible values when attempting to adjust the junction pressures when conducting the charge balance.

4.5.5 Numerical Equation Solver Convergence Comparison

In order to compare the computational cost associated with the different equation solvers it is important to analyze the convergence trends for a given simulation. In order to fairly evaluate the three equation solvers the number of function evaluations required to reach the specified tolerance was analyzed. A computationally expensive operating point, meaning an operating point relatively distant from the design point, from the test matrix was chosen to illustrate the difference between the three equation solver types. The results are shown for the Enthalpy Marching Solver in Figure 4.8.

As can be seen from the plot, Newton's method was the most computationally expensive and required 36 function evaluations to determine the final solution. This is due to the fact that Newton's method calculates the Jacobian to perform each iteration step, which also explains the step-by-step trend displayed in Figure 4.9 (Press et al., 1992). Broyden's method required 27 function evaluations to reach the final solution.

This method uses an approximation of the Jacobian at every iteration. Thus, the method often requires fewer function evaluations than Newton's method. Figure 4.9 shows that the convergence tends to oscillate slightly as the solver is converging. This can be attributed to the fact that the Jacobian is being approximated and the actual Jacobian is only calculated at the start of the solution procedure.

The Hybrid method was most efficient and only required 19 function evaluations to reach the solution. As can be seen from Figure 4.9, the Hybrid method calculated the Jacobian only twice compared to six times for Newton's method.

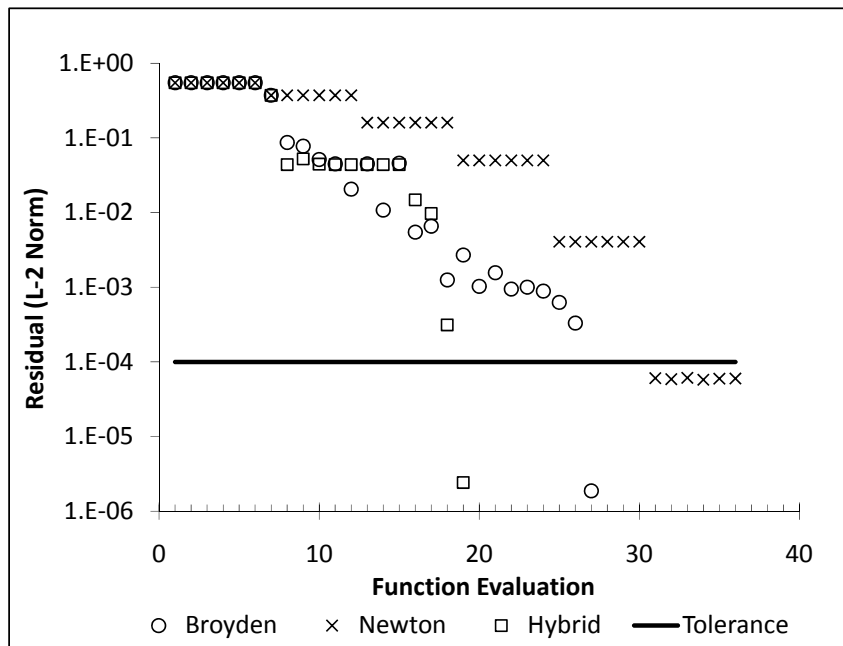


Figure 4.9 Solver convergence for the Enthalpy Marching Solver

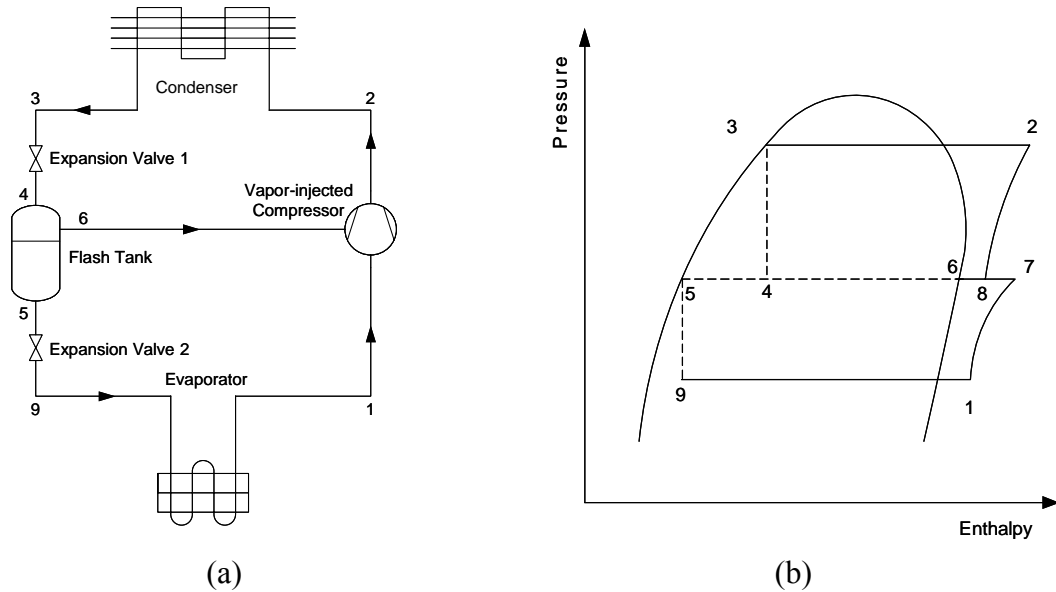
5 Steady State Simulation of Additional Cycle Types

The component-based nature of the Enthalpy Marching Solver presented in Chapter 4 allows it to be easily extended to simulate additional types of vapor compression systems. This chapter demonstrates this capability and describes the solution procedure to simulate two additional cycle types: the two stage flash tank cycle and a cascade vapor compression system. Both solvers were independently validated.

5.1 Two Stage Flash Tank Cycle

A two-stage flash tank cycle (FTC), as shown in Figure 5.1a, contains two additional components compared to the standard vapor compression cycle, namely an additional expansion valve and a flash tank separator. The standard compressor has been replaced with a vapor injected compressor where refrigerant is injected into an intermediate suction port of the compressor.

The corresponding cycle plotted on a P-h diagram is shown in Figure 5.1b. In a two-stage flash tank cycle the condensed liquid leaving the condenser is first throttled through the first stage expansion device and the two-phase refrigerant (state point 4) enters in the flash tank separator. In the flash tank the liquid and vapor components of the two-phase mixture are separated. The saturated vapor refrigerant is injected at an intermediate compressor suction port and the saturated liquid refrigerant is throttled through the second stage expansion device prior to entering the evaporator.



(a)
 (b)
Figure 5.1 Diagram of a two-stage flash tank cycle

5.1.1 Two Stage Flash Tank Cycle Solution Procedure

The simulation procedure used to model the vapor injection flash tank cycle, as shown in Figure 5.2, differs from the basic vapor compression system due to the constraint placed on the system by the assumption used to model the flash tank component. The flash tank component was modeled assuming saturated vapor ($x_5 = 1$) enters the intermediate suction port of the compressor and saturated liquid ($x_4 = 0$) enters the low stage expansion valve. During the experimental investigation of the flash tank cycle, it was determined that the flash tank performance was very sensitive to the high stage expansion valve setting. If the high stage expansion device was not set within a very narrow range, the flash tank would either completely fill with liquid refrigerant or completely drain of liquid refrigerant. Since the flash tank performance was highly dependent on the high stage expansion valve diameter, it was determined that the high stage expansion valve diameter should be output from the system simulation. Therefore,

the high stage expansion valve and flash tank were lumped together in a single component model (representative of the box surrounding the high stage expansion valve and flash tank). The high stage expansion valve diameter was calculated using the compressor discharge mass flow rate and assuming saturated vapor and saturated liquid were exiting the flash tank at a pressure of P_5 . The pressure drop through the flash tank was neglected, and thus the pressure at the inlet to the low stage expansion valve was set equal to P_5 .

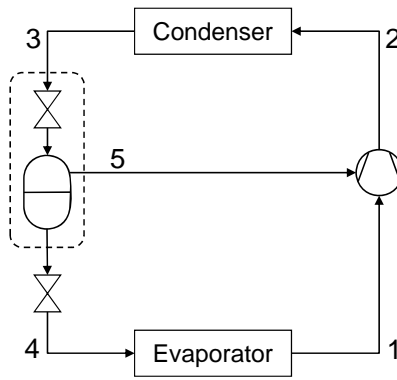


Figure 5.2 Diagram of two-stage flash tank cycle as modeled

Similar to the standard vapor compression system, the state point pressures and suction enthalpy are chosen as the unknown parameters that are iteratively solved for by the system solver. The injection enthalpy is required to execute the compressor model; however the injection enthalpy is easily calculated using the flash tank modeling assumption that saturated vapor is being injected into the compressor. The remaining state point enthalpies and the system mass flow rate are calculated as the solution procedure iterates.

Similar to the simulation of the standard vapor system, solution to the flash tank cycle commences with the execution of the compressor model using the suction enthalpy and pressure (h_1 and P_1), injection enthalpy and pressure (h_5 and P_5), and the discharge

pressure (P_2). The calculated compressor discharge mass flow rate and enthalpy are propagated to the condenser. The condenser calculates the enthalpy at state point 3 and an outlet pressure using pressure drop correlations. The high stage expansion valve/flash tank component is then run using the pressure at state point 3 (P_3), the condenser outlet enthalpy, compressor discharge mass flow rate, and pressure at state point 5 (P_5). The low stage expansion valve calculates a low side mass flow rate using the pressure at state point 5 (P_5) and corresponding saturated liquid enthalpy along with the pressure at state point 4 (P_4). The expansion valve mass flow rate and outlet enthalpy along with the pressure state point 4 (P_4) are then used to run the evaporator. The evaporator calculates an outlet enthalpy and pressure. The set of unknown values are shown in Equation 5.1.

$$\bar{x} = \begin{bmatrix} P_1 \\ P_2 \\ P_3 \\ P_4 \\ P_5 \\ h_1 \end{bmatrix} \quad (5.1)$$

The corresponding set of residual equations is shown in Equation 5.2.

$$\bar{r} = \begin{bmatrix} h_1 - h_{evap,out} \\ \dot{m}_{exp,low} - \dot{m}_{suction} \\ \dot{m}_{flash,vap} - \dot{m}_{injection} \\ P_3 - P_{cond,out} \\ P_1 - P_{evap,out} \\ h_{SC} - h_{cond,out} \end{bmatrix} \quad (5.2)$$

5.1.2 Two Stage Flash Tank Cycle Validation

An 11 kW R410A residential system with a scroll compressor was tested, by Wang (2008), at two cooling mode operating points and three heating mode operating points according to ASHRAE Standard 37-2005 (ASHRAE, 2005). The system was also tested

at an extended condition, which were an extreme high temperature for the cooling mode and an extreme low temperature for the heating mode. The operating test conditions are summarized in the Table 5.1. The baseline system was a standard vapor compression system and was tested at three additional operating points (and the validation results are included here for completeness). The flash tank cycle was tested at various injection pressures for each operating point. In total, the baseline system was tested at 10 operating points (4 cooling and 6 heating) and the flash tank cycle was tested at 42 operating points (24 cooling and 18 heating).

Table 5.1 ASHRAE test conditions and extended condition

Cooling					Heating				
Test	Indoor		Outdoor		Test	Indoor		Outdoor	
	DB (°C)	WB (°C)	DB (°C)	WB (°C)		DB (°C)	WB (°C)	DB (°C)	WB (°C)
A	26.7	19.4	35.0	N/A	High 1	21.1	≤15.6	16.7	14.7
B			27.8		High 2			8.3	6.1
Extended			46.1		Low			-8.3	-9.4
					Extended			-17.8	N/A

The indoor and outdoor heat exchangers were simulated using CoilDesigner, a heat exchanger simulation tool originally presented by Jiang (2003), and the details concerning the heat exchanger parameters can be found in Wang (2008). Each operating point was simulated using the experimental subcooling and superheat as input.

The system capacity and power consumption validation results for the baseline system are shown in Figure 5.3 and Figure 5.4. The average relative error in the system capacity was 4.8% with a maximum error of 12.4%. The system capacity of 8 of the 10 operating points was predicted to within $\pm 5\%$; however in all cases the capacity was over predicted by the simulation. The compressor power was simulated with an average error 4.2% with a maximum relative error of 6.5%. The compressor power consumption was

under predicted for all the operating points and the error in the power consumption was less than 5% for 7 of the 10 cases. The operating points with the largest error were the high ambient cooling case and the lowest ambient heating cases. The manufacturer coefficients for this compressor model were generated using test data at an ambient temperature of 35°C. Since the heat transfer between the compressor shell and the ambient was neglected, there is a high amount of error in the compressor simulation when the ambient temperature is significantly different from 35°C.

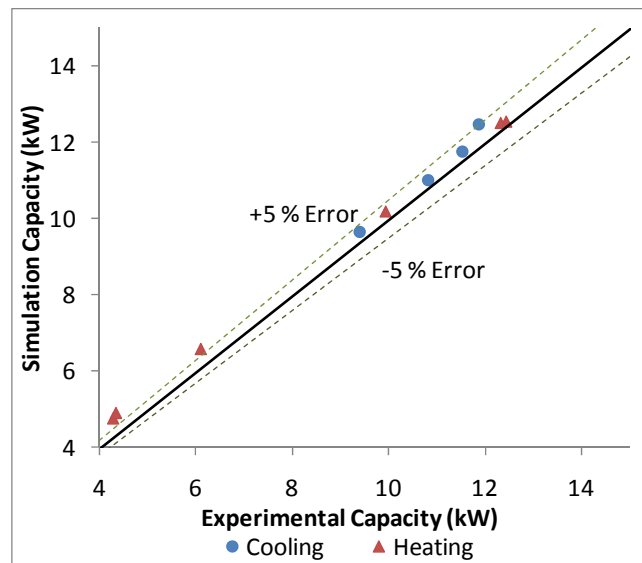


Figure 5.3 Baseline cycle validation results for system capacity

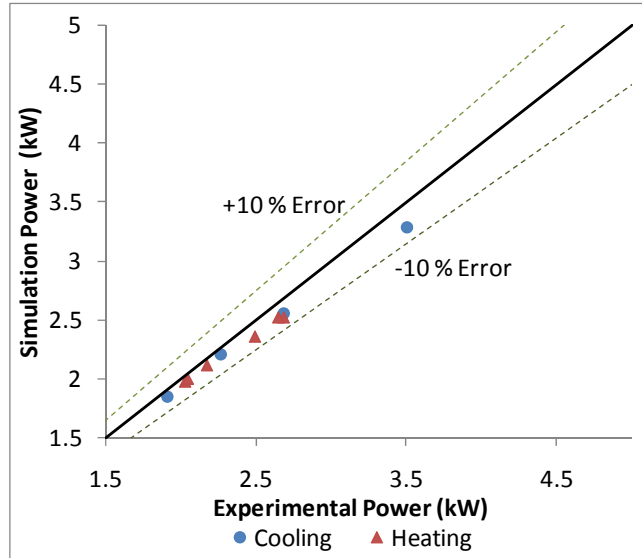


Figure 5.4 Baseline cycle validation results for compressor power consumption

As shown in Figure 5.5, the simulation accurately predicts the system mass flow rate with an average error of 3.4% and a maximum relative error of 7.2%.

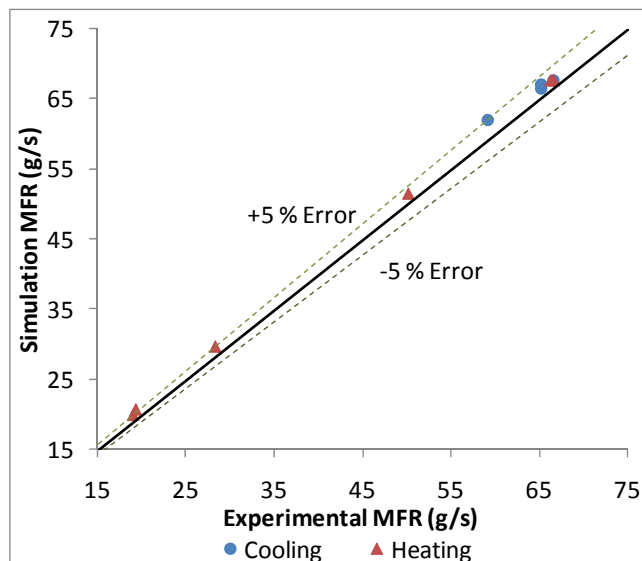


Figure 5.5 Baseline cycle validation results for system mass flow rate

The system capacity and power consumption validation results for the flash tank cycle are shown in Figure 5.6 and Figure 5.7. The average relative error in the system capacity was 1.3% with a maximum error of 4.5% and 31 of the 42 points falling within $\pm 2\%$. The compressor power consumption was predicted with an average relative error of

4.0% with a maximum error of 15.3% and 29 of the 42 points falling within $\pm 5\%$. Similar to the baseline system, the points with the most significant error were those operating points with the highest and lowest ambient temperatures.

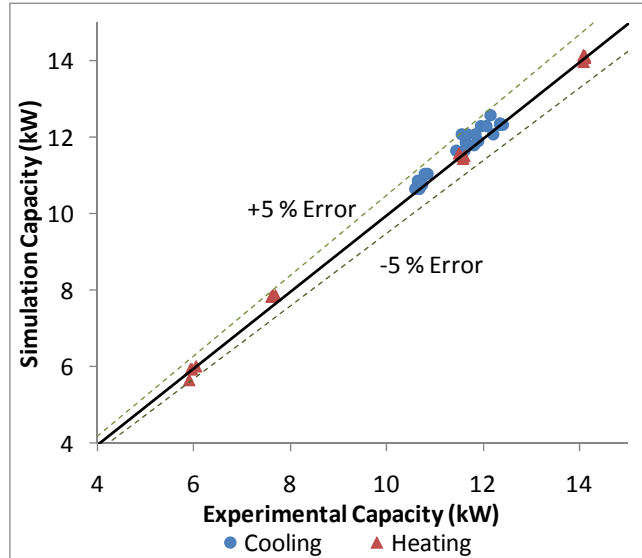


Figure 5.6 Flash tank cycle validation results for system capacity

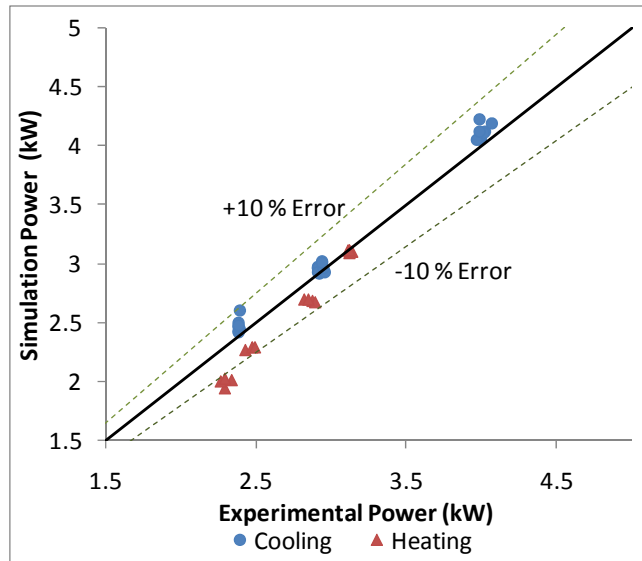


Figure 5.7 Flash tank cycle validation results for compressor power consumption

Figure 5.8 shows the suction and injection mass flow rates for the flash tank cycle. The suction mass flow rate was predicted with an average relative error of 1.2% and a maximum relative error of 6.1% with 38 of the 42 points falling within $\pm 3\%$ of the

experimental values. The injection mass flow rate was not as accurately predicted and had an average relative error of 10.3% and a maximum relative error of 45.6%. The maximum relative error corresponds to an absolute error of 3.9g/s, which does significantly affect the discharge mass flow rate. The high error of the simulated injection mass flow rate could have been a result of the flash tank modeling assumption of ideal phase separation. Even though sight glasses were used in the experiment to ensure saturated vapor was being injected into the compressor, it is possible that the injected refrigerant was indeed a high quality two phase mixture which results in a higher injection mass flow rate due to the increase in the injection refrigerant density.

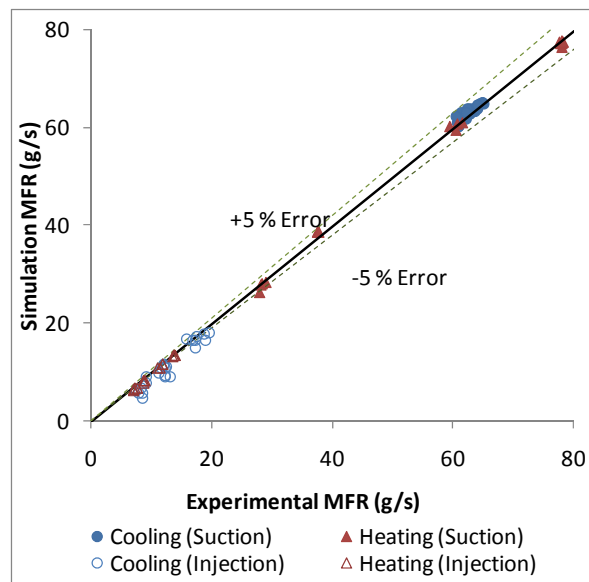


Figure 5.8 Flash tank cycle validation results for system mass flow rate

5.2 Cascade Vapor Compression System with Multiple Components

A simple cascade vapor compression system is shown in Figure 5.9. The system consists of two conventional vapor compression systems coupled through a cascade condenser. The evaporator in the low temperature system absorbs heat from the refrigerated space. The heat absorbed by the low temperature evaporator along with the

work input from the low stage compressor is rejected to the high temperature vapor compression system through the cascade condenser. The heat transferred to the high temperature vapor compression system in the cascade condenser and the work input from the high stage compressor is rejected in the primary condenser. One of the main benefits of such systems is that various refrigerants suitable for the corresponding temperature range can be used in each stage.

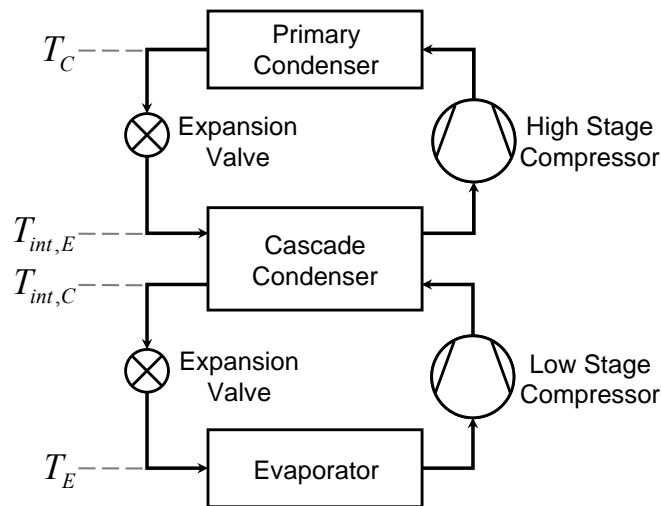


Figure 5.9 Diagram of a cascade vapor compression system

The use of a conventional HFC refrigerant, such as R404A, as the high temperature refrigerant along with CO₂ as the low temperature refrigerant is a suitable combination for low temperature refrigeration. In an R404A/CO₂ cascade system the heat rejection of the low temperature system occurs at a much lower temperature than a conventional CO₂ vapor compression system. The heat rejection occurs at a temperature below the critical temperature resulting in a higher COP.

In a conventional vapor compression system there are two temperature levels, namely the evaporating temperature, T_E , and the condensing temperature, T_C . For a properly designed system, these temperature levels are ultimately dictated by the

temperatures of the conditioned space and ambient. However, in a cascade system there are four temperature levels; the two additional temperatures being the condensing temperature of the low temperature system, $T_{int,C}$, and the evaporating temperature of the high temperature system, $T_{int,E}$. The two intermediate temperatures drive heat transfer from the low temperature system to the high temperature system. The four temperature levels for an ideal cascade vapor compression system are shown on the T-s diagram depicted in Figure 5.10. The corresponding P-h diagram is shown in Figure 5.11. Despite the carbon dioxide cycle operating in the subcritical region, the operating pressures remain higher than the corresponding pressures in the R404A high temperature system.

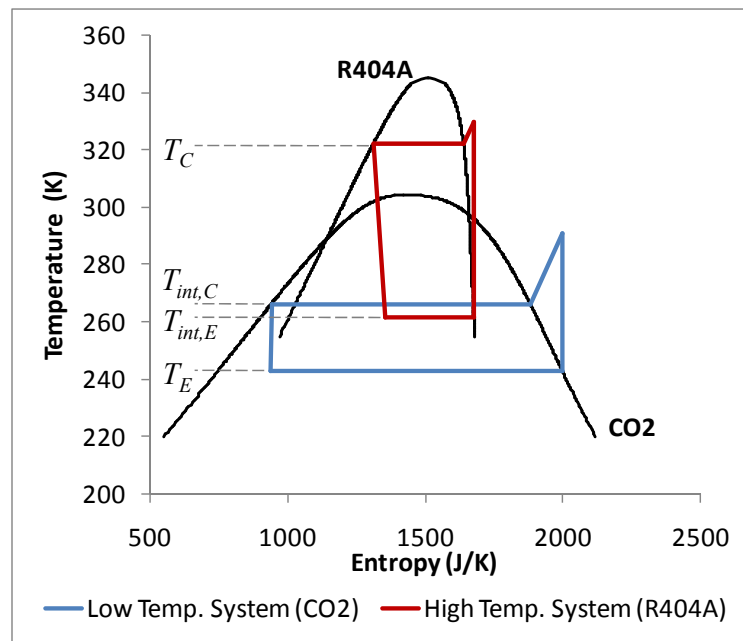


Figure 5.10 Temperature entropy diagram of a theoretical cascade system

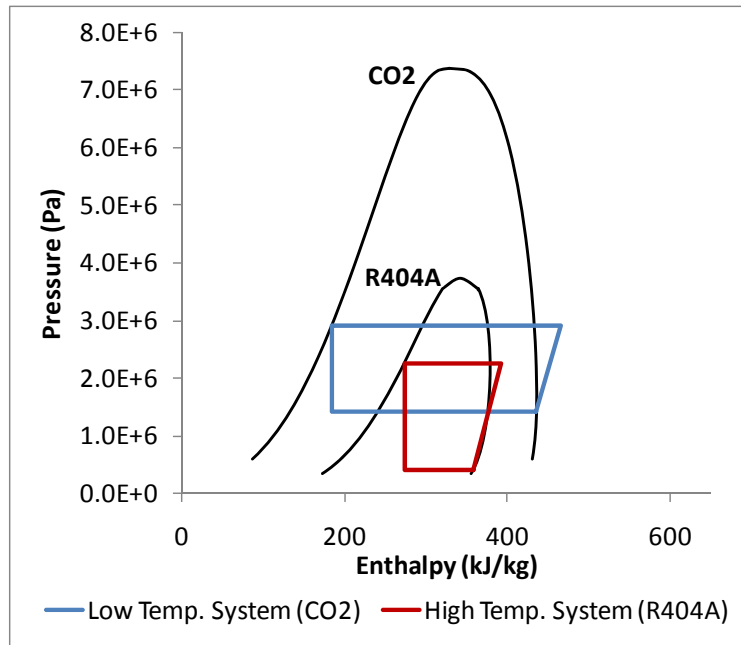


Figure 5.11 Pressure enthalpy diagram of a theoretical cascade system

5.2.1 Cascade System Solution Procedure

One approach to simulating a cascade vapor compression system is to simulate the low and high temperature systems individually, using the Enthalpy Marching Solver. In the system shown in Figure 5.12, the heat rejection in the condenser is being absorbed by a secondary fluid. Prior to simulating this system, the secondary fluid inlet condition and mass flow rate is typically specified prior to executing the condenser model. If the system shown in Figure 5.12 was being used as the low temperature system in a cascade vapor compression system, the secondary fluid inlet condition and mass flow rate would be provided through simulation of the high temperature system. Typical low temperature systems in cascade vapor compression systems contain additional components compared to a conventional vapor compression system. Thus, a generalized solution approach to solve non-cascade vapor compression system containing multiple components should be

implemented to handle complex system configurations, and this requirement is met with the Enthalpy Marching Solver.

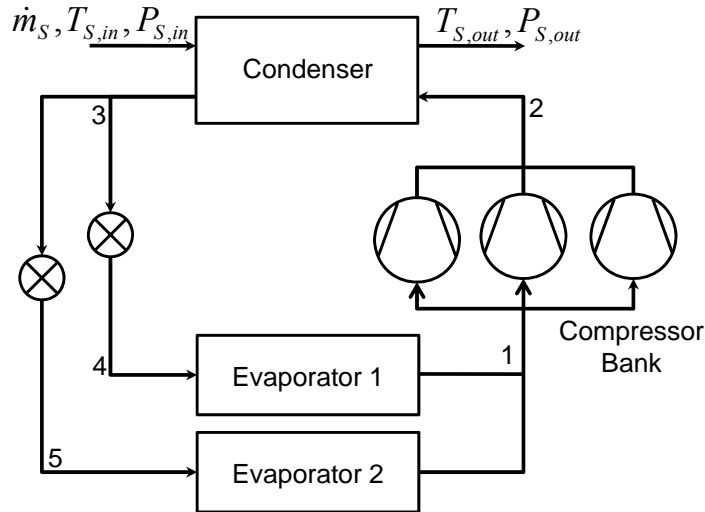


Figure 5.12 Diagram of a multi-component vapor compression system

As previously mentioned, in a cascade system heat is transferred from the low temperature system to the high temperature system through the cascade condenser. The cascade condenser model serves as the condenser in the low temperature system and evaporator in the high temperature system.

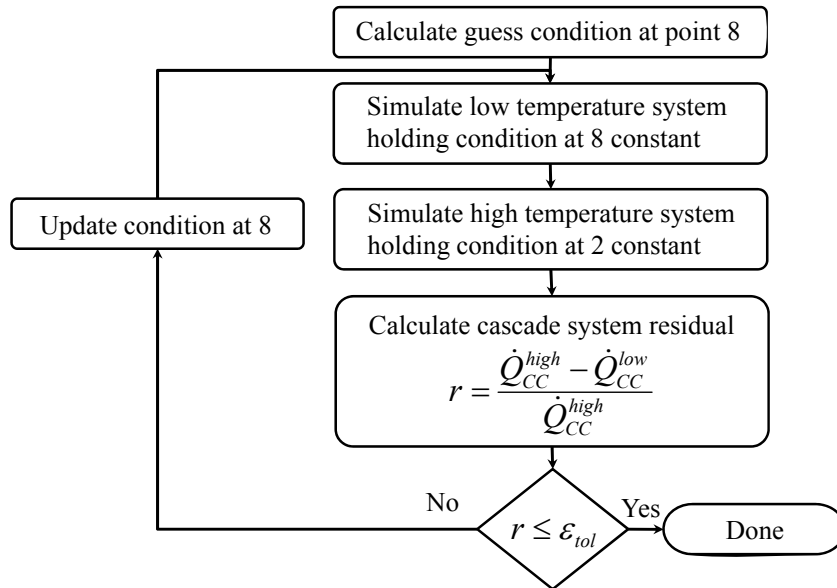


Figure 5.13 Flow chart describing the cascade simulation solution approach

A flow chart describing the approach implemented to simulate the cascade system is shown in Figure 5.13. The solution procedure starts by guessing an inlet condition to the cascade condenser at the point of the high temperature system evaporator inlet (state point 8 in Figure 5.14). Using the guessed condition and holding that condition constant, the Enthalpy Marching Solver is used to solve the low temperature vapor compression system. Upon arriving at the solution, the inlet condition to the cascade condenser in the low temperature system will be determined (state point 2 in Figure 5.14). This condition is then held constant while the high temperature vapor compression system is solved. Since state point 8 is likely to change after simulating the high temperature system, the cascade condenser heat load of the low temperature system and high temperature system will not match. Since under steady state operation the heat being rejected from the low temperature system must equal the heat being absorbed by the high temperature system, state point 8 is successively updated until the calculated heat load of the cascade condenser is equivalent in both the low and high temperature systems. A normalized residual, r , is used to determine if the solution procedure has reached convergence, as shown in Equation 5.3.

$$r = \frac{\dot{Q}_{CC}^{high} - \dot{Q}_{CC}^{low}}{\dot{Q}_{CC}^{high}} \quad (5.3)$$

In the above equation, \dot{Q}_{CC}^{high} is the cascade condenser heat load calculated when the model is being run as the evaporator in the high temperature system, and similarly \dot{Q}_{CC}^{low} is the cascade condenser heat load calculated when the model is being run as the condenser in the low temperature system. A tolerance value of 1.0E-4 was used to determine if the

cascade solver converged, which corresponds to an error between the two capacities of less than 1W for a 10kW system.

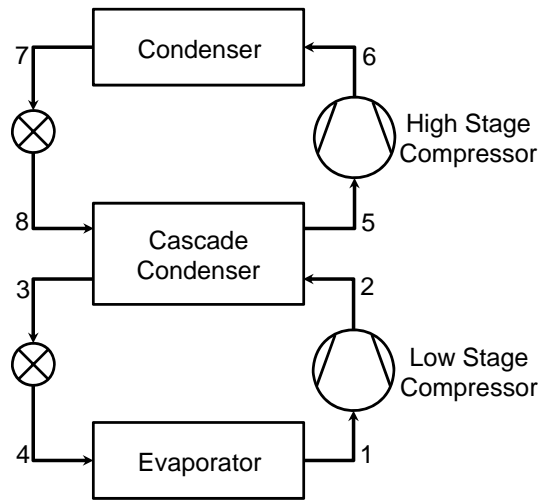


Figure 5.14 Diagram of a cascade vapor compression system junction numbers

As a general note, the high and low temperature systems can handle the cascade condenser model very elegantly since an object-oriented component-based framework has been used to implement the solver. The cascade condenser component model is only loaded once in the computer memory, however the component model is added to both the low and high temperature systems. Ports 1 and 2 of the component model are used in the low temperature system and ports 3 and 4 are used by the high temperature system. When the cascade condenser is being run as the condenser in the low temperature system, the inlet properties at ports 1 are modified as the solver iterates, however the inlet properties at port 3 remain constant. The opposite is true when the model is being run as the evaporator in the high temperature system.

5.2.2 Cascade System Validation

5.2.2.1 Experimental System

Experimental results from a cascade system using R404A as the high temperature refrigerant and CO₂ as the low temperature refrigerant were used to validate the simulation tool. The experimental system is shown in Figure 5.15.

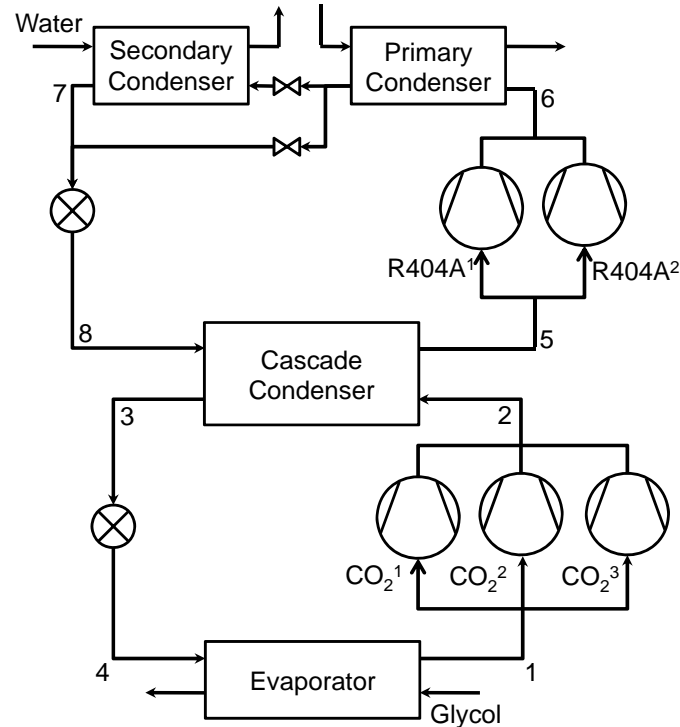


Figure 5.15 Diagram of experimental cascade system

The high temperature system consisted of two compressors of varying capacity and a primary and secondary condenser. The water flow rate through the primary condenser was adjusted for each case to achieve the condensing temperature listed in Table 5.2 and in cases 2-6 a secondary condenser had to be used to further reduce the R404A condensing temperature. The glycol flow rate through the CO₂ evaporator was adjusted to maintain a constant evaporating temperature for all six cases. Each of the compressors in the high temperature system could run in either a loaded configuration (all four cylinders

used to compress refrigerant) or unloaded configuration (two of four cylinders used to compressor refrigerant).

Table 5.2 Desired R404A saturation temperatures and R404A condenser configuration

Case	R404A Cond. Temp. (°C)	CO ₂ Evap. Temp. (°C)	R404A 2 nd Cond.
1	48.9	-31.7	Off
2	40.6	-31.7	Off
3	32.2	-31.7	On
4	32.2	-31.7	On
5	21.1	-31.7	On
6	10.0	-31.7	On

Table 5.3 lists the compressor configurations for both the high temperature and low temperature systems. Though only a single compressor is run for each case in the high temperature system, cases 2-5 utilize two CO₂ compressors running simultaneously in a parallel arrangement. The low temperature system compressor bank consisted of three compressors of various sizes. Brazed plate heat exchangers were used as the secondary R404A condenser, cascade condenser, and CO₂ evaporator. The primary R404A condenser was a water-cooled shell and tube heat exchanger.

Table 5.3 Cascade system compressor configuration

Case	R404A ¹	R404A ²	CO ₂ ¹	CO ₂ ²	CO ₂ ³
1	Unloaded	Off	Off	On	Off
2	Loaded	Off	Off	Off	On
3	Unloaded	Off	On	On	Off
4	Unloaded	Off	On	On	Off
5	Unloaded	Off	On	On	Off
6	Off	Unloaded	Off	Off	On

5.2.2.2 Modeling Procedure and Assumptions

The compressors in the high and low temperature systems were modeled using manufacturer data. For the high temperature system, compressor coefficients for the

loaded and unloaded operation were used along with the compressor polynomial equation provided by ARI Standard 540-1999. The CO₂ compressors were specifically manufactured to operate in the subcritical region with condensing temperatures in the range of 0 to -20°C and coefficients according to ARI Standard 540-1999 were derived using manufacturer rated performance data.

The cascade condenser component model was developed for the purpose of this study, and the details for which can be found in Winkler *et al.* (2008c).

5.2.2.3 Validation Results

The low and high temperature system capacity and power consumption validation results are shown in Figure 5.16 and Figure 5.17. For the low temperature system, the average error in system capacity was 2.6% with a maximum error of 3.6%. Capacity results for the high temperature system are similar with an average error of 2.5% and a maximum error of 2.9%. The compressor power was accurately predicted for the low temperature system with an average error of 2.9% and a maximum error of 5.1%. For the high temperature system, the power consumption was predicted with an average error 4.5%, however the maximum error was fairly high with an error of 11.4%. It is difficult to determine the source of this error since it was the only case in which R404A compressor 1 was being run fully loaded and pressure ratio for this case was predicted to within 2.3%.

The low and high temperature system mass flow rate results are shown in Figure 5.18. The average error for the low temperature system mass flow rate was 2.7% with a maximum error of 3.6%. For the high temperature system the average error was 4.4% with a maximum error of 6.8%. The maximum error in the mass flow rate prediction occurred for the cases with the maximum error in predicted saturation temperatures.

The predicted saturation temperatures are shown in Figure 5.19 and all saturation temperatures were predicted to within $\pm 3^\circ\text{C}$. The error in the saturation temperatures is rather small compared to the temperature gradient between the refrigerant and secondary fluid in the low temperature evaporator and high temperature condensers. The high temperature system evaporating temperature was predicted with an average error of 1.5°C , and thus the temperature gradient across the cascade condenser was accurately accounted for. System saturation temperatures are the primary driving force behind the heat transfer between the refrigerant and the surrounding environment and thus it is important that the saturation temperatures be accurately predicted. However, it is possible to accurately predict the saturation temperatures while failing to accurately predict the pressure ratio, which is the primary factor dictating the compressor power consumption. The pressure ratio for the low temperature system was predicted with average error of 2.8% and a maximum error of 4.3%. The pressure ratio of the high temperature system was not as accurately predicted and there was an average error of 9.4% with a maximum error of 15.2% between the simulated and experimental values. This seems to be attributed to the simplifications used in modeling the condensers. The maximum error in the pressure ratio prediction did not coincide with the maximum error in the high temperature system compressor power prediction.

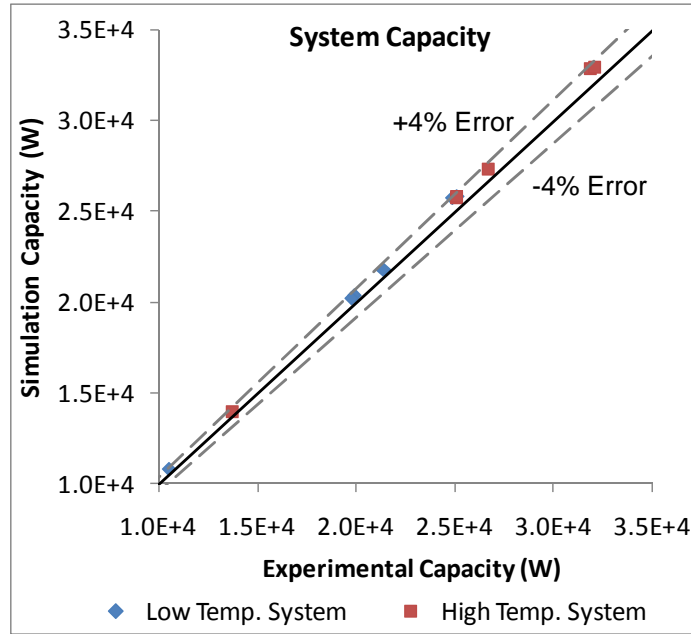


Figure 5.16 Cascade system validation results for system capacity

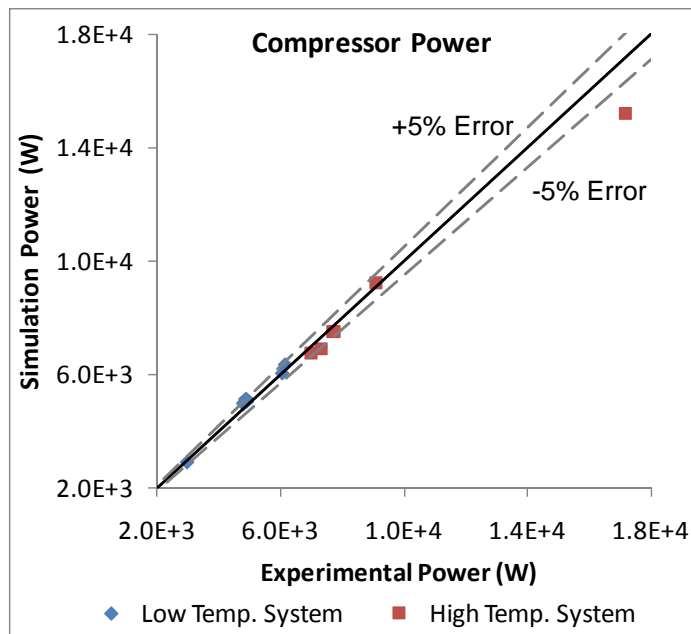


Figure 5.17 Cascade system validation results for compressor power consumption

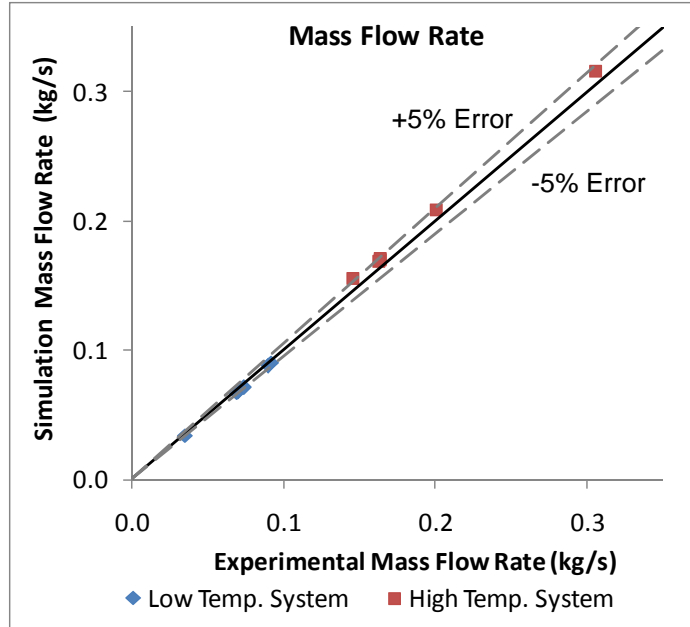


Figure 5.18 Cascade system validation results for system mass flow rate

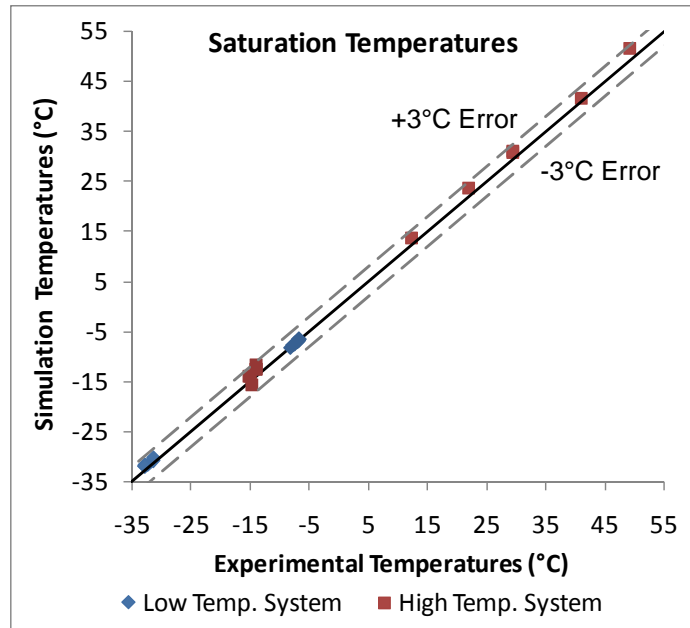


Figure 5.19 Cascade system validation results for saturation temperatures

6 Transient Component Simulation

This chapter discusses the component models that will be used by the transient solution engine in the simulation tool. However, the component-based framework implemented by the simulation tool allows for the insertion of additional component models into the program in the future.

6.1 Tank and Tube Heat Exchanger Simulation

To allow for the simulation of multi-component vapor compression cycles without solving the coupled form of the mass, energy, and momentum conservation equations, a new heat exchanger model has been developed. The heat transfer calculation and pressure drop calculation have been decoupled and independently solved by two types of structures; namely heat transfer elements and pressure loss elements. Thus, the transient heat exchanger model would consist of a set of heat transfer elements and pressure loss elements.

The approach used to model the heat exchangers is similar in nature to the methodology implemented by SINDA/FLUINT, and for lack of better terminology the names used to describe the elements used in the approach are also similar to the names adopted by SINDA/FLUINT (Cullimore *et al.*, 2004). The advantage of implementing a similar approach is that the SINDA/FLUINT environment has been proven to be stable, valid, and relatively fast. With that said, improvements can be made to the simulation by assuming that a vapor compression system is being modeled, and thus allowing for the simulation environment to be more useful to the design engineer. The fact that SINDA/FLUINT generates a FORTRAN file each time the program is run is evidence in itself that different numerical procedures will be used.

6.1.1 Heat Transfer Elements (Tanks)

The heat transfer elements, which henceforth will be called tanks, are transient devices that solve the conservation of mass and energy equations. The tank models are the portion of a heat exchanger that transfer heat between the refrigerant and the secondary fluid through the heat exchanger wall, and store refrigerant charge. Since the tank models do not solve a form of the momentum equation there exists a single pressure value for each tank and this tank pressure is updated as the simulation marches forward in time. As with any heat exchanger model, there is an enthalpy distribution from the heat exchanger inlet to the heat exchanger outlet and since this is a transient model there is a mass flow distribution between the inlet and outlet as well. It is important to keep in mind that a heat exchanger could be constructed from a single tank or a set of multiple tanks.

Figure 6.1 shows a conceptual diagram of a heat exchanger tank model. For each time step there is a certain mass of refrigerant, M , inside the tank at a pressure, P with a certain amount of internal energy, U . The refrigerant mass, pressure, and internal energy change as the simulation progresses in time, and thus time derivatives for each of these terms are calculated. During the calculation procedure, the inlet mass flow rate, \dot{m}_{in} , inlet enthalpy, h_{in} , and outlet mass flow rate, \dot{m}_{out} , are used to perform the refrigerant-side heat transfer calculations. The outlet enthalpy, h_{out} , is propagated to the downstream component and only changes when the model is updated for the next time step.

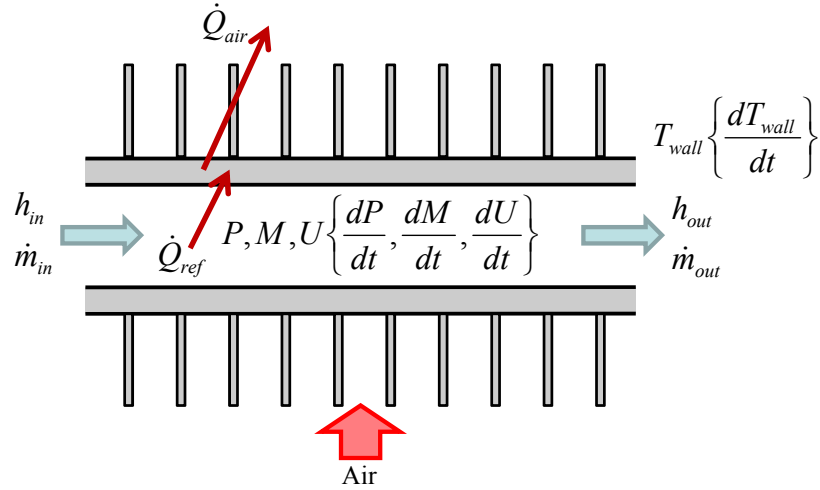


Figure 6.1 Conceptual diagram showing the tank model

The initial conditions that must be specified include the refrigerant pressure, refrigerant charge, and wall temperature. On the refrigerant-side, the boundary conditions are the inlet enthalpy and the inlet and outlet refrigerant mass flow rate. On the secondary fluid side the boundary conditions include the inlet air temperature and total mass flow rate. Thus, the time dependent variables for the tank model include the refrigerant pressure, refrigerant enthalpy distribution, the tank wall temperature, and the refrigerant charge.

The tank model is based on the work done by Rossi and Braun (1999), in which the heat exchanger tube is discretized using a finite volume approach to solve the differential form of the conservation of mass and energy equations. Assuming homogenous, one-dimensional flow, the conservation of mass and energy equations are shown below where x refers to the incremental length along the tank.

$$\frac{\partial \rho}{\partial t} + \frac{\partial(\rho v)}{\partial x} = 0 \quad (6.1)$$

$$\frac{\partial(\rho u)}{\partial t} + \frac{\partial(\rho v h)}{\partial x} + \delta \dot{Q}_{ref} = 0 \quad (6.2)$$

The tank is discretized using a finite volume approach to numerically solve the differential form of the conservation equations. This is accomplished by dividing the tank into several control volumes of equal size as shown in Figure 6.2.

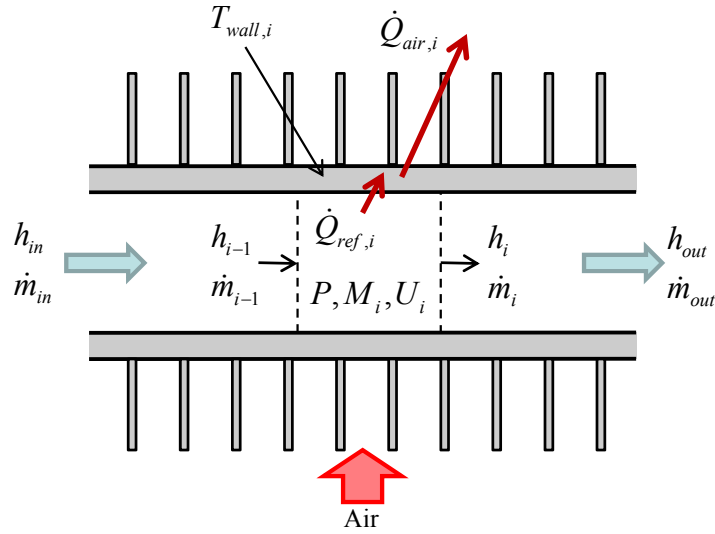


Figure 6.2 Discretized tank model

The conservation equations can be re-written with respect to the i^{th} control volume, assuming the region has an internal volume V_i .

$$\frac{\partial(\rho V)_i}{\partial t} + \dot{m}_i - \dot{m}_{i-1} = 0 \quad (6.3)$$

$$\frac{\partial(\rho u V)_i}{\partial t} + \dot{m}_{i-1} h_{i-1} - \dot{m}_i h_i + \dot{Q}_{ref,i} = 0 \quad (6.4)$$

Assuming the density, ρ , can be calculated as a function of any two independent thermodynamic properties, namely pressure and enthalpy, the following use of the chain rule can be applied to further reduce and linearize Equations 6.3 and 6.4.

$$\frac{\partial \rho_i}{\partial t} = \left. \frac{\partial \rho}{\partial P} \right|_{h,i} \frac{dP}{dt} + \left. \frac{\partial \rho}{\partial h_i} \right|_P \frac{dh_i}{dt} \quad (6.5)$$

Since each control volume has an equivalent internal volume the final linearized form of the discretized mass balance can be written as follows.

$$V_i \left[\left. \frac{\partial \rho}{\partial P} \right|_{h,i} \frac{dP}{dt} + \left. \frac{\partial \rho}{\partial h_i} \right|_P \frac{dh_i}{dt} \right] = \dot{m}_{i-1} - \dot{m}_i = \frac{dM_i}{dt} \quad (6.6)$$

Using the definition of enthalpy and assuming all regions have an equivalent volume; Equation 6.4 can be manipulated to the following

$$V_i \frac{\partial(\rho h - P)}{\partial t} + \dot{m}_{i-1} h_{i-1} - \dot{m}_i h_i + \dot{Q}_{ref,i} = 0 \quad (6.7)$$

which can be further reduced using Equation 6.5 to the final linearized form of the discretized energy balance equation.

$$V_i \left[\left(h_i \left. \frac{\partial \rho}{\partial P} \right|_{h,i} - 1 \right) \frac{dP}{dt} + \left(h_i \left. \frac{\partial \rho}{\partial h_i} \right|_P - \rho_i \right) \frac{dh_i}{dt} \right] = \dot{m}_{i-1} h_{i-1} - \dot{m}_i h_i - \dot{Q}_{ref,i} = \frac{dU_i}{dt} \quad (6.8)$$

Equations 6.6 and 6.8 yield a set of $2N$ linear ordinary differential equations, where N represents the number of cells used to represent the tank model. The unknown variables that must be solved for during each time step can be placed in a state vector, as shown in Equation 6.9 and be solved for by placing the equations in a matrix form.

$$\bar{x} = \left[\frac{dP}{dt} \quad \frac{dh_1}{dt} \quad \dot{m}_1 \quad \dots \quad \frac{dh_{N-1}}{dt} \quad \dot{m}_{N-1} \quad \frac{dh_N}{dt} \right]^T \quad (6.9)$$

The heat transferred to the refrigerant must be calculated prior to solving for the variables in Equation 6.9. Using the enthalpy for a given cell, h_i , the tank pressure, and refrigerant mass flow rate the refrigerant-side heat transfer coefficient, α_i , can be calculated. The heat transferred to or from the refrigerant can be calculated

$$\dot{Q}_{ref,i} = \alpha_i \frac{A_i}{N_{cells}} (T_i - T_{wall,i}) \quad (6.10)$$

where A_i is the total internal surface area of the tank, T_i is the refrigerant temperature of cell i , and $T_{wall,i}$ is the wall temperature of cell i . Similarly, the heat transferred to the secondary fluid can be calculated using the overall air-side heat transfer coefficient, U_{air} .

$$\dot{Q}_{air,i} = U_{air} \frac{A_{o,eff}}{N_{cells}} (T_{wall,i} - T_{air,in}) \quad (6.11)$$

where $A_{o,eff}$ is the effective outer surface area of the tank calculated according to Equation 6.12.

$$A_{o,eff} = \eta_s (A_t + A_f) \quad (6.12)$$

where A_t is the outer surface of the tubes, A_f is the surface are of the fins, and η_s is the fin surface effectiveness calculated accordingly.

$$\eta_s = \frac{A_t + \eta_{fin} A_f}{A_t + A_f} \quad (6.13)$$

The imbalance of the heat transferred to the refrigerant the heat transferred to the air changes the wall temperature of the tank.

$$\frac{(MC)_{tank}}{N_{cells}} \frac{dT_{wall,i}}{dt} = \dot{Q}_{ref,i} - \dot{Q}_{air,i} \quad (6.14)$$

6.1.1.1 Heat Exchanger Dehumidification

The tank model must handle the process of dehumidification if a particular cell wall temperature falls below the inlet air dew point temperature and Equation 6.11 is only valid when there is no dehumidification occurring on the surface of the heat exchanger. When the heat exchanger wall temperature is below the dew point temperature of the inlet air stream the water vapor in the air condenses on the heat exchanger surface, and thus the total heat transfer from the air consists of latent and sensible heat transfer. Equation 6.11 includes only the sensible heat transfer portion of the total heat transfer,

and therefore an alternative calculation procedure is required to calculate the air-side heat transfer when dehumidification occurs.

The total heat transfer for a given cell with the air is represented by Equation 6.15, where h_d represents the mass transfer coefficient, h_{fg} is the latent heat of water at the wall temperature, and ω_{wall} is the humidity ratio of the saturated air at the wall temperature.

$$\dot{Q}_{air,i} = U_{air} \frac{A_{o,eff}}{N_{cells}} (T_{wall,i} - T_{air,in}) + h_d \frac{A_{o,eff}}{N_{cells}} (\omega_{wall,i} - \omega_{air,in}) h_{fg} \quad (6.15)$$

The use of Equation 6.15 requires the air-side mass transfer coefficient, and in the modeling of the dehumidification process through a heat exchanger the mass transfer coefficient is most often related to the air-side heat transfer coefficient, h_{air} , using the Colburn analogy (McQuiston and Parker, 1994).

$$\frac{h_{air}}{C_{p,a} h_d} = Le^{2/3} \quad (6.16)$$

According to McQuiston and Parker (1994), $Le^{2/3}$ is approximately equal to one under typical moist air conditions, and thus the mass transfer coefficient can be calculated using the air heat transfer coefficient.

$$h_{air} = C_{p,a} h_d \quad (6.17)$$

Jiang (2003) reviews several dehumidification models and points out the advantages of the Enthalpy Potential Method described by McQuiston and Parker (1994). The main advantage of this method is the accuracy of the approach while eliminating the need for additional iterations through the use of a few assumptions. McQuiston and Parker (1994) conclude that the enthalpy gradient between the heat exchanger wall and the air stream drives the simultaneous heat and mass transfer between the surface and moist air. Equation 6.18 states that the total heat transfer with the air is driven by the enthalpy

potential, Δh_m , between the wall and air stream. The sensible air-side heat transfer coefficient was removed in the derivation of Equation 6.18 by assuming the Le number of air to be equal to one.

$$\dot{Q}_{air,i} = \dot{m}_{air,i} (h_{air,in} - h_{air,out,i}) = h_d \frac{A_{o,eff}}{N_{cells}} \cdot \Delta h_{m,i} \quad (6.18)$$

The enthalpy potential for a given cell, $\Delta h_{m,i}$, is calculated using the following equation.

$$\Delta h_{m,i} = h_{wall,i} - \frac{h_{air,in} - h_{air,out,i}}{2.0} \quad (6.19)$$

The outlet air enthalpy, $h_{air,out,i}$, can be directly calculated through substituting Equation 6.19 into Equation 6.18 with some additional rearranging of terms, and thus the total heat transfer with the air, $\dot{Q}_{air,i}$, can also be calculated.

The air outlet humidity ratio can be calculated in a similar way since it is the water vapor concentration gradient between the air and the wall that dictates the rate of water removal.

$$\dot{m}_{air,i} (\omega_{air,in} - \omega_{air,out,i}) = h_d \frac{A_{o,eff}}{N_{cells}} \cdot \Delta \omega_{m,i} \quad (6.20)$$

$$\Delta \omega_{m,i} = \omega_{wall,i} - \frac{\omega_{air,in} - \omega_{air,out,i}}{2.0} \quad (6.21)$$

Again, through substituting Equation 6.21 into Equation 6.20 the air outlet humidity ratio, $\omega_{air,out,i}$, can be calculated and thus the water condensate mass flow rate can be calculated accordingly.

$$\dot{m}_{water,i} = \dot{m}_{air,i} (\omega_{air,in} - \omega_{air,out,i}) \quad (6.22)$$

The latent and sensible air-side heat transfer can consequently be calculated.

$$\dot{Q}_{latent,i} = \dot{m}_{water,i} h_{fg} \quad (6.23)$$

$$\dot{Q}_{sensible,i} = \dot{Q}_{air,i} - \dot{Q}_{latent,i} \quad (6.24)$$

The outlet air temperature, $T_{air,out}$, can be calculated using total sensible air heat transfer.

$$T_{air,out,i} = T_{air,in} + \frac{\dot{Q}_{sensible,i}}{\dot{m}_{air,i} C_{p,a}} \quad (6.25)$$

6.1.2 Pressure Drop Elements (Friction Tubes)

Since the tank models only take into account heat transferred between the refrigerant and the wall and the mass of refrigerant, additional elements must be used to incorporate pressure drop calculations into the heat exchanger model. A detailed solution the conservation of momentum equation would require the mass, energy, and momentum equations to be coupled and solved for simultaneously. Therefore, additional assumptions will be made when formulating the Pressure Loss Elements, which from henceforth will be called friction tubes.

Since the heat transfer and charge calculations occur in the tank model, the friction tubes will be considered to be isenthalpic and contain no refrigerant charge. Thus, the only process occurring in the friction tubes is a change in refrigerant pressure.

There will be two unique types of friction tubes. The first will be reserved for the inlet and outlet of the heat exchanger, while the second type will only be utilized internally within the heat exchanger to connect a multiple tanks within a heat exchanger.

6.1.2.1 Inlet and Outlet Friction Tubes

These friction tubes will be placed at the inlet and outlet of the heat exchanger and will be used to determine the inlet and outlet mass flow rates for the heat exchanger. Recall, the boundary conditions required to solve the tank model include in the inlet enthalpy and the inlet and outlet refrigerant mass flow rate. The inlet and outlet friction

tube models will use the boundary conditions imposed by the system to solve the heat exchanger model.

The heat exchanger sequence is shown in Figure 6.3. In this diagram, a tank model is connected to an inlet friction tube and an outlet friction tube. The inlet friction tube will determine the inlet refrigerant mass flow rate using the inlet pressure, inlet enthalpy, and the current tank pressure. Similarly, the outlet friction tube will use the current tank pressure and outlet enthalpy, and the heat exchanger outlet pressure to calculate the outlet mass flow rate.

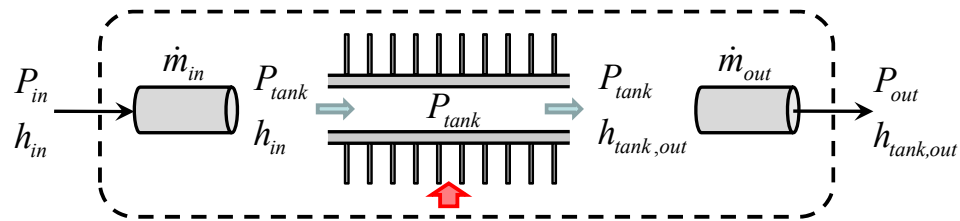


Figure 6.3 Inlet and outlet friction tubes

Notice that the type of boundary condition being implemented by the heat exchanger differs from that of the tank model. The heat exchanger operates using the inlet enthalpy and boundary pressures, whereas the tank model uses the inlet enthalpy and inlet and outlet mass flow rates.

The inlet and outlet friction tube models will assume that the mass flow rate instantly changes with pressure. This assumption is required to satisfy an overall mass balance once the heat exchanger is placed in the vapor compression system; meaning the amount of mass flowing out of the compressor must equal the amount of mass flowing into the condenser. This constraint will be further discussed in Chapter 7. Since the refrigerant mass flow rate is assumed to instantly adjust based on the inlet and outlet

pressures, the friction factor can be used to calculate the pressure drop through the friction tube.

$$DP_f = f \frac{\rho L}{2D} v^2 \quad (6.26)$$

A correlation for the friction factor, f , must be used to calculate the pressure drop in Equation 6.26. However, since the friction tube model must calculate a refrigerant mass flow rate using the inlet and outlet pressure, Equation 6.26 must be solved for the refrigerant velocity, v , which then must be used to calculate the refrigerant mass flow rate. Generally, the friction factor is a function of refrigerant mass flow rate, and thus Equation 6.26 is a highly non-linear function of refrigerant mass flow rate and can be numerically challenging to solve due to discontinuities associated with refrigerant phase change. Therefore, an explicit equation for the refrigerant mass flow rate as a function of pressure drop would be most suitable for this model in order to avoid additional iteration and numerical instability.

The use of an explicit equation for the refrigerant mass flow rate requires the use of a friction factor correlation that can be analytically solved for the refrigerant mass flow rate. Using the following friction factor correlation (ASHRAE, 2001)

$$f = \frac{0.3164}{\text{Re}^{0.25}} \quad (6.27)$$

along with the following definition of the Reynold's number

$$\text{Re} = \frac{\rho v D}{\mu} \quad (6.28)$$

the refrigerant mass flow rate can be explicitly expressed as a function of the frictional pressure drop.

$$\dot{m} = \rho Av = \rho \pi \left(\frac{D}{2} \right)^2 \left(\frac{DP_f}{\frac{0.3164}{2} \frac{L}{D^{1.25}} \rho^{0.75} \mu^{0.25}} \right)^{1/1.75} \quad (6.29)$$

The above relation has been shown to be accurate for single phase fluids (ASHRAE, 2001). A similar approach has been used for a variety of two-phase pressure drop correlations as well.

6.1.2.2 Internal Friction Tubes

The friction tubes used to connect the tanks within a heat exchanger will be treated slightly differently. A friction tube model connecting two tank models is shown in Figure 6.4. For the internal friction tube the inlet pressure and enthalpy are provided from the upstream tank model and the outlet pressure is provided from the downstream tank model. Both the inlet and outlet pressures effect the mass flow through the friction tube.

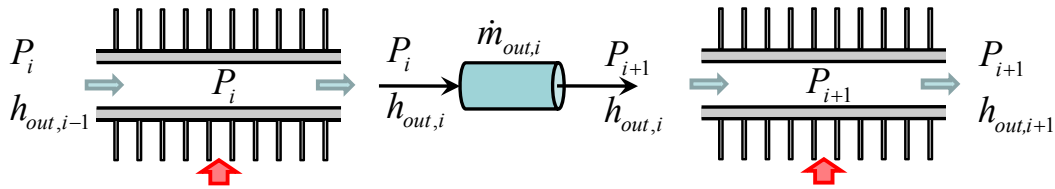


Figure 6.4 Internal friction tube connected to two tanks

To relax the assumption that the friction tube refrigerant mass flow instantly adjusts based on the inlet and outlet pressures, a form of the transient momentum equation must be used. The use of the transient momentum equation between two adjacent tank models will help to provide numerical stability when the tank models are calculating their corresponding pressure derivatives since the mass flow rate through the friction tube will not instantaneously change. A simplified form of the momentum equation, shown in Equation 6.30, states that the difference between the frictional pressure drop, DP_f , and the

pressure difference from inlet to outlet must result in an acceleration or deceleration of the refrigerant mass, M .

$$M \frac{dv}{dt} = F = A_c (P_{in} - P_{out} - DP_f) \quad (6.30)$$

This form of the momentum equation assumes homogenous flow and neglects body forces. The left hand side of Equation 6.30 can be reduced as follows.

$$M \frac{dv}{dt} = \rho A_c L \frac{dv}{dt} = L \frac{d(\rho A_c v)}{dt} = L \frac{d\dot{m}}{dt} \quad (6.31)$$

A final simplified form of the momentum equation can be attained by substituting Equation 6.31 into Equation 6.30.

$$\frac{d\dot{m}}{dt} = \frac{A_c}{L} (P_{in} - P_{out} - DP_f) \quad (6.32)$$

Equation 6.32 will be used to update the refrigerant mass flow rate through the internal friction tube as the simulation progresses in time. An initial mass flow rate must be provided and for most practical purposes will be assigned a value of zero. A zero mass flow rate assumes that the system has been idle for a significant amount of time and pressures within the system have equilibrated.

6.1.3 Heat Exchanger Modeling Procedure

To simulate a heat exchanger, a series of tanks and friction tubes can be connected. The sequence starts with an inlet friction tube followed by an alternating series of tank and friction tube models. The final tank model is connected to the outlet friction tube. A representative diagram showing the entire heat exchanger is shown in Figure 6.5. The final result is a transient heat exchanger model that calculates an inlet and outlet mass flow rate using the inlet refrigerant condition and outlet pressure.

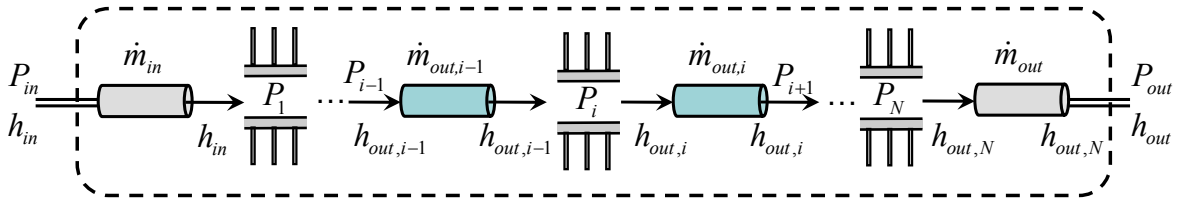


Figure 6.5 Tank tube heat exchanger

The minimum number of elements required to simulate a heat exchanger is three: an inlet friction tube, a tank, and an outlet friction tube. In this case, the pressure drop accuracy would be limited; however the heat transfer can be accurately modeled due to the discretization of the tank models. When additional tank models are being used to model the heat exchanger, the resolution of the tank discretization can be reduced.

6.1.3.1 Modeling of Multiple Row Heat Exchangers

Most heat exchangers consist of multiple tube rows, as shown in Figure 6.6.

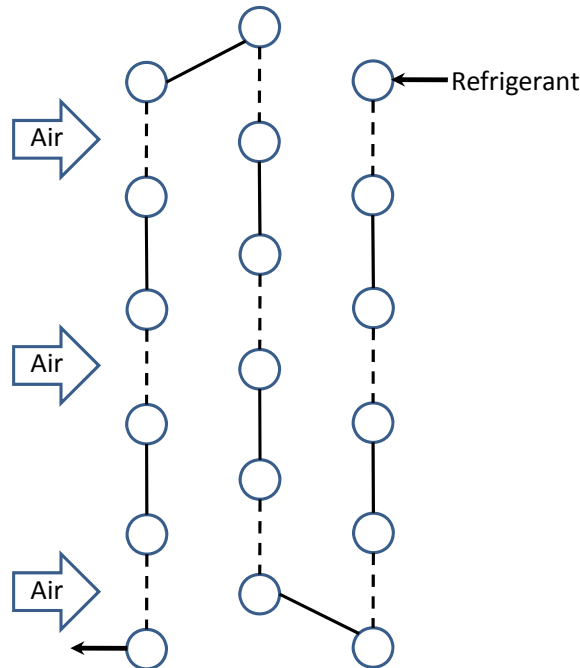


Figure 6.6 An example of a multiple row heat exchanger

The heat exchanger shown in Figure 6.6 consists of three rows and the air properties change as the air flows past each tube. It is important to take into account the change in

air properties when simulating a heat exchanger in order to accurately capture the gradients dictating air-side heat transfer. As described in Section 6.1.1, the inlet air condition is a required input in order to run the tank model and it is possible for the calculated outlet air condition for one tank to be set as input to run an additional tank in the heat exchanger.

In order to model the change in air properties as the air flows through the heat exchanger, the multiple row heat exchanger shown in Figure 6.6 can be modeled using a minimum of three tanks. Each tank is used to model a row of the heat exchanger, as shown in Figure 6.7. The refrigerant flows from tank 1 to tank 3, while the air flows from tank 3 to tank 1. The outlet air properties calculated by tank 3 are averaged and set as input to tank 2. The use of only three tanks to simulate the heat exchanger places a large emphasis on the averaging of air properties since the precision of the air-side discretization has been reduced. A validation of multiple row heat exchanger is presented in Section 6.1.7.2.

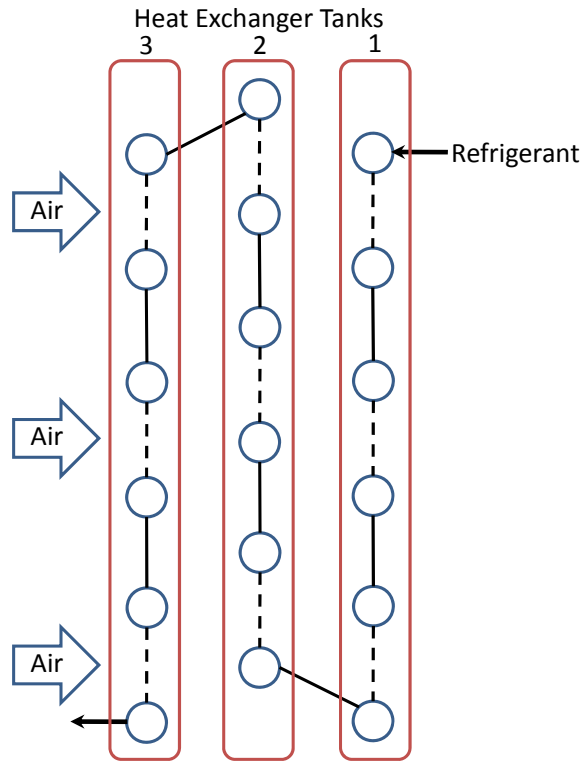


Figure 6.7 Using three tank to model a multiple row heat exchanger

Since under transient operation the heat load on the air-side and refrigerant-side are calculated independently, the air-side can be propagated through the heat exchanger without additional iteration. The air-side propagation is assumed to be steady and thus mass storage on the air-side is neglected. This assumption is valid since the air speed and heat exchanger width found in typical applications results in the air flowing through the heat exchanger in approximately 0.04 seconds, which is a much shorter time scale than the transient effects of interest.

6.1.4 Heat Exchanger Model Dependence on Number of Tanks

The heat exchanger model can be constructed out of any number of tank and tube models. Though a larger number of tank models might lead to a more accurate simulation, a larger number of tanks will increase the computational time. In order to determine the dependence of heat exchanger performance on the number tank models used to represent

the heat exchanger a series of numerical experiments were run by varying the number of tanks used to represent a particular heat exchanger. The steady state results of the tank and tube heat exchanger simulation were compared to the results predicted by CoilDesigner. CoilDesigner, originally presented by Jiang (2003), is a detailed steady state simulation tool for air-to-refrigerant heat exchangers and has been extensively validated against experimental results (Jiang, 2003; Aute *et al.*, 2004; Schwentker *et al.*, 2005; Jiang *et al.*, 2006; Schwentker *et al.*, 2006; Wang, 2008a). CoilDesigner is used extensively in industry for the design and optimization of heat exchangers and has started to become the industry standard for heat exchanger simulation.

The heat exchanger simulated was a single bank, single circuit evaporator with the following input parameters.

Table 6.1 Test heat exchanger input parameters

Refrigerant	R134a
Number of Rows	1
Number of Tubes	8
Tube Length (m)	0.5
Tube Outer Diameter (mm)	9.53
Tube Thickness (mm)	1.0
Tube Spacing (cm)	2.54
Fin Type	Plate Fin
Fins per Inch	20
Fin Thickness (mm)	0.1
Ref. Two Phase HTC (W/m^2K)	5020
Ref. Vapor HTC (W/m^2K)	780
Ref. Two Phase DP Correlation	Jung-Radermacher
Ref. Vapor Phase DP Correlation	Blasius
Air-side HTC Correlation	Kim-Yoon-Web

In order to reduce the level of uncertainty in comparing the various runs, the heat transfer coefficients were assumed constant for the two refrigerant phase regimes present in the heat exchanger. The CoilDesigner Input File Translator, discussed in the previous section,

was used to ensure consistent input parameters between CoilDesigner and the Tank and Tube Heat Exchanger model.

Enthalpy profiles through the evaporator model constructed from a various number of tank models is shown in Figure 6.8. The enthalpy profile predicted by CoilDesigner is shown in black and as the number of tank models increases the enthalpy profile approaches the enthalpy profile predicted by CoilDesigner.

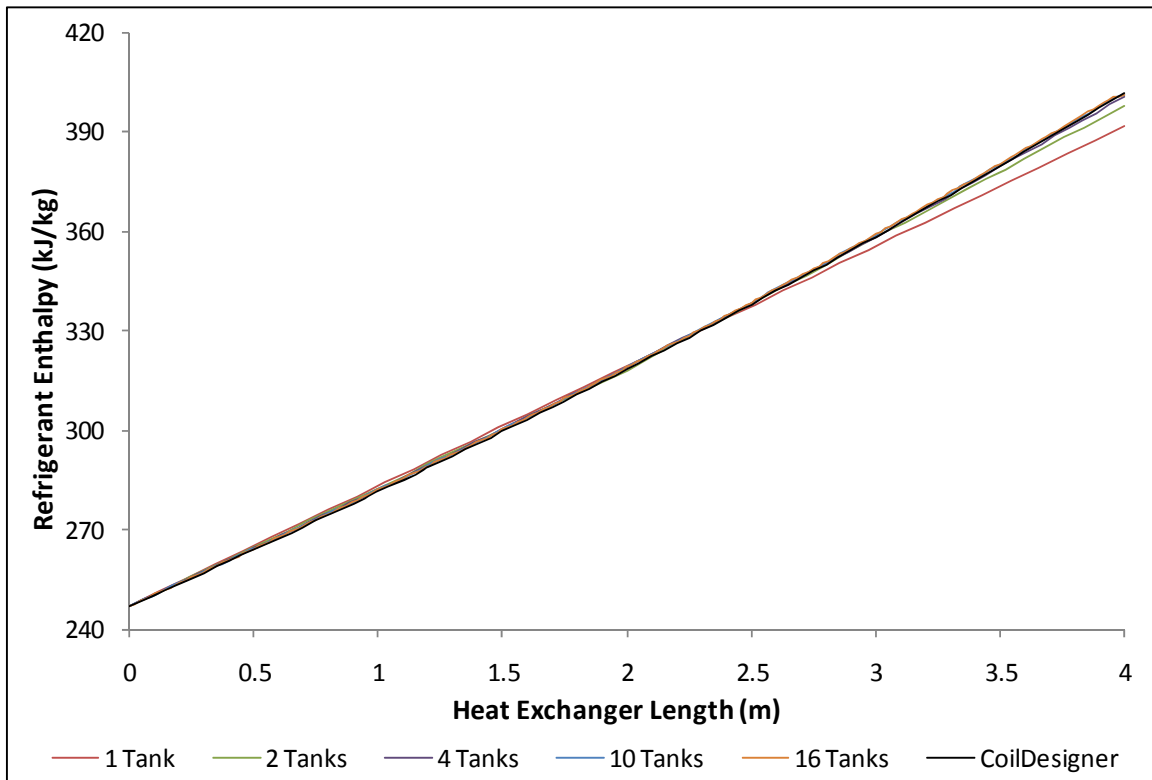


Figure 6.8 Refrigerant enthalpy profile along the heat exchanger length for heat exchanger models constructed from various number of tank models

The percent difference in predicted heat load between CoilDesigner and various Tank and Tube Heat Exchangers models are plotted in Figure 6.9. When a single tank model is used to represent the heat exchanger, the percent difference between the two models is greatest with the Tank and Tube Heat Exchanger predicting a heat load of 6.42% less than CoilDesigner. The percent difference between the two models

asymptotically approach zero as the number of tank models increases. By the time ten tank models are used to construct the Tank and Tube Heat Exchanger, the difference between the two models becomes insignificant with a percent difference of only 0.42%.

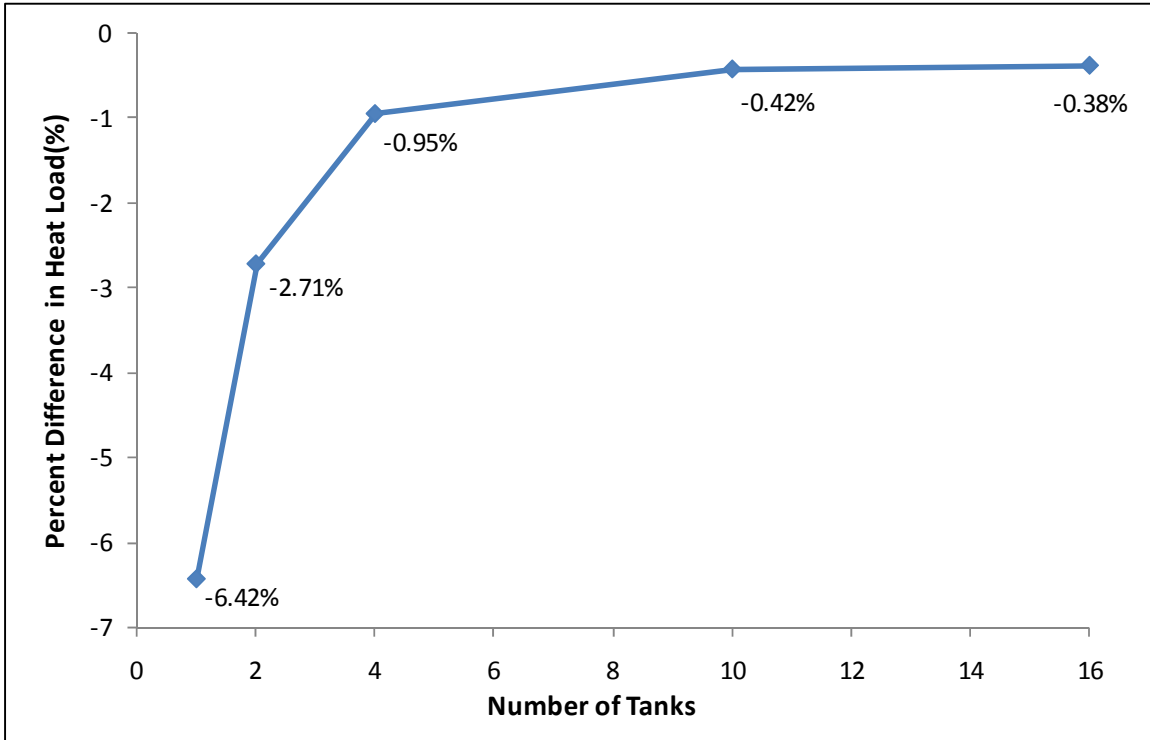


Figure 6.9 Percent difference in heat load compared to CoilDesigner

Pressure profiles through the evaporator model constructed from various number of tank models are plotted in Figure 6.10. Similar to the enthalpy profile, as the number of tank models increases the results approach that predicted by CoilDesigner. The enthalpy profile, as shown in Figure 6.8, appears continuous due to the tank model being discretized to perform the heat transfer calculations. However, the heat exchanger model uses friction tubes placed in between the tank models to calculate the pressure drop. The pressure drop calculation is discretized in equal lengths based on the number of tank models used to construct the heat exchanger model. For example, if a single tank is used to represent the heat exchanger, the pressure drop would be modeled using two friction

tubes. This is evident in Figure 6.10 for the pressure profile for a single tank heat exchanger. In this profile, there are three distinct pressure values; namely, the inlet, the tank pressure, and the outlet. The tank pressure in this profile is the outlet pressure to first friction tube and the inlet pressure to the second friction tube. Continuing with this trend, the two tank heat exchanger pressure profile displays four pressure values since three friction tubes were used in the modeling of the heat exchanger for this case.

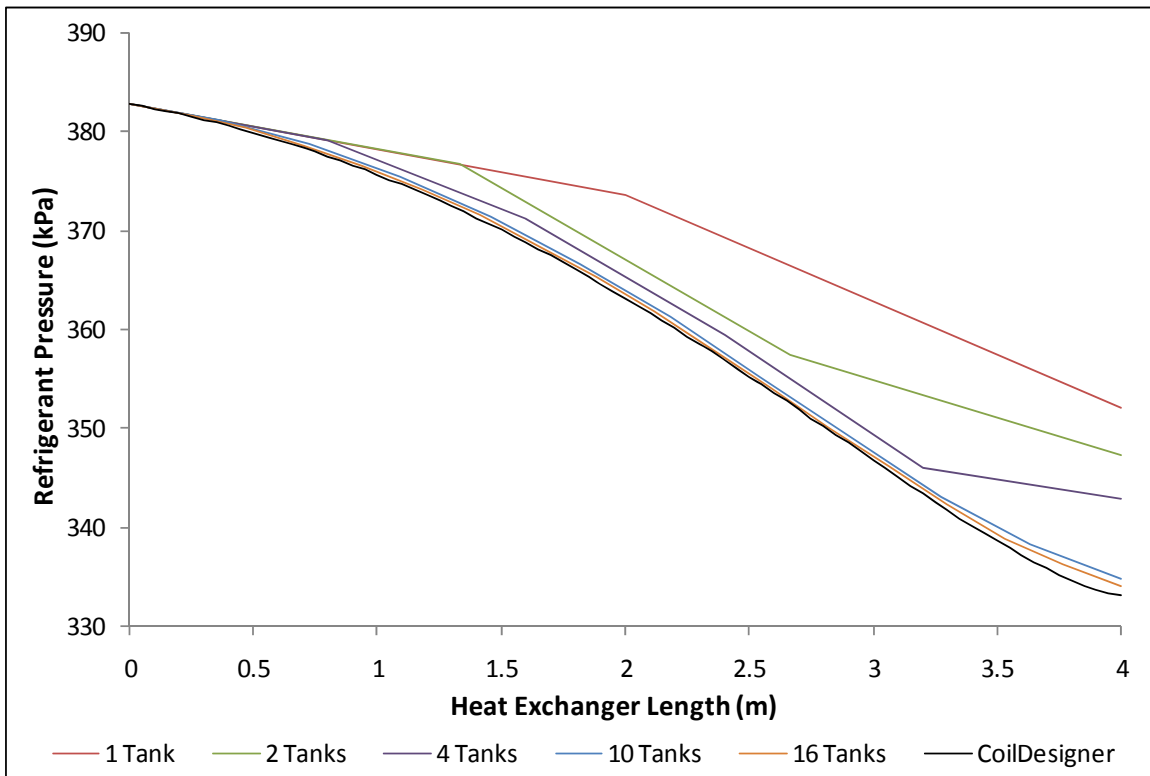


Figure 6.10 Refrigerant pressure profile along the heat exchanger length for heat exchanger models constructed from various number of tank models

The percent difference in pressure drop between the Tank and Tube Heat Exchanger and CoilDesigner for heat exchangers constructed from a various number of tank models is shown in Figure 6.11. Similar to the results for the heat load, the difference in the pressure drop prediction becomes much less as the number of tanks used to model the heat exchanger increases. However, the percent difference between the two

models is 1.84% when 16 tanks are used to construct the Tank and Tube Heat Exchanger model.

CoilDesigner models the heat exchanger by subdividing each tube into a number of segments. The heat exchanger modeled for this comparison consisted of eight tubes and each tube was subdivided into ten segments. It has been shown the heat exchanger performance predicted by CoilDesigner does not significantly change when the number of segments exceeds ten for heat exchangers of the size modeled in this example (Schwentker *et al.*, 2005). With regard to this example, the pressure drop calculation has been discretized into a total of 80 segments for CoilDesigner, but only 16 segments for the Tank and Tube heat exchanger model. Thus, the difference in pressured drop calculations is due to the different discretization schemes.

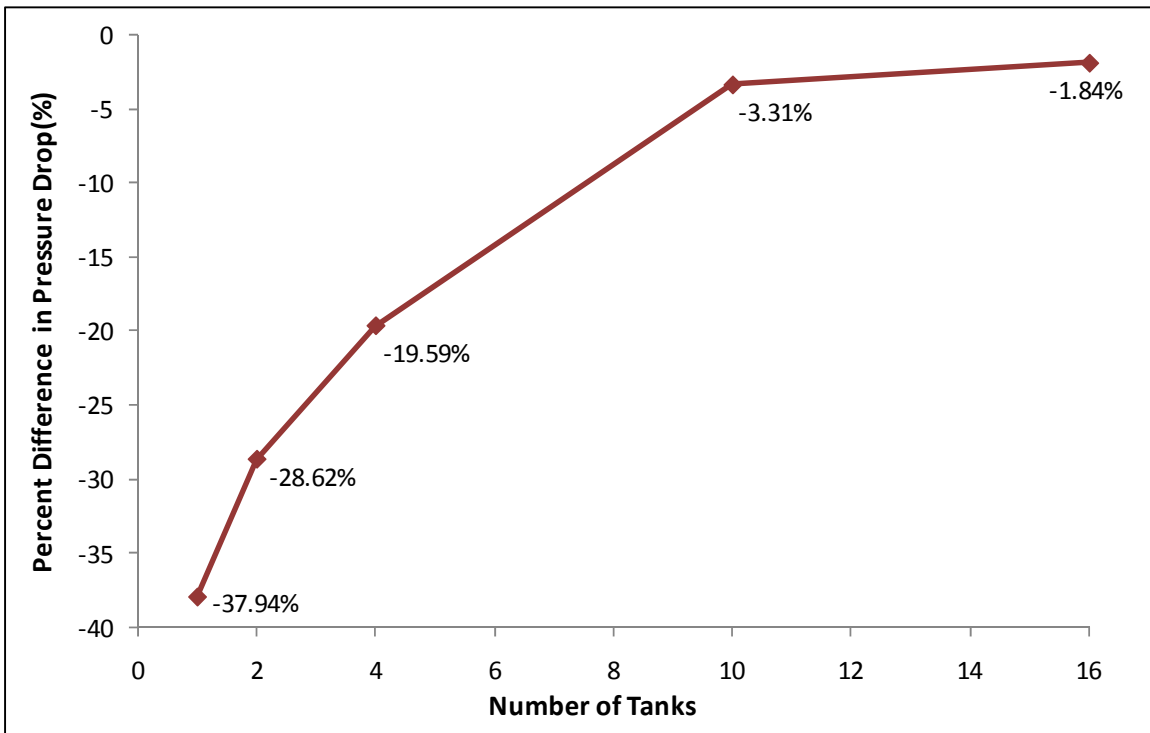


Figure 6.11 Percent difference in pressure compared to CoilDesigner

Though the tank models are further discretized to perform the heat transfer calculations, the difference in predicted heat load between CoilDesigner and the Tank and Tube Heat Exchanger model decreases as the number of tanks used to construct the heat exchanger increases. This is due to the effect the pressure drop through the heat exchanger has on the heat transferred to the refrigerant. As the pressure drops through an evaporator, the refrigerant temperature also decreases since the refrigerant present in the heat exchanger is a two phase mixture. As the refrigerant temperature decreases due to the pressure drop, the temperature gradient between the refrigerant and incoming air increases. For example, the predicted pressure drop for the single tank heat exchanger, as shown in Figure 6.10, is much less than pressure drop predicted by CoilDesigner and thus the saturation temperature is higher. This would result in an under prediction of the predicted heat load as shown in Figure 6.8.

6.1.5 Numerical Issues

The tank model is discretized using a finite volume approach and the refrigerant side heat transfer coefficient (HTC) is evaluated using the refrigerant properties for each given cell. Different HTC correlations are used depending on the refrigerant phase, however, the correlations tend to be discontinuous across different phase regimes. The discontinuity in heat transfer coefficient can lead to numerical instabilities as the phase transition point moves throughout the heat exchanger during transient operation. Harmes *et al.* (2008) avoids this issue by essentially average the HTC at the inlet and outlet of each cell.

Figure 6.12 shows HTC trend through a typical R134a evaporator operating at a saturation temperature of 283.15K. The two phase HTC correlation is plotted using the evaporative HTC correlation provided by Shah (1982) and the vapor HTC is plotted

using the correlation provided by Dittus and Boelter (1930). The correlations are plotted versus refrigerant enthalpy ranging from a quality of 0.22 to a superheat 10.0K. The discontinuity in HTC is evident. To avoid numerical instabilities associated with this discontinuity, the two phase HTC correlation has been replaced with a cubic spline from a quality of 0.90 to 1.0 to provide a smooth transition in HTC between the two phase regimes.

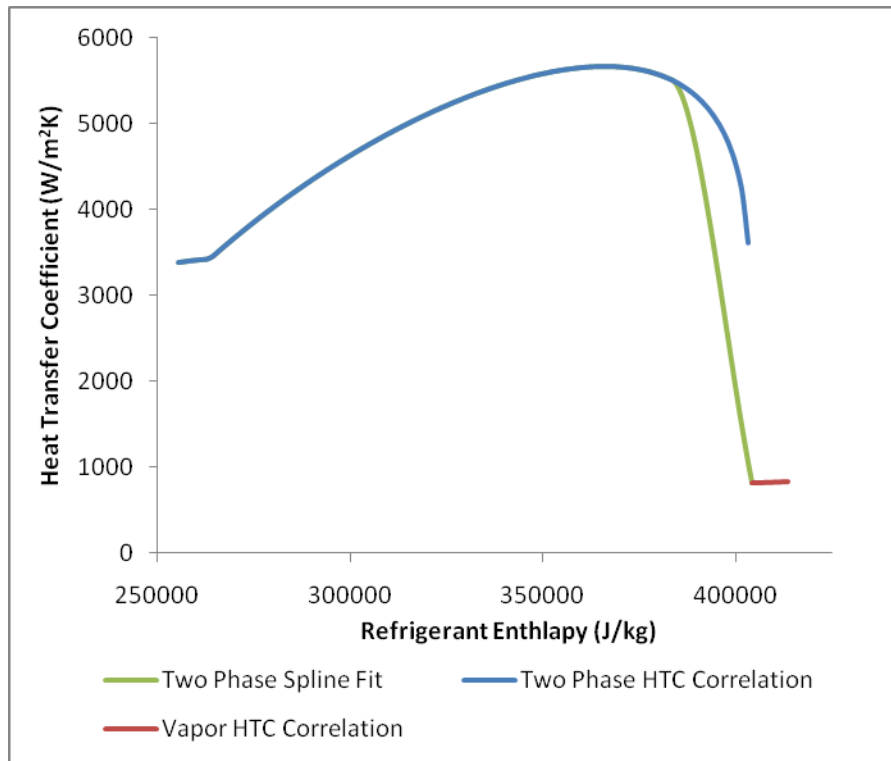


Figure 6.12 Heat transfer coefficient correlation trends

6.1.6 CoilDesigner Input File Translator

In order to make the seamless transition between conducting steady state and transient simulations, the user should only have to enter input parameters a single time. A CoilDesigner input file translator was created to construct a Tank and Tube Heat Exchanger directly from a CoilDesigner file since it is expected that users will utilize CoilDesigner as the heat exchanger component model when conducting steady state

simulations. The file translator essentially reads all the inputs from the CoilDesigner file and uses the preliminary calculations in the CoilDesigner solver to determine required inputs for the Tank and Tube Heat Exchanger model. Example inputs that are calculated by the CoilDesigner solver include the secondary heat transfer area, air-side heat transfer coefficient, heat exchanger thermal mass, etc. The calculations conducted by the CoilDesigner solver required to create the Tank and Tube Heat Exchanger Model occur only once during the initialization phase of the simulation.

6.1.7 Steady State Heat Exchanger Validation

The Tank and Tube Heat Exchanger model was validated using steady state experimental results for the outdoor and indoor heat exchanger in a residential R410A heat pump system. The transient performance of the Tank and Tube Heat Exchanger model has been validated through the simulation of the entire vapor compression system and is presented in Section 7.4. The heat exchanger model was validated as a standalone model under steady state conditions since the inlet refrigerant conditions can be held constant during the entire simulation. A steady state simulation also allows the Tank and Tube Heat Exchanger model performance to be compared to the simulation results predicted by CoilDesigner. The heat exchangers used in the validation were the indoor and outdoor heat exchangers in a residential 3-ton R410A heat pump.

Experimental data for both the cooling and heating modes was used in validating the performance of the Tank and Tube Heat Exchanger model. When operating in cooling mode the outdoor heat exchanger serves as the condenser and when operating in heating mode the outdoor heat exchanger serves as the evaporator. The indoor unit was validated for the cooling case only, in which it was serving as an evaporator. Thus, the Tank and

Tube Heat Exchanger model has been validated using experimental results for both a condenser and evaporator.

6.1.7.1 Single Row Heat Exchanger

The outdoor heat exchanger was a single row, tube-fin heat exchanger. The physical parameters used in simulating the heat exchanger are listed in Table 6.2. Though the heat exchanger consists of four circuits, since all four circuits are identical it was assumed each circuit received the same refrigerant mass flow rate. Thus, only a single circuit was model during the validation and the refrigerant mass flow rate, air flow rate, and heat load were scaled appropriately.

Table 6.2 Outdoor heat exchanger input parameters

Refrigerant	R410A
Number of Circuits	4
Number of Rows	1
Number of Tubes per Circuit	9
Tube Length (m)	1.8
Tube Outer Diameter (mm)	9.53
Tube Thickness (mm)	0.765
Tube Spacing (cm)	2.62
Fin Type	Wavy
Fins per Inch	25
Fin Thickness (mm)	0.1
Air Flow Rate (m ³ /s)	1.321

The outdoor heat exchanger was first modeled and validated using CoilDesigner. The CoilDesigner Input File Translator, as described in Section 6.1.6, was used to construct the Tank and Tube Heat Exchanger model. The outdoor heat exchanger was first validated using CoilDesigner because this is the likely procedure to be implemented by future users of this simulation tool. This procedure will also once again display the consistency between a detailed steady state heat exchanger model and the Tank and Tube Heat Exchanger model.

The correlations and correction factors used by CoilDesigner to best reproduce the experimental results were also used by the Tank and Tube Heat Exchanger model. Correction factors are used as multipliers against the heat transfer coefficient and pressure drop calculated by the correlations. A set of correction factors for the air-side and the refrigerant-side were constructed for both modes of operation in order to best match the experimental results. Correction factors are used to tune the model and take into account the error in heat transfer coefficient and pressure drop correlations. The correction factors, listed in Table 6.3 and Table 6.4, were held constant for both cooling and heating modes for the corresponding operating conditions. Even though the same pressure drop correlations were used for the condensing and evaporating cases, it is not uncommon to have to use different correction factors since the operating conditions are vastly different.

Table 6.3 Heat transfer correlations and corresponding correction factors

	Cooling Mode		Heating Mode	
	Correlation	Correction Factor	Correlation	Correction Factor
Air-side	Kim, Yoon, Web	0.75	Kim, Yoon, Web	0.75
Refrigerant Vapor Phase	Gnielinski	0.85	Gnielinski	0.7
Refrigerant Two Phase	Jung, Radermacher	0.85	Shah	1.0
Refrigerant Liquid Phase	Gnielinski	0.85	---	---

Table 6.4 Pressure drop correlations and corresponding correction factors

	Cooling Mode		Heating Mode	
	Correlation	Correction Factor	Correlation	Correction Factor
Air-side	Kim, Yoon, Web	1.0	Kim, Yoon, Web	1.0
Refrigerant Vapor Phase	Blasius	2.1	Blasius	0.7

Refrigerant Two Phase	Jung, Radermacher	2.1	Jung, Radermacher	0.6
Refrigerant Liquid Phase	Blasius	2.1	---	---

The cooling mode and heating mode air-side and refrigerant-side inlet conditions are listed in Table 6.5 and Table 6.6, respectively. The air flow rate was constant for all cases since the outdoor fan was run at a constant speed. The air flow rate was previously listed in Table 6.2.

Table 6.5 Cooling mode air-side and refrigerant-side inlet conditions

Air-side Inlet Conditions		Refrigerant-side Inlet Conditions		
T (°C)	RH	T_{sat} (°C)	T (°C)	\dot{m} (g/s)
19.88	38	32.83	67.60	59.20
28.05	38	40.22	71.29	65.19
35.05	20	46.73	79.97	66.62
46.35	20	57.17	100.58	65.21
49.79	20	60.31	108.41	63.49

Table 6.6 Heating mode air-side and refrigerant-side inlet conditions

Air-side Inlet Conditions		Refrigerant-side Inlet Conditions		
T (°C)	RH	T_{sat} (°C)	x	\dot{m} (g/s)
16.6	82.3	11.02	0.272	66.57
8.4	73.1	2.39	0.275	50.19
-8.4	63.0	-12.63	0.297	28.37
-17.4	62.9	-20.78	0.313	19.26
-18.0	94.7	-21.14	0.315	18.99

The heat load validation results for the outdoor heat exchanger are displayed in Figure 6.13. The CoilDesigner results and the Tank and Tube Heat Exchanger model results are shown for comparison purposes. The maximum error in the heat load prediction for the Tank and Tube Heat Exchanger model for the cooling mode was 2.8% and for the heating mode was 1.4%. The average relative error for the Tank and Tube Heat Exchanger model in the heat load prediction for all 10 cases was 1.27% compared to

0.60% for CoilDesigner. However, it is expected that the results for CoilDesigner to be slightly more accurate since the correction factors were determined using CoilDesigner.

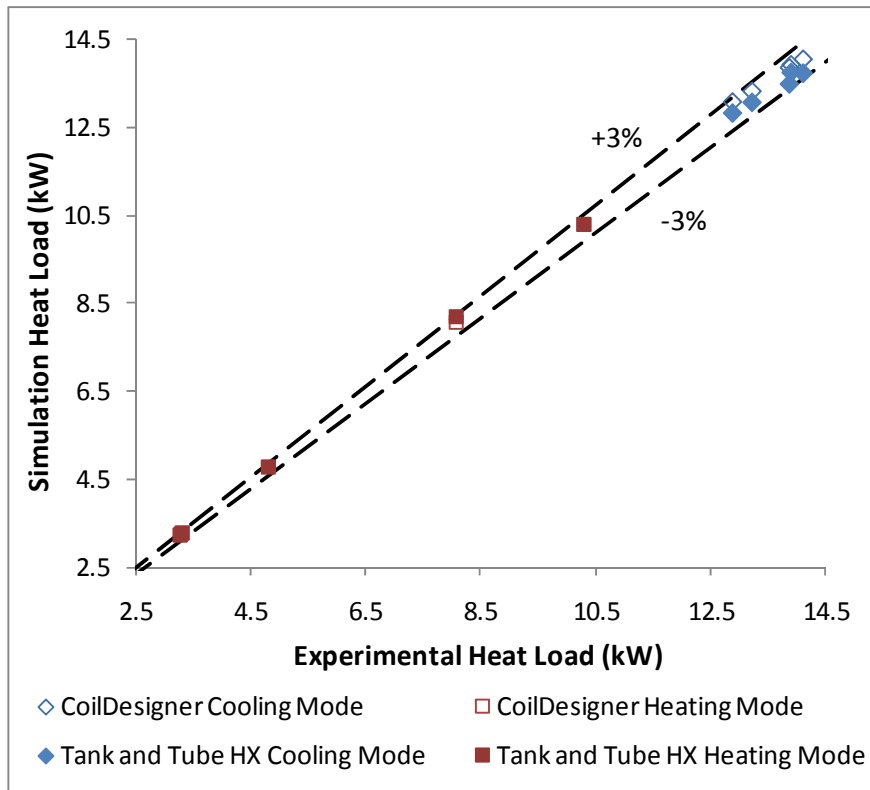


Figure 6.13 Heat load validation results for the outdoor heat exchanger

The refrigerant-side pressure drop validation results for the Tank and Tube Heat Exchanger model and CoilDesigner are plotted in Figure 6.14. The predicted pressure drop for the Tank and Tube Heat Exchanger and CoilDesigner are quite similar, however there is a significant amount of error for both models. For the few points where the Tank and Tube Heat Exchanger model and CoilDesigner predict slightly different refrigerant pressure drop, CoilDesigner is generally the more accurate of the two models. This is likely due to the discretization scheme used to model the heat exchanger. Ten segments were used to model each heat exchanger tube in CoilDesigner; resulting in a total of 90 cells used to perform the pressure drop calculation. Ten tanks were used to model the

heat exchanger in the Tank and Tube Heat Exchanger model, and thus the pressure drop calculation was not as refined when compared to CoilDesigner.

As shown in Figure 6.14, the cooling mode points are more accurately modeled than the heating mode points. The average relative error of the Tank and Tube Heat Exchanger model pressure drop prediction for the cooling mode points was 7.45% compared to an average relative error of 20.0% for the heating mode points.

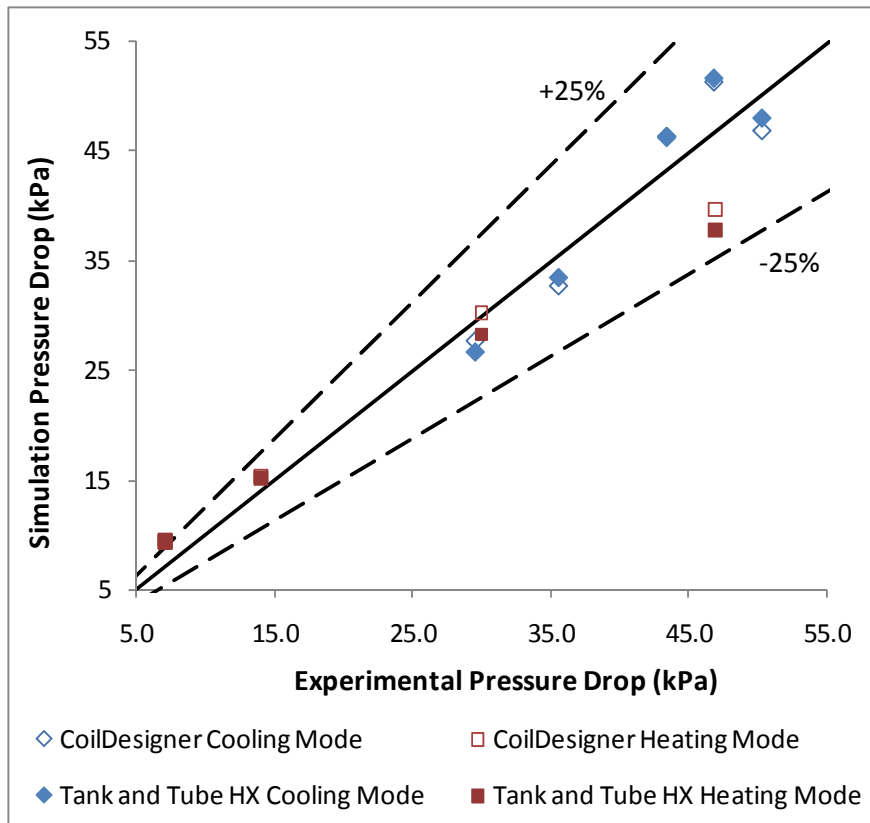


Figure 6.14 Refrigerant pressure drop validation results for the outdoor heat exchanger

6.1.7.2 Multiple Row Heat Exchanger

The indoor heat exchanger was a multiple row, tube-fin heat exchanger. The physical parameters used in simulating the heat exchanger are listed in Table 6.7. As with the outdoor heat exchanger, all six circuits are identical and thus it was assumed each circuit received the same refrigerant mass flow rate. Thus, only a single circuit was

modeled during the validation and the refrigerant mass flow rate, air flow rate, and heat load were scaled appropriately.

Table 6.7 Indoor heat exchanger input parameters

Refrigerant	R410A
Number of Circuits	6
Number of Rows	3
Number of Tubes per Circuit	18
Tube Length (m)	0.46
Tube Outer Diameter (mm)	10.5
Tube Thickness (mm)	0.55
Tube Horizontal Spacing (cm)	2.05
Tube Vertical Spacing (cm)	2.65
Fin Type	Louver
Fins per Inch	14
Fin Thickness (mm)	0.1
Air Flow Rate (m ³ /s)	0.565

As shown in Table 6.7, the indoor heat exchanger contained three rows and each of the rows was simulated using a single tank for each row. This configuration, as shown in Figure 6.7, was selected since it is the fewest number of tanks suitable for modeling a three row heat exchanger if the air-side propagation is to be included in the simulation.

The same procedure described for the outdoor heat exchanger was used to validate the indoor heat exchanger. The correlations and correction factors used in modeling the indoor heat exchanger are shown in Table 6.8 and Table 6.13. There was not a refrigerant liquid section in the heat exchanger since the indoor heat exchanger was only validated under cooling mode operating.

Table 6.8 Heat transfer correlations and corresponding correction factors

	Correlation	Correction Factor
Air-side	Chang, Wang	1.0
Refrigerant Vapor Phase	Gnielinski	1.0
Refrigerant Two Phase	Jung, Radermacher	1.0

Table 6.9 Pressure drop correlations and corresponding correction factors

	Correlation	Correction Factor
Air-side	Chang, Wang	1.0
Refrigerant Vapor Phase	Blasius	2.3
Refrigerant Two Phase	Jung, Radermacher	2.3

The indoor heat exchanger was validated using four experimental data points, shown in Table 6.10. The inlet air-condition remained relatively constant for all four test cases.

Table 6.10 Air-side and refrigerant-side inlet conditions

Air-side Inlet Conditions		Refrigerant-side Inlet Conditions		
T (°C)	RH	T (°C)	x	\dot{m} (g/s)
26.4	51.7	10.2	0.18	65.2
26.4	51.7	11.1	0.23	66.6
26.4	52.0	12.1	0.31	65.2
26.4	52.1	12.2	0.34	63.5

The heat load validation results for the outdoor heat exchanger are displayed in Figure 6.15. Again, the CoilDesigner result and the Tank and Tube Heat Exchanger model results are shown for comparison purposes. The maximum error in the heat load prediction for the Tank and Tube Heat Exchanger model was 5.4% compared to 4.5% for CoilDesigner. The average relative error for the Tank and Tube Heat Exchanger model in the heat load prediction for all the test cases was 3.6% compared to 2.1% for CoilDesigner. It is expected that CoilDesigner will more accurately capture the heat load performance since air-side discretization is more resolved. A total of 36 segments were used to model each tube row in CoilDesigner and the propagation of air properties through the heat exchanger was more precise. Even though only three tanks were used to

model the indoor heat exchanger, the difference in performance between the Tank and Tube Heat Exchanger and CoilDesigner was found to be not very significant.

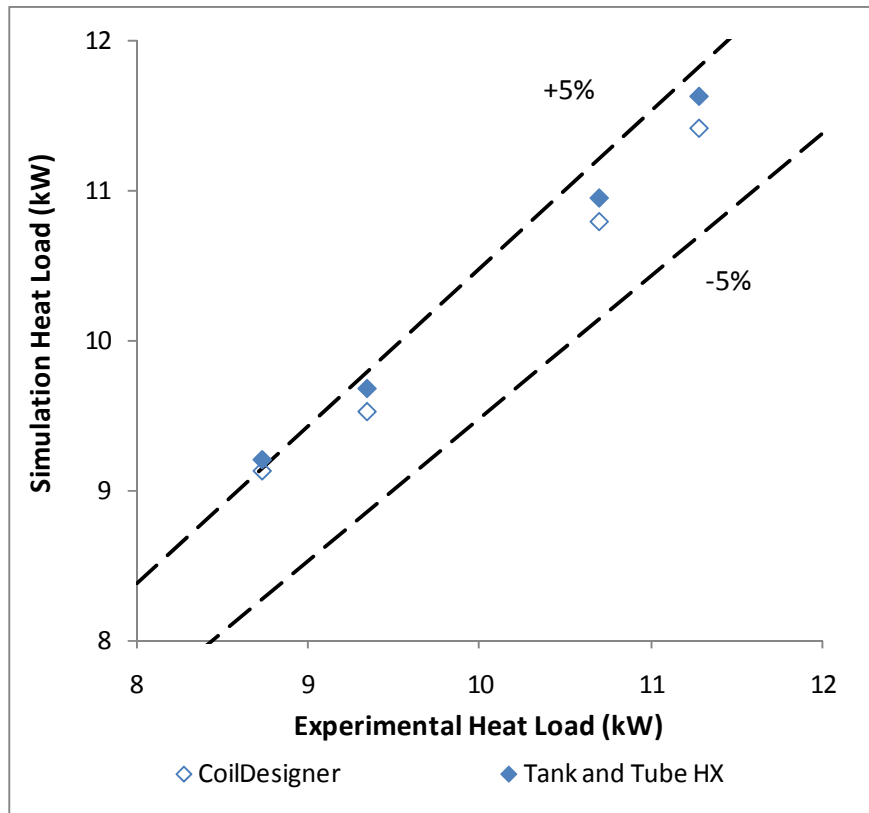


Figure 6.15 Heat load validation results for the indoor heat exchanger

The refrigerant-side pressure drop validation results for the Tank and Tube Heat Exchanger model and CoilDesigner are plotted in Figure 6.16. The average relative error in the pressure drop prediction for the Tank and Tube Heat Exchanger Model was 8.9% compared to 4.0% for CoilDesigner. The pressure drop error for the Tank and Tube Heat Exchanger is much higher than CoilDesigner due to the discretization on the refrigerant-side. For the outdoor heat exchanger, ten tanks were used to simulate the heat exchanger, whereas only three were used in the indoor heat exchanger. A total of 108 cells were used in CoilDesigner to discretize the refrigerant-side.

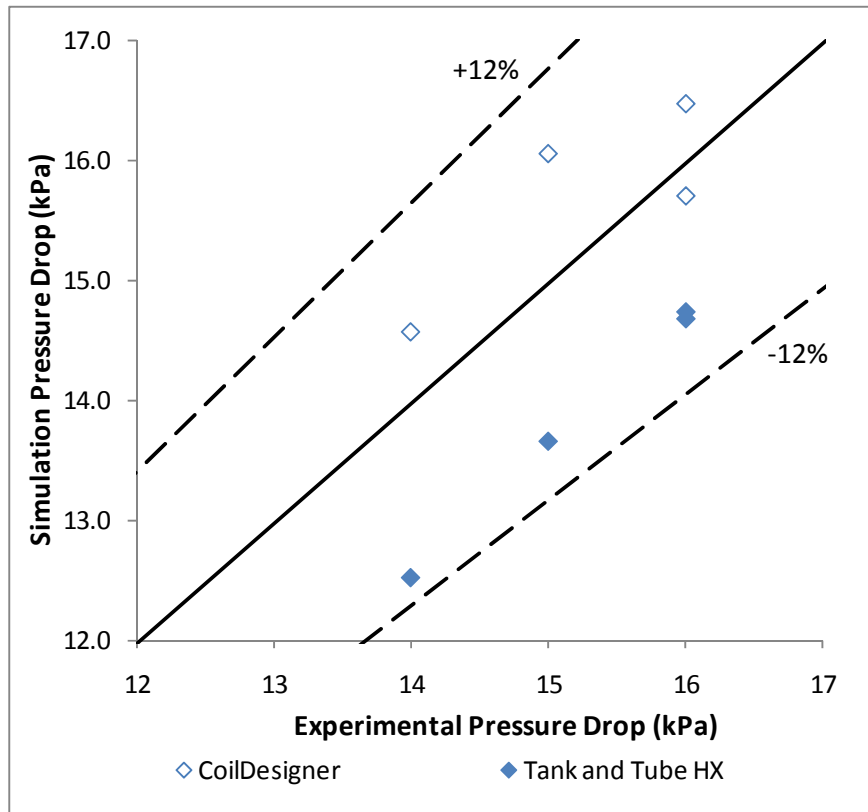


Figure 6.16 Pressure drop validation results for the indoor heat exchanger

6.2 Compressor Simulation

The compressor models described in Section 1.3.3 are transient models and cannot be directly utilized in a steady state simulation. Though steady state compressor models have been used in transient simulations, these models do not capture important transient effects, such as the compressor shell temperature. Most of the compressor models presented in the literature require a set of input parameters that are not readily available to design engineers. The development of a new compressor model suitable for steady state and transient calculations will ensure consistent results between the two types of simulation.

6.2.1 Compressor Modeling Approach

Figure 6.17 displays the various processes that occur as the refrigerant flows through a typical suction cooled, hermetic, reciprocating compressor. Reciprocating compressors are used in a large variety of vapor compression systems; including low temperature, medium temperature, and air conditioning applications (ASHRAE, 2000).

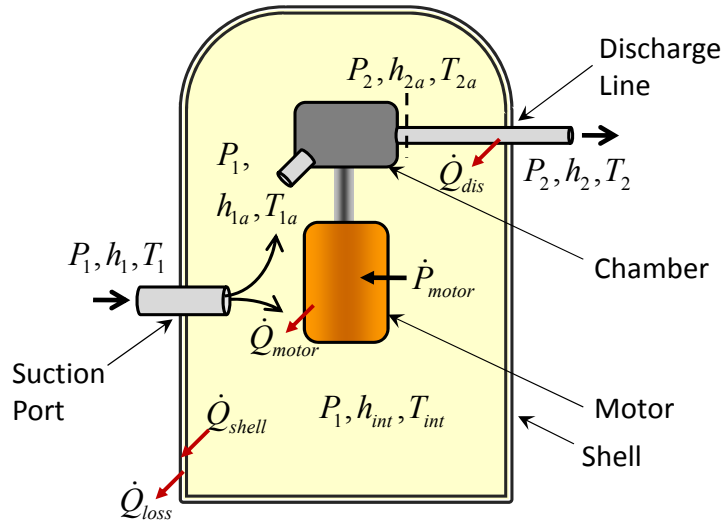


Figure 6.17 Reciprocating compressor model schematic

The refrigerant enters the compressor through the compressor suction port (P_1, h_1) and flows into the compressor shell. While in the compressor shell, a portion of the refrigerant is heated by the compressor motor and the refrigerant discharge line, and transfers heat to the compressor shell prior to entering the compression chamber (P_{1a}, h_{1a}). The remaining refrigerant flows directly into the compression chamber. In the compression chamber, the refrigerant is compressed, thus increasing the refrigerant pressure and temperature (P_{2a}, h_{2a}). Prior to exiting the compressor, the compressor flows through the discharge line in which heat is rejected to the low pressure refrigerant within the compressor shell (P_2, h_2).

Figure 6.18 displays processes that occur as the refrigerant flows through a suction cooled, hermetic, scroll compressor (ASHRAE, 2000). Scroll compressors are most commonly used in residential and commercial air conditioning, refrigeration, and heat pump applications. Scroll compressors are also used in automotive air-conditioning systems (ASHRAE, 2000).

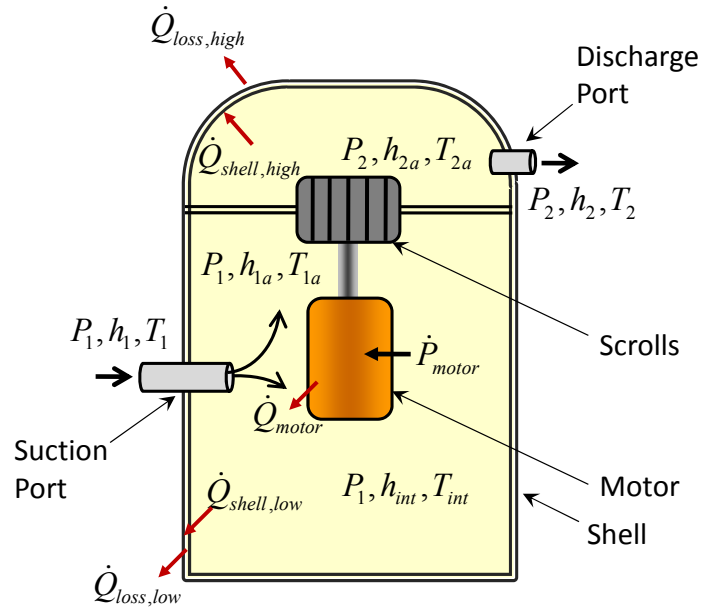


Figure 6.18 Scroll compressor model schematic

Similar to the reciprocating compressor, a portion of the refrigerant flowing into the scroll compressor cools the motor and exchanges heat with the compressor shell prior to entering the scrolls (P_{1a} , h_{1a}). The remaining refrigerant flows directly into the compressor scrolls. In the scroll compressor, the high pressure and low pressure regions within the shell are separated by an interface. The heat transferred from the high pressure refrigerant to the low pressure refrigerant through this interface is neglected. The refrigerant is compressed in the compressor scrolls, thus increasing the refrigerant pressure and temperature (P_{2a} , h_{2a}). The refrigerant exiting the compressor scrolls rejects heat to the compressor shell prior to exiting the compressor (P_2 , h_2).

Sections 6.2.1.2 through 6.2.1.4 describe the compressor modeling procedure and present the equations sets used to model both the reciprocating and scroll compressors. Both compressor models utilize the same approach to calculate the refrigerant mass flow rate and refrigerant outlet condition. However, the approach implemented to calculate the compressor shell heat loss, and thus power consumption, differs based on the geometry of the compressor type being simulated. This thesis presents models for the reciprocating and scroll compressors. Additional compressor types include rolling piston compressors, rotary vane compressors, screw compressors, and centrifugal compressors; models for which have not been included in this thesis. However, the general modeling approach can be applied to these types of compressors as well.

6.2.1.1 Boundary Conditions

The compressor dictates the vapor compression system refrigerant flow rate. Thus, nearly all compressor models in the literature calculate the refrigerant mass flow rate given the inlet condition and outlet pressure. Prior to being executed, the inlet pressure, inlet enthalpy, and outlet pressure are passed to the compressor model. The compressor model uses the boundary conditions along with the required physical parameters to calculate the compressor mass flow rate, outlet enthalpy/temperature, and power consumption.

6.2.1.2 Compressor Model Formulation and General Equation Set

The mechanisms of heat transfer within the compressor, as shown by Figure 6.17 and Figure 6.18, are dependent on the type of compressor. However, the outlet condition (h_2) can be calculated independently of the type of compressor. The compressor isentropic efficiency is generally available to most design engineers interested in conducting system-level simulation of vapor compression systems. The compressor

isentropic efficiency reported by compressor manufactures is calculated using the refrigerant conditions measured at the compressor suction and discharge ports, and thus the isentropic efficiency can be used to calculate the compressor outlet condition independent of the type of compressor.

A variety of compressor models presented in the literature assume a polytropic process. Such models use the polytropic work and polytropic efficiency to simulate the compressor. Though the polytropic work and polytropic efficiency remain more consistent over a variety of applications when compared to an isentropic analysis, the input parameters required to calculate the polytropic work and the polytropic efficiency are generally not known with a high level of certainty. For example, the refrigerant polytropic coefficient is used to calculate the polytropic work. The polytropic coefficient for a particular refrigerant is generally difficult to attain from the literature and assuming that the polytropic coefficient remains constant over a variety of operating conditions is generally not a valid assumption.

Therefore, using the isentropic efficiency to calculate the outlet condition is the most meaningful choice. Thus, the refrigerant outlet enthalpy can be calculated using Equation 6.33

$$h_2 = h_1 + \frac{h_{2,s} - h_1}{\eta_{isen}} \quad (6.33)$$

where $h_{2,s}$ is the isentropic enthalpy at P_2 and η_{isen} is the isentropic efficiency of the compressor. The isentropic efficiency in 6.33 can be entered as a constant value or as a user-defined function dependent on the operating conditions.

The compressor mass flow rate is calculated using the compressor volumetric efficiency. The volumetric efficiency provided by compressor manufacturers is generally

calculated using the suction density, ρ_1 , even though the refrigerant temperature entering the compression chamber has been increased from T_1 to T_{1a} . The refrigerant mass flow rate is calculated using Equation 6.34

$$\dot{m} = \eta_{vol} \rho_1 D_v \frac{RPM_{motor}}{60} \quad (6.34)$$

where η_{vol} is the compressor volumetric efficiency, D_v is the displacement volume of the compressor, and RPM_{motor} is the compressor speed.

The equations used to calculate the outlet condition and mass flow rate are independent of compressor type. However, the heat transfer processes occurring within the compressor, as shown in Figure 6.17 and Figure 6.18, are dependent on the compressor type and thus the heat transfer calculations must be representative of the type of compressor being modeled. Under steady state operation, after the compressor shell temperature has reached a steady value, the rate of heat transfer from the refrigerant to the shell is equivalent to the rate of the heat transfer from the shell to the ambient. Therefore, Equation 6.35 states that the change in refrigerant enthalpy is equal to the compressor power consumption, \dot{P}_{comp} , minus the heat loss from the compressor shell, \dot{Q}_{loss} . It can also be concluded from Equation 6.35 that the error in predicting the heat loss from the compressor shell will be evident in the error of either the predicted refrigerant outlet enthalpy or the compressor power consumption.

$$\dot{m}(h_2 - h_1) = \dot{P}_{comp} - \dot{Q}_{loss} \quad (6.35)$$

Under transient calculation, there is an imbalance between the rate of heat transfer from the shell to the ambient and the rate heat transfer from the refrigerant to the shell, and thus Equation 6.35 no longer holds true. Rather, Equation 6.36 describes the energy

balance occurring within the compressor shell. The thermal storage of the refrigerant and oil within the compressor shell are neglected in this case.

$$\dot{m}(h_2 - h_1) = \dot{P}_{comp} - \dot{Q}_{shell} \quad (6.36)$$

Since minimizing the compressor power consumption is often one of the key objectives behind simulating a vapor compression system, one of the main goals of simulating a vapor compression system should be to accurately predict the compressor power consumption. Since the outlet enthalpy, h_2 , is calculated using Equation 6.33, according to Equation 6.36 the heat transferred from the refrigerant to the compressor shell must be calculated in order to predict the compressor power consumption accurately.

The heat rejected by the compressor motor is calculated using the compressor power consumption and motor efficiency as shown in Equation 6.37.

$$\dot{Q}_{motor} = (1 - \eta_{motor}) \dot{P}_{motor} \quad (6.37)$$

Equation 6.37 applies to any type of hermetic compressor where the refrigerant (suction or discharge) cools the compressor motor.

6.2.1.3 Reciprocating Compressor Heat Transfer Calculations

As shown in Figure 6.17, a portion of the refrigerant entering the compressor is heated by the compressor motor and rejects heat to the compressor shell while the remaining refrigerant flows directly into the compression chamber. The heat rejected to the compressor shell occurs at the intermediate temperature, T_{int} , and requires the overall heat transfer coefficient, $(UA)_i$, on the inside of the compressor shell.

$$\dot{Q}_{shell} = (UA)_i (T_{int} - T_{shell}) \quad (6.38)$$

$$T_{int} = fn(P = P_1, h = h_{int}) \quad (6.39)$$

The compressor shell is modeled as a single lump, and thus Equation 6.38 assumes that the compressor shell is at a uniform temperature. This is a valid assumption since the inside of the compressor shell only contacts low pressure refrigerant. The intermediate enthalpy, h_{int} , can be calculated using Equations 6.37, 6.38, and 6.42

$$h_{int} = h_1 + \frac{\dot{Q}_{motor} + \dot{Q}_{dis} - \dot{Q}_{shell}}{(1-r)\dot{m}} \quad (6.40)$$

where r is the portion of refrigerant that flows directly into the compression cylinder. The enthalpy flowing into the compression chamber is calculated using Equation 6.41.

$$h_{1a} = rh_1 + (1-r)h_{int} \quad (6.41)$$

The heat rejected by the refrigerant as it flows through the discharge line is calculated using the temperature gradient between refrigerant outlet temperature, T_2 , and the intermediate refrigerant temperature, T_{int} , along with the overall heat transfer coefficient of the discharge line.

$$\dot{Q}_{dis} = (UA)_d(T_2 - T_{int}) \quad (6.42)$$

The refrigerant outlet condition from the compression chamber can be calculated using the heat rejected by the discharge line as follows.

$$h_{2a} = h_2 - \frac{\dot{Q}_{dis}}{\dot{m}} \quad (6.43)$$

Equation 6.43 assumes that the heat rejected by the high pressure refrigerant while flowing through discharge line enters the low pressure refrigerant, and thus the thermal capacity of the discharge line is neglected. The compressor power is then calculated using the compressor motor efficiency, η_{motor} .

$$\dot{P}_{motor} = \frac{\dot{m}(h_{2a} - h_{1a})}{\eta_{motor}} \quad (6.44)$$

The refrigerant inlet condition to the compression chamber (Equation 6.41) and the compressor power consumption (Equation 6.44) are dependent on one another. Thus, the compressor power consumption must be iteratively solved for within the compressor model.

The compressor shell rejects heat to the environment, which can be calculated using the overall heat transfer coefficient on the outside of the compressor shell, UA_o , and ambient temperature, T_{amb} .

$$\dot{Q}_{loss} = (UA)_o (T_{shell} - T_{amb}) \quad (6.45)$$

During transient operation the compressor shell temperature will change with time. The initial shell temperature must be provided to the compressor model prior to running the simulation. The refrigerant within the compressor shell typically rejects heat to the compressor shell resulting in the shell temperature increasing over time. As the shell temperature increases, the temperature gradient between the compressor shell and the ambient increases, and thus the heat rejected from the shell to the surrounding ambient also increases. The rate at which the compressor shell changes temperature is determined by the thermal mass of the compressor, $(MC)_{com}$, and can be calculated accordingly.

$$(MC)_{com} \frac{dT_{shell}}{dt} = \dot{Q}_{shell} - \dot{Q}_{loss} \quad (6.46)$$

During steady state simulation, Equation 6.46 is equal to zero and thus the heat rejected by the shell to the ambient must equal the heat rejected by the refrigerant to the shell. Thus, the following equation can be numerically solved to determine the steady state shell temperature.

$$(UA)_i (T_{int} - T_{shell}) = (UA)_o (T_{shell} - T_{amb}) \quad (6.47)$$

6.2.1.4 Scroll Compressor Heat Transfer Calculations

The heat transfer calculations in a scroll compressor are different than a reciprocating compressor due to the fact that the high pressure refrigerant comes into contact with a portion of the compressor shell. Thus assuming a single temperature for the entire compressor shell is no longer a valid assumption. Therefore, the shell heat transfer calculations have been separated for the low and high side regions of the compressor shell.

$$\dot{Q}_{shell,low} = p_{A,low} \cdot U_{i,low} \cdot A_i (T_{int} - T_{shell,low}) \quad (6.48)$$

$$\dot{Q}_{shell,high} = (1 - p_{A,low}) \cdot U_{i,high} \cdot A_i (T_{out} - T_{shell,high}) \quad (6.49)$$

The intermediate temperature, T_{int} , and refrigerant enthalpy at the inlet to the compressor scrolls, h_{1a} , are calculated using a similar procedure as described for the reciprocating compressor (Equations 6.39 through 6.41).

In the case of the scroll compressor, the refrigerant enthalpy at the outlet of the scrolls is calculated using $\dot{Q}_{shell,high}$.

$$h_{2a} = h_2 - \frac{\dot{Q}_{shell,high}}{\dot{m}} \quad (6.50)$$

The compressor power consumption is calculated using Equation 6.44. Similar to the reciprocating compressor, the compressor power consumption must be numerically solved through iteration due to the dependence of h_{1a} on the compressor power consumption.

Since the compressor shell has been discretized into two regions, the heat transferred from the shell to the environment must be calculated separately for each region.

$$\dot{Q}_{loss,low} = p_{A,low} \cdot (UA)_o (T_{shell,low} - T_{amb}) \quad (6.51)$$

$$\dot{Q}_{loss,high} = (1 - p_{A,low}) \cdot (UA)_o (T_{shell,high} - T_{amb}) \quad (6.52)$$

In Equations 6.51 and 6.52, $p_{A,low}$ represents the portion of outer surface area allotted to the low pressure region of the compressor shell.

Similar to the reciprocating compressor model, the scroll compressor model wall temperature must be updated during the transient simulation; however both the lower and upper shell temperature must be updated. The change in compressor shell temperature can be calculated in a similar fashion as the reciprocating compressor through allocating a percentage of the total thermal mass, $p_{M,low}$, to both the low and high sections of the compressor shell.

$$p_{M,low} \cdot (MC)_{com} \frac{dT_{shell,low}}{dt} = \dot{Q}_{shell,low} - \dot{Q}_{loss,low} \quad (6.53)$$

$$(1 - p_{M,low}) \cdot (MC)_{com} \frac{dT_{shell,high}}{dt} = \dot{Q}_{shell,high} - \dot{Q}_{loss,high} \quad (6.54)$$

6.2.2 Summary of Required Input Parameters

A list of the required inputs parameters to simulate reciprocating and scroll compressors are included in Table 6.11. The final column in this table describes how a value for the corresponding parameter would be attained by design engineers utilizing the compressor model.

Table 6.11 Parameters required to simulate reciprocating and scroll compressors

Input Parameter	Description	Recip./ Scroll	Comments
η_{isen}	Isentropic efficiency	Both	Available from compressor manufactures.
η_{vol}	Volumetric efficiency	Both	
D_v	Displacement volume	Both	
RPM	Compressor speed	Both	

η_{motor}	Motor efficiency	Both	Typical value 75-90%.
r	Mass flow ratio directed to shell	Both	Typical value varies based on compressor type.
U_i	Refrigerant heat transfer coefficient on inside of shell	Recip.	Typical value for low velocity refrigerant vapor flowing across a plate.
A_i	Heat transfer area inside of shell	Both	Available from compressor manufacture mechanical drawings.
$U_{i,low}$	Refrigerant heat transfer coefficient on lower portion inside of shell	Scroll	Typical value for low velocity refrigerant vapor flowing across a plate.
$U_{i,high}$	Refrigerant heat transfer coefficient on upper portion inside of shell	Scroll	Typical value for low velocity refrigerant vapor flowing across a plate.
$A_{i,high}$	Upper portion heat transfer area inside of shell	Scroll	Available from compressor manufacture mechanical drawings.
U_o	Air overall heat transfer coefficient on outside of shell	Both	Typical value based air flow rate or natural convection.
A_o	Heat transfer area on outside of shell	Both	Available from compressor manufacture mechanical drawings.
$P_{A,low}$	Percent of surface area (inner and outer shell) for the lower region	Scroll	Available from compressor manufacture mechanical drawings.
$(MC)_{com}$	Thermal mass	Both	Available from compressor manufactures.
$P_{M,low}$	Percent of thermal mass for the lower region	Scroll	Available from compressor manufacture mechanical drawings.
T_{amb}	Ambient temperature	Both	User preference based on simulation.

6.2.3 Compressor Model Validation

This section of the thesis presents a validation study for the scroll compressor model using experimental results for a R410A residential heat pump system. As indicated by Table 6.11, the scroll compressor model requires a large set of inputs parameters and thus the input parameters and the various sources are listed in Table 6.12.

Table 6.12 Input parameters used during compressor model validation

Input Parameter	Value Used in Validation	Source
η_{isen}	$\eta_{isen}, \eta_{vol} = f\left(\frac{P_2}{P_1}\right)$	Curve fit generated using steady state compressor manufacture data
η_{vol}		
D_v	30.69 cm ³	Compressor datasheet provided by manufacturer
RPM	3500	
η_{motor}	75%	Chose realistic value to best match experimental results
r	0.33	
$U_{i,low}$	100.0	Chose realistic value to best match experimental results
A_i	0.215 m ²	Calculated using manufacturer drawings
$U_{i,high}$	150.0	Chose realistic value to best match experimental results
U_o	50.0	Chose realistic value to best match experimental results
A_o	0.261 m ²	Calculated using manufacturer drawings
$P_{A,low}$	0.80	Estimated using manufacturer drawings
M_{com}	30.62 kg	Compressor datasheet provided by manufacturer
C_{com}	465.0 J/kg·K	Assumed compressor was 70% steel and 30% copper
$P_{M,low}$	0.85	Estimated using manufacturer drawings and Figure 6.18
T_{amb}	-18.0°C – 49.8°C	Experimental data

The compressor modeled was a 9.2 kW Copeland Scroll PFV compressor (model number ZP32K3E-PFV) used in residential air-conditioning and heat pump applications. Experimental results for a wide range of operating conditions have been published (Wang, 2008a) and a previous simulation of the compressor has been completed (Winkler *et al.*, 2008a) using a set of coefficients provided by the compressor manufacturer along with the Air-conditioning and Refrigeration Institute (ARI) compressor modeling equation (ARI, 1999). The ARI provides a standard compressor rating procedure and equation

format in which compressor manufactures publish coefficients for use within the standardized compressor equation. The coefficients provided by compressor manufactures are attained using the compressor's steady state performance over a variety of evaporating and condensing temperatures. However, the ambient temperature and inlet superheat are held at a single constant value during these tests. As a result, the ARI compressor model neglects the compressor shell cooling effects on the performance. The published coefficients for the compressor power consumption and mass flow rate were used in the steady state validation as a means of comparison since compressor coefficients are commonly used in steady state simulation of vapor compression systems.

The experimental compressor mass flow rate and isentropic efficiency values were attained from the published compressor performance data sheet. The reported compressor mass flow rate and isentropic efficiency were used to generate the volumetric and isentropic efficiency curves mentioned in Table 6.12. The volumetric and isentropic efficiency relations of the compressor were modeled as a function of the refrigerant condensing and evaporating temperature. The curves representing the compressor volumetric and isentropic efficiency were generated using TableCurve 3D (SYSTAT Software, 2002).

6.2.3.1 Steady State Validation

The compressor steady state performance was tested under a variety of cooling and heating applications with the ambient temperature ranging from -17.95°C to 49.79°C. A summary of the experimental test conditions are listed in Table 6.13.

Table 6.13 Steady state compressor operating conditions

T_{amb} (°C)	$T_{sat,in}$ (°C)	$T_{sat,out}$ (°C)	T_{in} (°C)
49.79	11.09	60.31	22.81
46.35	10.57	57.16	22.06

35.05	9.04	46.73	18.57
28.05	8.13	40.22	18.69
19.88	5.37	32.83	21.55
16.59	8.99	46.17	13.74
8.35	1.16	42.30	4.46
-8.32	-12.96	35.91	-10.66
-8.40	-12.67	35.67	-9.41
-8.58	-13.10	35.83	-10.56
-17.41	-20.02	32.14	-16.58
-17.95	-20.32	31.86	-16.53

Figure 6.19 displays the validation results for the compressor power consumption for the Scroll Compressor Model and the ARI Compressor Model using the manufacturer provided power consumption coefficients. The Scroll Compressor Model predicts the compressor power consumption with an average relative error 4.77% and a maximum relative error of 10.20%. By comparison, the ARI Compressor Model underestimates the power consumption consistently by approximately 10% with an average relative error of 11.25% and a maximum error of 12.38%.

Figure 6.20 displays the validation results for the compressor mass flow rate for the Scroll Compressor Model as well as the ARI Compressor Model. The results for the two models are essentially identical due to the procedure in which the volumetric efficiency correlation for the Scroll Compressor Model was attained. Since the Scroll Compressor Model volumetric efficiency and the ARI Compressor Model mass flow rate coefficients were attained from the same published manufacturer dataset, it is expected that the two models would have similar results. The compressor mass flow rate was predicted by the Scroll Compressor Model with average relative error of 7.5% and a maximum relative error of 20.69%. The point of maximum relative error occurred at the lowest ambient

temperature and at a relatively low mass flow rate which limited the absolute error in the mass flow rate prediction to 3.92 g/s.

The reason for the high error in the mass flow rate prediction of both the Scroll Compressor Model and the ARI Compressor Model is due to the fact that the compressor performance is only published at a single ambient temperature of 35.0°C and inlet superheat of 11.1°C. The compression of the refrigerant does not occur at the compressor suction port, but rather through the compressor scrolls (as shown in Figure 6.18). Thus, the refrigerant density at the inlet to the compressor scrolls is being transferred through the compression process. The density of the refrigerant at the inlet to the compressor scrolls is affected by the amount of heat transferred to the refrigerant as it flows from the compressor suction port to the scroll inlet. Again, the volumetric efficiency (determined from Equation 6.34) correlation was generated using the compressor suction port density since the refrigerant condition at the inlet to the compressor scrolls is not published information.

Validation results for the compressor discharge temperature are plotted in Figure 6.21. Similar to the mass flow rate prediction, the discharge temperature predicted by the Scroll Compressor Model and the ARI Compressor Model are quite similar. This is due to the fact that the Scroll Compressor Model uses the isentropic efficiency to calculate the outlet refrigerant enthalpy and the isentropic efficiency is determined from a correlation generated using published compressor data. Again, the isentropic efficiency reported by the compressor manufacturer was attained by testing the compressor at a fixed ambient condition and fixed refrigerant suction superheat. The compressor

discharge temperature was predicted to within $\pm 3.0^{\circ}\text{C}$ with an average absolute error of 1.41°C .

Figure 6.22 displays the predicted compressor shell temperature for the top of the compressor shell and the side of the compressor shell. The top of the compressor shell is in thermal contact with the high pressure side of the compressor (as shown in Figure 6.18) and side of the compressor shell is in thermal contact with the low pressure side of the compressor. The results plotted in Figure 6.22 are for the Scroll Compressor Model exclusively since the ARI Compressor Model does not provide a means of estimating the compressor shell temperature.

As shown in Figure 6.22, the Scroll Compressor Model more accurately predicted the compressor shell temperature located at the top of the compressor. The error in the compressor shell temperature prediction for the top of the compressor ranged from 7.43°C to -0.67°C with an average absolute error of 3.09°C . The compressor shell temperature prediction at this location was over predicted for all but two of the twelve operating points. The shell temperature prediction for the side of the compressor shell was predicted with an error ranging from 11.90°C to -12.06°C . The average absolute error was 6.93°C for this location. The error associated with the side shell temperature predicted followed the ambient temperature. At high ambient temperatures, the compressor shell temperature at this location was over-predicted while at low ambient temperatures the shell temperature at this location was under-predicted. In all cases however, the compressor shell temperature at the side of the compressor was higher than the ambient, and thus heat was always rejected by the compressor shell to the ambient.

It is important to note, that according to Wang (2008b) there is a high level of uncertainty in the compressor shell temperature measurements. This is due to the fact that for certain test cases, the tape holding the thermocouple to the compressor shell failed and thus the thermocouple was not in thermal contact with the compressor shell (Wang, 2008b). For the cases in which the thermocouple was not in contact with the compressor shell, the measured temperature would be lower than the actual shell temperature. The uncertainty of the shell temperature measurements was not taken into account during this validation since it cannot be determined exactly for which cases the thermocouples were not in contact with the compressor shell.

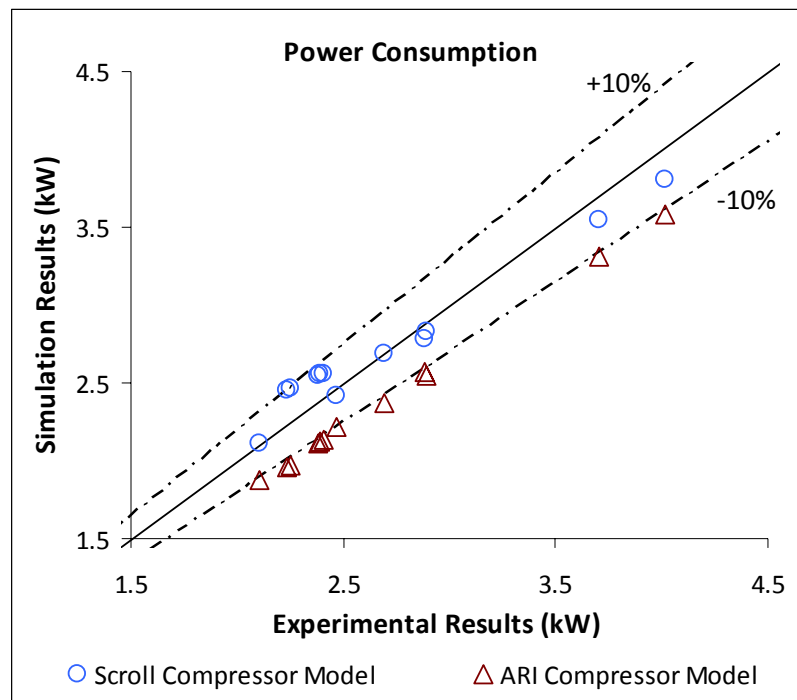


Figure 6.19 Compressor power consumption validation results (steady state operation)

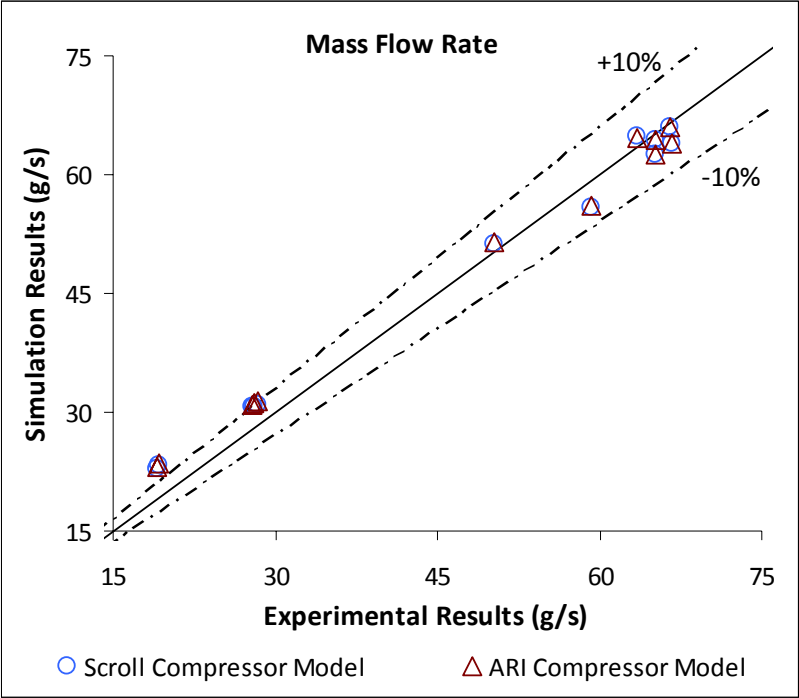


Figure 6.20 Compressor mass flow rate validation results (steady state operation)

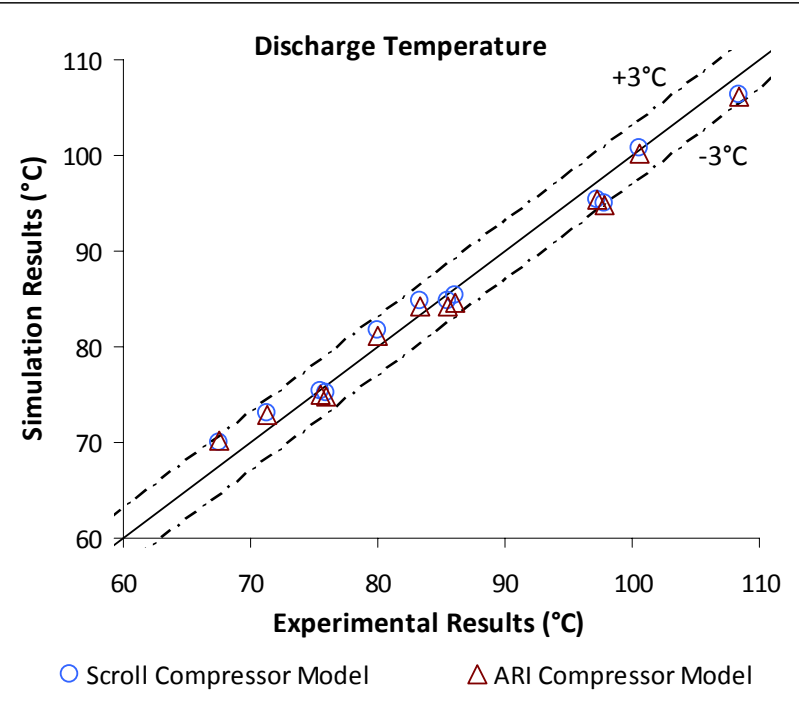


Figure 6.21 Discharge temperature validation results (steady state operation)

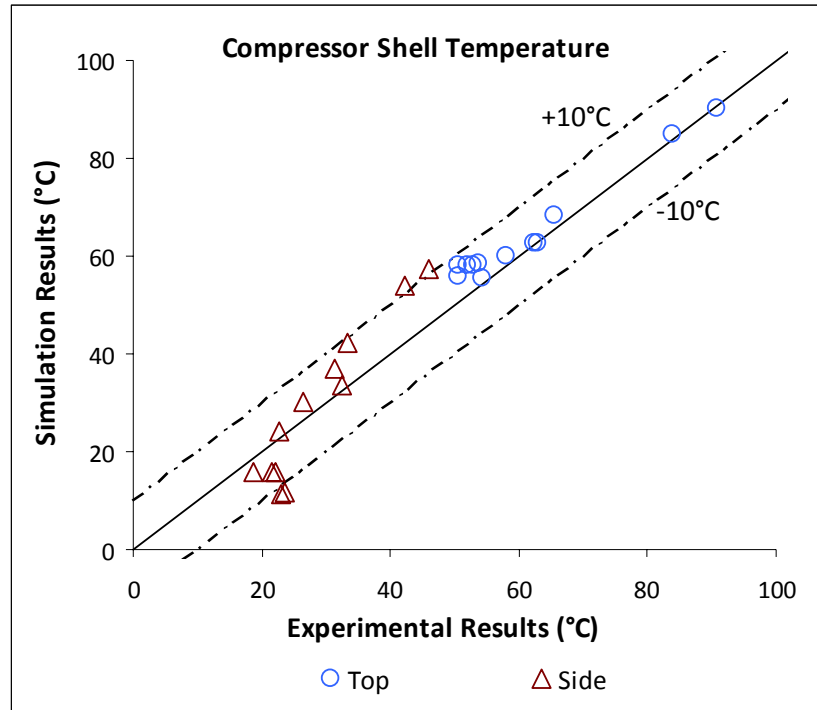


Figure 6.22 Compressor shell temperature validation results (steady state operation)

6.2.3.2 Transient Validation

The compressor startup performance was tested at a single operating condition. During the startup test, the vapor compression system was operating in cooling mode with an ambient temperature of 35°C. The system was turned on after the system had come to a state of equilibrium; meaning the pressure in the condenser and evaporator had equalized and the compressor shell temperature was close to the ambient temperature. After the compressor was turned on, the system was run for a period of 60 minutes and data was sampled every second.

Simulating the transient performance of a compressor without simulating the behavior of the entire system would typically not be feasible since the other components in the vapor compression system determine how the evaporating and condensing temperatures of the system change as the system reaches steady state. The evaporating

and condensing temperatures are required to execute the compressor model, and thus it makes most to simulate the entire vapor compression system when investigating the transient performance of the compressor. However, in order to validate the compressor model without incorporating the uncertainty of the other component models, the transient performance of the compressor was modeled using the experimental values for the suction pressure, suction temperature, and discharge pressure. Thus, the simulation was run using a time step of one second and directly used the experimental values for suction pressure, suction temperature, and discharge pressure at each time step. The experimental suction and discharge pressures used to run the transient simulation are displayed in Figure 6.23.

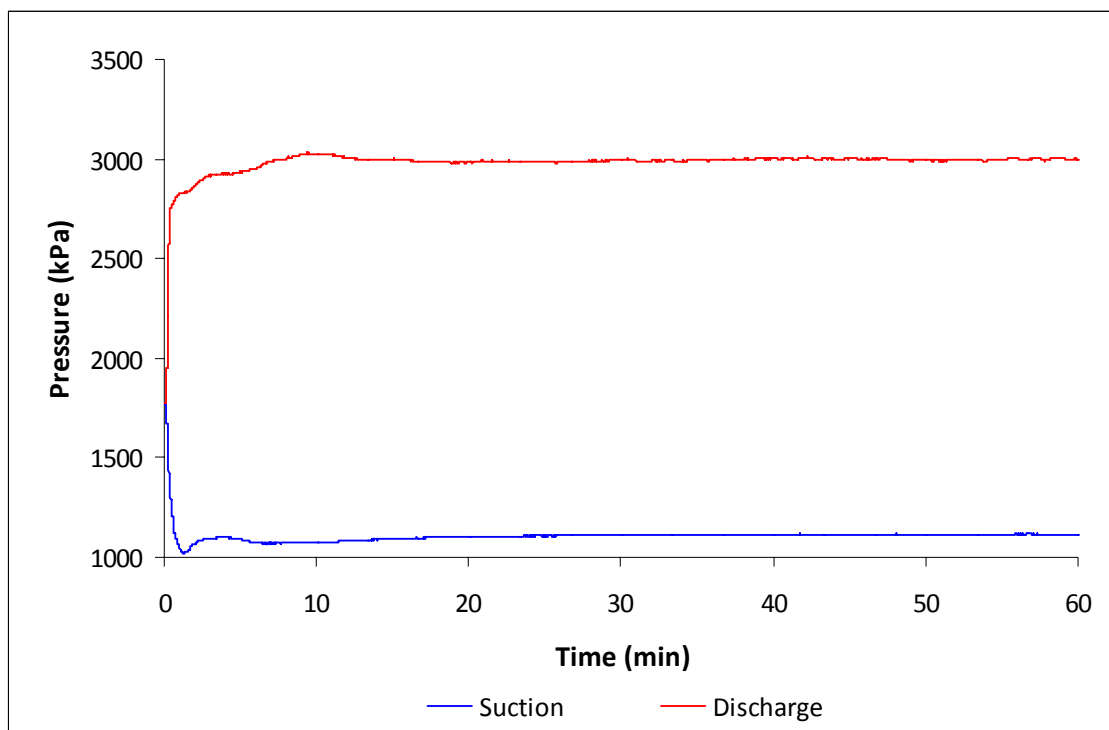


Figure 6.23 Experimental suction and discharge pressures during startup test

The validation results for the compressor mass flow rate are shown in Figure 6.24. The difference between the measured and predicted mass flow rate during the first minute

of operation can be attributed to the refrigerant condition at the inlet of the mass flow rate meter. As indicated by Wang (2008), a Coriolis flow mass flow meter was located at the condenser outlet to avoid data fluctuation associated with reading the mass flow rate of two phase flow. However, during the initial startup of the vapor compression system, there is generally a delay in the development of subcooled liquid at the exit to the condenser. During this period the mass flow rate can not be accurately modeled, explaining the initial trends in the experimental mass flow rate. Also during this initial startup period, the pressure ratio across the compressor is small; thus resulting in a high volumetric efficiency. Other than the initial startup period lasting approximately one minute, the mass flow rate predicted by the Scroll Compressor Model agrees well with the experimental values. The steady state value was predicted with a relative error of 3.3%.

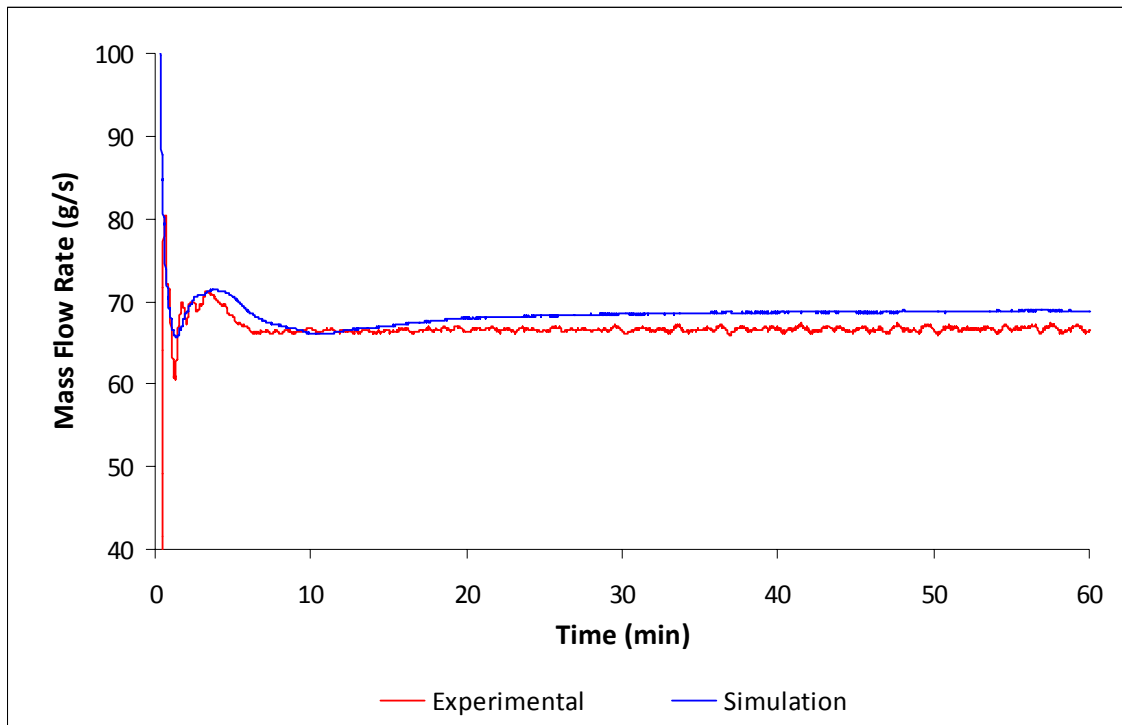


Figure 6.24 Compressor mass flow rate validation results (transient operation)

The validation results for the compressor discharge temperature are shown in Figure 6.25. The simulation results show good agreement with the experimental values as a steady state is reached, however during the first 30 minutes of the simulation the discharge temperature is over-predicted by the model. Though the model captures the experimental trends, the maximum error in the predicted discharge temperature after the initial startup (after the first 2 minutes of simulation) is approximately 8.0°C.

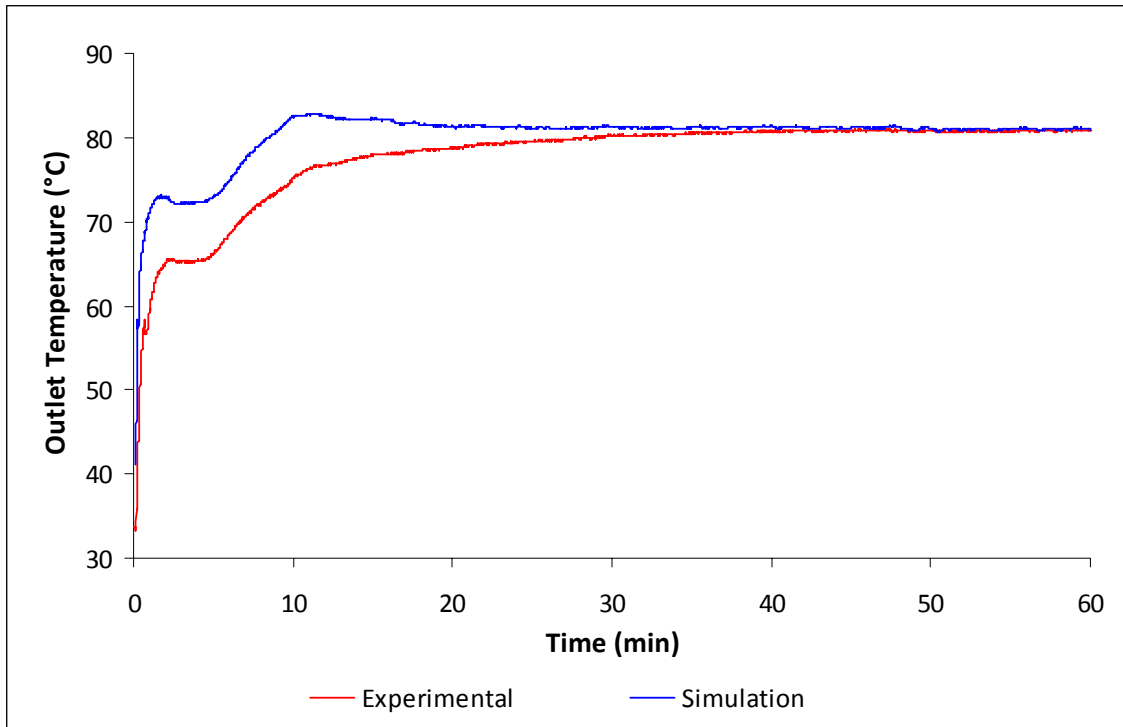


Figure 6.25 Compressor outlet temperature validation results (transient operation)

The compressor model uses the isentropic efficiency along with the refrigerant inlet condition to calculate the outlet condition. As previously mentioned, the isentropic efficiency values used to execute the simulation were taken from steady state manufacturer data, and thus the compressor model shows good agreement with the experimental values as steady state performance is reached. During the experiment, when the compressor is turned on the compressor shell temperature is close the ambient

temperature and proceeds to heat up as the compressor runs. Thus, the discharge refrigerant temperature is lower than the steady state values since heat is rejected from the refrigerant to the compressor shell. The error in the discharge temperature is due to the fact that the isentropic efficiency is used to directly calculate the refrigerant condition as the compressor discharge.

The validation results for the compressor power consumption are shown in Figure 6.26. Again, the model shows good agreement with the experimental results as steady state is reached with a relative error in the steady state power consumption of 1.68%. During the startup period, the model over predicts the power consumption.

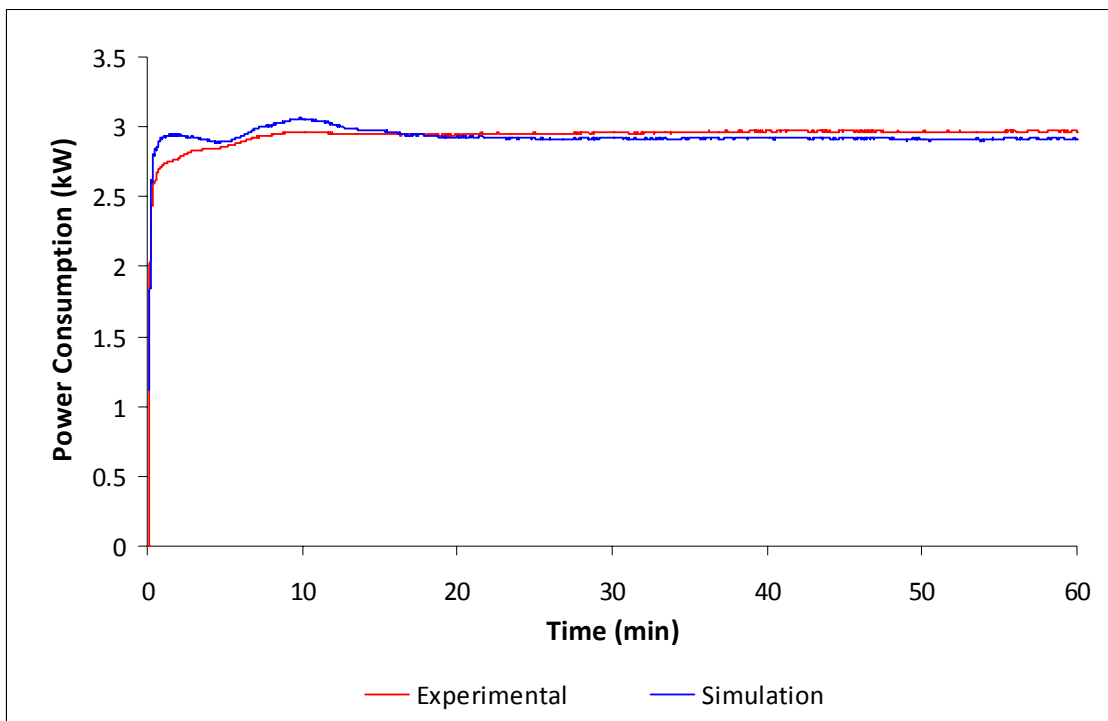


Figure 6.26 Compressor power consumption validation results (transient operation)

The power consumption predicted by the model increases much faster than the experimental results. The slight peaks in the simulated power consumption match the peaks in the discharge temperature shown in Figure 6.25 occurring at approximately 2

and 10.5 minutes into the simulation. As previously mentioned, the discharge temperature is calculated using the isentropic efficiency. According to Equation 6.36, if the outlet enthalpy, h_2 , (and thus the outlet temperature) is over predicted, either the power consumption or heat rejected from the refrigerant to shell will be over predicted as well. Therefore it is expected that the power consumption would be over predicted during the time spans in which the discharge temperature was also over predicted.

The simulated and experimental compressor shell temperatures for the top and side of the compressor shell are shown in Figure 6.27. The steady state temperature for the top of the compressor shell was under predicted by 11.6°C and the temperature for the side of the compressor shell was under predicted by 3.2°C.

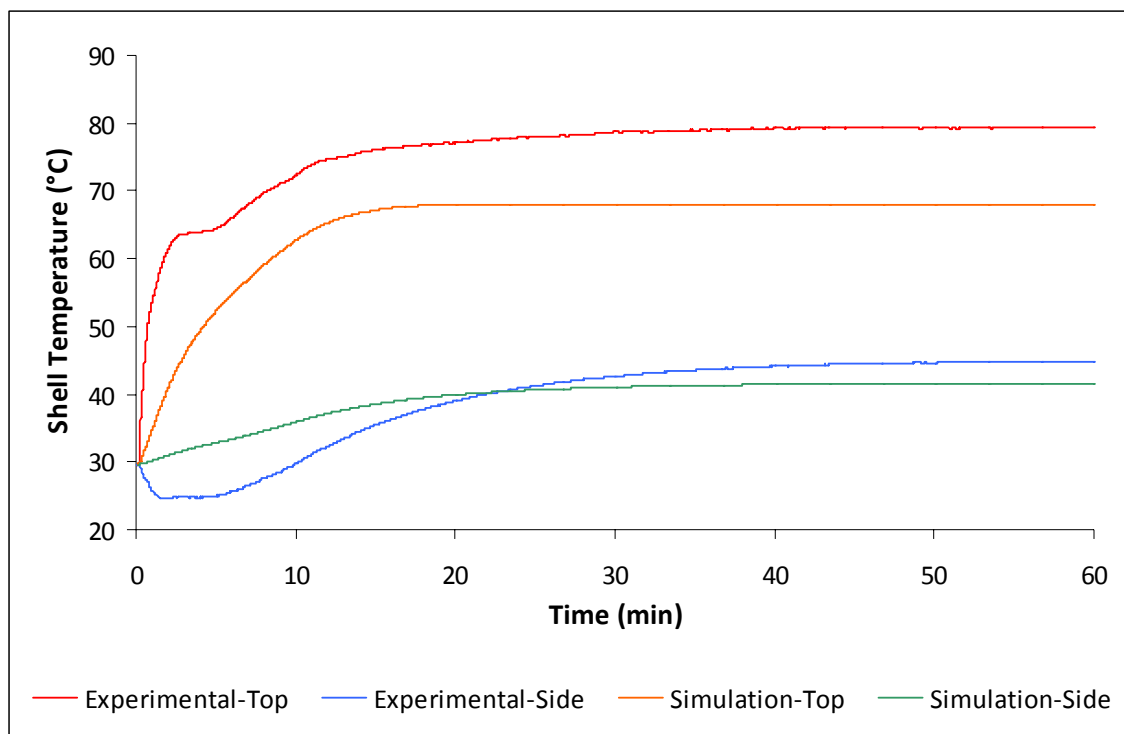


Figure 6.27 Compressor shell temperature validation results (transient operation)

The rate of change of the compressor shell temperature for the compressor side and top, as shown in Equations 6.53 and 6.54 respectively, are dependent on the rate of heat

transferred from the refrigerant to the shell, the rate of heat transferred from the shell to the ambient, and the thermal mass of the compressor. Since the predicted shell temperatures for both regions reasonably agreed with the experimental values during the steady state validation, it can be assumed that heat transfer was calculated fairly accurately. Even though the Scroll Compressor Model assumes the heat transfer coefficients to be constant during the simulation, since the refrigerant mass flow rate through the compressor does not significantly change after the initial startup period (as shown in Figure 6.24) the heat transfer coefficients are not likely to drastically change during the course of the transient simulation.

The rate at which the side temperature of the compressor shell changes differs from the experimental trends much more noticeably than the top of the compressor. Since it can be concluded that the heat transfer was modeled reasonably well, the differing trends in the side temperature is likely due to the thermal mass of the compressor not be accurately modeled. The Scroll Compressor Model does not take into account the thermal mass of the oil within the compressor shell. Even though the mass of the compressor was available from manufacturer data, the type and amount of materials used within the compressor were not known. The experimental values show a decrease in temperature immediately following the compressor being turned which does not appear in the simulation. This was likely due to the location of the thermocouple used to measure the side compressor temperature. If the thermocouple was located relatively close the compressor suction port, the cold refrigerant entering the compressor would affect the measured shell temperature for this location. This phenomenon was not captured by the model since the Scroll Compressor Model treats the lower portion of the compressor as a

single lump and therefore a single temperature value is used to represent the shell temperature for the lower region of the shell.

The cause of the error in the temperature prediction at the top of the compressor shell could not be determined. As shown in Figure 6.22, the simulated temperature at the top of the compressor shell during the steady state tests was over predicted for 10 out of 12 experimental values and the largest under prediction had an error of only -0.67°C . However, after executing the transient simulation, the temperature at the top of the compressor shell was under estimated by 11.6°C . The error in the temperature at the side of the compressor shell was consistent with the steady state data displayed in Figure 6.22. The transient pull down test was conducted at the same operating conditions as one of the steady state cooling tests ($T_{amb} = 35.05^{\circ}\text{C}$ as shown in Table 6.13) and thus the steady state performance of compressor and the system should be fairly similar to the steady state test. However, there are quite large discrepancies between the two tests as shown in Table 6.14. The system operating conditions ($T_{sat,suction}$, $T_{sat,discharge}$, $T_{suction}$, and $T_{discharge}$) for the two tests are fairly similar, however there is a large difference in the compressor shell temperatures. Unfortunately, the cause of these differences could not be determined.

Table 6.14 Steady state and transient performance comparison

Parameter	Steady State Test	Transient Test
$T_{sat,suction}$ ($^{\circ}\text{C}$)	9.04	10.85
$T_{sat,discharge}$ ($^{\circ}\text{C}$)	46.73	49.05
$T_{suction}$ ($^{\circ}\text{C}$)	18.57	17.88
$T_{discharge}$ ($^{\circ}\text{C}$)	79.97	80.80
$T_{shell,top}$ ($^{\circ}\text{C}$)	65.54	79.33
$T_{shell,side}$ ($^{\circ}\text{C}$)	33.32	44.80
\dot{m} (kg/s)	66.62	66.67
\dot{P} (kW)	2.88	2.97

Though the predicted compressor shell temperatures did not perfectly agree with the experimentally measured values, the model did capture the trends during transient test and despite the uncertainty in the measurements the model showed good agreement with the steady state results.

6.3 Expansion Device Simulation

The expansion device component models in the literature that are used in transient simulations of vapor compression system often employ the following assumptions:

- Refrigerant charge in the expansion device is neglected
- Mass flow rate distribution through the expansion device is neglected
- Refrigerant mass flow rate is modeled using a quasi-steady state approach

The assumption that the refrigerant charge in the expansion device is negligible is a valid assumption since the internal volume of the expansion device is extremely small compared the internal volume of the heat exchangers. Though liquid refrigerant enters the expansion valve, the liquid quickly flashes to two phase refrigerant which decreases the density and reduces the mass of refrigerant present in the expansion device.

This assumption in turn leads to an additional assumption that the refrigerant mass flow rate exiting the expansion device is equivalent to the mass flow rate entering the expansion device. Thus, the refrigerant mass flow rate distribution through the expansion device is neglected. In certain expansion devices (such as a fixed orifice, thermostatic expansion valve, electric expansion valve, short tube orifice, etc.) this is an acceptable assumption (MacArthur, 1984; Rossi and Braun, 1999; Shah *et al.*, 2004; Bendapudi *et al.*, 2005). However for capillary tubes, assuming the inlet and outlet mass flow to be equal is not ideal. Capillary tubes are often modeled using empirical correlations derived

from steady state performance data due to the complexity and computational expense required to perform accurate simulations. The available empirical correlations are derived from steady state performance data and require negligible computational expense (ASHRAE, 2002; Choi *et al.*, 2003). Due to the computational benefits of using empirical correlations to model the capillary tube, empirical correlations have been used to model the expansion device in transient simulation (Anand, 1999).

The third assumption listed above assumes the refrigerant mass flow rate through the expansion device is instantly affected by a change in condensing and evaporating pressures. This assumption, similar to the others, is utilized by nearly all the expansion device models used in the simulation of vapor compression systems presented in the literature.

Based on the assumptions listed above, it is suitable to use steady state expansion device models in the transient simulation. Thus, the integrated steady state and transient simulation tool can utilize the same library of expansion device models presented in Section 3.3. However, a time dependent variable might be required when simulating a thermostatic expansion valve in a transient simulation to take into account the thermal mass of the refrigerant bulb.

7 Transient System Simulation

The transient simulation of various component models does not produce very meaningful results unless the entire vapor compression system is analyzed. The basic four component vapor compression system using tank and tube heat exchanger models is shown in Figure 7.1. The system consists of four junctions used to connect the component models.

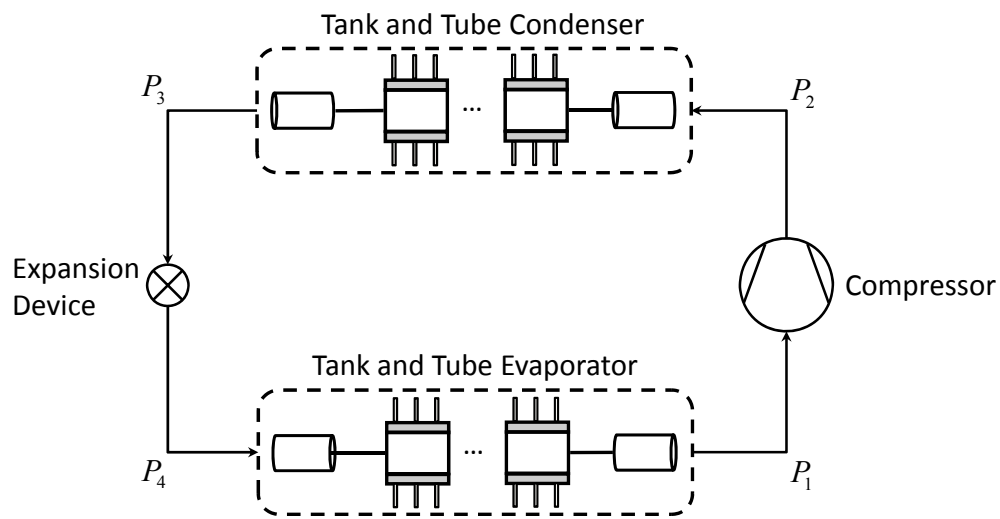


Figure 7.1 Basic four component system and unknown variables

7.1 System Simulation Procedure

7.1.1 System Level Solution Variables and Conservation Equations

The compressor and expansion device are the two components in the vapor compression system responsible for regulating the refrigerant flow rate. As a result, nearly all compressor and expansion device models in the literature calculate a mass flow rate given the inlet condition and outlet pressure. Recall, the heat exchanger models described in Section 6.1 calculate an inlet and outlet mass flow for a given inlet and outlet pressure. Thus, all the components in the system simulation shown in Figure 7.1 will calculate an inlet and outlet mass flow rate using the system junction pressures.

By definition, junctions in the cycle cannot store mass or energy; therefore the total mass and energy flowing into a junction must equal the total mass and energy flowing out of a junction. This constraint will result in four unique mass balance equations for the system shown in Figure 7.1. The conservation of energy at each junction can be handled by the execution order of the components since the outlet enthalpy from the heat exchanger is only modified after the time step has been completed. Therefore, for the basic system shown in Figure 7.1 four mass balance equations must be used to solve for the four unknown pressure values.

The four unknown variables can be placed in a vector as shown in Equation 7.1.

$$\vec{x} = [P_1 \quad P_2 \quad P_3 \quad P_4]^T \quad (7.1)$$

The system of residual equations used to solve for the unknown pressures is shown in Equation 7.2.

$$\vec{r} = \begin{bmatrix} \dot{m}_{comp,in} - \dot{m}_{evap,out} \\ \dot{m}_{cond,in} - \dot{m}_{comp,out} \\ \dot{m}_{exp,in} - \dot{m}_{cond,out} \\ \dot{m}_{evap,in} - \dot{m}_{exp,out} \end{bmatrix} \quad (7.2)$$

However, since the mass flow rate through the compressor and expansion device are assumed to behave quasi statically with respect the inlet and outlet pressures, the compressor and expansion device inlet and outlet mass flow rates (in Equation 7.2) can be replaced by a single term. Thus, Equation 7.2 can be simplified accordingly.

$$\vec{r} = \begin{bmatrix} \dot{m}_{comp} - \dot{m}_{evap,out} \\ \dot{m}_{cond,in} - \dot{m}_{comp} \\ \dot{m}_{exp} - \dot{m}_{cond,out} \\ \dot{m}_{evap,in} - \dot{m}_{exp} \end{bmatrix} \quad (7.3)$$

Equation 7.3 must be solved for simultaneously using a non-linear equation solver. Various non-linear equation solving algorithms exist in the literature, however the Hybrid method selected from the investigation described in Chapter 4 was chosen as the most suitable option. The numerical solver iterates until the specified convergence criteria is satisfied.

$$\|\vec{r}\|_2 \leq \varepsilon_f \quad (7.4)$$

The solution algorithm must be constructed in a generic nature to handle additional components. The nice feature of this algorithm is that it can be easily extended to cycles with additional components. For a system consisting of N_J junctions, the set of unknown variables can be expressed as follows.

$$\vec{x} = [P_1 \quad \dots \quad P_{N_J}]^T \quad (7.5)$$

Similarly, there are N_J mass balance equations.

$$r_i = \sum_{j=1}^{N \text{ Instreams}} \dot{m}_j - \sum_{k=1}^{N \text{ Outstreams}} \dot{m}_k \quad \forall i = 1 \dots N_J \quad (7.6)$$

This set of equations must be solved to convergence for each time step. Once the system pressures have been found, the transient variables are updated and the simulation steps forward in time.

A flow chart describing the transient simulation solution procedure is shown in Figure 7.2. The evaporator and condenser models must be provided with initial refrigerant conditions, which are used to execute the first time step and must be provided by the user. The initial conditions are used to determine guess values for the junction pressures to solve the initial time step. To solve subsequent time steps, using pressure values from the previous time step provides very accurate guess values since the system

pressures do not experience large changes over a single time step. This procedure reduces the number of iterations required to solve each time step.

The outlet enthalpy of the compressor is treated quasi-statically (same as the mass flow rate) and is dependent on the suction and discharge pressures. Thus in order to eliminate enthalpy values from the set of unknown values, the enthalpies in the cycle must be properly propagated.

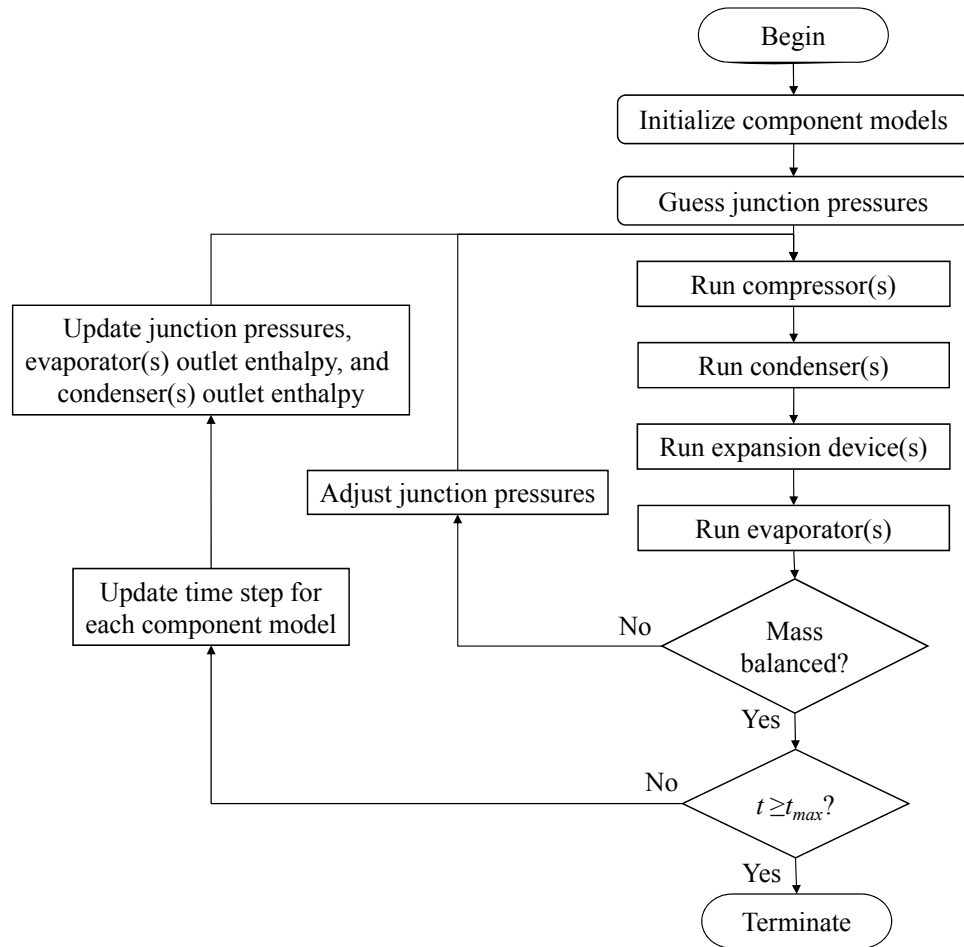


Figure 7.2 Flow chart describing the transient simulation solution procedure

7.1.2 Solution Procedure

The solution procedure developed to balance the cycle for transient simulations discussed above has similarities to the steady state solution procedures discussed in

Section 4.2 and is at essence a combination of the Junction Solver and Enthalpy Marching Solver. The transient solution scheme solves for the junction pressures by conducting system level mass balances at each junction in the cycle. Similar to the Junction Solver, this allows the approach to be easily extended to handle cycles containing additional components beyond the basic four component cycle. The solution scheme propagates the refrigerant enthalpy through the cycle in the same fashion as the Enthalpy Marching Solver allowing for the refrigerant enthalpy values to be removed from the set of unknown values. The reduction in the number of unknown values reduces the number of required function evaluations to solve each time step.

One of the disadvantages of the Junction Solver was the high computational cost associated with evaluating the heat exchanger models using the inlet and outlet pressures to calculate the refrigerant mass flow rate. Though this approach has been adopted by the transient system solver presented above, the high computational cost of evaluating the refrigerant mass flow rate has been eliminated due the procedure implemented by the inlet and outlet friction tubes. Recall from Section 6.1.2.1, the heat exchange inlet and outlet mass flow rate is calculated using a correlation derived to explicitly calculate refrigerant mass flow rate as a function of inlet and outlet pressure.

7.2 Time Stepping Procedure

After the solution for a given time-step has been reached, the simulation must be advanced forward in time. An explicit integration scheme was implemented to solve the differential equations since an implicit scheme is computationally more expensive and explicit schemes remain stable when using relatively small step sizes. Various integration methods exist; however fourth-order Runge-Kutta (Press *et al.*, 1992) has been shown to

be numerically stable for larger time steps than other methods (Bendapudi *et al.*, 2005). The time integration must occur in each component model, as opposed to at the system level, since the simulation is component-based. After a time-step has been solved, the system solver calls the update time step method in each component model and passes to each component model a common step size. Component models maintain the corresponding derivative information and update the transient variables accordingly.

7.2.1 Variable Time Step Procedure

A variable time step procedure for the transient simulation of vapor compression systems has been discussed by various authors (Anand, 1999; Rossi and Braun, 1999). Thus, a variable time step procedure has not been investigated in the current work and all the transient simulations were performed using a fixed time step value. Since the component models are provided with the time step size for each step, implementing a variable time step procedure is possible.

7.3 Transient and Steady State Comparison - Example Simulation

The simulation results presented in this section are for a simple test system, constructed to verify the steady state simulation tool and the transient simulation tool were indeed predicting similar results. Though experimental results were not used in this example, a validation using experimental results is shown in Section 7.4. The system was initially designed using steady state simulation techniques and then the transient simulation was used to perform a pull-down analysis, where essentially the system is turned on immediately following a long off period.

7.3.1 System Description

The system simulated was a typical four component 3 kW air-conditioner. The heat exchangers were designed by conducting steady state simulations using CoilDesigner. It should be pointed out that a number of validation studies of CoilDesigner (Aute *et al.*, 2004; Schwentker *et al.*, 2005; Jiang *et al.*, 2006) and the steady state solver (Winkler *et al.*, 2006; Winkler *et al.*, 2008a) have been presented. The condenser and evaporator were both single bank, single circuit heat exchangers consisting of eight tubes. Typical inlet air conditions for air-conditioning applications were used for both heat exchangers and were held constant during the transient simulation. The complete set of heat exchanger input parameters are shown in Table 7.1. The Tank and Tube Heat Exchanger model was used to simulate the heat exchangers in the transient simulation and the CoilDesigner Input File Translator, described in Section 6.1.6, was used to determine and calculate the necessary Tank and Tube Heat Exchanger model inputs from the CoilDesigner input files.

Table 7.1 Example simulation heat exchanger input parameters

	Evaporator	Condenser
Tube Length (m)	0.5	2.0
Tube Outer Diameter (mm)	9.525	9.525
Tube Thickness (mm)	1.0	1.0
Tube Vertical Spacing (cm)	1.0	1.0
Fin Type	Plate Fin	Plate Fin
Fins per Inch	20.0	20
Fin Thickness	0.1	0.1
Inlet Air Temperature (°C)	26.67	32.0
Air Flow Rate (m ³ /s)	0.1879	0.8941

The system used a reciprocating compressor and suitable input parameters were chosen for the type of system. The model described in Section 6.2.1.3 was used for the steady state and transient simulation. Recall, Section 6.2.1.3 describes the differences between the steady state and transient calculation procedures. The inputs for the

compressor model are shown below. A low value for the compressor thermal mass was selected to reduce the simulation time required for the pull down simulation to come to steady state.

Table 7.2 Example simulation reciprocating compressor input parameters

Isentropic Efficiency	0.65
Volumetric Efficiency	0.90
Displacement Volume (cm ³)	92.5
Compressor Speed (RPM)	1000.0
Motor Efficiency	0.90
Ambient Temperature (°C)	32.0
Thermal Mass (J/kg-K)	10.0
Outer Surface Area (m ²)	0.153
Outer Heat Transfer Coefficient (W/m ² -K)	40.0
Inner Surface Area (m ²)	0.125
Inner Heat Transfer Coefficient (W/m ² -K)	200.0

The steady state and transient simulations used a fixed orifice expansion device. The diameter was determined by manual adjustment during the steady state design process until a desired amount of superheat at the evaporator outlet was achieved.

The system subcooling was input during the steady state simulation and thus, the total system charge was calculated. The charge output from the steady state simulation was used as input in the transient simulation and the charge was initially allocated according to the internal volume of the heat exchangers.

It is important to point out the input parameters selected to test the simulation are best estimates; however the exact values of these parameters are not of paramount importance since the values are to remain consistent between the steady state and transient simulations.

7.3.2 Simulation Results

The following plots show transient and steady state results. The steady state results are indicated using horizontal lines since the values are independent of time. The transient simulation was only run for 20 seconds since the simulation reaches a steady state rather quickly due to the low thermal mass of the heat exchangers and the compressor.

The system pressures shown in Figure 7.3 represent the state points shown in Figure 7.1. The simulation starts with pressure being the same throughout the entire system, but the discharge pressure (junction 2 pressure) increases rapidly since this is at the compressor outlet. The difference between the pressure at junction 2 and the pressure at junction 3 is due to the pressure drop through the condenser. Similarly, the difference in pressure at junctions 4 and 1 is due to the pressure drop through the evaporator. The slight kink in the junction pressure at approximately 2.5 seconds is due to start of the superheated region in the evaporator. This occurs because of the discontinuity in the friction factor between two phase and vapor correlations.

The transient results match the steady values very well and the slight difference in the pressure drops is due to the discretization scheme. The heat exchanger models (CoilDesigner) in the steady state simulation were discretized into 40 control volumes (5 control volumes per tube for 8 tubes) whereas the Tank and Tube Heat Exchanger models used during the transient simulation consisted of only a single tank.

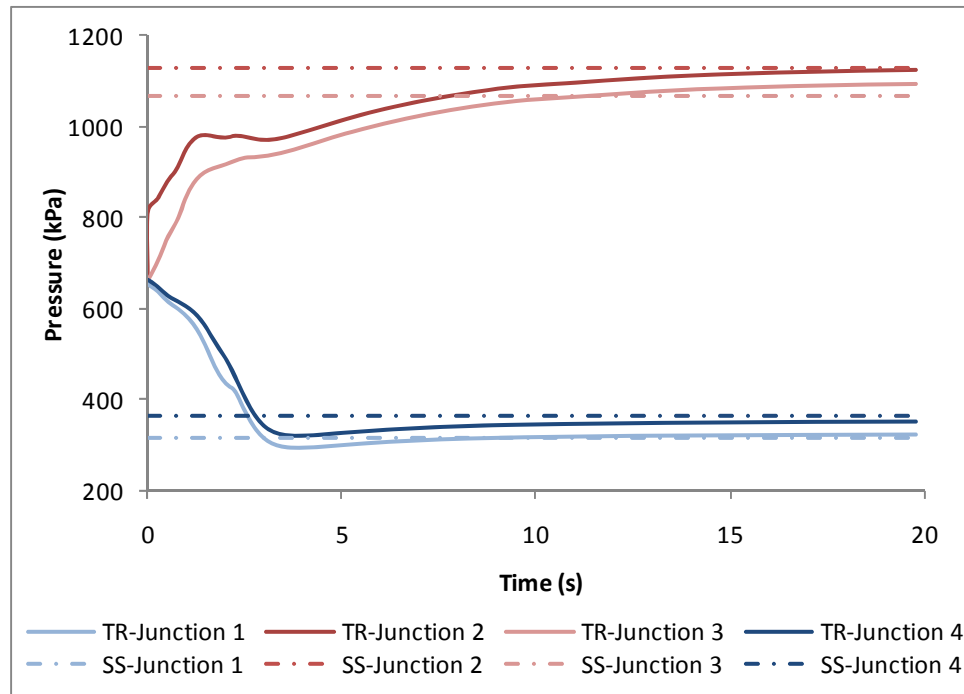


Figure 7.3 Example simulation results - system pressures

The heat exchanger capacities are plotted in Figure 7.4. During the transient operation, the imbalance in the air-side and refrigerant-side heat load goes into changing the material temperature. During steady state, the air-side and refrigerant-side heat loads are equivalent, and hence there is only one line plotted for each heat exchanger for the steady state results. For testing purposes, the initial wall temperature for both heat exchangers was set to 25.0°C, which is slightly cooler than the condenser inlet air temperature. Thus, the air-side heat load for the condenser is negative, meaning the air is cooling down, for the first few seconds until the condenser wall temperature increases beyond that of the inlet air temperature.

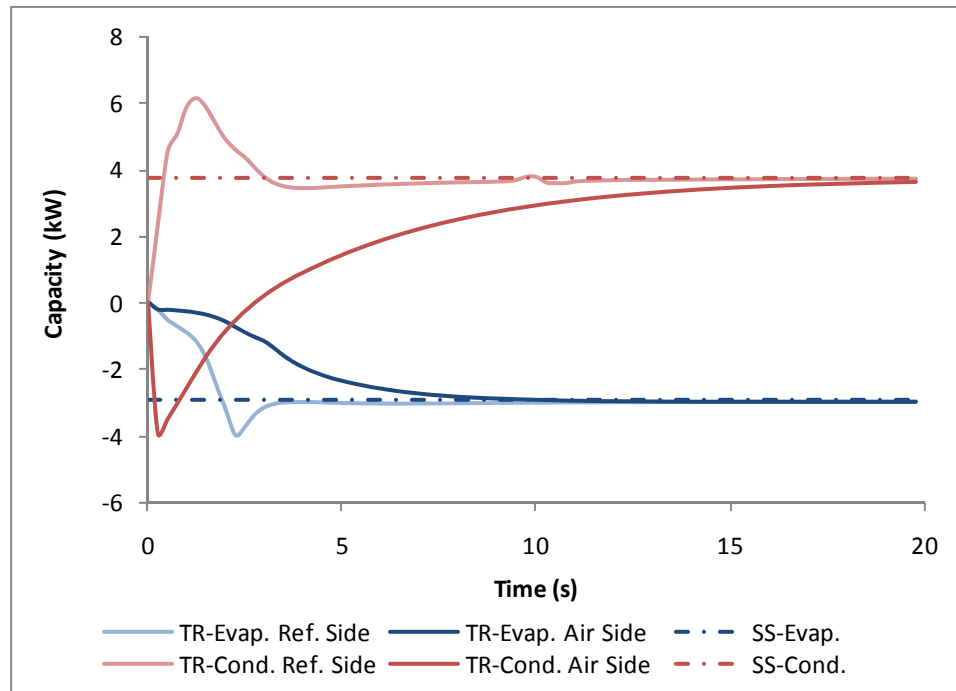


Figure 7.4 Example simulation results – heat loads

The refrigerant-side heat load for the condenser reaches a maximum because initially the increase in saturation temperature of the refrigerant in the condenser increases faster than the material temperature. Thus, the temperature gradient between the refrigerant and wall is very high in the beginning, but then decreases as the saturation temperature stabilizes and the wall temperature catches up. The minimum heat load depicted in the evaporator refrigerant-side heat load is due to the start of the superheated region. As the superheated region in the evaporator forms, the temperature gradient between the wall and the refrigerant decreases along with the refrigerant-side heat transfer coefficient.

Again, the steady state values between the two simulations for the condenser and evaporator heat loads have a high level of agreement.

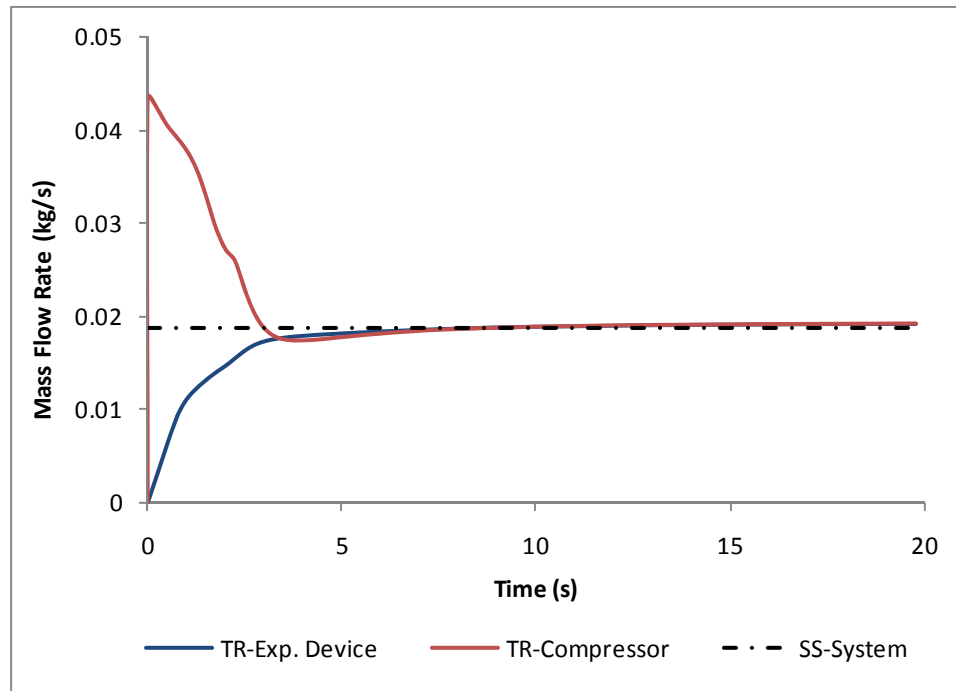


Figure 7.5 Example simulation results – mass flow rate

The mass flow rates are plotted in Figure 7.5. When the system initially starts there is an imbalance in the mass flow rate between the compressor and expansion device. The mass flow rate through the expansion device is dictated by the pressure difference between the inlet and outlet, and when the system starts from an equilibrium state the pressure difference across the expansion device is very small resulting in a low mass flow rate. The opposite is true for the compressor. During the initial start-up period, the pressure ratio across the compressor is small resulting in a high volumetric efficiency and the suction density is high due high suction pressure. Thus, the compressor and expansion device mass flow rate are different during the first few seconds of the simulation. When operating at steady state, the mass flow rate is equal throughout the entire system, and thus there is only a single value as shown in Figure 7.5.

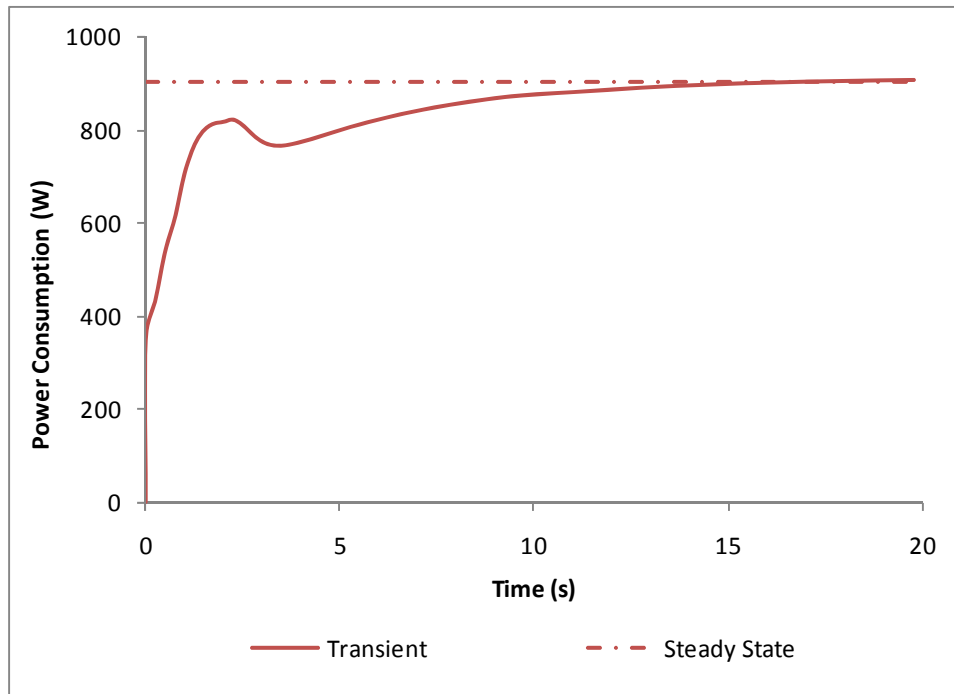


Figure 7.6 Example simulation results – compressor power consumption

The compressor power consumption is displayed in Figure 7.6. The compressor power consumption is most affected by the pressure ratio. Thus, the peak in compressor power occurring at approximately 2.5 seconds coincides with the peak in the discharge pressure, shown in Figure 7.3. The transient and steady state simulations overlap rather well.

The distribution of system charge is shown in Figure 7.7. Due to the imbalance in mass flow rate between the compressor and the expansion device, during the startup period charge moved from the evaporator to the condenser. A majority of the system charge exists in the condenser due to the refrigerant being in the subcooled state at the outlet.

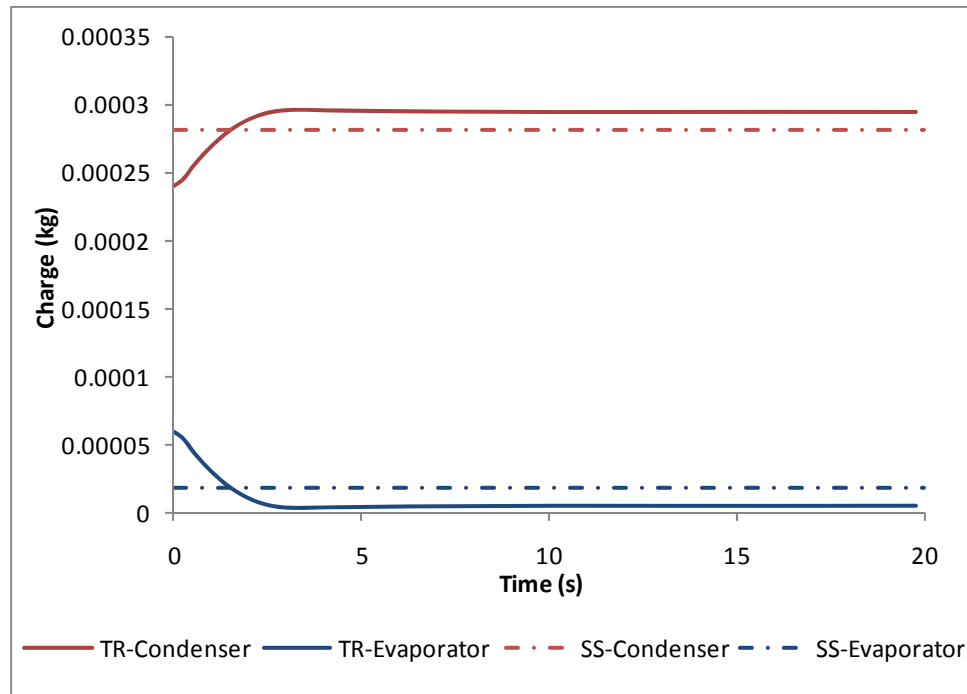


Figure 7.7 Example simulation results – system charge distribution

Tracking the system charge during startup is a very difficult task since it requires both the expansion device and compressor to predict the transient mass flow rate accurately. The expansion device model does not uniquely handle two-phase flow at the inlet, which exists during the startup period. Also, transient compressor simulations often limit the mass flow rate during the startup to take into account the pressure drop through the valves. These two contributing factors are reasons for the discrepancies in the charge allocation between the steady state and transient simulations shown in Figure 7.7. It should also be pointed out that charge prediction in steady state simulations is a very challenging task since it is inherently coupled to void fraction correlations which are generally not very accurate over a wide range of operating conditions.

7.3.3 Results Comparison

A table summarizing the simulation results is presented below. The previous plots of the transient performance indicate the system has indeed reached a steady state. The

transient results presented in the table are the results from the last time step of the simulation. These results are used to make comparisons to the steady state simulation since it is important for the steady state results predicted by the transient simulation to match the steady state simulation results.

Table 7.3 Comparison of steady state and transient results for the example system

	Steady State Simulation	Transient Simulation	Error
Cooling Capacity (kW)	2.949	2.961	0.42%
Power Consumption (W)	903.3	907.5	0.46%
Mass Flow Rate (kg/s)	0.0187	0.0192	2.56%
Subcooling (°C)	8.3	8.7	-0.40°C
Superheat (°C)	5.1	1.8	3.30°C
Condenser Pressure Drop (kPa)	57.6	30.8	46.5%
Evaporator Pressure Drop (kPa)	50.8	31.1	38.8%
Condenser Charge (kg)	0.2814	0.2940	4.5%
Evaporator Charge (kg)	0.01808	0.00554	69.4%

The cooling capacity, power consumption, mass flow rate, and subcooling compare very well. As previously mentioned, the difference in discretization scheme leads to differences in the pressure drop predictions; however, as shown in Figure 7.3 the system operating pressures are predicted quite closely. A single tank heat exchanger model was utilized to show the most important output parameters (cooling capacity, power consumption, operating pressures, and mass flow rate) can show a high level of agreement with a much more detailed steady state simulation tool since the single tank heat exchanger model is the computationally cheapest option. The difference in pressure drop shown in Table 7.3 is not unexpected since the pressure drop prediction dependence on number of tanks was shown in Figure 6.11 and the pressure drop could be accurately captured with an increased number of tanks (Figure 6.14). This disagreement in pressure

drop prediction also leads to a few degrees of error in the superheat prediction, since the superheat at the evaporator outlet is dependent on the evaporator pressure drop.

7.4 Transient Validation Study

This section of the thesis presents a validation study using experimental results. The experimental data consists of a single pull down test where the system was turned on after remaining idle for a significant amount of time. Though a pull down test is useful in validating the model, additional experimental data, such as cycling behavior, would be most useful in determining the discrepancies between the experimental and simulated values.

7.4.1 System Description and Procedure

The system modeled was a 9.5 kW residential R410A air-conditioner. The procedure used to perform the validation was to first validate the individual component models using steady state experimental results. The validation results for the condenser and evaporator (along with the physical description of the two heat exchangers) was presented in Section 6.1.7 and the validation and physical description of the scroll compressor used in the system was presented in Section 6.2.3. The experimental setup used a thermostatic expansion valve as the throttling device, however due to lack of specific information a fixed orifice expansion device was used in the simulation.

The system charge output from the steady state system simulation was used as input to the transient simulation. The actual system charge from the experimental results was not used since the system contained additional auxiliary components not included in the simulation. The entire system charge was assumed to be located in the evaporator and condenser. The initial charge allocation between the two heat exchangers was unknown

and manually adjusted to achieve the startup trends that best matched the experimental values.

The experimental study used to perform this validation was collected and presented by Wang (2008a). The vapor compression system was tested using a wind tunnel, and thus the inlet air conditions to evaporator coil were held constant. The evaporator in an air-conditioner is being used to service a cooling load and ideally the load/space air temperature would be monitored in a pull down scenario.

7.4.2 Validation Results

A comparison of the simulated and experimental suction and discharge pressures are shown in Figure 7.8. The final steady state values show good agreement with experimental values and the change in suction pressure during the initial startup period shows good agreement as well.

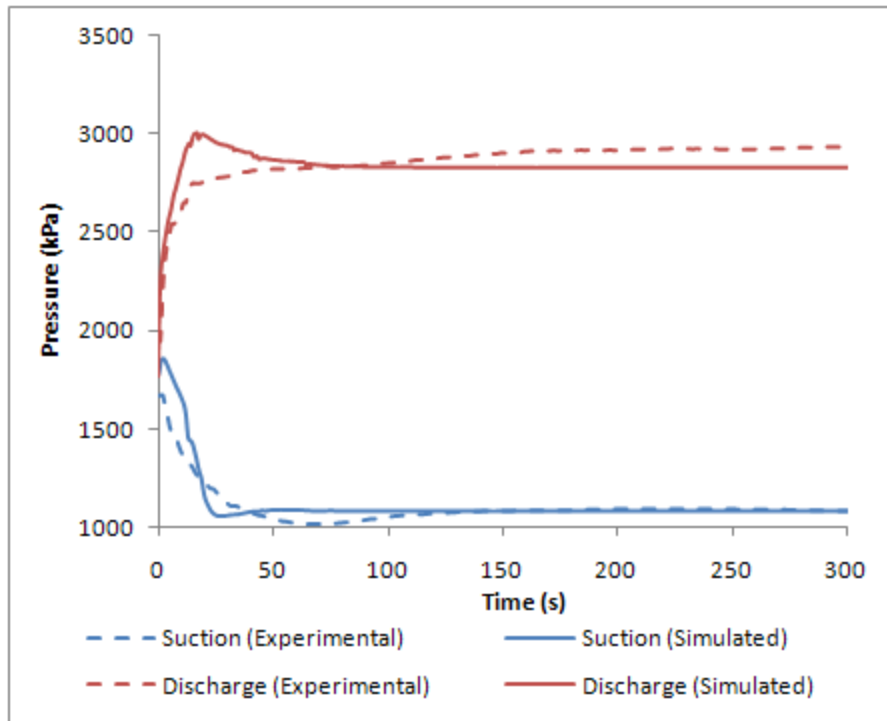


Figure 7.8 Transient validation results – system pressures

The error in the startup pressure predictions is due to the level of difficulty in accurately capturing the charge migration as the system starts up. The accumulator, which ultimately reduces the compressor mass flow rate during the transient period, was not included in the simulation. In addition, the compressor mass flow rate during the startup period was likely over estimated resulting in the peak in simulated discharge pressure since the compressor mass flow rate was not limited in anyway. It is not uncommon for transient compressor models to limit the mass flow rate to a maximum value during the start up period; however this value often lacks physical significance and was not used.

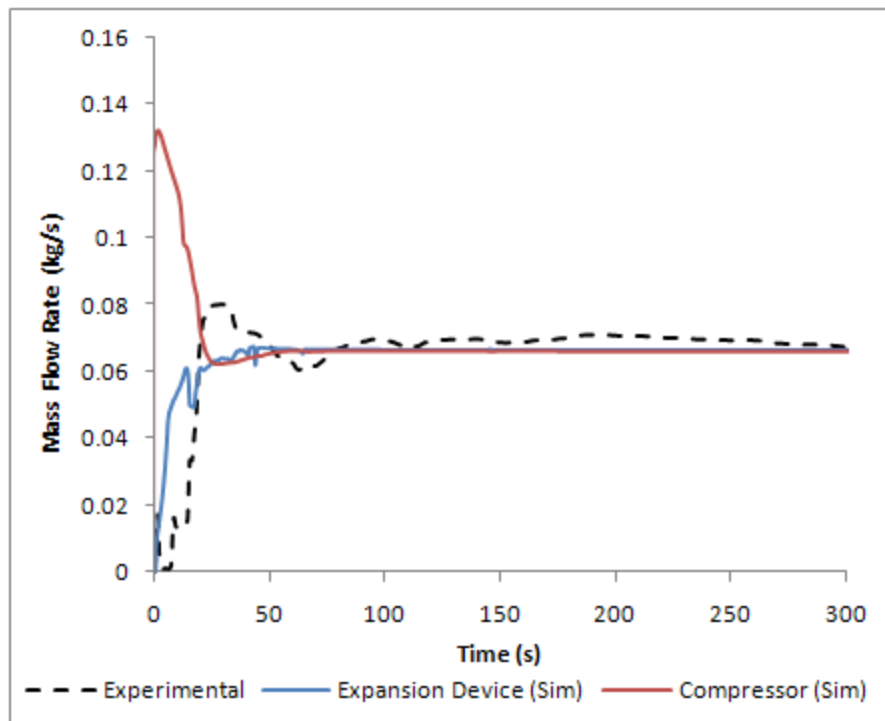


Figure 7.9 Transient validation results – refrigerant mass flow rates

The simulated and experimental refrigerant mass flow rates are shown in Figure 7.9. In the experimental setup, the refrigerant mass flow rate was measured at the condenser outlet (Wang, 2008a) and thus should be compared to the simulated expansion device

mass flow rate. Since the mass flow rate was measured at the condenser outlet and mass flow meters can only measure single phase flow, the mass flow rate was not measured during the few seconds of the startup period since two-phase flow was likely exiting the condenser. The peak in the experimental mass flow rate is not seen in the simulated results, but this is likely due to the slight differences in the experimental system configuration. The simulated and experimental values show very good agreement at steady state. Ideally during a transient experimental setup, the refrigerant mass flow rate would be measured at the compressor outlet to better capture the mass flow rate time dependence; however that was not done in this case.

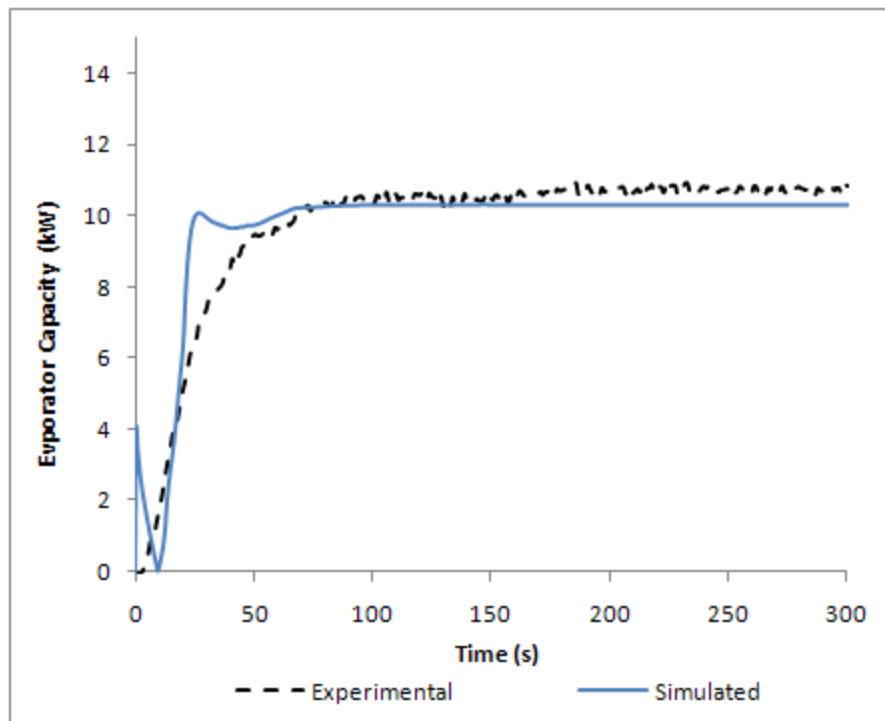


Figure 7.10 Transient validation results – air-side capacity

The evaporator air-side capacity is shown in Figure 7.10. The evaporator air-side capacity in an air-conditioning application tends to be very important since it is the air-side capacity that is cooling the load. The simulated air-side capacity reaches a steady

state value slightly faster than the experiment; however the two converge upon a similar steady state value. The simulated air-side capacity reaches a steady value due to two factors.

Generally, when conducting transient simulation of a vapor compression system it is very difficult to accurately account for all the thermal mass of the equipment. A photograph of the evaporator used in the experiment is shown in Figure 7.11. The simulation does not take into account the thermal mass of the connecting piping and return bends (U-bends used to connect the heat exchanger tubes). The thermal mass of the supporting hardware is also not accounted for in the simulation. Thus, the total thermal mass of the heat exchanger is under predicted, which would contribute to the predicted air-side capacity reaching a steady state value much more than quickly than observed experimentally.

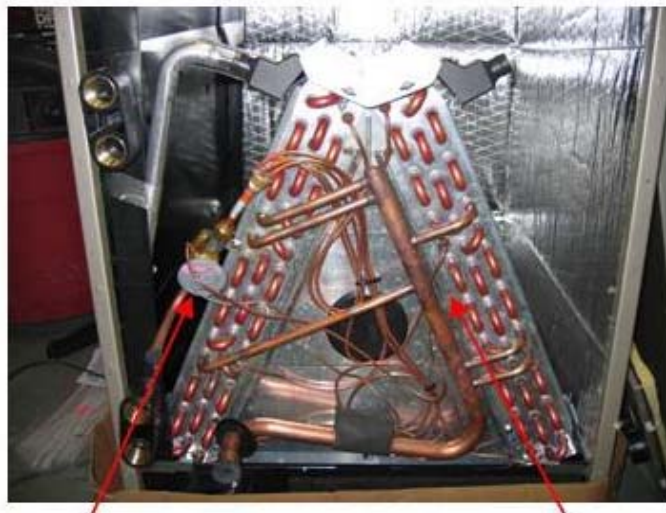


Figure 7.11 Photograph of evaporator (courtesy of Wang (2008a))

The total air-side capacity plotted in Figure 7.10 consists of the sensible load component and latent load component, and approximately 25-30% of the total air-side capacity is due to latent load component at steady state. Relative humidity sensors were

used to measure the evaporator inlet and outlet humidity, which was ultimately used to calculate the evaporator latent capacity. The design of the relative humidity sensor used in this experiment contributes to a very slow response time, resulting in a time lag of the latent capacity during the startup test (Muehlbauer, 2008). Thus, the latent load component of the total air-side capacity in the experimental data reaches a steady value slower than the true response.

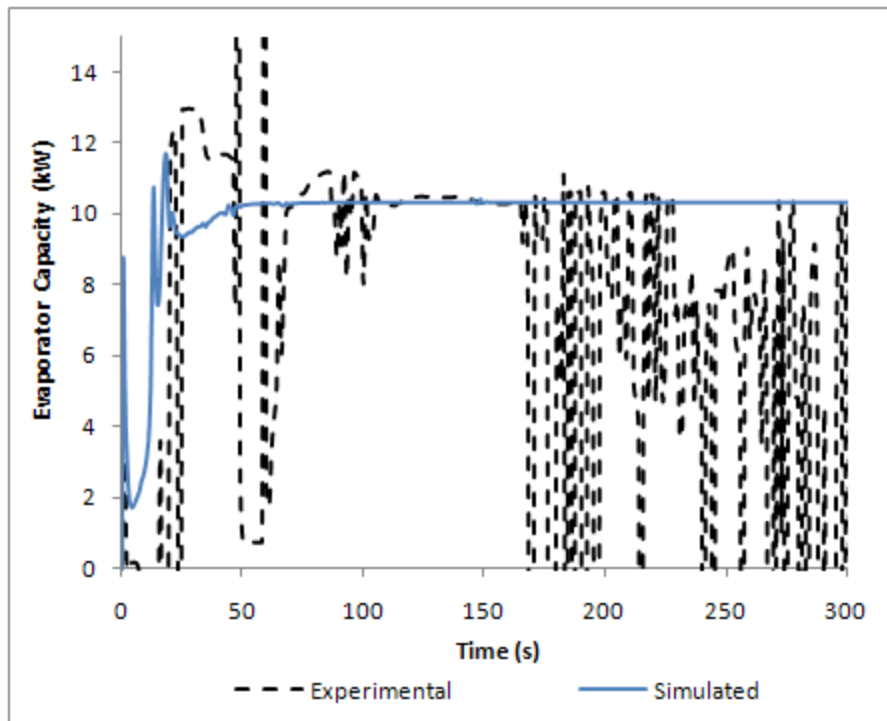


Figure 7.12 Transient validation results – refrigerant-side capacity

The refrigerant-side capacity during the startup period is shown in Figure 7.12. In order to experimentally measure the refrigerant-side capacity during the startup period refrigerant in the superheated vapor state must be exiting the evaporator, which does not occur until after the 300 second time period. Thus, the simulated and experimental refrigerant-side capacity during the startup period cannot be adequately compared and this plot is only shown for completeness. However, the simulated and experimental

refrigerant-side capacities both arrive at approximately the same steady state value, which is also supported by the agreement displayed in Figure 7.10.

The compressor power consumption comparison is shown in Figure 7.13. Though the simulation and experiment reach very similar steady state values, the startup performance is not accurately captured. This disagreement during the start up period is compounded by the following two previously discussed factors; (1) the over-predicted compressor discharge pressure during the startup period, and (2) the likely over-predicted compressor mass flow rate during the startup period.

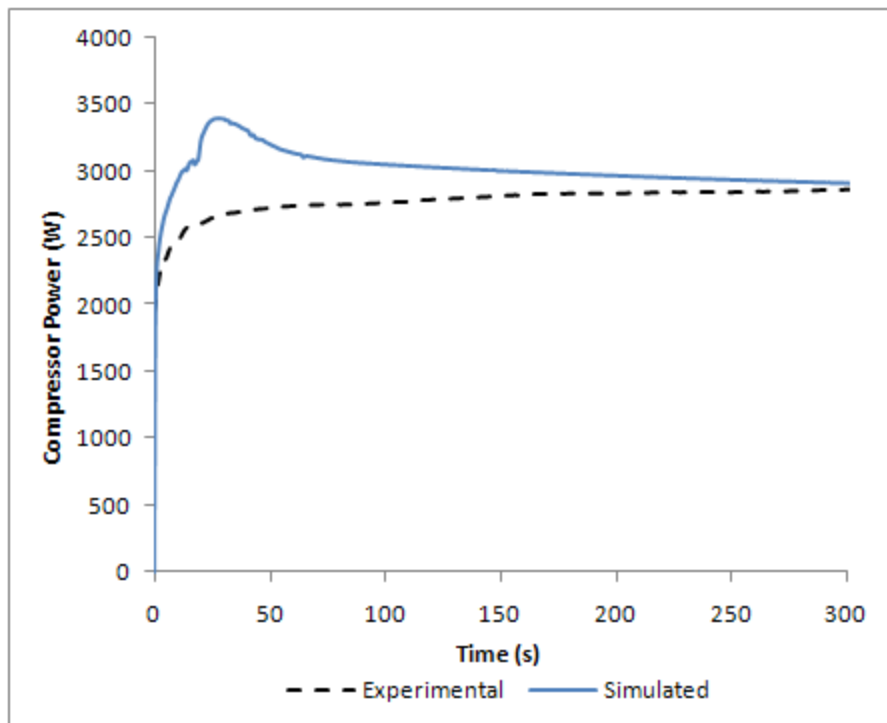


Figure 7.13 Transient validation results – compressor power consumption

7.4.3 Validation Discussion

The validation results for the key indicators describing the performance of a vapor compression system were presented in the previous section. Though the steady state performance results between the simulated and experimental values matched fairly

consistently, the startup trends were not as accurately captured as some of the transient vapor compression system simulation validations presented in the literature. This can be explained for the following reasons.

The component models in the transient simulation were only tuned using steady state experimental data. Meaning from the steady state experimental data only, suitable correction factor were utilized to adjust the heat transfer coefficient and pressure drop correlations. This process and results were described in Section 6.1.7. The tuning factors used to validate the heat exchanger models were determined by running steady state heat exchanger simulations using only CoilDesigner, and not the Tank and Tube Heat Exchanger model. No additional modifications were made to the component models prior to running the transient simulation, which is a process not mentioned in any of the sources found in the literature. This procedure was chosen since it is the procedure likely to be implemented by engineers using the simulation tool since steady state performance tests are more prevalent than transient tests.

The component models do not use any empirical numbers in their formulation other than the tuning (correction) factors used to adjust the heat transfer coefficient and pressure drop correlations. Typically empirical constants (such as an upper limit on refrigerant mass flow rate, constant polytropic coefficients, variable expansion device discharge coefficient, etc.) are used to improve the validation, which is not the case here. All the parameters used in the simulation are taken from the manufacture data and when heat transfer correlations didn't exist for the compressor shell, best estimates were made.

8 Summary and Conclusions

The main objective of this work is to develop a component-based simulation tool capable of simulating the transient and steady state performance of vapor compression systems. This objective has been completed and the conclusions are summarized as follows.

8.1 Component-Based Simulation

- Four component standards were developed to fulfill the needs of implementing a component-based framework for steady state and transient simulation of vapor compression systems.
 - A component-based framework supporting steady state and transient vapor compression components has been developed and implemented. The complete set of methods and properties used to satisfy the required system-to-component communication has been described.
 - A component standard supporting heat exchanger and load communication has been developed and implemented. The load standard allows heat exchangers to be coupled with multiple loads, generally an important level of detail to take into account when performing transient simulations.
 - A component standard supporting heat exchanger and fan component communication has been developed and implemented. The fan standards allows heat exchanger models to be coupled with fan components, which allows for (1) the fan power to be considered in the performance calculation,

and (2) the heat exchanger air flow rate to be determined based on the fan performance.

- A component standard specifically for control actuation has been developed and implemented. The control block standard is very important for transient simulation and allows for any control algorithm to be implemented by users of the program and incorporated into the simulation.
- A single component standard would have offered the simplest solution, however due to the very nature of the systems being simulated (vapor compression systems, heat exchanger and load models, heat exchanger and fan models, and controls), four component standards were required.

8.2 Steady State Component Simulation

- A library of various steady state vapor compression component models has been developed and incorporated into the simulation tool. The component model library allows user to select different component models based on the scope of the simulation and to modify them to simulate a wide range of systems.
- The steady state component library contains two air-to-refrigerant heat exchanger models, four compressor models, and four expansion device models.

8.3 Investigation into Steady State Solver Performance and Its Improvement

- A new steady state solution technique capable of simulating vapor compression systems with additional components has been developed and the performance has been compared with existing techniques in the literature.

- The new solver was found to be more robust and more efficient than the existing solution algorithms for the following reasons.
 - The solver inherently utilizes variables that have already been calculated by the component models. For example, the condenser uses the refrigerant mass flow rate calculated by the compressor.
 - The solver has fewer unknown variables reducing (a) the computational time to evaluate the numerical Jacobian and (b) the number of variables that needed to be resolved
 - Only a single enthalpy value is determined from the numerical equation solver, reducing the likelihood of property routine errors.
- Three numerical equation solvers were tested to determine the equation solver best suitable for the new vapor compression system solution algorithm. The Hybrid method out performed both Newton's method and Broyden's method in terms of robustness and the number of required function evaluations.
- A new guess value calculation procedure was implemented where component models are run in the preprocess phase to better determine the system operation. This method was shown to have a 40% reduction in the computational time compared to the original method despite the component models being run prior to simulating the entire system.
- Two system specification types were evaluated and it was found that cycle simulations solving for a specified amount of subcooling are more robust than cycle simulations solving for a specified system charge. This is due to the

sensitivity of the calculated system charge with respect to the refrigerant phase at the condenser outlet.

8.4 Transient Component Simulation

- A new transient heat exchanger model (Tank and Tube Heat Exchanger Model) has been developed based on a decoupled approach to modeling the heat transfer and pressure drop performance of the heat exchanger. The model implements a distributed parameter approach in order to track the refrigerant properties throughout the entire length of the heat exchanger. The model has been validated and the results have been compared with CoilDesigner, the typical steady state heat exchanger model to be used in the simulation tool.
- The heat exchanger model was shown to predict the experimental data heat load to within $\pm 5\%$ despite decoupling the heat transfer and pressure drop calculations.
- A CoilDesigner Input File Translator has been developed to convert a set of CoilDesigner inputs to the corresponding Tank and Tube Heat Exchanger Model. The translator fulfills the objective that users of the tool should only be required to specify all required inputs a single time to run either a transient or steady state simulation.
- A new transient and steady state compressor model has been developed. The model implements a unique solution procedure in that the heat transfer calculations are separated from the compression equations allowing for additional compressor types to be easily added to the model. The compressor model was validated and the model performed better than the standard ARI

compressor model while only using inputs taken from available manufacturer data.

8.5 Transient System Simulation

- A transient system solution procedure has been developed that can handle additional components. This satisfies the objective that users should be able to model vapor compression systems consisting of additional components to further enhance energy efficiency and thermal comfort.
- The transient and steady state simulations were compared to show consistency between the two simulation engines. The steady state results from the transient simulation and the results from the steady state simulation displayed a high level of agreement.
 - The transient and steady state simulation results displayed a high level of consistency despite the coarse discretization in the pressure drop calculations. Thus, in order to capture the most important performance variables (system capacity, power consumption, operating pressures, etc.) it is important to finely discretize the heat transfer calculations.
- A single pull down transient test was validated using experimental results. The component models were tuned only during a steady state validation and no additional adjustments to the models were made for the transient simulation.

9 List of Major Contributions and Future Work

9.1 Major Contributions

The simulation tool presented in this thesis provides the vapor compression industry with a single simulation tool capable of simulating the steady state and transient performance of a vapor compression system while taking advantage of the strengths of each approach. The major contributions include:

- An integrated steady state and transient component-based simulation tool for modeling vapor compression systems
 - Facilitating consistency between transient and steady state simulation results
 - Minimizing software development effort
 - Minimizing software maintenance effort
- A comprehensive vapor compression component-based modeling standard (framework) supporting vapor compression system components, loads, fans, and control sensors
- A faster, more robust steady state solution algorithm capable of modeling systems with additional components (published in Winkler *et al.*, 2008b)
- A new steady state guess value calculation procedure shown to enhance robustness and computational efficiency
- New transient component models further advancing the current state of research while enhancing the ease of use for future users of the simulation tool
- The following paper was published describing the steady state solver and characterizing its performance compared to two other solvers in the literature:

- [102] "Comprehensive Investigation of Numerical Methods in Simulating a Steady-State Vapor Compression System."
- The following papers are currently under development:
 - Winkler, J., Aute, V., and Radermacher, R. "An Integrated Steady State and Transient Vapor Compression System Simulation Tool, Part 1: Component Model Development." Journal: To be determined.
 - Winkler, J., Aute, V., and Radermacher, R. "An Integrated Steady State and Transient Vapor Compression System Simulation Tool, Part 2: Simulation Results Comparison and Validation." Journal: To be determined.
- The steady state feature of the simulation tool has been released and is currently being utilized by at least 8 companies worldwide, including: Daikin, Delphi, DriEaz, Emerson Network Power, Ingersoll Rand, Johnson Controls, Sanyo, and SubZero
- The procedure in which the steady state solver was developed allows it to be easily extended to solve additional cycle configurations, such as the two-stage flash tank cycle and cascaded vapor compression systems. This has been completed and presented in the following two papers:
 - [101] "Simulation and Validation of a Two-Stage Flash Tank Cycle using R410A as a Refrigerant."
 - [103] "Simulation and Validation of a R404A/CO₂ Cascade Refrigeration System."

9.2 Future Work

Even though this thesis continues to advance vapor compression system modeling capabilities, the following would further develop the tool and quite possibly make it more useful to the industry.

- Implement a moving boundary tank model since the moving boundary heat exchanger has been shown to more computationally efficient than the fixed volume approach. This would allow users to choose between a fixed volume and moving boundary model based on the desired output parameters.
- Develop transient auxiliary component models such as accumulators, receivers, etc.
- Develop a graphical user interface for the transient simulation engine
- Further develop the new transient compressor model to handle two-stage compressor configurations.
- Develop transient system solution algorithms to handle additional cycle configurations (such as a cycle with a suction line heat exchanger, two-stage flash tank cycle, and two-stage split cycle). The steady state solution technique was further advanced to handle additional cycle configurations (Winkler *et al.*, 2008a), and transient solution algorithms need to be given special attention.

References

- [1] Agrawal, N., Bhattacharyya, S., and Sarkar, J. "Optimization of Two-Stage Transcritical Carbon Dioxide Heat Pump Cycles." *International Journal of Thermal Sciences*, 2007, Vol. 46, pp. 180-187.
- [2] Almedia, M. S., Gouveia, M. C., Zdebsky, S. R., and Parise, J. A. "Performance Analysis of a Heat Pump Assisted Drying System." *International Journal of Energy Research*, 1990, Vol. 14, pp. 397-406.
- [3] Anand, G. *Transient and Steady State Model of a Household Refrigerator*. Master's Thesis, Department of Mechanical Engineering, University of Maryland, College Park, MD, 1999.
- [4] ANSI/ARI Standard 540-1999. *Positive displacement refrigerant compressors and compressor units.*, Air-Conditioning and Refrigeration Institute, 1999.
- [5] ASHRAE. "ASHRAE Handbook: Systems." American Society of Heating, Refrigerating, and Air-Conditioning Engineers, 2000.
- [6] ASHRAE. ASHRAE Handbook: Fundamentals. American Society of Heating, Refrigerating, and Air-Conditioning Engineers, 2001.
- [7] ASHRAE. ASHRAE Handbook: Refrigeration. American Society of Heating, Refrigerating, and Air-Conditioning Engineers, 2002.
- [8] ASHRAE, ANSI/ASHRAE 116-1995. *Methods of testing for rating seasonal efficiency of unitary air conditioners and heat pumps.*, American Society of Heating, Refrigeration, and Air-Conditioning Engineers, Inc., 1995.
- [9] Aute, V., Radermacher, R., and Naduvath, M. V. "Constrained Multi-Objective Optimization of a Condenser Coil using Evolutionary Algorithms." International Refrigeration and Air Conditioning Conference at Purdue. Purdue University, West Lafayette, IN, July 12-15, 2004.
- [10] Aynur, T. N., Hwang, Y., and Radermacher, R. "Field Performance Measurements of a VRV AC/HP System." International Refrigeration and Air Conditioning Conference at Purdue. Purdue University, West Lafayette, IN, July 17-20, 2006.
- [11] Bendapudi, S. A. and Braun, J. E. *A review of literature on dynamic models of vapor compression equipment*. HL 2002-9 Report #4036-5, Herrick Laboratories, 2002.
- [12] Bendapudi, S. A., Braun, J. E., and Groll, E. A. "A Dynamic Model of a Vapor Compression Liquid Chiller." Ninth International Refrigeration and Air Conditioning Conference at Purdue. Purdue University, West Lafayette, IN, July 16-19, 2002.

- [13] Bendapudi, S. A., Braun, J. E., and Groll, E. A. "Dynamic Model of a Centrifugal Chiller System - Model Development, Numerical Study, and Validation." *ASHRAE Transactions*, 2005, Vol. 111, Part 1, pp. 132-148.
- [14] Bourdouxhe, J. P., Grodent, M., Lebraun, J. J., Saavedra, C., and Silva, K. L. "A Toolkit for Primary HVAC System Energy Calculation – Part 2: Reciprocating Chiller Models." *ASHRAE Transactions*, 1994, Vol. 100, Part 2, pp. 774-786.
- [15] Bradley, D. *Personal communication*. Thermal Energy System Specialists, LLC, 2007.
- [16] Browne, M. and Bansal, P. "Steady-State Model of Centrifugal Liquid Chillers." *International Journal of Refrigeration*, 1998, Vol. 21, pp. 343-358.
- [17] Browne, M. and Bansal, P. "Transient Simulation of Vapour Compression Packaged Liquid Chillers." *International Journal of Refrigeration*, 2002, Vol. 25, pp. 597-610.
- [18] Chi, J. and Didion, D. "A Simulation Model of the Transient Performance of a Heat Pump." *International Journal of Refrigeration*, 1982, Vol. 53, pp. 176-184.
- [19] Choi, J., Kim, Y., and Kim, H. Y. "A Generalized Correlation for Refrigerant Mass Flow Rate through Adiabatic Capillary Tubes." *International Journal of Refrigeration*, 2003, Vol. 26, pp. 881-888.
- [20] Corberan, J. M., Gonzalvez, J., Montes, P., and Blasco, R. "'ART' a Computer Program Code to Assist the Design of Refrigeration and A/C Equipment." 2002 International Refrigeration and Air Conditioning Conference. Purdue University, West Lafayette, IN, July 16-19, 2002.
- [21] Corberan, J. M., Gonzalvez, J., Urchuegui, J., and Lendoiro, A. N. "Simulation of an Air-to-Water Reversible Heat Pump." 8th International Refrigeration Conference at Purdue. Purdue University, West Lafayette, IN, July 25-28, 2000.
- [22] Cullimore, B. A. *Vapor Compression Cycle Air Conditioning: Design and Transient Simulation*. C&R White Paper, C&R Technologies, 2000.
- [23] Cullimore, B. A., S. G. Ring, and D. A. Johnson. User's Manual SINDA/FLUINT. Littleton, CO: C&R Technologies, Inc., 2004.
- [24] Davis, G. L., and Scott, T. C. "Component Modeling Requirements for Refrigeration System Simulation." Proceedings of the 1976 Purdue Compressor Conference. Purdue University, West Lafayette, IN, July 6-9, 1976.
- [25] Dhar, M. *Transient Analysis of Refrigeration System*. Ph.D. Thesis, Department of Mechanical Engineering, Purdue University, West Lafayette, IN, 1978.

- [26] Ding, G. L. "Recent Developments in Simulation Techniques for Vapor-Compression Refrigeration Systems." *International Journal of Refrigeration*, 2007, Vol. 18, pp. 1119-1133.
- [27] Ding, G. L., Zhang, C., and Lu, Z. "Dynamic Simulation of Natural Convection Bypass Two-Circuit Cycle Refrigerator-Freezer and its Application, Part I: Component Models." *Applied Thermal Engineering*, 2004, Vol. 24, pp. 1513-1524.
- [28] Dittus, F. A. and Boelter, L. M. K. "Heat Transfer in Automobile Radiators of the Tubular Type." *University of California Publications in Engineering*, 1930, Vol. 2(13), pp. 443-461.
- [29] Domanski, P. A. "NIST Simulation Models." USNC/IIR Short Course on Simulation Tools for Vapor Compression Systems and Components. Purdue University, West Lafayette, IN, July 10-11, 2004.
- [30] Domanski, P. A., and D. Didion. Computer Modeling of the Vapor Compression Cycle with Constant Flow Area Expansion Device. Gaithersburg, MD: NBS Build Science Series 155, National Institute of Standards and Technology, 1983.
- [31] Domanski, P. A., D. Didion, and J. Chi. CYCLE D: NIST Vapor Compression Cycle Design Program, Version 3.0 User Guide. Gaithersburg, MD: National Institute of Standards and Technology, 2003.
- [32] Domanski, P. A. and McLinden, M. O. "A Simplified Cycle Simulation Model for the Performance Rating of Refrigerant and Refrigerant Mixtures." *International Journal of Refrigeration*, 1992, Vol. 15, pp. 81-88.
- [33] Dynasim AB. 2007. <<http://www.dynasim.com>>.
- [34] ElAziz, O. A., Winkler, J., Aute, V., and Radermacher, R. "Transient Simulation of a Transcritical Carbon Dioxide Refrigeration System." International Refrigeration and Air Conditioning Conference at Purdue. Purdue University, West Lafayette, IN, July 17-20, 2006.
- [35] Ellison, R. D. and Creswick, F. A. *A Steady-State Computer Design Model for an Air-to-Air Heat Pump*. ORNL/CON-16, Energy Division, Oak Ridge National Laboratory, 1978.
- [36] Emerson Climate Technologies. *System Design Simulator*. Ver. 4.1.0, 2004.
- [37] Energy Information Administration. *Regional Energy Profile - U.S. Household Electricity Report*, 2005.
- [38] Fischer, S. K. and Rice, C. K. *The Oak Ridge Heat Pump Models: I. A Steady State Computer Design Model for Air-to-Air Heat Pumps*. ORNL/CON-80/RI, Energy Division, 1983.

- [39] FKW - Research Center for Refrigeration and Heat Pumps, Ltd. *Cycle Calculation Program - KMKreis*. Ver. 6.2, 1998.
- [40] Gado, A. *Development of a Dynamic Test Facility for Environmental Control Systems*. Ph.D. Thesis, Department of Mechanical Engineering, University of Maryland, College Park, MD, 2006.
- [41] Gauthier, J. S. *Personal communication*. Gauthier Simulation, 2007.
- [42] Ge, Y. T. and Tassou, S. A. "Mathematical Modelling of Supermarket Refrigeration Systems for Design, Energy Prediction, and Control." *Proceedings of the Institute of Mechanical Engineers*, 2000, Vol. 214, Part A, pp. 101-114.
- [43] Gordon, B. W., Liu, S., and Asada, H. H. "Dynamic Modeling of Multiple-Zone Vapor Compression Cycle using Variable Order Representations." *Proceedings of the American Control Conference*. San Diego, CA, June 1999.
- [44] Grald, E. W. and MacArthur, J. W. "A Moving-Boundary Formulation for Modeling Time-Dependent Two-Phase Flows." *International Journal of Heat and Fluid Flow*, 1992, Vol. 133, pp. 266-272.
- [45] Grossman, G. and Gommed, K. "A Computer Model for Simulation of Absorption Systems in Flexible and Modular Form." *ASHRAE Transactions*, 1987, Vol. 93, Part 2, pp. 2389-2428.
- [46] Grossman, G. and Michelson, E. "A Modular Computer Simulation of Absorption Systems." *ASHRAE Transactions*, 1985, Vol. 91, Part 2B, pp. 1808-1827.
- [47] Grossman, G. and Zaltash, A. "ABSIM – Modular Simulation of Advanced Absorption Systems." *International Journal of Refrigeration*, 2001, Vol. 24, pp. 531-543.
- [48] He, X. D., Liu, S., Asada, H. H., and Itoh, H. "Multivariable Control of Vapor Compression Systems." *HVAC&R Research*, 1998, Vol. 4, 3, pp. 205-230.
- [49] Herbas, T. B., Berlinck, E. C., Uriu, C. A., Marques, R. P., and Parise, J. A. "Steady-State Simulation of Vapour-Compression Heat Pumps." *International Journal of Energy Research*, 1993, Vol. 17, pp. 801-816.
- [50] Hermes, C. J. and Melo, C. "A First Principles Simulation Model for Start-Up and Cycling Transients of Household Refrigerators." *International Journal of Refrigeration*, 2008, Vol. 318, pp. 1341-1357.
- [51] Hiller, C. C. and Glicksman, L. R. *Improving Heat Pump Performance via Compressor Capacity Control Analysis and Test, Volume 1*. Energy Laboratory Reports MIT-EL 76-0001, MIT Energy Laboratory, 1976.

- [52] Huff, H. J., Hwang, Y., and Radermacher, R. "Options for Two-Stage Transcritical Carbon Dioxide Cycle." Natural Working Fluids 2002, IIR-Gustav Lorentzen Conference. Guangzhou, China, .
- [53] Hwang, Y. and Radermacher, R. "Theoretical Evaluation of Carbon Dioxide Refrigeration Cycle." *HVAC&R Research*, 1998, Vol. 43, pp. 245-263.
- [54] Jiang, H. *Development of a Simulation and Optimization Tool for Heat Exchanger Design*. Ph.D. Thesis, Department of Mechanical Engineering, University of Maryland, College Park, MD, 2003.
- [55] Jiang, H., Aute, V., and Radermacher, R. "CoilDesigner: A General-Purpose Simulation and Design Tool for Air-to-Refrigerant Heat Exchangers." *International Journal of Refrigeration*, 2006, Vol. 29, pp. 601-610.
- [56] Jolly, P., Jia, X., and Clements, S. "Heat Pump Assisted Continuous Drying Part 1: Simulation Model." *International Journal of Energy Research*, 1990, Vol. 14, pp. 757-770.
- [57] Joudi, K. A. and Namik, H. M. "Component Matching of a Simple Vapor Compression Refrigeration System." *Energy Conversion and Management*, 2003, Vol. 44, pp. 975-993.
- [58] Kim, Y. and O'Neal, D. L. "Two-Phase Flow of R-22 through Short-Tube Orifices." *ASHRAE Transactions: Research*, 1994, Vol. 100(1), pp. 323-334.
- [59] Kim, Y., O'Neal, D. L., and Yuan, X. "Two-Phase Flow of HFC-R134a and CFC-12 through Short-Tube Orifices." *ASHRAE Transactions: Symposia*, 1994, OR-94-2-2, pp. 582-591.
- [60] Koury, R., Machado, L., and Ismail, K. "Numerical Simulation of a Variable Speed Refrigeration System." *International Journal of Refrigeration*, 2001, Vol. 24, pp. 192-200.
- [61] Li, H., Braun, J. E., and Shen, B. "Modeling Adjustable Throat-Area Expansion Valves." International Refrigeration and Air-Conditioning Conference at Purdue. Purdue University, West Lafayette, IN, July 12-15, 2004.
- [62] MacArthur, J. W. "Analytical Representation of the Transient Energy Interactions in Vapor Compression Heat Pumps." *ASHRAE Transactions*, 1984, Vol. 91, Part 1B, pp. 982-996.
- [63] MacArthur, J. W. and Grald, E. W. "Prediction of Cyclic Heat Pump Performance with a Fully Distributed Model and a Comparison with Experimental Data." *ASHRAE Transactions*, 1987, Vol. 93, Part 2, pp. 1159-1178.
- [64] Masuda, M., Wakahara, K., and Matsuki, K. "Development of a Multi-System Air-Conditioner for Residential use." *ASHRAE Transactions*, 1991, Vol. No. 1, pp. 127-131.

- [65] McQuiston, F., and J. Parker. Heating, Ventilation, and Air Conditioning, Analysis and Design. 4th ed. Wiley & Sons, Inc., 1994.
- [66] Modelica Association. *Modelica - A Unified Object-Oriented Language for Physical System Modeling, Language Specification*. Ver. 3.0, 2007.
- [67] More, J. J., Garbow, B. S., and Hillstrom, K. E. *User guide to MINPACK*. Argonne National Laboratory Report ANL-80-74, 1980.
- [68] Muehlbauer, J. *Personal Communication*, University of Maryland, 2008.
- [69] Murphy, W. E. and Goldschmidt, V. W. "Cyclic Characteristics of a Typical Residential Air Conditioner - Modeling of Start-Up Transients." *ASHRAE Transactions*, 1985, Vol. 91, Part 2A, pp. 427-444.
- [70] Murphy, W. E. and Goldschmidt, V. W. "Cycling Characteristics of a Residential Air Conditioner - Modeling of Shutdown Characteristics." *ASHRAE Transactions*, 1986, Vol. 92, Part 1A, pp. 186-202.
- [71] Otter, M. and Elmqvist, H. "Modelica Language, Libraries, Tools, Workshop and EU-Project RealSim." *Simulation News Europe*, 2000, Vol. December, pp. 3-8.
- [72] Parise, J. A. "Simulation of Vapour-Compression Heat Pumps." *Simulation*, 1986, Vol. 46, pp. 71-76.
- [73] Ploug-Sorensen, L., Fredsted, J. P., and Willatzen, M. "Improvements in the Modeling and Simulation of Refrigeration Systems: Areospace Tools Applied to a Domestic Refrigerator." *HVAC&R Research*, 1997, Vol. 34, pp. 387-403.
- [74] Press, W. H., et al. Numerical Recipes in C. Cambridge, London, United Kingdom: Cambridge University Press, 1992.
- [75] Rasmussen, B. P. and Alleyne, A. G. "Control-Oriented Modeling of Transcritical Vapor Compression System." *Transactions of the ASME*, 2004, Vol. 126, pp. 54-64.
- [76] Richardson, D. H. *An Object Oriented Simulation Framework for Steady-State Analysis of Vapor Compression Refrigeration Systems and Components*. Ph.D. Thesis, Department of Mechanical Engineering, University of Maryland, College Park, MD, 2006.
- [77] Richardson, D. H., Aute, V., Winkler, J., and Radermacher, R. "Numerical Challenges in Simulation of a Generalized Vapor Compression Refrigeration System." 2004 International Refrigeration and Air Conditioning Conference. Purdue University, West Lafayette, IN, July 12-15, 2004.
- [78] Richardson, D. H., Jiang, H., Lindsay, D., and Radermacher, R. "Optimization of Vapor-Compression Systems Via Simulation." 2002 International Refrigeration and Air Conditioning Conference. Purdue University, West Lafayette, IN, July 16-19, 2002.

- [79] Robinson, D. M. and Groll, E. A. "Theoretical Performance Comparison of CO₂ Transcritical Cycle Technology Versus Hcfc-22 Technology for a Military Packaged Air Conditioner Application." *HVAC&R Research*, 2000, Vol. 64, pp. 325-348.
- [80] Rossi, T. A. *Detection, Diagnosis, and Evaluation of Faults in Vapor Compression Cycle Equipment*. Ph.D. Thesis, Department of Mechanical Engineering, Purdue University, West Lafayette, IN, 1995.
- [81] Rossi, T. A., and Braun, J. E. "A Real-Time Transient Model for Air-Conditioners." 20th International Congress of Refrigeration, IIR/IIF. Sydney, Australia, .
- [82] Sanaye, S. and Malekmohammadi, H. R. "Thermal and Economical Optimization of Air Conditioning Units with Vapor Compression Refrigeration System." *Applied Thermal Engineering*, 2004, Vol. 24, pp. 1807-1825.
- [83] Sarkar, J., Bhattacharyya, M. R., and Gopal, M. R. "Simulation of a CO₂ Transcritical Heat Pump Cycle for Simultaneous Cooling and Heating Applications." *International Journal of Refrigeration*, 2006, Vol. 29, pp. 735-743.
- [84] Schwentker, R. A., Aute, V., Radermacher, R., and Mercer, K. "Simulation and Design Tool for Microchannel Heat Exchangers." Fifth International Conference on Enhanced, Compact, and Ultra-Compact Heat Exchangers: Science, Engineering, and Technology. Whistler, British Columbia, Canada, September 11-16, 2005.
- [85] Schwentker, R. A., Winkler, J., Aute, V., and Radermacher, R. "A Simulation and Design Tool for Flat Tube, Louvered-Fin Heat Exchangers." SAE 2006 World Congress. Cobo Center, Detroit, MI, April 3-6, 2006.
- [86] Shah, M. M. "Chart Correlation for Saturated Boiling Heat Transfer: Equations and further Study." *ASHRAE Transactions*, 1982, Vol. 88 (1), pp. 185-196.
- [87] Shah, R., Alleyne, A. G., and Bullard, C. W. "Dynamic Modeling and Control of Multi-Evaporator Air Conditioning Systems." *ASHRAE Transactions*, 2004, Vol. 110, Part 1, pp. 109-119.
- [88] Shen, B., Groll, E. A., and Braun, J. E. "ACMODEL: A Steady-State System Simulation Model for Unitary Air Conditioners and Heat Pumps." USNC/IIR Short Course on Simulation Tools for Vapor Compression Systems and Component Analysis. Purdue University, West Lafayette, IN, July 10-11, 2004.
- [89] Solar Energy Laboratory, University of Wisconsin-Madison. *TRNSYS 16*. Ver. 16, 2007.
- [90] Stoecker, W. F. "A Generalized Program for Steady-State System Simulation." *ASHRAE Transactions*, 1971, Vol. 77, Part 1, pp. 140-147.
- [91] Stoecker, W. F. Refrigeration and Air Conditioning. 2nd ed. McGraw-Hill, 1983.

- [92] Stoecker, W. F. Design of Thermal Systems. 3rd ed. New York: McGraw-Hill, 1989.
- [93] SYSTAT Software. *TableCurve 3D Version 4.0.*, 2002.
- [94] Tassou, S. A., Marquand, C. J., and Wilson, D. R. "Modelling of Variable Speed Air-to-Water Heat Pump Systems." *Journal of the Institutue of Energy*, 1982, Vol. 59, pp. 59-64.
- [95] The CAPE-OPEN Laboratories Network. *1.0 Standard Documentation Set.*, 2003.
- [96] Tummescheit, H., Eborn, J., and Prolss, K. "Air Conditioning - a Modelica Library for Dynamic Simulation of AC Systems." Proceedings of the 4th International Modelica Conference. Hamburg, Germany, March 7-8, 2005.
- [97] Vargas, J. V. and Parise, J. A. "Simulation in Transient Regime of a Heat Pump with Closed-Loop and on-Off Control." *International Journal of Refrigeration*, 1995, Vol. 18, pp. 235-243.
- [98] Wang, X. *Performance Investigation of Two-Stage Heat Pump System with Vapor-Injected Scroll Compressor*. Ph.D. Thesis, Department of Mechanical Engineering, University of Maryland, College Park, MD, 2008a.
- [99] Wang, X. *Personal communication*. Air-Conditioning, Heating, and Refrigeration Institute, 2008b.
- [100] Winkler, J., Aute, V., and Radermacher, R. "Component-Based Vapor Compression Simulation Tool with Integrated Multi-Objective Optimization Routines." 2006 International Refrigeration and Air Conditioning Conference. Purdue University, West Lafayette, IN, July 17-20, 2006.
- [101] Winkler, J., Wang, X., Aute, V., and Radermacher, R. "Simulation and Validation of a Two-Stage Flash Tank Cycle using R410A as a Refrigerant." 2008 International Refrigeration and Air Conditioning Conference. Purdue University, West Lafayette, IN, July 14-17, 2008a.
- [102] Winkler, J., Aute, V., and Radermacher, R. "Comprehensive Investigation of Numerical Methods in Simulating a Steady-State Vapor Compression System." *International Journal of Refrigeration*, 2008b, Vol. 31, pp. 930-942.
- [103] Winkler, J., Aute, V., Radermacher, R., and Shapiro, D. "Simulation and Validation of a R404A/CO₂ Cascade Refrigeration System." 2008 International Refrigeration and Air Conditioning Conference. Purdue University, West Lafayette, IN, July 14-17, 2008c.